Alma Mater Studiorum - University of the Basque Country

Departamento de Física
Programa de Doctorado de Física

Observational Tests of Wave and Particle Dark Matter Predictions

PhD

Author:
Alvaro Pozo

Director:
Dr.Tom Broadhurst

Donostia International Physics Center (DIPC)
Año Academico 2022-2023

Le dedico el resultado de este trabajo a toda mi familia. A mis padres, abuelos, hermano y pareja que me apoyaron y contuvieron los momentos malos y en los menos malos. Gracias por enseñarme a afrontar las dificultades sin perder nunca la cabeza ni morir en el intento. Por ultimo querría agradecer al DIPC toda la ayuda que me ha dado para poder llevar a cabo esta tesis.

Abstract

Recent discoveries of large halos of stars and dark matter around some of the lowest mass galaxies defy expectations that dwarf galaxies should be small and dense. Furthermore, these halos are seen to surround a dense core within each dwarf, with a clear density transition visible between the core and the halo at a radius of 1.0kpc. This common core-halo structure is hard to understand for standard heavy particle dark matter where featureless, concentrated profiles are predicted, whereas dark matter as a Bose-Einstein condensate, ψDM, naturally accounts for the observed profiles, predicting a dense soliton core in every galaxy surrounded by a tenuous halo of interfering waves. We show that the stellar profiles of the well studied "dwarf Spheroidal" (dSph) class, and also the equally numerous "ultra faint dwarfs" (UFD) are accurately fitted by the core-halo structure of ψDM, suggesting two boson species which are reinforced by parallel relations seen between the central density and radius of UDF and dSph dwarfs respectively, which both match the steep prediction, $\rho_c \propto R_c^{-4}$, for soliton cores in the ground state. Here we also compare these stellar profiles with hydrodynamical simulations where the previously observed core-halo structure is predicted to be visible in the ψDM context, but not for CDM.

Contents

Chapter 1

Introduction

Dark Matter (DM) is still one of the most unresolved puzzles of modern physics. It is amply established that DM is the dominant form of matter in the Universe, the nature of which is widely understood to lie beyond the Standard Model of particle physics (Ellis et al., 1984). DM has been uncovered by wide-ranging, independent observations ranging from the perturbations spectrum of the Cosmic Microwave Background (CMB) to large-scale structures, including the Baron Acoustic Oscillations and individual galaxy rotation curves and stellar dispersions. The community has accurately established and accepted that the DM comprises 85% of the total mass density of the Universe, with the remaining 15% only in the form of baryonic matter, including stars, gas, and black holes. Decades of study and work have led the community to consider DM predominately composed of some form of unknown heavy particles, usually called "WIMPs" weakly interacting massive particles motivated by super-symmetry. Black holes represent a possible similar contender usually classed as "MACHO's" or massive-compact-halo-objects for which predictions differ from WIMPs mainly in terms of the lensing and collisional/accretion effects expected for astrophysical-sized black holes. This latter idea is now revived with the detection of many surprisingly massive binary black hole mergers by the LIGO/VIRGO team and also because of the strongest absence of WIMPs in laboratory experiments (Aprile et al., 2018). For over 30 years, these two classes of the model have been simulated approximately as "cold dark matter" as they are not dynamically relativistic in cosmological simulations and hence "cold" of structure formation (Davis et al., 1985; Efstathiou et al., 1990) focusing cosmologists on testing the predictions of CDM.

With the lack of any evidential detection of weakly-interacting massive particles, the favored particle theory explanation for many years, this alternative possibility of "MACHOs" kind objects as DM has seen increased their amount of supporters. The LIGO data of the past years has motivated if the primordial black holes (PBHs) could be the main DM contributors between these compact objects in the DM halos (Carr & Hawking, 1974; Carr, 1975; Meszaros, 1974; Clesse & García-Bellido, 2015). For this purpose, some recent works have been done to understand if some of these LIGO detections could somehow be DM detection, considering the BH binaries as a signature of DM (Bird et al., 2016). This idea is based on the concept that if BHs

in a galactic halo pass sufficiently close, they radiate enough energy in gravitational waves to become gravitationally bound. The bound BHs will rapidly spiral inward due to the emission of gravitational radiation and ultimately merge in less than a Hubble time. This could be possible if BHs will have $\sim 30M_{\odot}$, something that will match with the expected window of $20M_{\odot}$ to $100M_{\odot}$ of PBHs as a candidate of DM (Bird et al., 2016). Moreover, PBHs are predicted to be distributed spatially more like DM than luminous matter, where distinguishing them from traditional astrophysical sources seems to be the main issue nowadays. Is it supposed that PBHs mergers should occur in smaller dominated DM halos than in the luminous ones where traditional stellar BHs mergers should dominate.

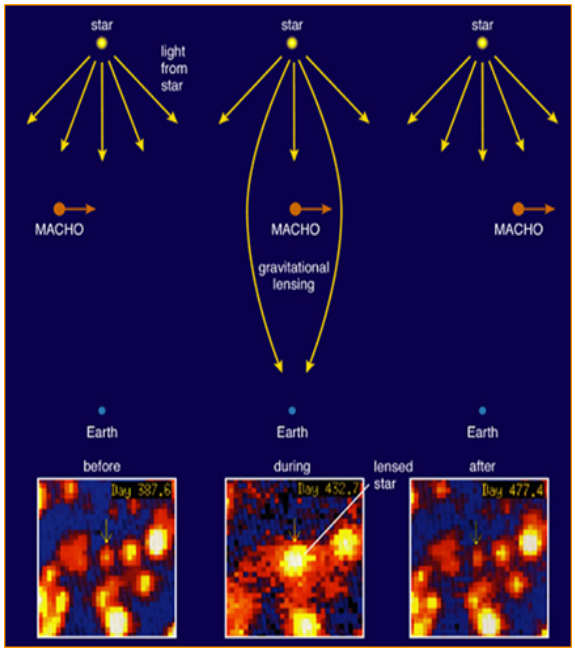

Figure 1.1: Brightness temporal magnification of a lighting source due to the gravitational microlensing product of and intermediate MACHO. Credit Wesley (2004)

In this scenario, a recent LIGO detection of two $\sim 30M_{\odot}$ has recently been suggested as a PBH DM detection (Bird et al., 2016), due to being inside the expected range of $20M_{\odot}$ to $100M_{\odot}$ (Carr et al., 2010; Monroy-Rodríguez & Allen, 2014)(Lower masses are excluded by microlensing surveys (Wyrzykowski et al., 2011; Tisserand et al., 2007a), higher masses would disrupt wide binaries (Monroy-Rodríguez & Allen, 2014; Yoo et al., 2004; Quinn et al., 2009), and it has been argued that PBHs in this mass range are excluded by CMB constraints (Ricotti, 2007; Ricotti et al., 2008)). Nevertheless, the resulting merger rate they found for PBHs of $\sim 30M_{\odot}$ was quite smaller compared to the estimated one from LIGO, of 2-53 $Gpc^{-3}yr^{-1}$. However, they pointed out that the rate is expected to be higher in higher density regions and in regions of lower DM velocity dispersion that are expected to be in Milky-Way-like halos. Moreover, even if the obtained merger rate conflicts with the expected one, with more precise treatments of the small-scale galactic phase-space distribution, conservative lower estimates of the merger rate for PBH DM suggest that the LIGO/VIRGO network should see a considerable number of PBH mergers

over its lifetime (Bird et al., 2016).

The stochastic GW (Gravitational wave) background could be another important source of information. These models predict a wide mass distribution that extends to small BHs and redshift values that seem related to stellar formation history. As we have already commented, PBHs mass function is limited by microlensing analysis to $30M_{\odot}$ in his lower limit, making the resulting merger rate more significant per volume for PBHs than traditional BHs at high redshifts. This prediction goes in hand with the obtained information by the LIGO-Virgo collaboration, where 11 pairs of BBH (Binary black hole) events are suggestive that lensing of GWs may be taking place at a much higher rate than previously realized by the LVT. If this is confirmed, it will imply that models that predict more merger rates at z>1, as the BDS (Bardeen de-Sitter) model, would be in the good direction. In this scenario, the predicted stochastic background of GWs will highly differ from the predicted by the standard model one, which expects a much higher rate at lower redshifts than at higher (Diego et al., 2021).

Some constraints have seemed to rule out the option of PBHs as an important DM candidate, based on the ideality of galaxy clusters to study the microlensing by these objects (An effect that happens when these MACHO objects pass in front of a visible baryonic source, that suffer a temporal magnification due to gravitational lensing (Paczynski, 1986), check figure 1.1) due to being possible to find critical curves free from a similar event with stellar impact. These works have made analyses of multiply imaged quasars (QSOs) that suggest that the observed microlensing signals are incompatible with the hypothesis that PBHs of $\sim 30M_{\odot}$ could form a high proportion of the dark matter(Mediavilla et al., 2017), limiting it to a 20%, but with the most likely mass of microlenses being below 1 $M_{\odot}$. Even if the accretion disk around the QSOs were an order of magnitude larger than they are considered (something that could imply a higher percentage of DM being constituted by PBHs), most of the works seem to conclude that applying a realistic extended mass function, PBHs in the range of $20M_{\odot}$ to $100M_{\odot}$ could only imply a $\sim 10\%$ of the DM (Carr & Kühnel, 2020; Diego et al., 2018). Even more, recent results from MACHO and EROS collaboration have discarded MACHO objects as the main DM contributor in the galactic halos in the range from $10^{-7}M_{\odot}$ to a few solar masses, as it has been known "The End of the MACHO Era" (Yoo et al., 2004; Alcock et al., 2000, 1998). This end of the "Macho era" is based on several constraints of a wide diversity of works: Microlensing events on the Large Magellanic cloud seem not to show any evidence to discard high masses of dark objects, but they favor exclusion of objects between $0.3M_{\odot}$ to $30M_{\odot}$ from contributing more than $4 \times 10^{11}M_{\odot}$to the Galactic halo (Alcock et al., 2000), where the small number of events with levels higher than background levels (2-4) were insignificant compared to the expected amount (60-80) if MACHOs would entirely make the dark matter. Suggesting a more realistic percentage of 20% MACHO halo fraction. Something reinforced by EROS whose detections on the range of 10 days suggested a MACHO fraction less to 25% in the range from $10^{-7}M_{\odot}$ to $10^{-4}M_{\odot}$ and less to the 40% for objects less massive than one solar mass (Alcock et al., 1998, 2000). At the same time, MACHOs with masses superior to $M > 43M_{\odot}$ also seem to be directly discarded by Yoo et al. (2004), con-

cluding that objects below $43M_{\odot}$ can not form the bulk of DM in normal size galactic halos. All these points clearly seem to disfavor the possible window for MACHOs from $10^{-7.5}M_{\odot}$ to $10^{43}M_{\odot}$, and smaller, cause baryonic matter below $10^{-7.5}M_{\odot}$ ould have evaporated away in a Galactic time scale (de Rujula et al., 1992). But the end of this "MACHO era" seems to be inevitable as the values of the upper limits (upper $43M\odot$) have been excluded too from a catalog of 251 halo binaries, with the next resulting limits-exclusions values(Monroy-Rodríguez & Allen, 2014): $112M_{\odot}$, $85M_{\odot}$, $21 - 68M_{\odot}$, $28 - 78M_{\odot}$, $3 - 12M_{\odot}$ and superior to 10^6 (de Rujula et al., 1992). In summary, even MACHOs have been major candidates for dark matter in the past; nowadays, they seem to be a failed CDM scenario, where such massive objects should be dominant in the dark matter total mass. The recent community's efforts have gradually reduced their mass window to $100 - 10^6 M_{\odot}$,(Yoo et al., 2004; Monroy-Rodríguez & Allen, 2014; Alcock et al., 2000, 2001).

The most popular CDM scenario, the paradigm of Weakly-Interacting-Massive-Particle (WIMP), has been leading the study of DM physics since it was proposed decades ago. The so-called "WIMP miracle" tells us that the DM relic abundance observed can be generated without tuning much of the WIMP couplings if the underlying physics appears at a weak scale. Thus, this paradigm could be naturally accommodated in theories addressing electroweak symmetry breaking (EWSB). As we know, the Standard Model of particle physics only parametrizes EWSB, but it fails to explain its dynamical origin. The incapacity of the standard model of particle physics to describe types of matter outside the baryonic one (stars, gas...ordinary matter), and to find a candidate for DM, has motivated a wide variety of alternative DM theories. Like the current most accepted one of weakly interacting massive particles (WIMPs) to the quantum chromodynamic axion and axion-like particles (ALPs) generic in string theory, defended here. The failure to detect any sign of these WIMP at high energies with the LHC or with subterranean experiments(different experiments to detect WIMPs like Xenon100 (2012), PandaX-II (2017) / LUX (2017), and XENON1T (2018) have a failure, not been able to observe any signal with a significant confidence level) has recently made the community turn around in the apparently more promising ALPs. Moreover, the past discovery of the Higgs boson at the LHC in 2012 increased the theoretical and experimental interest related to the axions, as the Higgs boson is proof of the existence of an apparently elementary spin-zero boson undergoing spontaneous symmetry breaking, something that was somewhat controversial and unknown previously (Chadha-Day et al., 2022; Aprile et al., 2018). A proof that should validate the theoretical existence of the axion. This fact in combination with the eternal lack of WIMPs in the LHC, has extremely favored the plausibility of the ALPs as the solution for the long searched dark matter particle.

The wave dark matter scenario is the most promising ALPs based DM scenario. The strength of this wave dark matter theory is based on the capacity to resolve the small-scale structures contradictions that WIMPs-based theories have challenged without success in the past decades. These small-scale contradictions called the "Small Scale Crises," are basically defined by the "cuspy core problem" (which relays on the contradiction of the observed galaxies' flat density profile at their center

and the prediction of Navarro-Frenk-White (NFW) cusps (Navarro & Frenk, 1996) based on many-body simulations of collisionless CDM), the "missing satellite problem" (Collisionless CDM cosmology predicts that dwarf satellites in the Milk Way should be significantly more numerous than observed, more than 500 vs. ∼20) and the "Too big to fail problem" (A proposed solution to the missing satellites problem is the argument that many of the dwarf galaxies have had their stars stripped from them during tidal interactions and hence we are prevented from being able to see them. Nevertheless, many of the dwarf satellites predicted are so massive that there is no way they could not have visible stars). Any viable model of DM explains these three problems well. Here is where alternative theories like wave dark matter (Hu et al., 2000) and self-interacting DM (Spergel & Steinhardt, 2000) seem to triumph whereas WIMPs are in tension with the data as we discuss below. Focusing on wave dark matter, the pioneering work led by Schive in 2014 (Schive et al., 2014a), predicted a solitonic standing wave cores of de Broglie scale in galaxies caused by a Bose-Einstein condensate. In this soliton, wave DM behavior should make an indistinguishable signature to test observationally and differ from the WIPM scenario. Such observational proof should lead wave dark matter to the top in this scientific race of answering the DM puzzle.

Many other alternative DM theories have been postulated these decades, such as spanning ultralight bosons to heavy fermions, warm dark matter, and primordial black holes, among others. Check figure 1.2. Although all these ranges of theories, whether DM shares any interactions with the familiar particles described by standard particle physics, other than gravity, is still unknown. Despite our huge ignorance, it has become very clear from observational surveys that DM constitutes most of the matter in the Universe and governs the formation of structures by collapsing under its own gravity to form galaxies. Further, to achieve this DM must be non-relativistic or cold, even in early times. Otherwise, the initial density perturbations destined to become galaxies would have been erased by free streaming of the DM.

The main objective of this thesis is to test the distinctive predictions of Wave DM. For that purpose, many semi-analytical computations based on Schröedinge-Poisson equations have been done willing to find and compare that wave-like behavior at astronomical scales. In particular, new observations of high and low redshifts galaxies will be done to compare the rich wave-like structure in the de Broglie scale with such a standing wave core, the soliton. This central solitonic core should also be rounded by an excited state interference patron, forming the galactic halo. Many computations and analyses have been done to demonstrate the wave-like predictions within the observations, such as the stellar velocity dispersions in the galaxies, the solitonic imprint in the stellar density in galaxy cores, and extended DM haloes between others. These extended DM halos of some dwarf galaxies clusters spread to many kpcs despite their low masses (Torrealba et al., 2016, 2019), have recently increased the tension at galactic scales. Moreover, the existence of some "enormous" dwarfs called "ghostly" galaxies of very low densities directly contradicts heavy particle-based DM expectations. Low-density galaxies are naturally explained by a wide soliton, the product of a less massive galaxy halo. Successfully describing the recently discovered

new type of galaxies, "Ultra-diffuse galaxies".

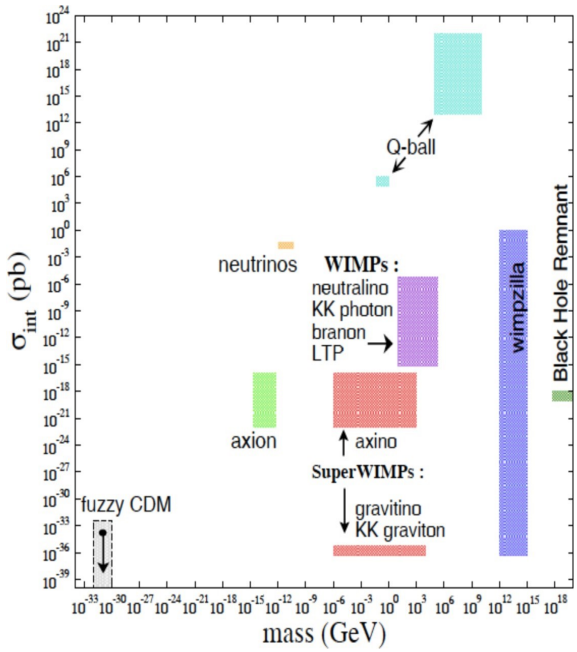

Figure 1.2: Postulated DM models on a mass versus interaction cross-section plot. Observe the high particle mass difference between the fuzzy dark matter (wave dark matter) and the concept of Weakly Interacting Massive Particles (WIMPs). This mass discrepancy makes them irreconcilable. Credit Gardner & Fuller (2013).

These extended halos are here naturally explained with our wave dark matter pioneering simulations based on the stellar profiles of the galaxies. In particular, we have shown how wave dark matter naturally predicts the observed extended stellar profiles in the isolated dwarfs that are far enough to be tidally affected by the Milky Way. Vanishing any opportunity for standard cold dark matter to describe these extended profiles as tidal tails. Observations from the JPCAM high-resolution T250 telescopy of the OAJ (Observatorio Astronómico Javalambre) in Teruel, with dedicated images of these local dwarfs, could help test these results. Moreover, the wide range of astrophysical and cosmological instruments, such as the Hubble Space Telescope (HST) and the recently launched James Webb Space Telescope (JWST), will provide us with more precise measurements that would help us to narrow the DM unknowns. These tools will help distinguish the WIMP scenario from its alternatives, such as fuzzy-wave DM. For that purpose, future setting-ups of the JWST survey program and its forefront data of deep imaging (and the HST data) for DM detection will facilitate the study of the underlying theory and fundamental laws that predict DM physics. For that purpose, the already commented JWST deep images survey program feels to be one of the keys due to its potential to provide deep images of groups of the lens covering the mid-and near-infrared wavelength and providing us with much higher quality images than the ones from the Hubble in terms of depth, resolution, and redshift. Many dwarf galaxies are expected at high redshift for CDM (small galaxies form earlier), while a lack of them should be detected for wave dark matter at $z > 10$ (Check figure 2.14 in section 2.1.3). Stellar

early formations should also be detected for wave dark matter, being both points only possible to answer with the JWST.

So what do we actually really know about dark matter? By Chadha-Day et al. (2022)

1. Cosmic density (strong evidence: cosmic microwave background anisotropies (Collaboration et al., 2018b)). Expressed as a fraction of the total density of the Universe, DM makes up 26 % of the Universe, compared to 6% in ordinary matter, and 68% in vacuum energy.

2. Local density (strong evidence: Milky Way stellar motions). The local density of dark matter is around 0.3 to 0.4 GeV cm^{-3}, equivalent to one proton every few cubic centimeterss, or one solar mass per cubic lightyear. The local density is around 10^5 times the average cosmic density.

3. No preferred galactic length scale (strong evidence: galaxy clustering and evolution). DM must be non-relativistic (v $\sim$ c would allow DM to move significant distances during galaxy formation), and have negligible pressure (which would imprint sound waves during galaxy formation). This discounts standard model neutrinos and other "hot" or "warm" DM. For bosons, the de Broglie wavelength (which can be modeled as an effective pressure) must be small compared to the galaxy clustering scale.

4. Early appearance of DM (strong evidence: galaxy clustering). DM had to be present, and gravitating, in the Universe long before the cosmic microwave background formed, and its gravitational influence began before the Universe was one year old. For light bosonic DM (like the axion) this corresponds to the latest epoch of particle creation.

5. Lack of significant interactions (strong evidence: the "Bullet Cluster" (Clowe & Markevitch, 2004)). DM cannot interact with itself or ordinary matter too strongly.

Chapter 2

General Context

This section will introduce the previously mentioned dark matter concept and the two main DM theories of this work: The current accepted standard Cold dark matter (CDM) and the alternative proposition of Wave dark matter (ψDM).

2.1 Dark Matter

Dark matter still remains one of the biggest unresolved puzzles in cosmology, even if its existence is required to explain galaxy formation, as well as astronomical observations of the observable universe's current structure. Dark Matter constitutes the 85% of the matter in the Universe and the %27 of the total content of the universe. In this thesis, I focus on the Nature of dark matter by studying the properties of dwarf galaxies because they are known to be dominated by dark matter, with large mass-to-light ratios (Read & Gilmore, 2005; Amorisco & Evans, 2012).

Dark Matter is not known to have any electromagnetic interaction(it does not absorb, reflect or emit light). This makes dark matter extremely difficult to detect directly, making its gravitational interaction with ordinary matter the best spot chance. This is why it has long been thought that DM must be a stable, long-lived particle that lies outside the Standard Model of particle physics. Although there still hasn't been any direct observation of any such DM particle, there are many indirect observations that reinforce its existence and explain its physical behavior: Galaxy rotation curves (explaining why the rotation velocity of the stars doesn't decrease in the outer zones of a galaxy, as predicted in a situation of ordinary matter alone, where $Vc \propto r^{-1/2}$, while observations have long shown flat behavior, independent of radius, something more like; $Vc \sim$constant), stellar velocity dispersions, the total mass of galaxy clusters, mass constraint due to gravitational lensing (the mass distribution of a galaxy cluster or any other supermassive object, can be computed, observing the lensing effect of such object on the light of the light source beyond it, concluding a baryonic faction $\sim$0.18 at the virial radius (McCarthy et al., 2007; Eckert et al., 2013)), the necessity of a non-electromagnetic-interaction matter existence for the universe's current structure formation and its imprint on the Cosmic

microwave background, between many others. Continuing with these last listed points, dark matter also permits the primordial perturbations in the density field of the baryonic matter, as it is observed in the temperature anisotropy fluctuations of the CMB, making it possible to grow and form the cosmic structures we observe today (Kuhlen et al., 2012). Moreover, in the models where dark matter and dark energy are not decoupled from the other components of the universe, dark matter should decouple from the primordial plasma earlier than baryonic matter, making possible an earlier growth of the primordial fluctuations in the dark matter density field, and making them also bigger than the baryons' in the recombination epoch, where these ones are still coupled to the density perturbation of the background radiation field that generates the CMB anisotropies. After the recombination epoch, baryons should be dominated by the dark matter's dominating gravitational potential sources, forming after many Gyrs, the actual halos, and observed cosmic structures such as galaxies, etc.(Bertone et al., 2005; Boyarsky et al., 2009; Feng, 2010; Kawasaki & Nakayama, 2013)

The first claims for dark matter existence using observable stellar motions were made by Kapteyn (1922), followed by Oort (1932), also claiming the necessity of more mass than the visible stars to fit the observable data. Fritz Zwicky found the first clear evidence for DM using the galaxies in the Coma cluster. He correctly determined that the motions of the Coma cluster's stars were dominated by the mass of a non-stellar matter. Zwicky concluded that there must be considerably more matter than the mass of the visible stars in all the galaxies in the Coma cluster, and so he concluded that there was a lot of "Dark Matter" (he used the term "Dunkel Matierie" as he wrote his papers in German) (Zwicky, 1933). Many theories have been postulated in order to resolve the dark matter puzzle, being WIMP-based (weakly interacting massive particles) Cold dark matter (CDM) the most recognized theory nowadays.

To fully understand the nature of dark matter, one must determine the fundamental laws and theory of DM physics. Nowadays, observations on scales larger than a few Megaparsecs clearly show the consistency of DM with being collisionless (Clowe & Markevitch, 2004; Clowe et al., 2006; Bertone & Tait, 2018). However, as we have already pointed out in the introduction, on small galactic scales of a few kpcs, observations seem to differ from expectations (Aprile et al., 2018), allowing for many plausible theories with exotic small-scale physics and particle masses spanning over 30 orders of magnitude. We have already introduced the nowadays leading theory based on WIPMs, which is considered the 'backbone' of the Universe, CDM. Apart from the small scale problems, it has been highly successful in describing the large-scale structures (Bertone & Tait, 2018). However, the lack of direct and indirect detections of such particles (de Martino et al., 2020b) have opened the door to alternative theories such as warm dark matter (WDM), which is often associated with fermions ,in particular, "sterile" neutrinos, of particle mass of a few keV (typically treated as collisionless), or Peccei-Quinn axions (de Martino et al., 2020b) which are bosons of mass $\sim 10^{-5} - 10^{-3}$eV, and also the possibility of ultralight wave dark matter (ψDM") of mass $\sim 10^{-22}$eV, which is described by a classical scalar field and exhibits wave phenomena on scales of the de Broglie wave-

length (Navarro & Frenk, 1996; Hu et al., 2000; Spergel & Steinhardt, 2000; Schive et al., 2014a; de Martino et al., 2017).

Both, Warm dark matter and ψDM produce smoother structures at low scales than CDM, as a product of their thermal motion (Hui, 2020), or quantum pressure (Hui, 2020; Schive et al., 2014a), respectively. Moreover, the presence of dwarf galaxies with masses $\sim 10^9 M_\odot$, as well as measurements of the 'lumpiness' of the dark matter distribution, favor WDM and ψDM proposed particle masses; $\sim$ 3keV for WDM and $\sim 10^{-22}$eV for wave dark matter(Hu et al., 2001; Maldacena, 2001). Much more work is needed for wave dark matter as the simulations done to constrain this theory have all been done without considering the impact of its wave behavior in baryons (with few exceptions as Mocz et al. (2019, 2020)), something that might be crucial to understand it accurately.

Competing DM theories differ in terms of their early growth of structure with differing predictions for the formation of galaxies. For example, at redshift $\sim$ 30 (10^8 years after the BIG Bang), CDM expects a population of subhalos of masses from 10^5 to $10^7 M_\odot$ with a not less denser filament connection (Wang, 2014) than WDM and ψDM. Moreover, galactic stellar structures formation should happen earlier than for WDM and ψDM, where these structures should form later due to the initial suppression of the dark matter power spectrum by particle free-streaming (Doré, 2014). The main difference of ψDM with WDM should be the interference patterns and soliton cores. As star and galaxy formation has been studied with hydrodynamical simulations that ignore the wavelike aspects of the dark matter superfluid (Arkani-Hamed & Maldacena, 2015), wave and warm dark matter differences still have not been discerned to the maximum. This reinforces the importance of accurately simulating the wave dark matter wave structures for a precise formation history and large-structure knowledge.

2.1.1 Cold Dark Matter

The origin of Dark Matter is understood to lie "beyond" the standard model of particle physics, which describes only 16% of the total cosmological mass density (Cyburt et al., 2016; Collaboration et al., 2016). It is also clear that DM is non-relativistic due to the earliest limits of observation given by the Cosmic Microwave Background and galaxy power spectrum. Furthermore, DM behaves collisionlessly for pairs of clusters undergoing a collision, implying there is no significant self-interaction other than gravity, in particular, the iconic Bullet cluster (Markevitch et al., 2004; Clowe et al., 2006) and other massive examples (Molnar & Broadhurst, 2018). This "Cold Dark Matter" collisionless and Jeans unstable to forming structures on all astrophysical scales down to a particle physics model-dependent small-scale cutoff (e.g. $\sim$ Earth mass / 10^{-4} kpc for a 100 GeV WIMP (Broadhurst et al., 2020)) , has long been synonymous with heavy particles of some new form, that must be unusually stable and interact only via gravity, and principally

motivated by supersymmetric extensions of the Standard Model (Ellis et al., 1984). This model has been considered to be the standard model for the evolution of the Universe (ΛCDM) due to its good agreement with many independent observations; The temperature fluctuations of the Cosmic microwave background (CMB) (Collaboration et al., 2018a,b, 2020b,c,e), the power spectrum of the matter density perturbations (Percival et al., 2001; Pope et al., 2004; Tegmark et al., 2004), the luminosity distances to supernovae SNeIa (Riess et al., 1998, 2004; Davis et al., 2007; Kowalski et al., 2008; Amanullah et al., 2010; Suzuki et al., 2012), and the expansion rate of the Universe (Jimenez et al., 2003; Simon et al., 2005; Stern et al., 2010).

This model predicts a spatially flat universe, and it can successfully explain and describe the observed homogenous and isotropic Universe, as well as the dynamics of the large cosmic structures. All these results are a product of some of its cosmological, more important characteristics like its density value $\Omega_{\Lambda,0} = 0.686^{\pm}0.020$ (which it is in units of the critical density $\rho_c = 3H_0^2/8\pi G$) product of its characteristic cosmological constat (Λ), that naturally explains the observed present accelerated expansion period (Collaboration et al., 2018b). Dark matter is supposed to be the second contributor to the Universe's total energy density; in this scenario where dark matter is necessary to explain the motions and formation of large structures, which the ΛCDM model has demonstrated to be efficient, determines a dark matter-energy density of $\Omega_{DM,0} = 0.314 \pm 0.020$, while the predicted density of ordinary matter is much lower $\Omega_{b,0} = 0.0221 \pm 0.0003$ (Collaboration et al., 2018b). Leads us to the previously mentioned flat curvature of the Universe of $\Omega_{k,0}h^2$(the Hubble constant)$=-0.037^{0.044}_{0.042}$ (Collaboration et al., 2018b). However, there are some discrepancies between its predicted values for$\Omega_{\Lambda,0}$ and $\Omega_{k,0}$ and the observed ones. For example, the predicted value for $\Omega_{\Lambda,0}$, gives us maximum vacuum energy of $\rho_\Lambda \sim 10^{-47}GeV^4$, which is too small compared to the value resulting from the quantum field theory, where quantum chromodynamics predicts a value of $\rho_\Lambda \sim 10^{71}GeV^4$. In this scenario, constant reviews of the cosmological constant and dark energy have been done, trying to solve the issue, but the continuing discrepancy has not alleviated the so-called "fine-tuning problem" (Weinberg, 1989), proposing different solutions as the anthropic principle or a cyclic model of the Universe (Rubakov, 2000; Steinhardt & Turok, 2006; Weinberg, 1987; Capolupo, 2019). Furthermore, the measured Hubble constant from the nearby Universe seems to differ also from the value anticipated by the ΛCDM model, as well as with the normalization of the power spectrum of the mass density perturbations on cosmic scales, σ_8, inferred from the CMB and large-scale structure surveys (Collaboration et al., 2018b). First, the Hubble constant from the CMB measurements $H_0 = 67.77{\pm}0.60kms^{-1}Mpc^{-1}$(Collaboration et al., 2018b) has a discrepancy of 4.4σ with the observer local value of $H_0 = 73.52 \pm 1.62kms^{-1}Mpc^{-1}$ (Riess et al., 2016, 2019). Similarly, the σ_8 obtained by the Planck collaboration is $\sigma_8 = 0.8149{\pm}0.0093$, which denotes a $S_8 = 0.811 \pm 0.011$ ($S_8 \equiv \sigma_8(\Omega_m/0.3)^{0.5}$), while the Kylo Degree Surveys estimates a values of $S_8 = 0.745 \pm 0.039$, implying a discrepancy of 2.3σ. Moreover, some recent interpretations from the Planck experiments are more consistent with a spatially closed Universe (even if still is a big consensus that Planck's data favors a flat universe, consistent with ΛCDM), in contrast to the flat one from ΛCDM (Di Valentino et al., 2020).

It is well known and has been previously mentioned in this work that WIMPs are supposed to be the pillar of the CDM model. These particles are naturally foreseen in the supersymmetric (SUSY) extension of the Standard Model of particle physics (Jungman et al., 1996). Furthermore, it has been suggested that they could be the product of certain compactifications of extra dimensions (Servant & others Tait, 2003). These WIMPs within the range of 1GeV to 10 TeV predict what has been called the "WIMP miracle", which computed annihilation cross-section that sets the density number of the dark matter particles, is consistent with the observed dark matter density $\Omega_{DM,0} \sim 0.3$ (Collaboration et al., 2018b). Many experiments have been done to detect such heavy particles directly or indirectly. In experiments like LUX and XENON 1t (Aprile et al., 2011), dark matter particles are expected to crash with the atomic nucleus of a detector that should liberate a piece of energy, directly confirming these particles. On the other hand, indirect detections include the search for neutrinos that should appear in the annihilation of pair of WIPMs in the center of the Earth or the Sun, as these particles are expected to accumulate in the gravitational potential wells. Experiments like IceCube and Super-K (Choi et al., 2015) have been designed for such detections. Moreover, the WIMPs annihilation should imprint the cosmic rays that can be detected on the Earth with the location of positrons and antiprotons (Avrorin et al., 2015; Bergström et al., 2013). Finally, similar results are expected in collisions between WIMPs and fermions, checked in the Large Hadronic Collider (LHC) (Tanabashi et al., 2018).

However, enthusiasm for WIMP-based CDM is now fading with the continued absence of any such particle in stringent direct laboratory searches (Aprile et al., 2018) and astrophysical DM annihilation searches (Archambault et al., 2017) and because of long recognised tension in this context with the basic observed properties of low mass galaxies (Moore, 1994; Bullock & Boylan-Kolchin, 2017).

Black holes as dark matter have been revived recently due to the puzzling large black holes inferred from the gravitational wave detections by LIGO/Virgo (Bird et al., 2016). Black holes act effectively as collisionless "particle" DM, like WIMP's (except when coalescing). However, the LIGO inferred black hole mass scale of $30M_{\odot}$ is not present in Galactic microlensing searches, nor in the light curves of individual lensed stars recently discovered through high columns of cluster DM, limiting any such PBH contribution to a small fraction of the DM (Diego et al., 2018; Kelly et al., 2018; Oguri et al., 2018). Nevertheless is also important to point out the achieves of the ΛCDM model since it was proposed to solve the difficulty in forming galaxies by the present day from the very tiny temperature fluctuations observed in the CMB (Peebles, 1982). The CDM galaxy formation models showed to be in high agreement with quite a lot of observations as the large-scale clustering of galaxies, the approximate mass ranges of galaxies, galaxy scaling relations (such as the Faber-Jackson and Tully-Fisher relations), observational constraints on galaxy formation, the age of the universe, and the amplitude of CMB fluctuations (Blumenthal et al., 1984).

The excellent agreement of CDM with large scales observations (larger than 1 Mpc) has encouraged the community to consider CDM as the primordial dark

matter theory. However, they are more than one question that CDM still cannot answer, like the formation of high massive galaxies at high redshift than hoped (Genzel et al., 2003; Glazebrook et al., 2004). Nevertheless, the main challenge that CDM has to face are all the small scales observations that directly attack CDM simulations, where this new ultra-light boson dark matter theory seems to be in much better agreement: Cuspy-halo problem, missing satellite problem, extremely ghostly dwarfs, and extended dark matter halos in classical and ultra-faint dwarfs that disagree with the expected concentrated CDM halos.

2.1.2 The NFW profile for CDM halos

The Navarro–Frenk–White (NFW) profile is a spatial mass distribution of dark matter fitted to dark matter halos identified in N-body simulations by Julio Navarro, Carlos Frenk, and Simon White (Navarro & Frenk, 1996). This model was designed to describe the dark matter halo's structure in standard cold dark matter cosmology. The model is helpful to describe dark matter halos behavior for an object with masses from dwarfs to Milky way kind galaxies. In this model, the halo concentration is fully correlated with its total mass, whereas it is dependent to the epoch formation. Halo profiles are approximately isothermal over a large range in radii but are significantly shallower than r^{-2} near the center and steeper than r^{-2} near the virial radius.

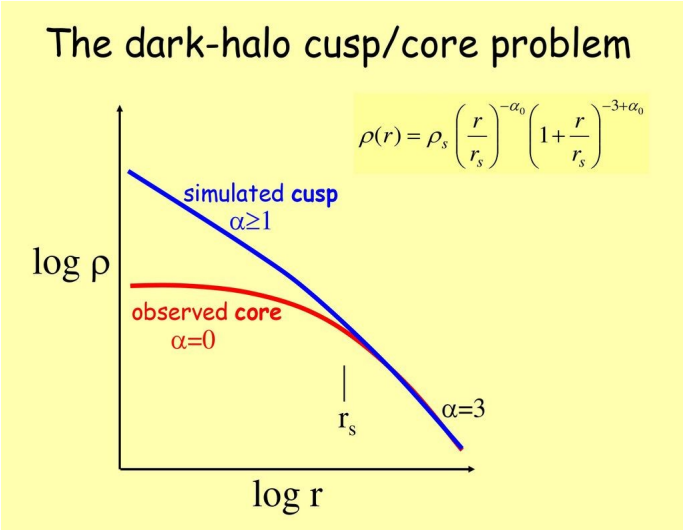

Figure 2.1: Cusp Vs Core density profile. The blue line represents the NFW density profile while the red one shows the observed flat central profile. The NFW profile simulates an increasing profile rising to the infinitive in the center, inconsistent with the data. Credit Bryant (2018).

These CDM halos, when azimuthally averaged, are found to follow the NFW density profile (Navarro & Frenk, 1996) so that the full radial profile may be ap-

proximated as:

$$\rho_{DM}(r) = \frac{\rho_0}{\frac{r}{r_s}\left(1+\frac{r}{r_s}\right)^2} \tag{2.1}$$

where ρ_0 is the halo's dark matter density that varies from halo to halo, and r_s is the scale radius, where $R_{vir} = c \times r_s$. R_{vir} is the virial radius, the radius of the sphere where the enclosed mass (M_{200}) is 200 $\times$ ρ_{crit} (where ρ_{crit} is the critical density of the universe). The scale radius is the point where the profile changes in slope ("-1" for the inner part and "-3" for the outer part), while c is the "concentration parameter" that defines the relation between the virial and the scale radiuses. It is important to remark that the scale radius helps define an object's concentration. A big scale radius means a less concentrated object than one with a bigger scale radius.

This model also demonstrates that the main reason cause dynamics and luminosities are uncorrelated could be the necessity of systematically increasing the mass-to-light ratios with luminosity (Navarro & Frenk, 1996). The authors already expose in the original work two of the main problems that are also two of the main motivations of this thesis: The inconsistency of the inner regions of many classical dwarfs and low surface brightness galaxies, which have less central mass than predicted, known as the "cuspy-core" problem, and the discrepancy between the number of satellite galaxies seen when a Milky-Way type galaxy is simulated, and the dwarf galaxies observed around our own Milky Way, known as the "missing satellite" problem. Another CDM potential issue is the "too big to fail" problem, characterized by predicting more dense dark matter halos than are observed among the Milky Way satellite galaxies. But as it is a problem specifically focused on the dwarfs, we will be deeper explained in the corresponding section 2.2. All these small-scale problems of the CDM model are a product of its scale-invariant spectrum of density fluctuations with substantial power on small mass scales. As the behavior of the power spectrum on extremely small scales depends on the specific physics of the dark matter particles, this model based on weakly interacting massive particles has power spectra that extend without suppression all the way to Earth masses, producing all these inconsistencies with the observable data, like the cuspy profiles and the lack of small mass dwarfs that should we see around Milky Way kind galaxies. Something that ψDM solves, as in scales smaller than the Jean scale, the pressure will dominate, suppressing the small scale structures, making a real difference from CDM to ψDM (More thoroughly explained in section 2.1.3).

The cusp-core problem refers to the discrepancy between the observed central dwarfs' DM density profiles and the computed ones by NFW in standard CDM N-body simulations (Del Popolo & Le Delliou, 2009). The central mass inferred by stellar kinematics of the galaxies is ~ 5 times smaller than anticipated by the CDM model, a considerable discrepancy that is difficult to alleviate (Weinberg, 2015). This cuspy inner profile results from the CDM N-body simulations that describe the dark matter mass density profile ($\rho(r)$) by a steep power law in the central regions of the halos. This density profile was seen to follow the next relation: $\rho \sim r^{\alpha}$, with $\alpha = -1$ (Navarro et al., 1997; Navarro & Frenk, 1996). It was also suggested in more recent works that the inner slope could be dependent on the total mass of the halo, becoming stepper as a result of a more negative α of -1.5 (Jing, 2000a; Moore

et al., 1999a). Almost the entire simulations show a cuspy density in the center of every galaxy, with a substantial density increment in small radiuses, while the rotation curves of the majority of the dwarfs suggest a cored central density profile (Carignan, 1989). This central mass inconsistency of the small masses galaxies is graphically represented by the differences between a cuspy profile that goes to infinity at the center or a cored profile in the galaxy's central regions.

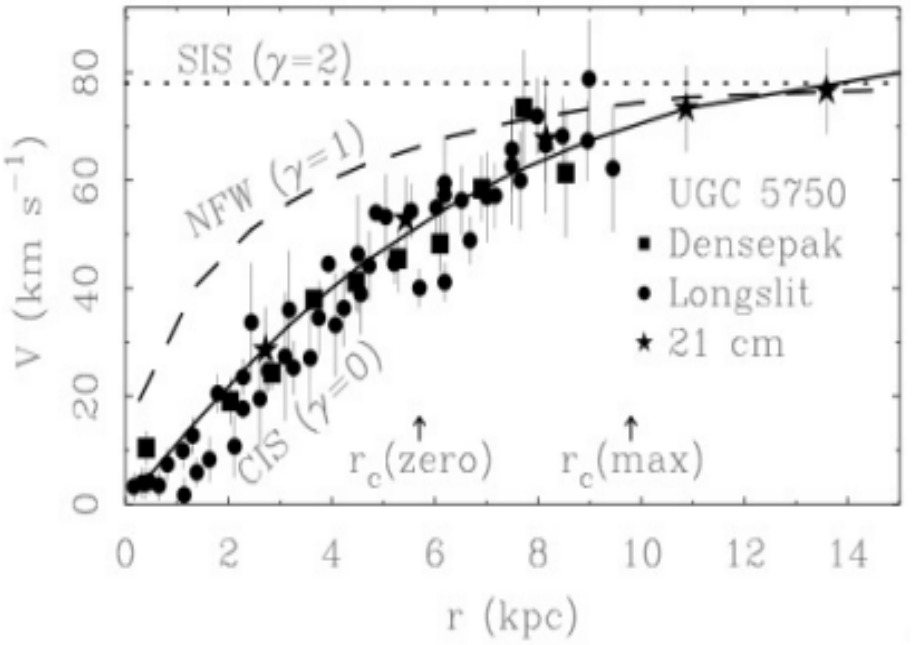

Figure 2.2: UGC 5750 dwarf's rotation curve: Notice how the NFW profile (long-dashed line) nor the singular isothermal sphere (SIS, dotted line) can fit the measured rotation curves of the galaxy. In contrast, the cored profile, apart from being the only acceptable option, seems to agree excellently with the data. Credit Chen & McGaugh (2010); de Martino et al. (2020a)

The discrepancy between the expected cusp NFW profiles and the observed profiles seems far to be alleviated due to the point that dwarf galaxies, which are expected to be some of the darkest matter-dominated objects in the universe, should provide the the best match to the DM halo predictions of CDM. Moreover, even if they are dwarfs with several orders of magnitudes in terms of luminosities (from $10^2$to $10^{10}L_{\odot}$ (McConnachie, 2012; Javanmardi et al., 2016)), all of them seem to show similar velocity dispersion values, indicating an analogous dark-baryonic proportion, and in consequence, theoretically similar profiles (Mateo et al., 1993). Plenty of similar and independent analyses have reinforced this discrepancy between the expected cuspy and the observed cores. For example, the measured HI rotation curve of the dwarf irregular galaxy DDO 154 (Carignan & Freeman, 1988), is more consistent with a cored inner profile. Some recently discovered ultra-faint galaxies in the local groups have half-light radiuses of just a few kpcs that are difficult to explain for the CDM model in an isolated situation, with tidal iterations and baryonic feedback as the only possible explanations (Willman et al., 2005; Zucker

et al., 2006a,b; Torrealba et al., 2016; Caldwell et al., 2017; Torrealba et al., 2019). In the same way, this cuspy profile has been noticed to be too steep not only for classical dwarfs but also for LSB (Light surface brightness), which rotations curves seem to agree with cored inner regions than with cuspy ones (Borriello & Salucci, 2007; de Blok & Bosma, 2002; de Blok et al., 2003; Gentile et al., 2004) (see figure 2.2). Similar observations and conclusions have been obtained from dwarf irregular galaxies like NGC 6822 (Weldrake et al., 2003), and NGC 3741 (Gentile et al., 2007). In summary, the analysis made to the rotation curves of all these dwarfs suggests inner slopes of $\alpha = -0.22 \pm 0.08$ (Spekkens et al., 2005), with a mean slope $\alpha = -0.32 \pm 0.24$ obtained from some of the most irregular low surface brightness galaxies as the steepest, very far from the $\alpha = -1$ required value (Spekkens et al., 2005; de Blok et al., 2003). Finally, the appearance of a new kind of extended galaxies(Crater II (Caldwell et al., 2017), Antlia II (Torrealba et al., 2019)],NGC 1052-DF2 and NGC 1052-DF4 (van Dokkum et al., 2018c,d,a, 2019a; Danieli et al., 2019; Haslbauer et al., 2019)), called as ultra-diffuse galaxies seem to be inexplicable for the CDM model (Pozo & others., 2021b), where galaxies with such extended profiles and cores seem to contradict CDM expectations in all the aspects.

NFW has been exposed to be insufficient in describing the density profile in the center of these galaxies, whereas the here explained ψDM (wave DM) profile is able to reproduce the required central constant density (Marsh & Pop, 2015; Schive et al., 2014a,b). Nevertheless, some authors seem to claim that these flat density profiles are not unequivocally forced to discard NFW as the correct solution, claiming that the baryonic effects such as radiation pressure of massive stars, gas cooling, tidal effects, or the supernova feedback (Ogiya & Mori, 2014; Spekkens et al., 2005; Macciò et al., 2012) can alter dark matter gravitational potential wells, solving this cusp-core discrepancy inside the NFW context. For example, an inner Lindblad-like resonance, which couples the rotating bar to the orbits of the star through the cusp, was suggested to cause an angular momentum transfer from the bar pattern to the dark matter halo (Weinberg & Katz, 2002), transforming a cuspy profile into a cored one; nevertheless, some new investigations claimed just the contrary result (Dubinski et al., 2009). Another solution, and one of the most popular ones for the CDM community, is based on the previously presented baryonic feedback, more concretely, in supernova feedback. The wind created in a supernova seems to be effective in order to transform cuspy profiles into cored ones (Mashchenko et al., 2006) by transferring the gas and the dark matter particles from the center to outer zones (Mashchenko et al., 2008), flattening the dark matter density profile. Similar results are expected from the stellar winds in this scenario, but with a more negligible effect than supernovas (Gnedin & Zhao, 2002; Mashchenko et al., 2008). Another option would be radiative cooling, which would make gas collapse and generate cyclical starbursts, periodically contributing to the flattening of the inner cuspy cold dark matter profile (Ogiya & Mori, 2014). Nevertheless, these proposals seem not reasonable to solve the problem in a simple universal way, non its effects on cosmological scales. Moreover, simulations done by Mocz et al. (2020, 2019) already suggested that the baryonic feedback does not significantly alter the dark matter dynamics, being unable to transform cusps to cores. These Auriga and EAGLE simulations show that gas outflows and the cyclical starburst cannot transform a

cuspy profile into a cored one (Bose et al., 2019). Another possible solution could be carried out by the dynamical friction between gas clumps with masses between 10^5 and $10^6 M_\odot$ in the initial phases of the galaxies formations (El-Zant & Shlosman, 2001; Romano-Díaz et al., 2008). In this scenario, the friction between these clumps would transfer angular momentum to the dark matter particles, making it possible to change their position to the outer zones of the halo, flattening the inner part. Even if these clumps are known to have masses in the order of $10^6 M_\odot$ (Kaufmann, 2006), the existence of such gas clumps could imply an inefficient star formation and cloud fragmentation (Nipoti & Binney, 2015), that would imply halos $\leq 10^7 M_\odot$ and gas clumps of $\sim 10^4 M_\odot$, and in consequence orders of magnitude smaller than the needed ones to solve the cusp core problem (Jardel & Sellwood, 2009).

The missing satellite problem is the lack of observable satellite galaxies around the Milky way, compared to the simulations of Milky Way-type galaxy results. This CDM simulation expects quite more satellite galaxies around Milky way type galaxies of $\simeq 10^{11} M_\odot$, for which high-resolution CDM cosmological simulations predict thousand of subhalos with masses equal or superior to $10^7 M_\odot$. However, this value is ∼20 times larger than the observed amount of such satellites around the Milky Way and Andromeda (Bullock & Boylan-Kolchin, 2017; Kauffmann et al., 1993; Klypin et al., 1999; Moore et al., 1999b). The origin of this discrepancy between the observations and the number of galaxies for CDM comes from its power spectrum, in which its behavior on small scales is totally dependent on the physics of the applied dark matter particles; in the case of the WIMPs, the power spectra extends without suppression to Earth masses (Green et al., 2004), allowing in the CDM scenario to the early formation of plenty low mass subhalos that would form the right amount of nowadays expected extra couples of satellites. This problem was first confirmed by Klypin et al. (1999), which clearly showed how the expected low mass satellite amount doesn't fit with simulations in Milky and Andromeda cases (check figure 2.3). Although the difficulty of detecting ultra-faint galaxies has constantly fed the doubts about whether the observations were talking against the theoretical results (Bullock, 2010), arguing that the higher sensitivity of the detection tools is discovering a higher amount of ultra-faint galaxies. The actual number still seems to be relatively low for CDM, being four times lower than expected (Simon & Geha, 2007), and with no prospect of detecting enough in the future to resolve it. Furthermore, the densest subhalos predicted by CDM from the ELVIS ΛCDM simulations (Garrison-Kimmel et al., 2014a) are much denser than the denser subhalos of Milky's biggest satellites.

Another popular solution is based on the point that small subhalos below $10^8 M_\odot$ would not have detectable stars or gas due to being not massive enough to gravitationally attract (or contain form tidal forces) cold gas to form stars and/or physical phenomena are undergoing within these subhalos that prevent the formation of luminous stars, preventing us from detecting these dwarf galaxies(Kim et al., 2018). This solution has carried out another small-scale problem for the cold dark matter paradigm, usually referred like the "too-big-to-fail" problem. This problem estates that the predicted galaxies are too big not to have visible stars or to have seen their start formation process truncated due to tidal forces.

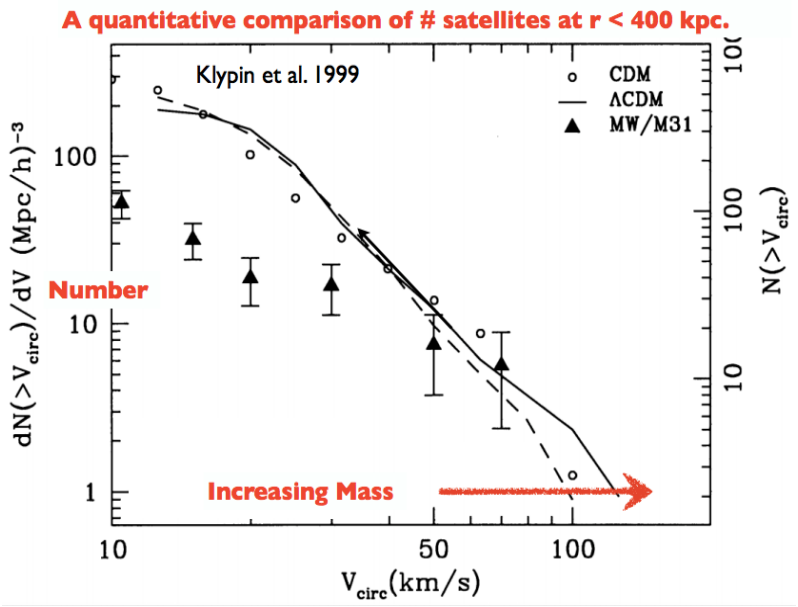

Figure 2.3: Number of satellite galaxies vs circular velocity (or mass). The observable amount of low-mass satellite galaxies in MW and M31(black data points) shows a high discrepancy with CDM's theoretical results, white dots, and ΛCDM, represented with a solid line. The models expect a rising trend while we search for low mass galaxies (low circular velocities), whereas the data shows a much flatter one below 50 km/s. Credit Kim et al. (2019).

As for the "cuspy-core" problem, it has been argued by some authors that there is no need to add another dark matter alternative theory to explain the observed discrepancies that have carried out the "missing satellite" problem. The abundance matching (AM) technique (Bullock & Boylan-Kolchin, 2017)(for comparing the distribution of the dark matter halo when using galaxy luminosities) seems to be able to solve the problem for galaxies of $\sim 10^9 M_\odot$, after applying the observed star formation rate (Read & Erkal, 2019). For galaxies smaller than $\sim 10^9 M_\odot$, assuming the suppression of star formation by UV reionization may plausibly correct the discrepancy (Bullock & Boylan-Kolchin, 2017; Efstathiou et al., 1992; Sawala et al., 2016) while for galaxies smaller than $\sim 10^8 M_\odot$, an atomic cooling must be considered (Bullock & Boylan-Kolchin, 2017; Rees & Ostriker, 1977). The stellar mass of the galaxies can be easily estimated by fitting broad-band photometric data with a Spectral Energy Distribution model (Walcher et al., 2011; Mitchell et al., 2013). In contrast, the total galaxy mass Mhalo can be inferred from either gravitational lensing or HI rotation curves (Mandelbaum et al., 2006; Moster et al., 2010; Katz et al., 2017). These models are all consistent with each other, predicting more than 80 satellites with stellar masses bigger than $10^3 M_\odot$, in clear discrepancy with observations that might be alleviated assuming a low total mass for the Milky way, something that seems unreasonable nowadays (Hargis et al., 2014). Nevertheless, one of the biggest victories of this technique came out from an improved version of AM (Abundance matching) by Brook et al. (2014) with the successful match between the predicted amount of satellites around Milky with stellar masses sup-

pression to $10^3 M_\odot$ with and without considering the reionization (Brook et al., 2014; Dooley et al., 2017). Although (Brook et al., 2014) obtained a satisfying result for the CDM community, it has been recently considered that the stellar mass might have some important issues in its efficiency to predict the real amount of satellites by AM; the suppression of star formation due to either the infall of the galaxy toward a larger galaxy (Geha et al., 2012; Gatto et al., 2013) or tidal stripping (Read et al., 2006a; Tomozeiu et al., 2016) introduces an intrinsic scatter in the M_*-M_{halo} relation (Ural et al., 2015; Read et al., 2017). These issues could be alleviated by replacing the stellar mass with the star formation rate.

The Too big to fail is a discrepancy that arises when we observe the dark matter density profiles of the most luminous satellites of the Local Group and the predicted densities by the CDM model. Briefly, the expected densest dwarfs by the CDM model are ~ 5 times denser than the observed densest ones around Milky and Andromeda (Boylan-Kolchin et al., 2011; Read et al., 2006b; Boylan-Kolchin & Bullock, 2012). As we have already commented, this problem also arises in one of the postulated possible solutions for the missing satellite problem, which argues about a lack of stars in some dwarfs that may make them undetectable, impossible to be true for their dark matter densities that will be able to retain gas and form stars, making them observable. We must remark that the TBTF problem is an independent problem from the missing satellite problem and instead is related to the stellar mass dark matter halo relation; it is an internal dark matter distribution issue where the mismatch between the observed and predicted dark matter central densities depend upon the specific realization of the dark matter halo substructure (Boylan-Kolchin et al., 2011; Boylan-Kolchin & Bullock, 2012).

This problem arises when comparing the predicted and observed circular velocity (V_{circ}) at the half-light radius of the galaxies, where, due to being dwarfs, one of the most dark matter dominated objects, they are expected to be dominated by dark matter at all their extension, so that the dynamical mass of a dwarf ($M_{dyn}(< 1/2)$) should be representative of its dark matter content at least until that radius. In conclusion, the computed V_{circ} at the half-light radius is equal to the observed one (Boylan-Kolchin & Bullock, 2011). This requirement seems to be completed by just the subhalos that are far from the density values of the predicted densest ones by ΛCDM; in other words, the most luminous and denser dwarfs of the local group have smaller $V_{circ}(r_{1/2})$. For example, 10 of the most massive subhalos computed by the Aquarius simulations (Springel et al., 2008), have circular velocities values that are pretty higher than observed ones, of V_{max}>25km/s instead the observed values of V_{max} ∼12-25km/s (Boylan-Kolchin & Bullock, 2012). These problems seem to be universal, as has been observed in the whole Local group's dwarfs, with similar conclusions in Andromeda's system. Moreover, isolated galaxies stand out for the same issue, showing much lower circular velocities and not enough dense galaxies than expected in a CDM scenario (Tollerud et al., 2014; Kirby et al., 2014) simulated with the ELVIS model(Garrison-Kimmel et al., 2014b). Moreover, this discrepancy between the predicted amount of too dense halos and observed less dense ones grows up when we analyze the same problem in other systems out from the Local Group (Garrison-Kimmel et al., 2014b). For example, the observed galaxies around M94

and M101 are less dense than predicted by CDM simulations, where M94 is a group formed by a Milky way kind galaxy with just two satellites of stellar masses around $10^6 M_\odot$, very far from the 10 suggested by CDM models (Smercina et al., 2018). In the same way, M101 galaxies have a luminosity function similar to the ones from Milky, suggesting a similar lack of intermediate-mass galaxies (Danieli et al., 2017). On the other hand, the lack of the found Ultra-faint galaxies(the half compared to the Milky way's) seems to note out the missing satellite problem in this system (Bennet et al., 2020).

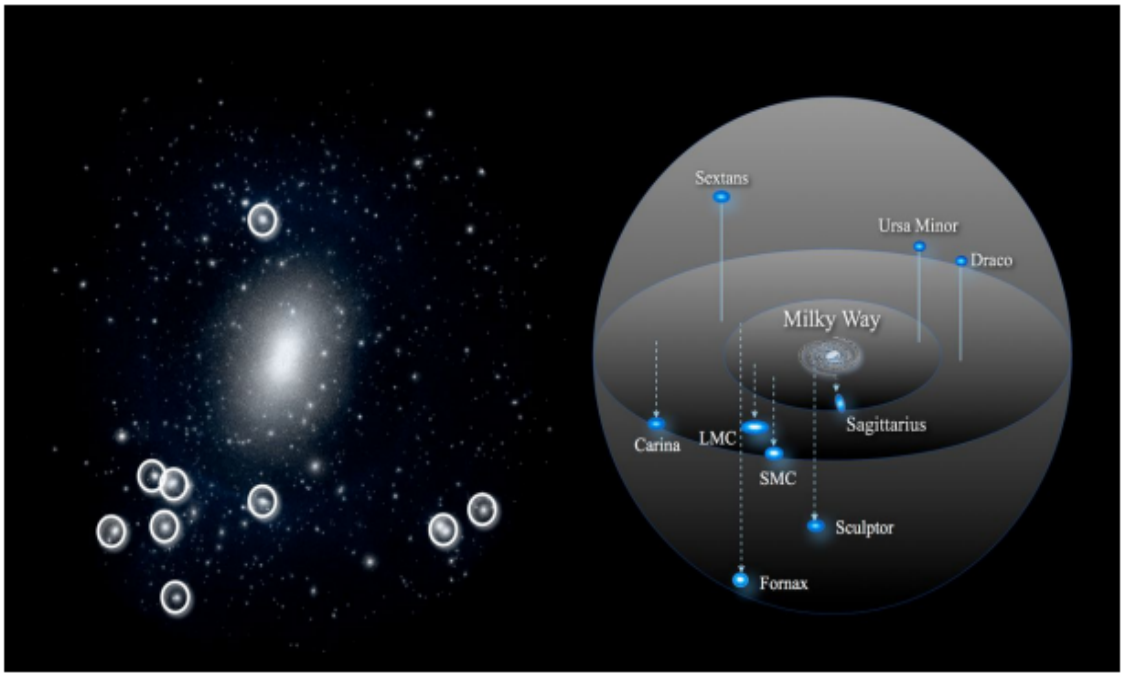

Figure 2.4: The TBTF problem in the Milky Way. The left panels show the predicted nine densest satellites from the ELVIS ΛCDM simulations Garrison-Kimmel et al. (2014b) for a Milky Way-like galaxy of $10^{12} M_\odot$ while the right panel shows the current distribution of the real densest satellites. The densities of the densest real satellite are ~ 5 times smaller than the predicted ones, while the estimated amount of subhalos by the simulations largely exceeds the observed ones. This last point is related to the previously commented missing satellite problem. Credit Weinberg (2015).

Recently it has been claimed that the mass of the milky way is half of the widely adopted, established value, and this lower mass is claimed by them to be sufficient to alleviate the TBTF problem for CDM (Boylan-Kolchin & Bullock, 2012). A Milky way with a mass of $\sim 5 \times 10^{11} M_\odot$ will just show a discrepancy of ∼3 extra subhalos, whereas the actual accepted values of $\sim 10^{12} M_\odot$ (Xue et al., 2008; Brown et al., 2010; Gnedin et al., 2010) or $\sim 2 \times 10^{12} M_\odot$ (Sakamoto et al., 2003; Sohn et al., 2018) have a discrepancy between 6 and 12 subhalos more or less, too much to be considered as a consistent statistical fluctuation. Nevertheless, there is no evidence to indicate that the mass of the Milky way has been overestimated, and the apparent Universal characteristic of the TBTF problem due to appearing in Andromeda's

group and outside the Local group makes the Milky's possible mass overestimate inefficient to solve it entirely. So as for the other small-scale issues, baryonic feedback seems to be the best option. As suggested for resolving the cusp-core problem, N-body/hydrodynamical simulations claim that repeated bursts of star formation feedback from supernovas can significantly decrease the amount of dark matter in the center (flattening the core) in consequence, drastically reducing the circular velocity (Brooks & Zolotov, 2014; Dutton, 2016; Buck et al., 2019). However, for APOSTLE simulations (Sawala et al., 2016; Fattahi et al., 2016, 2018), FIRE simulations(Garrison-Kimmel et al., 2019), and EAGLE models for galaxy formation (Crain et al., 2015; Schaye et al., 2015), the best option for solving the TBTF problem seems to be the subhalo disruption and the mass loss due to tidal disruption. Furthermore, the amount of subhalos with stellar masses superior to $10^5 M_\odot$ is still close to 10, vaguely resolving the issue.

2.1.3 Wave Dark Matter

These three small-scale (cuspy-core, missing satellite and too big to fail problems) issues are not just the only ones whose CDM has to face. In many cases, the CDM profiles are too compact for the measured velocity dispersion, asking for unreasonable low values of "c" (the concentration parameter), something that ψDM matter has shown to be able to solve with the presence of a soliton in the center of every galaxy, as we describe now in this section.

This soliton would provide the galaxy with a flatter central density, consistent with the observable inner low velocities. More massive galaxies of high internal momentum are predicted to have narrower, denser solitons of approximately 100pc in radius. This is supported by the rising central velocity dispersion recently measured in the Milky Way (de Martino et al., 2020b). For lower mass galaxies, wider solitons are predicted, reaching 3kpc in a scale close to the lower limiting "Jeans mass", below which galaxies form in Wave-DM as the bosons cannot be confined below the de Broglie scale. This limiting soliton size appears to match well the newly discovered Antlia II galaxy, which is extremely "ghostly" despite its large size and proximity orbiting the Milky Way (Torrealba et al., 2019) at only 130kpc. Such extensive galaxies seem impossible to exit in the CDM paradigm, where much more concentrated halos are expected. Antlia II has been identified via proper motions with Gaia(Torrealba et al., 2019), and we have its extreme represents the limiting case fo Wave-DM with mean velocity dispersion of only $\simeq 6.5$km/s, with an unprecedentedly low stellar surface brightness. All these ψDM characteristics and answers to CDM misconceptions will be explained in the following chapters of the work.

ψDM matter is a non-relativistic alternative DM theory based in axions, this light boson solution for the universal DM is gaining credence on the strength of the first simulations to evolve the coupled Schrödinger-Poisson equations, dubbed ψDM, (Schive et al., 2014a) that reveal distinctive, testable predictions for the non-linear

structure of this wave-like form of DM. The Uncertainty Principle means bosons cannot be confined to a scale smaller than the de Broglie one, so this “pressure" naturally suppresses dwarf galaxy formation and generates rich structure on the de Broglie scale, as revealed by the first simulations (Schive et al., 2014a,b; Mocz et al., 2017; Veltmaat et al., 2018) in this context. The most distinctive ψDM prediction is the formation of a prominent solitonic standing wave at the base of every virialised potential, corresponding to the ground state, where self gravity of the condensate is matched by an effective pressure due to the Uncertainty Principle. The solitons found in the simulations have flat cored density profiles that have been shown to accurately match the known time independent solution of the Schrödinger-Poisson equation (Schive et al., 2014a,b, 2016), for which the soliton mass scales inversely with its radius. Furthermore, a scaling relation between the mass of this soliton and its host virial mass has been uncovered by the ψDM simulations, $m_{soliton} \simeq m_{halo}^{1/3}$, such that a more compact dense soliton should be found in more massive galaxies (Schive et al., 2014b) and can be understood from the virial relation (Veltmaat et al., 2018).

On scales larger than the de Broglie scale, the evolution of structure in ψDM simulations is indistinguishable from CDM simulations, starting from the same initial conditions, as desired given the well established agreement between CDM and the statistics of large scale structure and the CMB. Hence, although the light bosons contrast completely with the heavy fermions from supersymmetry, they actually provide a very viable non-relativistic explanation for the observed coldness of dark matter.

These characteristics make wave dark matter a good candidate for resolving the previously mentioned problems ("cusp-core", "missing satellites", and "too big to fail"), as their solitonic flat cores profiles provide less dense halos than predicted by CDM. This happens because of the “quantum pressure” product of the Heisenberg uncertainty principle that balances the self-gravity of the soliton (Schive et al., 2014a) on the de Broglie scale. Forming solitonic, standing wave cores in the ground state (rather than a divergent cusp) within galaxies which are surrounded by a granular halo where the density is fully modulated between constructive and destructive interference on the de Broglie scale (Schive et al., 2014a). This is quite unlike the smooth divergent NFW profile of CDM halos. Moreover, the existence of some star clusters at the center of certain dwarfs "conflict directly with" the cuspy NFW profile and has favored the ψDM model as the soliton core provides a shallow, tide free, central potential provided the star cluster orbits within the soliton (Schive et al., 2020; Contenta et al., 2018).

This revolutionary cored profile seems to go in hand with the observational data from the dark matter-dominated dwarfs, which are understood to have dark matter cores. The kpc size of these dwarf cores provides a simple estimate of the boson mass that is close to 10^{-22}eV (Schive et al., 2014a; Chan et al., 2020; Broadhurst et al., 2020). This general value for the boson mass has been recently reinforced with the detection of the new "ghostly" galaxy Antlia-2, famous for its low surface brightness and relatively large radius. This, along with the low mass and density

of this galaxy, matches well with the wave dark matter predictions where such an internally low momentum galaxy should have a wider soliton, compatible with a boson mass of 10^{-22}eV. Explaining the observed extended stellar profile with a soliton of 3 kpcs (Broadhurst et al., 2020).

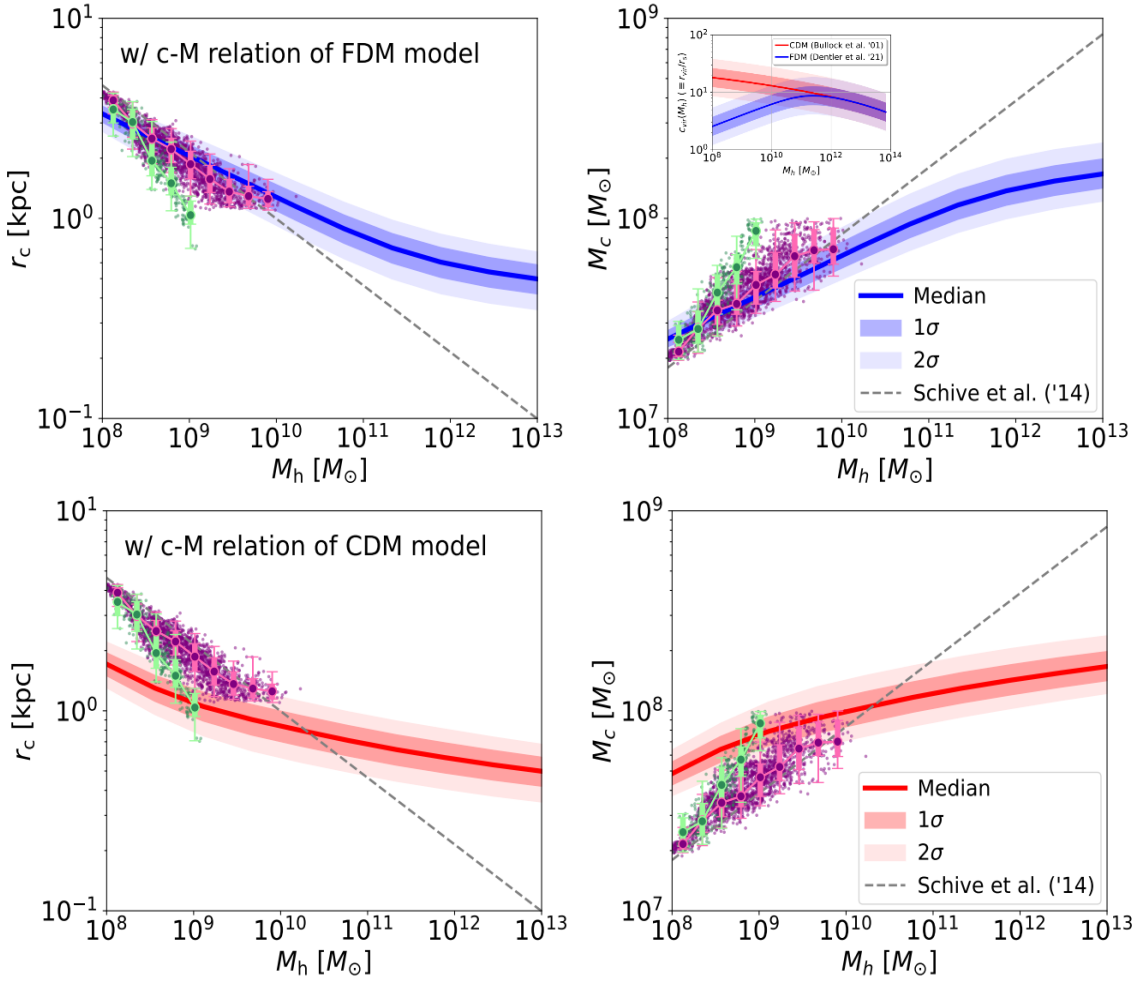

Figure 2.5: Predicted core-halo relations for ψDM and CDM models. The Small panel represents the analytical expressions for the c-M relation of ψDM (blue) and CDM (red) models. The upper panels show the computed core-halo relation for the ψDM models, and its discrepancy/agreement with the simulated numerical predictions while the lower panels show exactly the same but for the CDM model. For both panels, the thick solid line represents the median. The shadowed areas represent the 1, and 2σ errors around the mean in order to accurately fit the well know large scatter measured in c-M simulations (Bullock, 2001; Jing, 2000a; Bhattacharya et al., 2013; Diemer, 2015). The gray dashed lines represent fitting function found numerically by Schive et al. (2014a) while the green and purple data points show the estimated results from soliton mergers simulations (Chan, 2022) and cosmological simulations (May & Springel, 2021) respectively. Credit Taruya & Saga (2022)

Figure 2.5 shows the resulting core-halo relations for wave dark matter and cold dark matter models, adopting the c-M relations of each DM model. The results from

the c-M CDM relation, which predicts high-concentration halos, are much shallower than the trend predicted by the numerical simulations. In contrast, the obtained results from the c-M ψDM coincide better with the results obtained from the numerical simulations. The predicted core-halo relation seems to agree surprisingly well with the scaling relation from Schive et al. (2014a) (where; $r_c \propto M^{-1/3}$ h and $M_c \propto M^{1/3}$ h.) until $10^9 M_\odot$, but with important discrepancies for halos bigger to $10^9 M_\odot$ (Taruya & Saga, 2022). Nevertheless, it is important to remark that the data points result of the cosmological numerical simulations (purple data points of figure 2.5) have been done with small box size, L = 10 h^{-1} Mpc. In contrast, the soliton merger simulations (green data points of figure 2.5) were done with an L=300 kpc. Moreover, these simulations have not been made with a strictly cosmological setup, where the initial conditions of the former simulations is not precisely consistent with the wave dark matter model having a small-scale cutoff. Something that could explain the observed discrepancy of the computed c-M relation upon $10^9 M_\odot$. In addition, the analytical c-M relation for the ψDM model is not designed to account for the low-mass halos considered here. In this respect, the predicted core-halo relations adopting the c-M relation of (Dentler et al., 2022) might not be accurate at $10^{11} M_\odot$. The observed smaller scatter in the core-halo relation for smaller halos seems to result from the preference of the ψDM model for low concentration halos at small scales. Something that is also observable for the numerical simulations. Making the core-halo ψDM relation much stronger than the predicted one from the CDM model (Taruya & Saga, 2022).

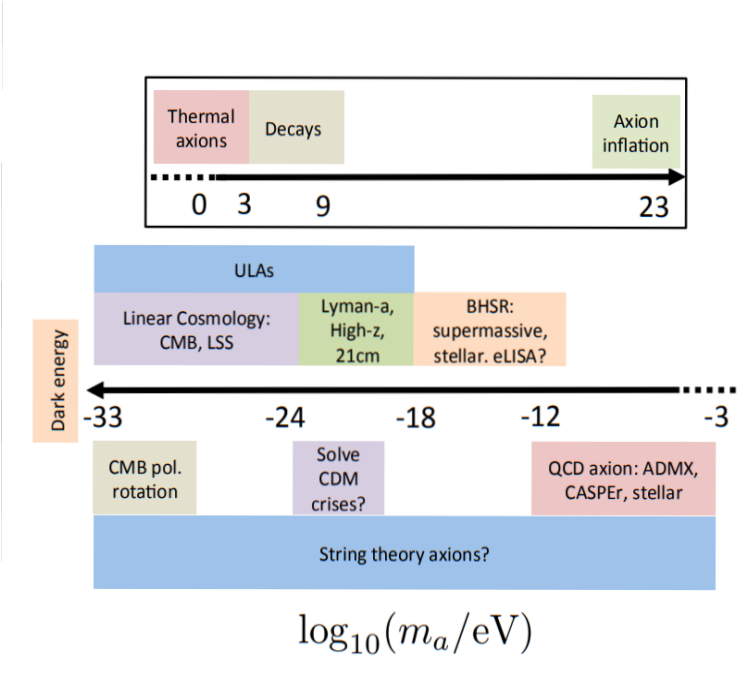

Figure 2.6: Summary of constraints and probes of axion cosmology. Credit Marsh (2016).

JWST may definitively test the rich non-linear coherent wave structure of fuzzy DM's unique signature, imaging the substructure around Einstein rings at the de

Broglie scale. Moreover, they are assumed to be more different ways to look for wave dark matter: distinguish fuzzy DM from the WIMPs by exploiting cosmological birefringence (Carroll et al., 1990), analyze linearly polarized light such as the one from pulsars (Liu et al., 2020) to detect the polarization angle variation that may happen because of topological interactions between axion and photons when linearly polarized light travels in the axion-like DM media and the galaxy formation delay between wave dark matter and CDM scenarios (deeper explained in point 6 of the wave main characteristics list enumerated in next pages).

The boson mass, m_ψ, is the only free parameter for ψDM, this simplicity is one of its great strengths as predictions for the DM is unique once a particular value of the boson mass is specified. The boson mass has been previously estimated to be approximately $m_\psi \simeq 10^{-22}$ eV (Schive et al., 2014a), by identifying the large DM-dominated cores observed in dSph galaxies as solitons. Independent analyses of other dSph galaxies have supported this value (Chen et al., 2017; Broadhurst et al., 2020). With this value, we can normalize the ψDM simulations and predict the absolute values of soliton properties as a function of halo mass for comparison with the observations.

Axions are recognized as a viable candidate of DM and the primary physical particle of the thesis of this work. With a null spin and uncharged and hence only gravitational self interaction. They are postulated to have extremely light masses, from 10^{-33} to 10^{-3}eV (Marsh, 2016), where this upper value is limited by the nuclear reactions in stars and actual supernova explosion mechanics. They are supposed to weakly interact with normal matter and are not very susceptible to weak and strong nuclear forces, so gravitational interactions are their only interaction with ordinary matter. They are a natural solution of the standard model and the string theory predicted by quantum chromodynamics, and they were postulated as a natural solution to the CP problem (Peccei & Quinn, 1977a; Peccei, 1977), where the QCD(quantum chromodynamics) violated the CP symmetry. The axion would be the particle of the needed field to solve this problem (Dine et al., 1981; Svrcek & Witten, 2006). Nevertheless is important to point out that the axions postulated to solve the CP problem are very different from the "axion-like" particles (ALPs) of String theory (they MUST not be confused). Both are axionic in terms of their axial rotation symmetry but not at all related. ALPs can have a wide range of mass, whereas QCD axions are thought to naturally be about 10^{-7} eV or a bit lower, but certainly not thought to be as light as 10^{-22}eV for the ALPs.

Many different kinds of tests have been proposed in order to detect ALPs in laboratories, such as for example measuring couplings to electrons, nucleons, electric dipole moments etc. Nevertheless, the first needed step would be to set the appropriate mass scale of the searched particle in such experiments, in order to target the oscillation frequency $f = m_\psi c^2/h$ Chadha-Day et al. (2022). Another very useful method to detect axions and ALPs, could be based in the argued interaction of these particles with electromagnetic fields. In this context, axions can interconvert with photons in the presence of a background magnetic field. Something similar to neutrino's oscillation, but in this case the strength of the mixing

would be totally related to the magnetic field's size. Astrophysical environments impossible to replicate on Earth, such as stars, galaxies, and clusters seem to be the perfect place to look for (Galaxy clusters host strong magnetic fields over very large distances). This means that if ALPs exist, some of these photons should convert to ALPs while they pass through these clusters, making some of the light from different sources disappear while they cross through the clusters. Even if definitive bounds are impossible due to essential knowledge of the magnetic fields of these clusters, the non-observation of this effect can be used to place bounds on the axion photon coupling (Reynolds et al., 2020). Another expected testing sources are the Supernovas, these explosions at the end of stars' life, produce a huge amount of neutrinos, photons, and ALPs, these last ones only if they exist. It was predicted that in the case of the supernova SN 1987A, these ALPs would have been converted into gamma rays photons through Milky Way's magnetic field, giving us the opportunity to get new constraints (Chadha-Day et al., 2022). The principal handicap of these tests, relies on the fact that photons traveling through the plasma of these astrophysical structures acquire low efficient masses avoiding axions or ALPs with higher masses mix with them. The CERN Axion Solar Telescope (CAST) experiment will also look up to these axion-photon conversions that should happen in stars, specifically, in the Sun (Anastassopoulos et al., 2017).

As we have previously commented, a light axion of $\simeq 10^{-22}$ eV would be a viable candidate for the Wave DM halos base particle, so their wave nature would manifest on astrophysical scales (Schive et al., 2014a,b). Under this proposal, dark matter halos are stable on small scales for the same reason that the hydrogen atom is stable: the Uncertainty Principle. Moreover, it is well known that if the dark matter is composed of ultra-light scalar particles m«1eV, the occupation numbers in galactic halos are so high that the dark matter behaves as a classical field obeying a collective, coherent Schrodinger wave equation(Schive et al., 2014a,b). Another important consequence of ψDM halos composed of axions of $\simeq 10^{-22}$ eV is the inherent cut-off at small scales of the power spectrum in this context. This boson mass suppresses small-scale structures in ψDM context below the de Broglie wavelength of $\sim$1kpc for such boson mass, making it the largest scale at which quantum mechanical effects will appear (Chavanis, 2011; Suárez & Chavanis, 2017), coinciding with the sizes of the observed stellar distribution is dawrfs(Marsh & Silk, 2014; Bozek et al., 2015). Nevertheless, these boson fluids seem to behave and form exact structures as CDM at large scales, showing consistent results with observations (Suárez & Chavanis, 2017; Matos et al., 2009). It is necessary to remark that to create the relevant cut-off in the power spectrum at small scales, it requires an axion mass larger than $\simeq 10^{-23}$ eV to still be consistent with the observed large structures (a constraint that comes from the Hubble Ultra Deep Field UV luminosity function and the optical depth to reionization as measured from CMB polarisation)(Bozek et al., 2015), and above $\simeq 10^{-24}$ eV for the observed stellar formation rates and halo masses functions (a constraint that comes from CMB temperature anisotropies) (Hlozek et al., 2015). We will explain these two ψDM cosmological results in detail at the end of this section.

Condensate of Bose-Einstein is considered as the fifth state of the mat-

ter. This state is revealed when a boson gas is cooled to temperatures near absolute zero. The bosons would occupy the lowest energy-quantum state, at which point microscopic quantum mechanical phenomena, particularly wavefunction interference, become apparent macroscopically. This phenomenon is only physically possible in a gas formed by bosons. Being the only particle with the same quantum state due to not filling Pauli's exclusion theorem, a product of their symmetric wave function, where fermions with spin 1/2 cant fill the same quantum state whereas bosons with spin 1 can. This state's two main associated characteristics are superfluidity(matter stops having friction) and superconductivity(null electrical resistance).

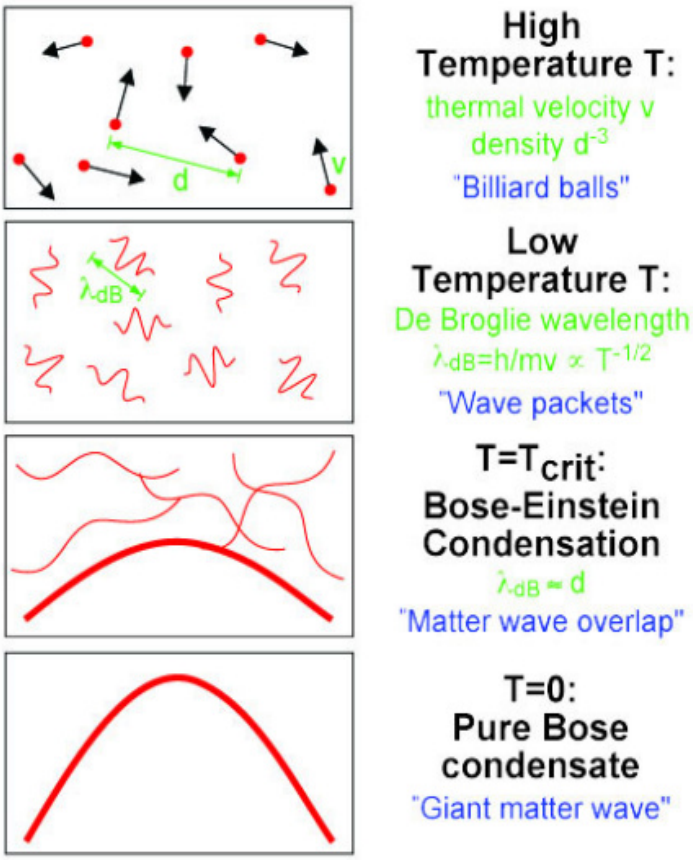

Figure 2.7: Bose-Einstein Condensation phases. At high temperatures, the particles of a weak interactive gas can be described as wave-packets with an extension of Δx, approximately given by Heisenberg's uncertainty relation $\Delta x = h/\Delta p$, being Δp the width of thermal momentum distribution. As Δx is similar to the thermal de Broglie wavelength λ_{dB}, as well as the temperature of the gas decreases, the λ_{dB} increases to a comparable size to the distance between the particles, increasing also Δx, the uncertainty of their exact position. When the temperature gets close to zero absolute, the Δx gets maximum being impossible to distinguish one particle from another. Vanishing the thermal cloud and leaving a pure Bose condensate. Credit Durfee & Ketterle (1998).

An ideal Bose gas is a collection of non-interacting N bosonic particles. Following

the laws of quantum mechanics, these particles have a wave nature that the de Broglie wavelength can characterize;

$$\lambda_B = \frac{h}{p} \tag{2.2}$$

and which can be used to obtain the de Broglie thermal wavelength for ideal gases with massive particles:

$$\lambda_{BT} = \frac{h}{\sqrt{3 m_b k_B T}} \tag{2.3}$$

Where m_b is the boson mass (as this scalar particle has to be a boson, not fermions, that can form a Bose-Einstein condensate by virtue of being "bosonic", whereas fermions cant all fall into one ground state like bosons, due tot he Pauli exclusion principle, with rare exceptions like the cooper pairs of electrons (of opposite spin) that can pair up to effectively become bosons and thus condensate as in superconductivity), T is the temperature, h Planck's constant, and k_B is Boltzmann's constant. At high temperatures, when λ_{BT} is smaller than the distance between particles, their thermal movement dominates the gas properties as localizable particles. But while the temperature decreases, λ_{BT} increases to values more significant than the distances between the particles, arising their wave behavior. In this situation, the different matter waves overlap, coordinating their state and producing the Bose-Einstein condensate. A single wave function defines all the system as a "super-atom". At his point, all de atoms are in the smaller quantum-energy state, being identical. As all of them share the same quantum state and have all the same minimum energy, they become indistinguishable from each other, behaving as a single super-atom.

This boson mass (the only free parameter, in the ψDM), has been estimated to be approximately $m_\psi \simeq 10^{-22}$ eV (Schive et al., 2014a), by identifying the large DM dominated cores observed in dSph galaxies as solitons. Independent analyses of other dSph galaxies have supported this value (Chen et al., 2017; Broadhurst et al., 2020). With this value, we can normalize the ψDM simulations and predict the absolute values of soliton properties as a function of halo mass for comparison with the observations. A gas-fluid formed by such axions will have a high-temperature condensation (critical temperature is $\sim$ TeV due to the high number density of axion particles), a temperature that will see its difference with the mean-field temperature enlarged while the universe expands and cools. This will make the axion gas a Bose-Einstein condensate due to the previously explained physical phenomenon of the boson gases cooled to temperatures near absolute zero. The expected de Broglie wavelength for such axions condensates is about $\sim$1kpc, and will set off the area in which quantum mechanical effects will appear. This de Broglie wavelength size coincides with the observed stellar distributions from galaxies (Marsh & Silk, 2014; Bozek et al., 2015). The needed boson mas constraint so this axion's Bose-Einstein condensates will reproduce CDM structure at large scales while at the same time,

they will be able to create the relevant cut-off in the power spectrum on small scales, has to be superior to $m_\psi > 10^{-23}$eV(Bozek et al., 2015). This constraint comes from the Hubble Ultra Deep Field UV luminosity function and the optical depth to reionization as measured from CMB polarisation, which stipulated a boson mass higher to $m_\psi > 10^{-24}$eV, as a product of the CMB temperature "anisotropy" (Hlozek et al., 2015).

This physical state where a vast group of indistinguishable bosons can coexist in thermal equilibrium, in the same quantum state can be described by the Bose-Einstein statistic:

This Bose-Einstein statistic is equivalent to Maxwell-Boltzmann statistic for high energies, originally postulated to describe these particle gases in classical mechanics.

In summary, these are the five main points that characterize wave dark matter:

1. **Extreme light particles**:

   $m_{22} \equiv m_\psi/10^{-22}\text{eV} \rightarrow 10^{31}$ lighter than CDM.
   Because of such small particle mass de Broglie wavelength becomes astronomical (kpc) scale
   Wavelike properties (e.g, interferences)

2. **Governed by Schröedinger-Poisson equations**:

   "Is a nonlinear modification of the Schröedinger equation with a Newtonian gravitational potential, where the gravitational potential emerges from the treatment of the wave function as a mass density, including a term that represents the interaction of a particle with its own gravitational field."

$$i\frac{\partial\Psi(x)}{\partial t} = -\frac{1}{2m_\psi}\nabla^2\Psi(x) + m_\psi\varphi(x)\Psi(x) \tag{2.4}$$

$$\nabla^2\varphi(x) = 4\pi G a(t)(|\Psi(x)|^2 - 1) \tag{2.5}$$

   Ψ is the wave function, φ is the Newtonian gravitational potential, and 'a' is the cosmic expansion scale factor. One of the most critical features of this model is that it has only one free parameter, m_ψ, the boson mass. So the most significant task in the wave DM model is to constrain the actual value m_ψ, as a result of observational data. That is the main purpose of this work. See

figure 2.11 to realize how a small variation of the mass can produce slightly different cosmological structures.

One of the essential properties of wave dark matter is that there is an effective quantum pressure that will suppress the small-scale structure. This feature can be easily noticed if rewriting the Schröedinger-Poisson equations into conservation laws, just like the Euler equation in hydrodynamics.

$$\frac{\partial p}{\partial t} + \nabla(p\vec{v}) = 0 \tag{2.6}$$

$$\frac{\partial \vec{v}}{\partial t} + \vec{v}\nabla\vec{v} = \nabla(\frac{1}{2m_\psi^2}\frac{\nabla^2 f}{f}) - \nabla\varphi \tag{2.7}$$

Where:
$\Psi = fe^{iS}$
p $= m_\psi f^2$
v $= m_\psi^{-1}\nabla S$

Eq.(2.6) is the continuity equation and Eq.(2.7) is the moment equation, where the below explained conditions are the conversions from wave equation to fluid. Applying those conversion variables, we get the momentum equation in hydrodynamics:

$$\frac{\partial \vec{v}}{\partial t} + \vec{v}\nabla\vec{v} = -\frac{1}{p}\nabla p - \nabla\varphi \tag{2.8}$$

Notice how the only difference between these last two momentum equations (equation(2.7) and (2.8)), is the first term on the right side, colored with blue, which represent the pressure. By rewriting the term of quantum fluid into a similar term in hydrodynamics, we can derive an expression for the already mentioned quantum pressure, which is a stress tensor:

$$P_{ij} = \frac{1}{m_\psi}(\partial_i f \partial_j f - \frac{1}{4}\delta_{ij}\nabla^2 f^2) \tag{2.9}$$

3. **The Uncertainty principle means bosons cannot be confined to a scale smaller than the de Broglie scale, so this “pressure" naturally suppresses dwarf galaxy formation and generates rich structure on the de Broglie scale, as revealed by the first simulations**Schive et al.

(2014a,b):

Representing the de Broglie wavelength in terms of boson mass:

$$\lambda_B = 1.2 \frac{m_\psi}{10^{-22} eV} \frac{100 kms^{-1}}{v} kpc \tag{2.10}$$

In combination with axion masses of $\sim 10^{-22}$eV, it provides ψDM models wave-like small-scale structures as a consequence of the de Broglie scale. Moreover, in scales smaller than the de Broglie wavelength, the quantum pressure dominates over gravity. The axion field is uniform and there is a minimum mass for a dark matter halo (Khlopov et al., 1985) due to the suppression of small-scale structures. At the same time, we will see how large-scale structures stay similar to CDM in the next point. This suppression of small-scale structures formation with such boson mass is the product of the inherent cut-off:

The power spectrum and the small scale cut-off in ψDM:

The small-scale cut-off is in relation to the power spectrum for ψDM and WDM caused by the pressure (quantum for ψDM and thermal heating pressure for WDM); this cut-off limits the minimal mass at which a structure can first form, limiting for example for a boson mass of $\sim 10^{-22}$eV any structure formation below $\sim 10^9 M_\odot$. CDM has no such pressure and, in consequence, no cut-off, stipulating almost no small-scale structure formation mass limits, and also, there is no smoothing of the core. For masses similar to 10^{-22}eV, this suppression of structures of scales below the Jeans scale is expected to suppress structures of $\sim 10 Mpc^{-1}$ and below.

Notice how the resulting pressure in equation (2.9) is related to the spatial derivative of density. This is the quantum pressure that involves a significant rule in wave dark matter, because after defining pressure, the corresponding Jeans limit can be computed, defining the point where gravity balances pressure. Above this Jean scale limit, gravity would dominate in both CDM and ψDM, expecting similar behaviors. But in scales smaller than this Jean scale, the pressure will dominate, suppressing the small-scale structures, making a real difference from CDM to ψDM in these scales smaller than the Jean scale. As we have just pointed out in the previous paragraph, this does not happen for CDM, as models based on weakly interacting massive particles, have power spectra that extend without suppression all the way to Earth masses. This "effective" pressure from the UP sets a lower scale for the structure of ψDM, given by the de Broglie scale. On scales larger (several times larger) than the de Broglie scale, the pressure is negligible and so ψDM can be expected to approximate the behavior of CDM and hence explains why the halos of ψDM have an NFW form like CDM. But the halos are not smooth like CDM they

have a pervasive structure on the de Broglie scale due to interference - however, when azimuthally averaged, the profile is NFW-like.

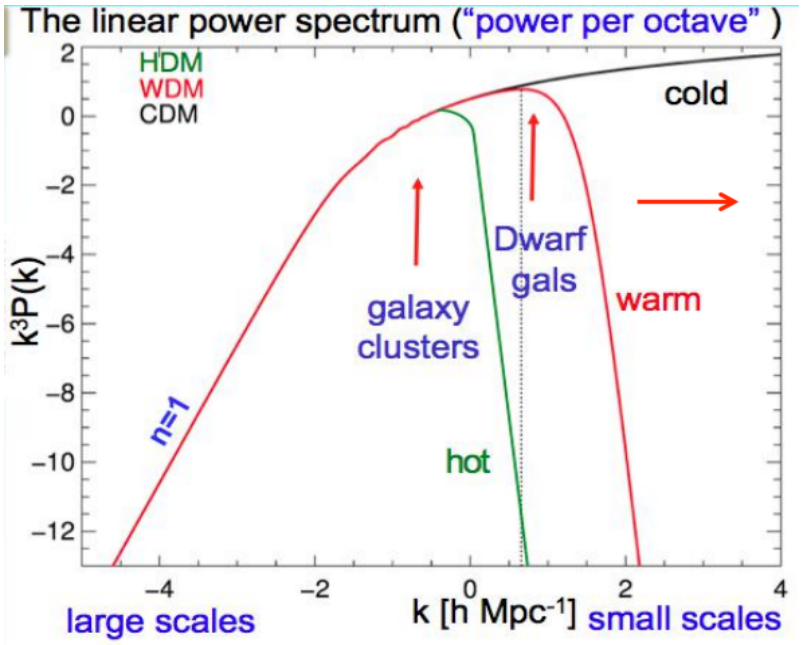

Figure 2.8: The small scale cut-off at the power spectrum. See how the power spectrum value dives to zero for WDM (ψDM is actually a sharper cut-off than WDM) at large frequencies(small-scales), a product of caustics pressures(quantum pressure for ψDM). Notice how there is no such cut-off for CDM, making possible the formation of DM structures at very small scales and low masses.

The matter power spectrum describes the density contrast of the universe (the difference between the local density and the mean density, the variance of the density field), P(k), as a function of scale. A higher frequency, k, will refer to smaller scales. In contrast, P will increase with the more significant difference between the local density and the universe's mean cosmological density, being zero when they are equal. It is the Fourier transform of the matter correlation function. Gravity competes with cosmic expansion on large scales, and structures grow at first according to linear theory. Later, these overdensities will grow so large they can collapse, "non-linearly" to make galaxies. This must be simulated as the linear theory approximation can no longer be applied. In this regime, the density contrast field is Gaussian, Fourier modes evolve independently, and the power spectrum sufficiently describes the density field. On small scales, gravitational collapse is non-linear and can only be computed accurately using N-body simulations. The fundamental behavior of the models at small scales will be defined by the physics of their primordial particles, giving different results for CDM (WIMPs) and ψDM (axions).

4. **The most distinctive waveDM prediction is the formation of a prominent solitonic standing wave at the base of every virialised potential,**

corresponding to the ground state, where self-gravity of the condensate is matched by an effective pressure due to the Uncertainty Principle. (Schive et al., 2014a,b):

This is because the soliton is all the bosons collected in the ground state of the bose-Einstein condensate (the lowest energy configuration is a soliton). All these bosons, zillions, all form one giant wave, and not an unrelated smooth mass of individual boson waves but one coherent "standing wave" that is totally smooth and lasts forever as a stable soliton, that is self-reinforcing the tendency of a wave to spread is countered by its self-gravity; In summary, this is the definition of a standing wave.

As ψDM large structure scale results seem not to differ from CDM, the most interesting property of wave dark matter occurs in scales smaller than the Jean scale. In such smaller scales, in very high density points, axions form the well known solitonic-core supported by an equilibrium between gravity and quantum pressure (Seidel & Suen, 1991) (Small right panel of figure 2.9).

5. **On scales larger than the de Broglie scale, the evolution of structure in waveDM simulations is indistinguishable from CDM simulations, starting from the same initial conditions, as desired given the well-established agreement between CDM and the statistics of large scale structure and the CMB.(Schive et al., 2014a,b)**

On large scales, however, the scalar field behaves just like a collisionless self-gravitating fluid, identical to CDM, and is therefore consistent with modern large-scale cosmological constraints. In this scale, gravity causes the axion field to develop inhomogeneities, and its clusters into ψDM halos (The whole orange structures of figure 2.9). The development of these inhomogeneities in the axion field is governed by gravity but also by axion self-interactions, but in a smaller proportion. These are governed by the non-linear Schrodinger equations presented on the upper side. Finally, the different halos are connected by dark matter filaments (Blue structures of figure 2.9) creating the appreciable "Cosmic Web" of figure 2.10.

For further understanding check out sections 3 and 3.1, where these ψDM halos' structures are well explained, specifically in figure 3.2, where the dark matter halos painted in orange of figure 2.9 can be seen with the color map used in figure 2.10 to differ the high density zones (cores) with the low ones (outer part of the halo). In this section, we will also explain the different behavior of these two structures.

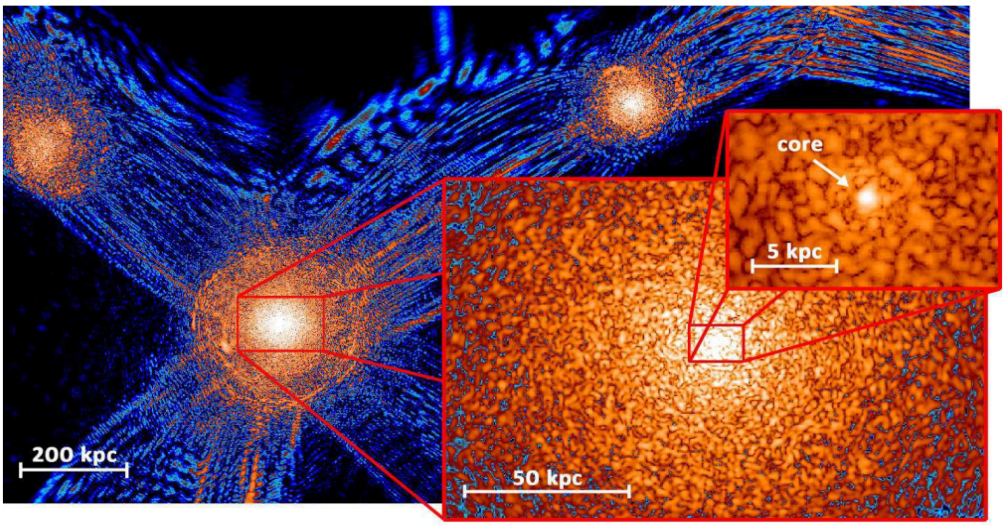

Figure 2.9: Cosmic web small scale: Cosmological simulations representing Wave dark matter density distribution on scales smaller than Jean scale and beyond. Notice how the interference patterns product of the wave behavior dominate the structure at these scales, connecting halos(density granules in this case, orange structures) by filaments (blue structures). At the center of every halo, we should localize the main difference with CDM, the solitonic core (labeled "core"), instead of a divergent cuspy profile. Credit Schive et al. (2014a).

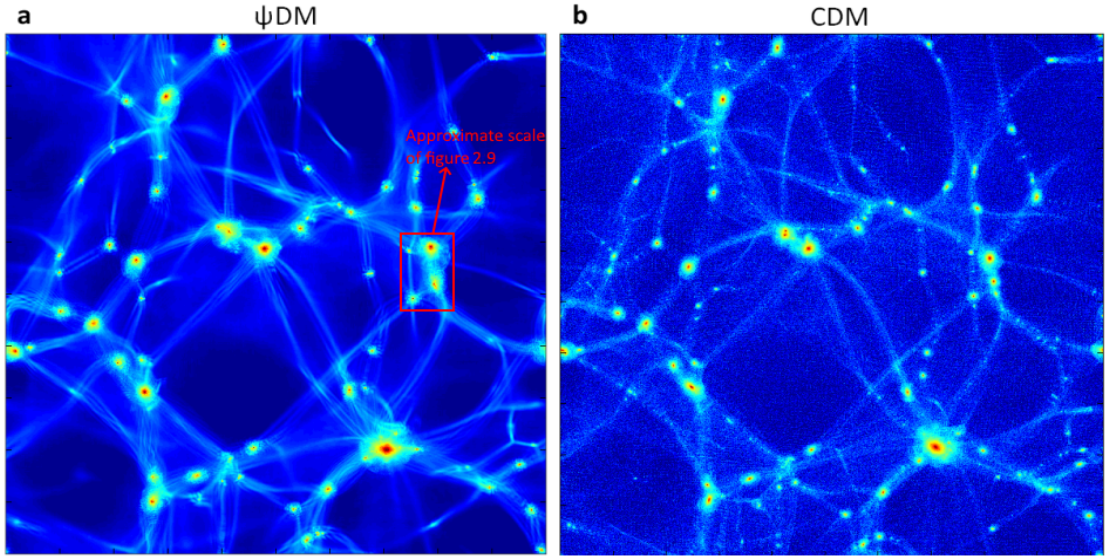

Figure 2.10: Cosmic web large scale: This figure shows cosmological simulations to represent the ψDM large scale structure vs. the CDM large scale structureSchive et al. (2014a). The predicted results by these two models are very consistent in these large scales, where gravity should dominate both DM models. So as a consequence, these two models should not differ at large scales, giving to ψDM the same cosmological observational consistency of CDM. Notice how now the halos are plotted with a color map from lower densities in green to higher in red in contraposition to the orange of figure 2.9. Representing this last color the position of the cores. Filaments are painted in blue also in this case. Credit Schive et al. (2014a).

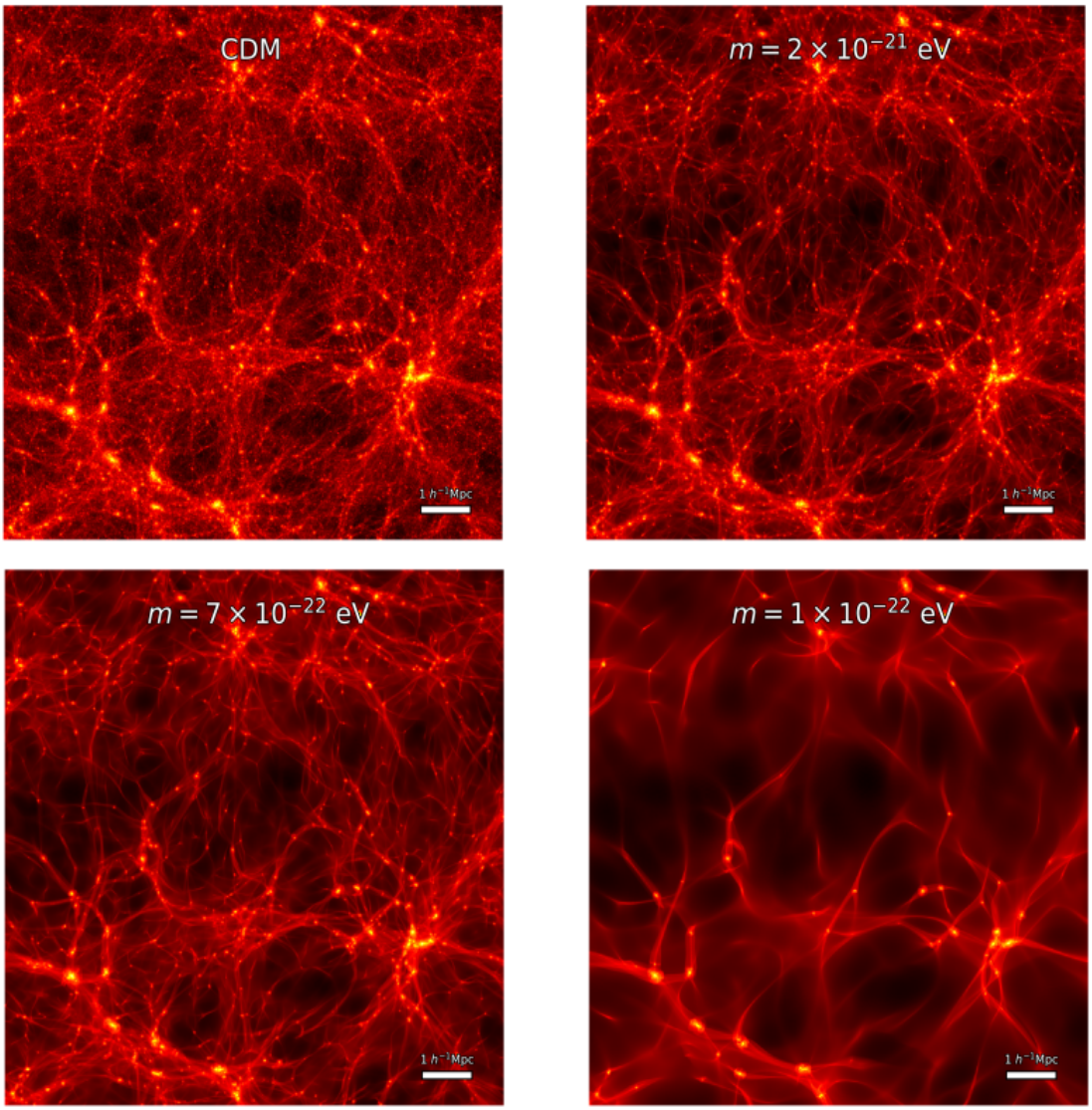

Figure 2.11: Cosmic web large scale: As in figure 2.10 figure shows cosmological simulations to represent the ψDM large scale structure vs. the CDM large. The main difference with figure 2.10 is that in this case, three different boson masses have been used in order to point out the weight of the boson mass in the resulting cosmological structures. Credit Dome et al. (2023).

6. **Cosmological formation**

In this point, we will describe how the sum of the previous 5 points affects galactic formation in the ψDM context, comparing it also with the CDM formation process. This structure's formation process starts very early in the Universe's time life, the potential wells of the dark matter halos start to form at very high temperature, when the ordinary matter is still ionized.

The differences in the power spectrum and their consequences on the structure formation process

In CDM, there is no power spectrum cut-off at small scales, allowing to form DM structures of low masses and concentrations. Nevertheless, whereas such a cut-off at small scales occurs for ψDM, limiting the minimum mass at which DM structures can start to be formed at scales below the de Broglie length, defined by the boson mass. This phenomenon is typically called the "suppression of DM structures at small scales", making for example, the formation of DM haloes below the $\simeq 10^9 M_\odot$ for boson masses of 10^{-22}eV, impossible to form. This limit carries out a direct consequence on the formation times between CDM and ψDM. More massive halos need more time to be concentrated, indicating that, as in CDM, there is no small scale formation limit, haloes below $\simeq 10^9 M_\odot$ will be formed before the first $\simeq 10^9 M_\odot$ halos are formed in the ψDM context. In both cases, we will see the formation of the first "filamentary" structures at the very first times (very high redshifts), forming earlier in CDM. In CDM the filaments are comprised of low mass subhaloes. In contrast, in ψDM/WDM, there is no fragmentation between them, as the filaments are not eaten so quickly due to the delayed halo formation product of the small-scale structures cut-off of the power spectrum. Instead, dark matter is distributed more continuously also alongside these filaments wherein ψDM the interference pattern is displayed due to the relative velocity of the matter converging onto the filament. Inside the virial radius, the main difference between the WDM and ψDM filaments structure is that for WDM, a caustic structure can be seen, while the interference pattern of ψDM, produces a much more turbulent density structure, due to being the superposition of many plane waves that encode the velocity dispersion in the halo (Mocz et al., 2020). These filaments should endure much more time (should be appreciable at much lower redshifts) in ψDM, as the earlier formation of the first halos in CDM should start breaking these filaments earlier due to gravitational attraction. Moreover, the longer life of these filaments in wave dark matter will favor the formation of much more stars inside these filaments, making a great difference in the location and extension of stellar profiles in CDM and ψDM galaxies, as well as making baryonic objects look "fuzzier"/more smoothed than in CDM (Mocz et al., 2019, 2020), postulating them as excellent DM tracers in ψDM (something that will make a great point of the thesis, being discussed here and in section 3.3). All these points have been recently confirmed with new simulations by May & Springel (2022), where they support a ψDM scenario with linked halos via continuous, smooth, and dense filaments while in CDM these filamentary structures break into subhalos much quicker (see figure 2.12). Moreover, they also pointed out that significant visual differences should be observed between ψDM and CDM in the outer part of the halos. Concretely, they argue (as I do in this work), that the main difference relays on the slopes and extent of the density profiles, making the ψDM profiles flatter and fall more slowly towards the outer regions of the halos; "reaching much further outwards before dropping to the background matter density" (May & Springel, 2022). Whereas for CDM, filaments are less extended and with quicker declining density profiles. This decline is expected to be of 500 h^{-1}kpc for CDM in contra-position to the one of ψDM,

that extends to 1 h^{-1}kpc (May & Springel, 2022).

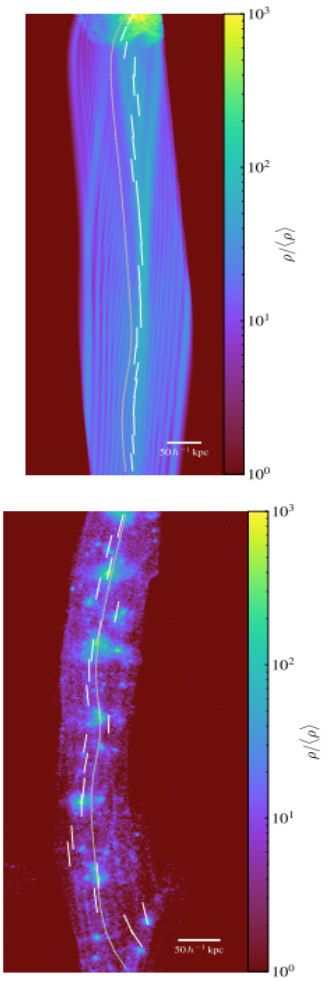

Figure 2.12: Projected density for ψDM and CDM filaments. Notice how the density profile is much more flat and continuous compared to CDM, where the filament seems to be broken into sub-halos along the whole structure. Credit May & Springel (2022).

At early times, dark matter and gas first collapse to filaments for wave dark matter as a product of lacking small scale power below a Jeans scale of $10^9 M_\odot$for $m_\psi = 10^{-22}$eV(Product of the small scale cut-off of the power spectrum). These filaments should never really maintain in a CDM scenario, where filaments should dissolve into a scale-free mass spectrum of small DM halos, commonly named subhalos (the fragmentation into subhaloes is a function of the mass resolution of the dark matter). This characteristic will also provide CDM to form stellar structures earlier than in ψDM. In such wave dark matter scenario, galaxy formation should begin at z$\sim$10 for a boson mass of 10^{-22}eV, with reionization completed only at z$\sim$8 (check figure 2.14). Nevertheless, these predictions seem well to agree with the surprisingly low optical depth of Thomspon scattering of the CMB and with the tentative turn down in galaxy number density at "$z > 8$" (Leung et al., 2018), implying that the galaxy

formation is not significant until $z > 8$. So the most interesting fact is that the galaxy formation should begin before for CDM than for ψDM, creating another potential observation by JWST. This lack of galaxies at high redshifts for wave dark matter is because the matter will not collapse into galaxies until the density is higher than the Jeans scale (set by the small scale cut-off of the power spectrum), so that lower boson results in a bigger Jean's mass, and hence, galaxies form later (Schive et al., 2016).

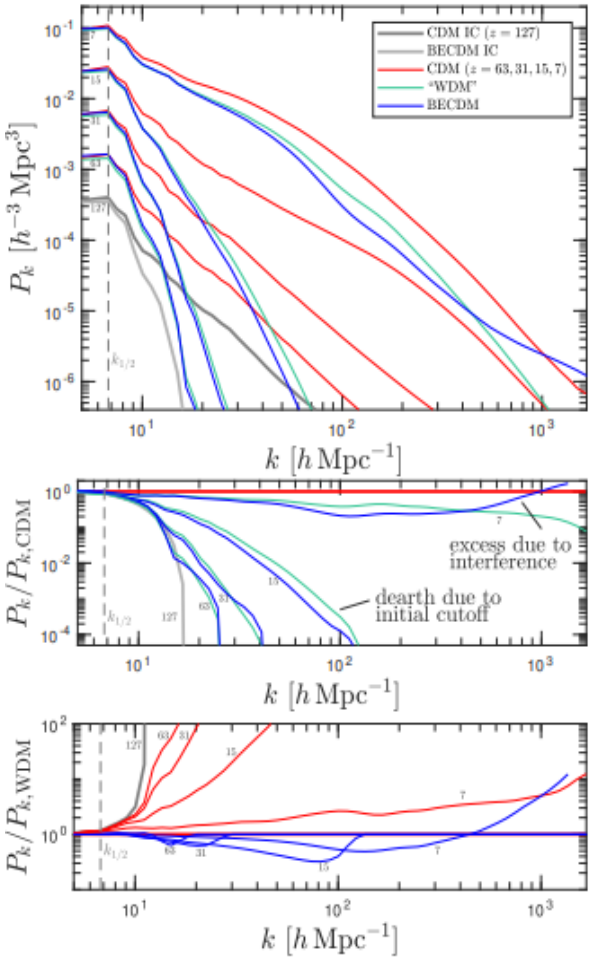

Figure 2.13: The dark matter power spectrum for CDM, WDM and ψDM. WDM and ψDM follow each other quite close in all the redshifts until z=15, indicating that the dynamic quantum potential has not significantly modified the structure. Both ψDM and WDM show a lack of power compared to CDM at high frequencies, revealing the cut-off at small scales. Notice how at z=7, at very small scales, there is an excess of power for ψDM compared to WDM and CDM as a consequence of the interference patterns proper of ψDM. Credit Mocz et al. (2020).

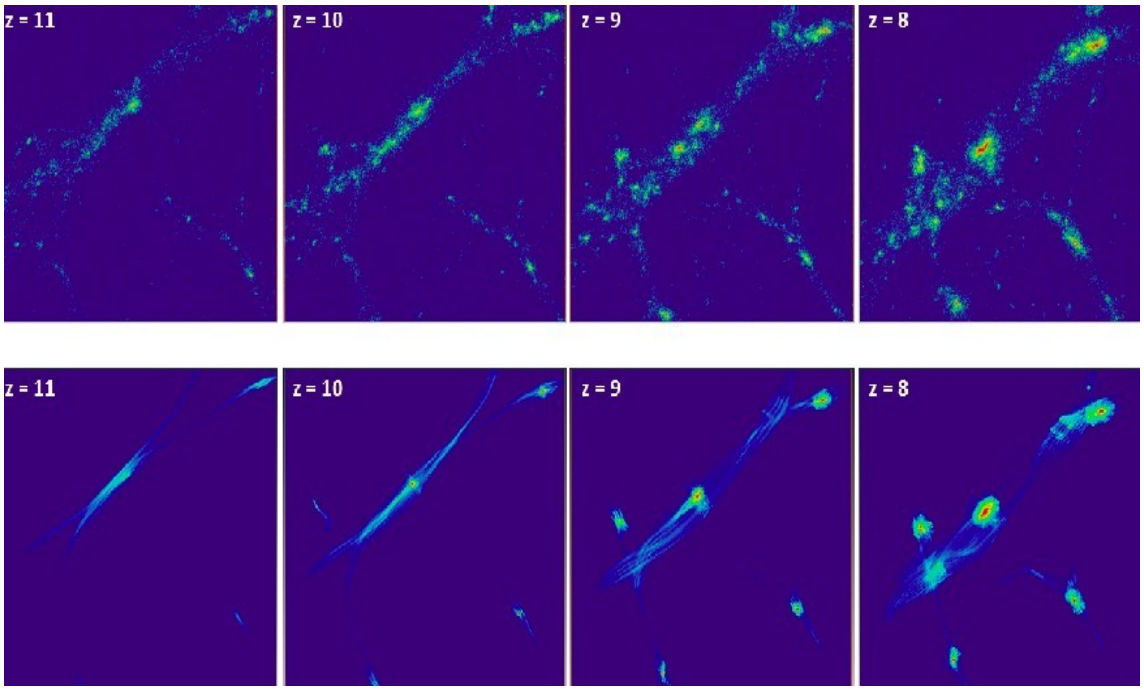

Figure 2.14: Galaxy formation with time: The top panels represent the galaxy formation evolution for CDM, whereas the ones below represent wave dark matter. Notice how in standard CDM the predicted dwarf formation is abundant at z $>$ 10, while for $m_\psi = 10^{-22}$eV ψDM, galaxies are suppressed as matter can not be confined below the Jeans scale due to the uncertainty principle. At z $>$ 10, the filaments are deprived of galaxies. These filaments are full of DM and gas, where dark matter's most significant gravitational potential should make gas trace DM. Moreover, the cooling of the gas should make stars form in these filaments, a characteristic imprint of wave dark matter (check figure 2.15). Something required to be tested by JWST, along with the presence of galaxies at these high redshifts. Important to note that the lack of galaxies at z $>$ 10 compared to CDM in wave dark matter is a direct result of the boson mass, and is more obvious for smaller boson masses. Credit Mocz et al. (2017).

These filaments are also expected for warm dark matter being apparently indistinguishable from wave dark matter at early times in terms of smooth filaments as with warm-DM as it also has an effective cut-off at high frequency in the power spectrum. Nevertheless, both WDM and CDM highly differ to ψDM: WDM and CDM, show a cuspy profile, whereas WDM's filaments represent a caustic dark matter distribution. Something that contrasts with ψDM where the caustics are regularized by the uncertainty principle with a wave-like interference DM structure. In filaments, the interference remains coherent due to a limited number of wave velocities from the initial collapse, and interference minima/maxima are aligned on scales of a few $\sim$ 100 kpc. Nevertheless, inside halos, the wave seems to be crossed in many capes as in classical collisionless dynamics (Mocz et al., 2019). However, interference patterns can be observed at kpc-scales for ψDM where the size of the interferences in filaments and halo seems to be possible to estimate (Mocz et al., 2019, 2018). At scales of the order of the de Broglie wavelength, the structures in dense regions can be highly

nonlinear, differing from WDM and CDM. Moreover, as we have highlighted in point 4 of the previous wave dark matter characteristics list, the quantum pressure in ψDM can become strong enough to counteract the self-gravity of the dark matter superfluid. This results in the formation of a prominent solitonic standing wave at the base of every virialised potential, characterized by a spherical soliton core of few kpcs at the center of every DM halo(Schive et al., 2014a). Versus much denser cusps in CDM (Navarro & Frenk, 1996) and WDM Mocz et al. (2019). See figure 2.15.

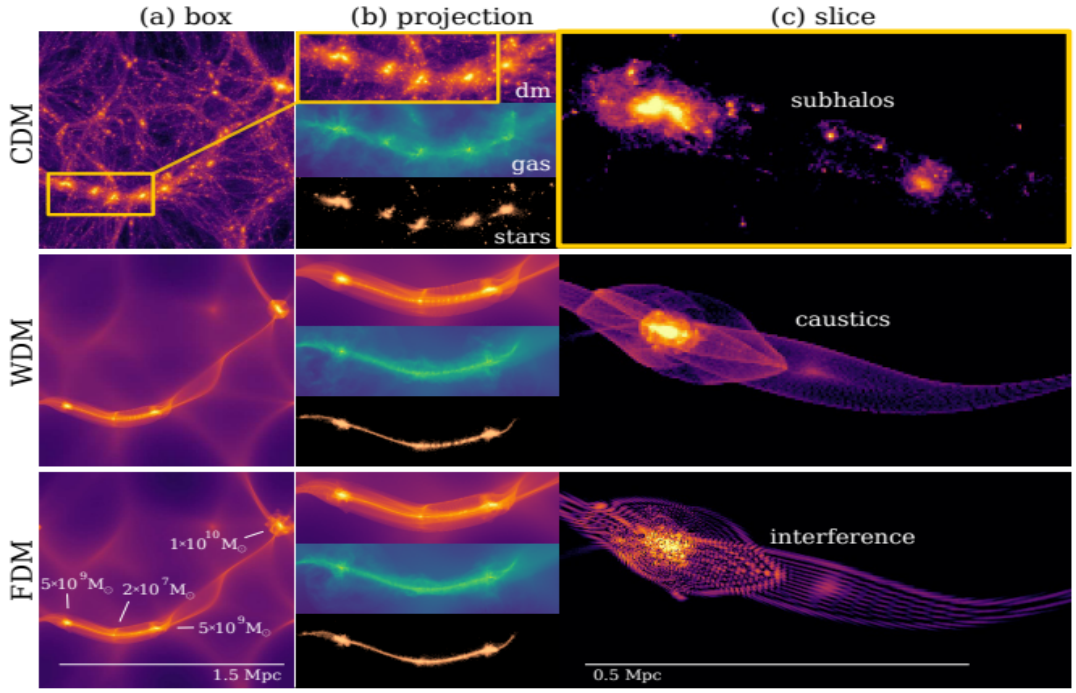

Figure 2.15: Cosmic filaments structure in ψDM/WDM/CDM. This figure shows the dark matter, gas, and stellar structure for CDM, WDM, and ψDM across the filaments and their main differences in large and small scales. **a) Projected dark matter distribution at large scales:** On large cosmological scales the projected dark matter density fields look similarly smooth in WDM and FDM while both still are consistent with CDM. As stipulated in point 3 of the previous wave DM characteristics list; the initial suppression prevents the formation of halos with masses below $M_{1/2} \sim 5^{10} M_{\odot}(m_{\psi}/10^{-22}eV)^{-4/3}$ Hui (2020). Obtaining a cosmic web dominated by dense filaments, which can fragment due to a linear instability to form halos Valinia & others. (1997). In contrast, CDM filaments hierarchically fragment into nearly-spherical subhalos. **b) Projections of dark matter, gas, and stars in a filament:** The main difference between WDM and ψDM with CDM is that the gas and stars seem to trace dark matter in the filaments, a point that would be taken into account for the assumption of section 3.3. **c) Slices of the dark matter through a filament:** In CDM, the dark matter fragments into subhalos on all scales. On the other hand, WDM shows a rich caustic structure while ψDM differs at the scales of the de Broglie wavelength where interference patterns arise. Credit Mocz et al. (2019)

As we have already commented, the power spectra match for CDM and ψDM on large scales (>Mpc), with the main difference being the cut-off on small scales due to the length-scale introduced by the de Broglie wavelength of the axion. This cut-off is expected to happen at $L_{cut-off} \simeq 1.4h^{-1}$Mpc for a boson mass of $\sim 2.5\times10^{-22}$eV (Mocz et al., 2020). These boson masses of $\simeq 10^{-}22$eV, due to the uncertainty principle, should suffer a quantum potential (pressure) that would prevent the gravitational collapse of any DM structure below the de Broglie wavelength(observable as the cut-off at small scales of the power spectrum), of some kpcs for this case. This would suppress the formation of galaxies and other DM structures below the $\simeq 10^9 M_\odot$, giving us a clear characteristic at high redshifts to discard or confirm the ψDM cosmological model. It is important to note that even though WDM shows a similar cut-off at small scales in the power spectrum, with similar consequences, the physical reason is quite different, being free-streaming instead of quantum pressures. This is the main point why the halo/filament structure is also different in both, being an interference pattern for ψDM due to his wave behaviour.

The motions and distribution of the observed luminous objects in these galaxies are totally dominated and defined by the dark matter potential wells. However, as the formed dark matter structures and their behavior are quite different for the different DM scenarios (CDM/WDM/ψDM), the distribution and motion of baryons will also be. Apart from the different haloes formation epoch and the filaments lifetime due to the initial cut-off of the power spectrum for the WDM/ψDM models, the wave behavior and the quantum pressures of ψDM provide different virialized DM halo structures. While for CDM and WDM cuspy profiles are expected (Navarro & Frenk, 1996; Lovell et al., 2014), in ψDM context, simulations of merging DM haloes clearly show the formation of solitonics structures at the de Broglie wavelength scale (Schive et al., 2014a; Mocz et al., 2017; Schwabe et al., 2016), even if these are more evident as we go lower in redshift, where large, more-spherically symmetric cores are formed embedded in filaments. In contrast to the early filaments fragmentation and cuspy haloes of CDM (see figures 2.14, 2.15 and 3.5). These simulations by Mocz et al. (2019, 2020), also seem to reinforce that the baryonic feedback has not a significant effect in these halos of $10^9 M_\odot$ to $10^{10} M_\odot$ in redshifts z>6, being unable to soft these cuspy profiles of CDM/WDM and discarding their possible transformation to a core. They conclude that baryonic feedback does not significantly alter the dark matter (Mocz et al., 2019, 2020).

Simulations by Mocz et al. (2020, 2019) confirmed that ψDM and WDM are practically identical to large cosmological scales, even with the presence of baryonic feedback. Both were also similar at small scales, having similar filaments behavior and structure, also producing a similar stellar formation in haloes and alongside the filaments, in contrast to CDM, where the earlier breaking of the filaments should avoid stellar formation in filaments. Moreover, the first stars should form in these filaments for ψDM/WDM rather than in the halos (Yoshida et al., 2003). Nevertheless, the global star formation in ψDM/WDM will occur quite later due to the delayed halo formation(product

o the small scale structure cut-off), being at z∼13, while in CDM will start at z ∼35. To be more precise, the quantum effects should also delay a bit the star formation in ψDM (z∼13) compared to WDM (z∼13.5). The star formation rate seems to be also smaller in ψDM/WDM, decreasing the possible disturbances of baryonic feedback, like supernovas, increasing the possibilities of being stars tracers of DM (See the hypothesis of section 3.3). Moreover, the simulations already proved that the baryonic gas is a good tracer of the dark matter density in the initial formation phases (Mocz et al., 2019, 2020), with a similar distribution of it in the intergalactic medium from WDM and ψDM. Making gas also follow the gravitational potential at large scales, limiting shock and cooling to unimportant roles in the ψDM context. This would be impossible without the quantum pressures that suppress the small scale structures formations, where the cosmic Jeans criterion avoids gas from collapsing in small scale structures (the Jeans mass is about$10^5 M_\odot$at z = 100 and $2 \times 10^4 M_\odot$ at z = 20 (Mocz et al., 2019, 2020)). In consequence, this initial suppression of the power spectrum limits the minimum dark matter halos that can form, making the baryonic objects look more smoothed and more homogenously distributed alongside the halos and filaments, being in good agreement with the dark matter density profile and therefore, tracing it (Mocz et al., 2019, 2020).

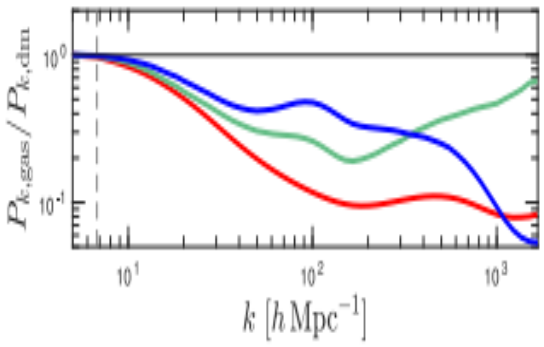

Figure 2.16: The ratio between gas and dark matter power spectrum in CDM (red), WDM (green), and ψDM (blue) remarks that baryons still can be traces of DM in ψDM context at z∼7. Credit Mocz et al. (2020).

On the other hand, that scenario is not expected for CDM, where the lack of the cut-off at small scales will allow baryonic formations at almost any scale, increasing the effect of baryonic feedback, and in sum, with the no minimum dark matter halo mass formation alongside with the quick filaments break, will produce a disengagement of baryonic density profiles with dark matter. A consequence of the not smoothed, extensive homogeneous baryonic-dark matter structures. The time where baryons should perfectly trace DM in WDM/ψDM, should endure from z=127 to z∼10, where baryons show the same lack of power at large frequencies(small scales) compared to CDM (due to the initial power spectrum cut-off). However, after the first halo formations and the starting fragmentation of the filaments, baryons should also start feel-

ing their own pressure, making their distribution not exactly to dark matter ones, but still partially tracking it (Mocz et al., 2019, 2020). The point why baryons really trace DM and still be imperfect tracers of DM at z=7 and later on is shown in figure 2.16, where simulations by Mocz et al. (2020) showed that the ratio between gas and dark matter is closer to unity at low frequencies(small values of "k"), than for CDM, showing a smoother distribution of the dark matter. Being also the one that stays closer to unity along the frequencies. The contrary effect is shown for CDM, where the less small-scale power for baryons allows them to feel the gas pressure earlier and stronger, making them not coupled to dark matter. So, in consequence, evidence of baryons tracing dark matter in actual galactic profiles should be irremediable evidence of ψDM (we will show the different examples of it in the results section 4).

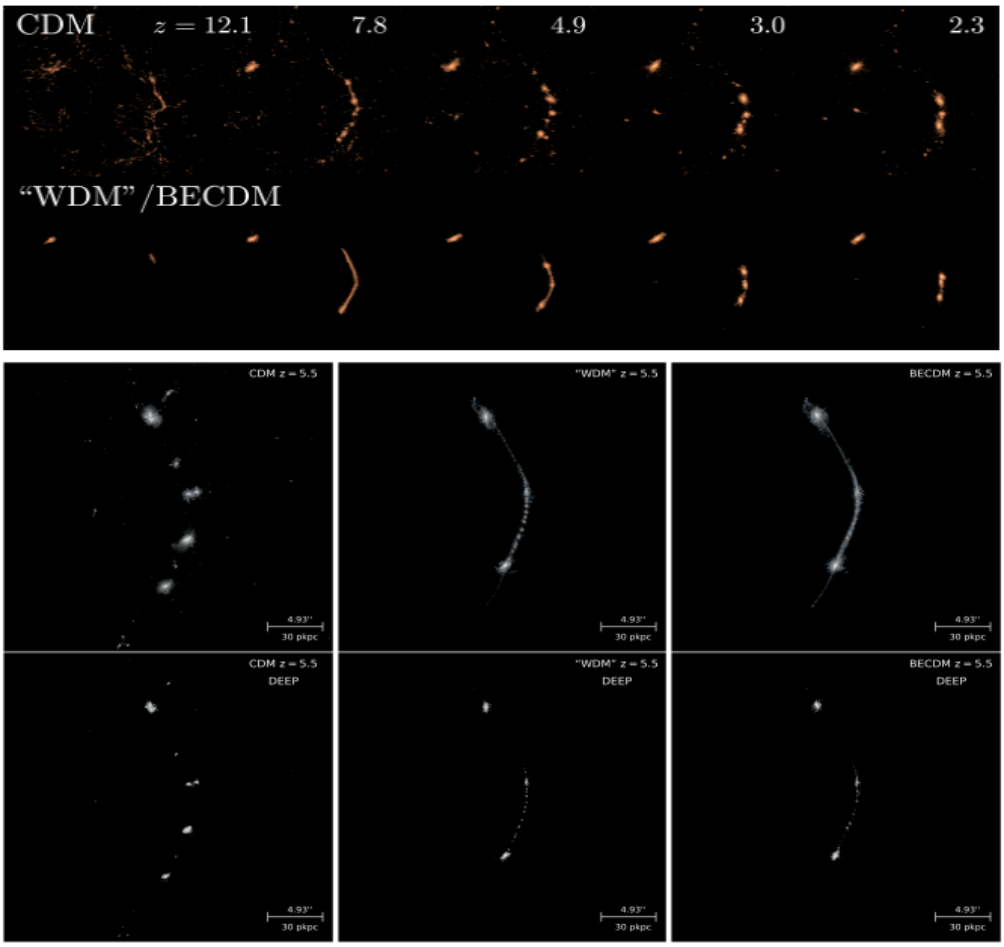

Figure 2.17: Evolution of the projected stellar densities for CDM and WDM/ψDM. Notice how for CDM, the stellar filaments have fewer stars, and they are almost totally accreted by the subhalos much earlier. For ψDM, stellar filaments are still a clear observable structure at z=5.5, with also some extended stars (possible remnants of these past full-filled stellar filaments) observable at z=2.3 for WDM, where similar results are expected for ψDM but still unable to do due to lack of resolution. Credit Mocz et al. (2020).

Finally, there are still some results in the simulations that strongly reinforce the stellar-DM tracer hypothesis. The distribution of gas and stars was clearly seen to have a cuspy profile for WDM/CDM, while in ψDM, stars seem to develop the solitonic core shape (Mocz et al., 2019). Moreover, by z$\sim$6, just half of the stars per unit volume are formed in low mass halos, indicating that they will be more embedded to DM due to their smaller own pressure and feedback. This lack of stars at such redshift also could indicate that the last stars formed in the filaments will be formed late enough to still see some of them in an extensive, distant position compared to the ones concentrated in the halo center (check figure 2.17). In order to test this last argument, a simulation was done until z=2.3 for WDM (Mocz et al., 2020) (looking to be similar for ψDM), with filaments finally being accreted into the haloes, but much more later than in CDM, and furthermore, with still some baryonic objects, primordially starts, in more extensive position and distant to the core as the imprint of these past stars full-filled filaments (check figure 2.17 and the hypothesis done in section 3.3).

Summary of cosmological formation differences between ψDM and CDM Mocz et al. (2020):

(a) ψDM stays filamentary much more time while in CDM filaments are fragmented into spherical subhalos

(b) ψDM forms fuzzy/smoother structures at small scales (few kpcs) due to quantum pressure

(c) ψDM forms solitons at the center of every halo(below the de Broglie scale) while CDM shows denser cuspy inner profiles

(d) In ψDM, the longer "survival" time of filaments makes the first stars born there before are fragmented, while in CDM, the early fragmentation of the filaments makes them born directly in the subhalos. This makes stars be distributed along the filaments, showing more extended stellar profiles than in CDM

(e) The distribution of stars and gas along the entire filaments exhibit central cores imprinted by dark matter. There is no equivalence in CDM

(f) ψDM halos show density granules, an interference pattern product of their wave behavior

(g) ψDM has a delayed stellar formation start compared to CDM, as well as a reduced formation rate. This suggests smaller baryonic feedback embedding stars more robustly to the dominating dark matter potential than CDM. Furthermore, these two points should have significant consequences on the reionization history and signatures of the universe.

Summary of cosmological formation differences between ψDM and WDM (Mocz et al., 2020):

(a) ψDM filaments show a quantum interference pattern while WDM show a caustic one

(b) The dark matter density profile stays cylindrical in the filaments and spherical in the solitonic cores for ψDM, while WDM has a cuspy central profile

(c) The dark matter cores are imprinted in the distribution of gas stars, both in filaments and halos. In contrast, gas and stars profiles are cuspy in WDM

(d) The star formation occurs a bit later for ψDM due to quantum potential (Δz$\sim$0.5), also reducing a bit the stellar formation compared to WDM.

2.1.4 The Ly-α forest challenge

The Ly-α forest is claimed to provide a constraint on the boson mass of ψDM that is significantly larger than the dwarf galaxy based estimated mass of 10^{-22}eV (Schive et al., 2014a,b). The larger the de Broglie wavelength, the lower would be the power spectrum of the forest below that scale. Due to the characteristic power spectrum cut-off of ψDM, would leave observable imprints in the structure of the intergalactic medium(IGM) at the scales probed by the Ly-α forest of distant quasars. This section will start by explaining the Ly-α forest concept, and its cosmological implication in the wave dark matter paradigm.

The Ly-α forest is the many narrow absorption lines that appear between the Lyman-α transition of the neural hydrogen at the redshift localization on the spectrum of the observed background, luminous object. These absorption lines occur due to the neutral hydrogen clouds located between us and the observed object. The different hydrogen clouds produce absorption lines at different redshifts as the universe expands. The ensemble of all these lines is known as the Ly-α forest, and it is located between the location where the absorption line will occur at a null distance(121,6nm), and the absorption line of the farthest cloud to us, so obviously, each line would represent a hydrogen cloud in the way that has absorbed the light that we are analyzing. So the Ly-α forest permits to analyze the characteristics of the intergalactic medium, the diffuse filamentary matter filling the space between galaxies, being a very useful constraint of DM properties on small scales (0.5Mpc/h$\leq \lambda \leq$ 20 Mpc/h) and high redshift regime (2$\leq \lambda \leq$5). This is due to the point that the thermal cut-off only limits the constraints of matter power spectrum in the flux power spectrum introduced by pressure and thermal motions of baryons in the photo-ionized IGM (Iršič et al., 2017a; Armengaud et al., 2017; Viel et al., 2005, 2013; Nori et al., 2019). Allowing us to measure the suppression in the matter power spectrum induced by ψDM.

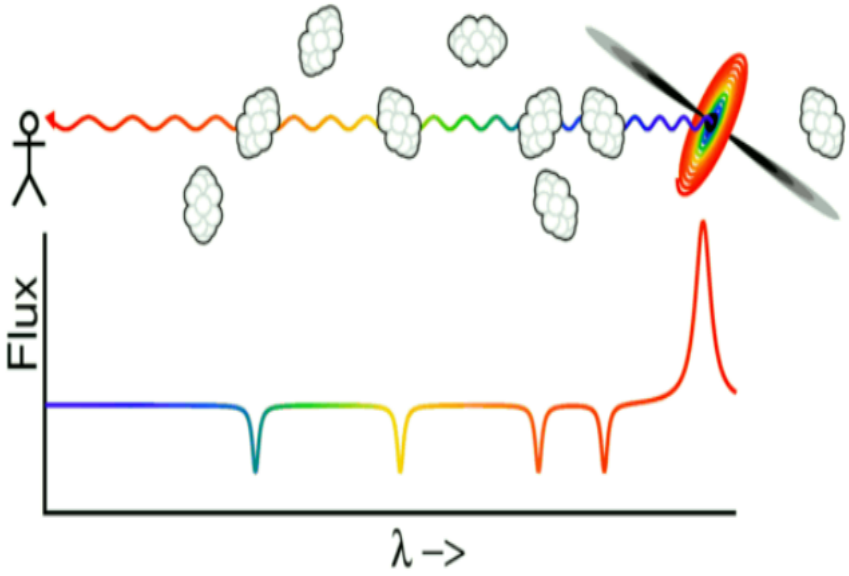

Figure 2.18: The observed Ly-α forest analysis for a distant quasar. Notice how different hydrogen clouds absorb his light at different redshifts, producing all the absorption lines of the forest. Credit Edward (2004).

So the Ly-α forest seems to be very useful to analyze the DM power spectrum at small scales, and the main difference between ψDM and CDM appears at those scales due to the wave-like nature of ψDM. on scales below the de Broglie wavelength and the Jean scale, the dominance of pressure should suppress small scale structures. For masses similar to 10^{-22}eV, this suppression occurs at sub-galactic scales, providing as a perfect target for the observations (Iršič et al., 2017a; Armengaud et al., 2017; Viel et al., 2005, 2013; Nori et al., 2019). This is due to the fact that for such axion masses, the resulting de Broglie wavelength and its quantum properties are large and strong enough to smooth the associated density fluctuations on the relevant small scales. One of the most implemented Ly-α forest observations, are the ones based on emissions from distant quasars by neutral HI in the intergalactic medium (IGM). These observations have longly claimed as an excellent high-redshift probe for spatial fluctuations of the matter density at comoving scales going down to $\sim$ 1-0.1 Mpc.

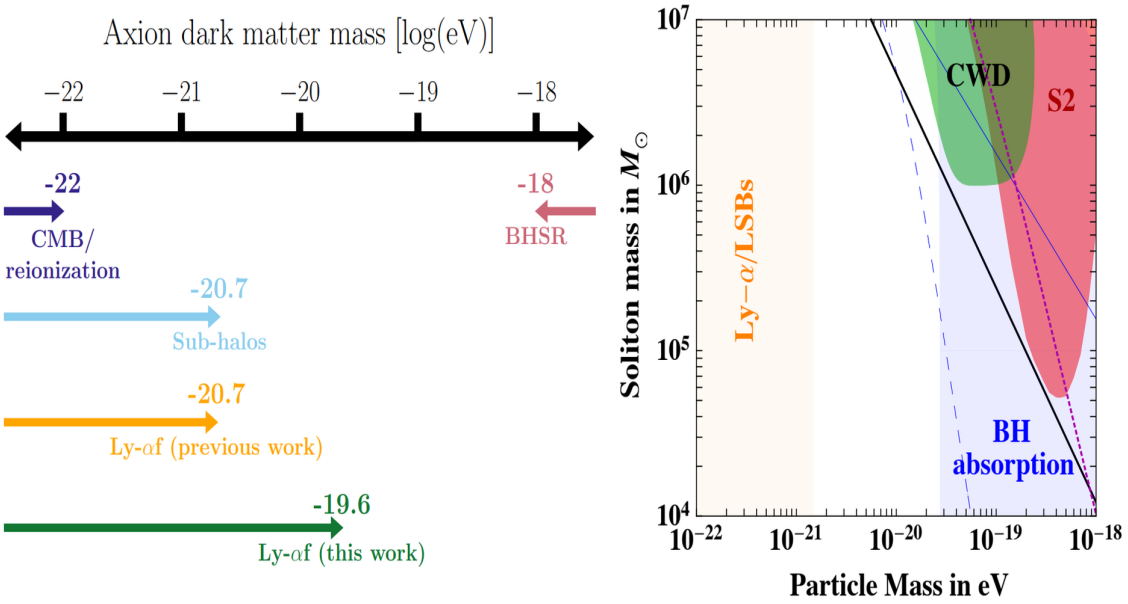

Figure 2.19: Different possible constraints for the boson mass. Important to remark that all these constraints have been estimated by analogy with warm dark matter's excess power in the forest clustering on small scale (few Mpc) with wave dark matter, as both have a mass cut-off, where they do not take into account the granular substructure and the mechanical feedback from stars and gas, which is clearly an important source for IGM turbulence and heating. Moreover, a narrow range of initial angle of θ, can alleviate the tension faced by the wave dark matter (Leong et al., 2019) **The left panel**: Compilation of possible excluded boson masses from different observational data. Axions of $10^{-33} \leq m_\psi \leq 10^{-24}$ eV are excluded by Planck (Collaboration et al., 2015, 2020a) cosmic microwave background (CMB) data (Hlozek et al., 2015; Hložek et al., 2018). A combination of the high-redshift UV luminosity function (Bouwens et al., 2015) and the optical depth to reionization (Spergel & Flauger, 2015) exclude axions of $m_\psi = 10^{-22}$ eV. The non-detection of supermassive black hole super-radiance (BHSR) excludes $10^{-18} \leq m_\psi \leq 10^{-16}$ eV (Arvanitaki, 2011; Stott & Marsh, 2018). The sub-halo mass function excludes $m_\psi \leq 2.1 \times 10^{-21}$ eV, while analyzes from the Lyman-alpha forest, exclude $m_\psi \leq 2 \times 10^{-21}$ eV. Axions below 2×10^{-20} eV are excluded by Rogers & Peiris (2021). Credit Rogers & Peiris (2021). **The Right panel**: Lyα constrains excluding $m_\psi < 10^{-21}$eV.Notice an extra more detailed exclusion of axions between $10^{-19} \leq m_\psi \leq 10^{-18}$eV, mainly product of (BHSR). Indicating that the soliton absorption time by the BH is smaller than the age of the universe Bar et al. (2019). The red region marks the constraint of the S2 orbiting star around the hypothetical soliton of the Milky Way while the green area represents the conflict with observations of a clockwise-rotating disk. Credit Bar et al. (2019). All these SMBH constraints will be explained deeper in section 2.1.5.

Constraints on the boson mass of ψDM have been claimed using the power spectrum of Ly-α forest clustering, by analogy with Warm-DM, assuming the transmission power spectrum of tenuous, highly ionized Hydrogen turns over at a scale set by the boson mass that has been assumed analogous to the turnover predicted by the free streaming scale of Warm-DM. Relatively high boson masses are inferred

this way, $\gtrsim 10^{-21} eV$, from the turnover scale observed in the forest in particular at $z > 5$ (Iršič et al., 2017a; Rogers & Peiris, 2021), which underpredict the kpc scale cores of dSph galaxies. These estimates do rely on several simplifying assumptions, including universal parameterizations for gas heating evolution and uniform UV radiation from star-forming sources after an instantaneous transition to reionization. It has been cautioned that plausible variation of these assumptions can accommodate Warm-DM with a colder, early IGM (Garzilli et al., 2017, 2021). Moreover, these analogues with Warm dark matter are in debate due to not taking into account the different matter power spectrum between ψDM and Warm DM, tha could critically change the results. In summary, these Ly-α constraints use models that only consider the cut-off in the initial power spectrum of dark matter and ignore wave effects like interference pattern fluctuations of the ψDM field which can add additional small-scale power.

We emphasize that forest predictions for Wave-DM are currently missing cosmological simulations incorporating gas hydrodynamics (firstly achieved by Philip Mocz (Mocz et al., 2017, 2018, 2019, 2020)), and that it is already clear that rich substructure is predicted at least for the DM in this context from the full density modulation caused by self-interference of the wave function on the de Broglie scale, pervading all galaxy halos and filaments (Schive et al., 2014a). This inherent substructure may be expected to affect the early gas distribution, particularly in the epoch before reionization is completed, where dense filaments predate galaxy formation in this context, the epoch of which is set by the boson mass. This early filament dominated era is expected to be similar for Warm-DM for which one detailed filament simulation exists, predicting that gas cools to very high density along DM filaments, with the possibility of early star formation (Gao & Theuns, 2007), which can therefore result in a "cosmic dawn" that is very different from LCDM. Furthermore, gas outflows and shocks are observed to be widespread at high redshift which can also be expected to enhance the variance in power on small scales in the gas. However, these are not included in the simulations relied on for Ly-α constraints, even for Warm Dark Matter. For Wave-DM, the distribution of the first galaxies will be more biased than for CDM, from the absence of low mass galaxies below the Jeans scale that is set by the boson mass (Schive et al., 2014b) and hence reionization is expected not only to be later than for CDM but with more significant spatial variance, enhancing the forest and 21cm power spectra. Empirical guidance is expected soon with deep JWST imaging into the era of reionization and also from 21cm mapping of early galaxies and filaments traced by stars and HI respectively.

There may be a gathering case for a significant AGN role in early reionization (Padmanabhan & Loeb, 2021) as implied by new high redshift $z \simeq 6$ detections of double peaked Lyα emitters (Hu et al., 2016; Bosman et al., 2020; Gronke et al., 2021). This adds to claims of unusually wide "gaps" in the forest at higher redshift $z > 5$ (Becker et al., 2015) and may be taken to indicate late and/or sparsely distributed sources of ionization (Gangolli et al., 2021). These observations lend support to the proposal that AGN are responsible for the bulk of reionization (Madau & Haardt, 2015), which would imply a different heating history and less uniform reionization, with possibly different conclusions regarding the interpretation of the

Lyman-forest power spectrum, especially on small scales.

Another heating source for the forest is gas outflows from galaxies that are observed to be ubiquitous at $z > 4$ in high-z surveys (Pettini, 1999; Frye et al., 2002), that will also act to increase spatial and velocity variance on small scales (Oppenheimer & Davé, 2006; Viel et al., 2013; Bertone & White, 2006) and may explain the apparent lack of damped Lyα absorption near massive high-z galaxies (Adelberger et al., 2005). General gas enrichment by these outflows may also be supported by the common presence of CIV absorption in the forest (Broadhurst & Scannapieco, 2000), now detected to the lowest detectable column densities with sizeable, $\simeq 0.1$, volume filling factors (Songaila & Cowie, 1996; D'Odorico et al., 2016).

If with further observations and simulations is it concluded that outflows and AGN heating do not significantly affect the scale or utility of the turnover in the Lyα forest transmission power spectrum for constraining boson mass, then it is still possible in the context of Wave-DM, with the dominant light boson considered here of $\simeq 10^{-22}$eV, to appeal to a larger initial field misalignment of the axion potential, which has been demonstrated to provide suitable excess small scale power to match the forest data(Leong et al., 2019) in the Wave-DM context. Additionally, it is also natural to consider adding a subdominant DM contribution from a heavier axion of $\simeq 10^{-20}$ eV to generate more small scale structure, and indeed this does account well for the newly appreciated DM dominated class of Ultra-Faint galaxies orbiting the Milky Way and perhaps also for the common presence of nuclear star clusters in all classes of galaxy (Luu et al., 2020). This multiple axion model is motivated by the discrete axion mass spectrum generically predicted by String Theory (Arvanitaki et al., 2010) which may lead to "nested" solitons (Luu et al., 2020) and will also boost small scale clustering of DM and gas to a level that may be predicted by future simulations (Hsu & Chiueh, 2021).

2.1.5 Supermassive black holes and Soliton accretion time

It is well known that almost all massive (not dwarf) galaxies host a supermassive black hole (SMBH) at their centers. This SMBH of millions of solar masses should dominate the central mass content and dynamics (Ferrarese & Merritt, 2000; Gebhardt et al., 2000). It has also been demonstrated that such SMBH mass is also related to many halo main characteristics, such as their total halo mass (Ferrarese, 2002; Bandara et al., 2009). Like the soliton, it is also directly connected with the total halo mass of a galaxy (section 3.1), the effect of these SMBHs in soliton densities has been recently analyzed (Davies & Mocz, 2020; Bar et al., 2019), where soliton's profiles were analyzed far away from the Schwarzschild radius, considering the SMBH a point mass inside the ψDM regime.

These two works conclude to limit the boson mass, getting a forbidden range of $10^{-22.12}$ to $10^{-22.06}$eV (from M87*, the SMBH of M87 galaxy) (Davies & Mocz, 2020) and from 2×10^{-20} to 8×10^{-19}eV(from Sgr A*) and $m_\psi \leq 4 \times 10^{-22}$eV (from M87*), in order to ensure soliton's lifetime in the presence of an SMBH (check the right panel of figure 2.19). These constraints were based on the possible produced effects of an SMBH in the well-known soliton-halo relation and in the soliton accretion time in the presence of an SMBH. However, they assumed that the soliton-halo relation should still hold in the presence of an SMBH, making the soliton mass unchanged by the SMBH. Even if the black hole's gravitational potential could reshape the soliton's density profile in certain cases. Nevertheless, they alerted that an inappropriate extrapolation of the soliton-halo relation could imply different results regarding boson masses and soliton surviving time(Bar et al., 2019).

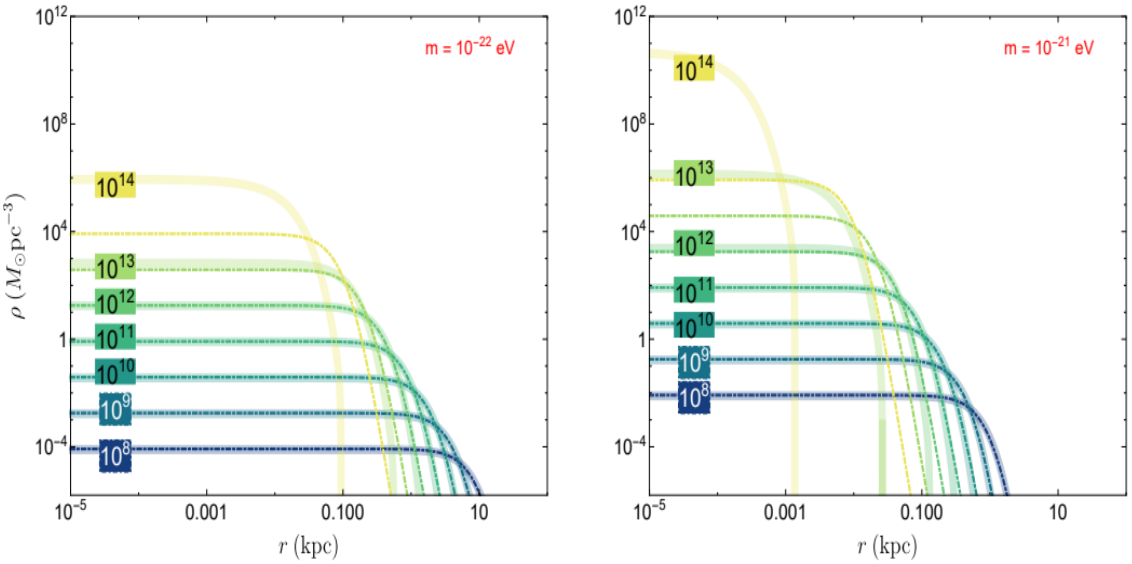

Figure 2.20: Effect of SMBH in different soliton's densities. Coloured dashed lines represent soliton's density profile while the shaded areas represent those profiles under an SMBH effects. Appreciate how the squeezing effect of the soliton increases along with bigger halo and boson masses. It is also appreciable how the soliton core scales inversely with black hole mass rather than the soliton mass. We must take into account how the solitons of galaxies below to $10^{11} M_\odot$ seem to be unaffected by the black hole for both m_ψ, precisely the M_h and m_ψ values analyzed in this work. Credit Davies & Mocz (2020).

Their simulations show that black hole's perturbation was only noticeable for halo masses bigger to $10^{13} M_\odot$ for $m_\psi = 10^{-22}$eV and for $M_h \geq 10^{12} M_\odot$ for more massive bosons of $m_\psi = 10^{-21}$eV. The black hole effect " squeezes" the soliton, raising its central density, producing at the same time a decrement of the core radius due to the direct relation between soliton mass and soliton radius. However, when the black hole dominates, this soliton radius decrement is inversely proportional to the black hole's mass, instead of the soliton's mass (Davies & Mocz, 2020).

The other important fact is the soliton accretion time, more exactly the time that the soliton can survive in the presence of a SMBH without being accreted. By the 'no-hair' theorem, the soliton cannot survive forever; the accretion timescale is given by Barranco et al. (2011):

$$t_{acc} = 5.6 \times 10^{18} \left(\frac{M_{\blacksquare}}{10^8 M_{\odot}} \right)^{-5} \left(\frac{m_{\psi}}{10^{-22} eV} \right)^{-6} yr \tag{2.11}$$

Where $M_{\blacksquare}$ is The mass of the black hole.

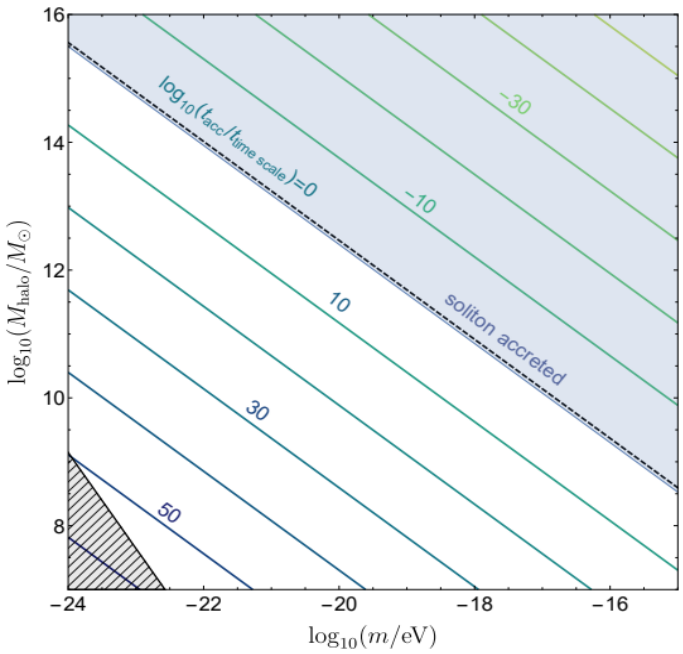

Figure 2.21: Soliton accretion time in function of the m_{ψ} and $M_h$values. The blue shaded area represents the solitons that would have already been destroyed in 10 Gyrs by the SMBH. Notice how the solitons of the galaxies analyzed in this work with m_{ψ} of $10^{-22} \leq 10^{-20}$eV and M_h of $10^8 \leq 10^{11} M_{\odot}$ have not seen their solitons accreted. Credit Davies & Mocz (2020).

The main thing to ensure is that the accretion time is longer than the two most crucial timescale factors; the age of the universe (∼14Gyr) and the re-condensation time of the soliton, to ensure that the soliton could survive until the present day. The total time was decreased to 10 Gyr in order to represent more accurately the time that the SMBH and the halo existed with similar masses to their measured values. In comparison, the re-condensation was already discarded to be relevant (Davies & Mocz, 2020). It is also known that black holes seem to grow exponentially with time, which would affect the possible surviving time of the soliton. All these calculations were made considering a constant mass for the black hole, where a possible less massive SMBH in the past would enlarge the surviving time of the soliton, due to being the accretion time a conservative (lower-limit) estimation(Davies & Mocz, 2020). Moreover, if the black hole grows across time, it will decrease its

possibility to break the soliton-halo relation, making it only possible at later times when the black hole really becomes a SMBH.

There have been some recent works that have shown the potential of SMBHs to constrain the viability of the ψDM model. For example, (Pantig & Övgün, 2022a) focused his analysis on the weak deflection angle, specifically in one of its applications; the formation of the Einstein ring. This work used realistic parameters from Sgr. A* and M87* to analyze the angular size of the Einstein rings due to the effect of a possible solitonic profile. A considerable deviation was founded for the light source near the SMBH compatible with the existence of a solitonic core, promoting it as a possible good experimental ψDM detection method. This deviation of the weak deflection angle seems to be bigger in the Schwarzschild case, implying that the soliton mass could be effectively added to the black hole's mass. The most observable effect of this join of the soliton mass with the SMBH mass is the increase of the photonsphere and shadow radii. It is also important to remark that this analysis was focused on solitons with a r_c proper for a boson mass of $10^{-23}\text{eV} \leq m_\psi \leq 10^{-21}\text{eV}$ (Pantig & Övgün, 2022a), the value postulated to resolve the small scale problems of CDM.

2.1.6 Axiverse

The string theory, in which the axions are a product of a potentially testable dynamical solution to the strong CP problem, also predicted the presence of a pin in which the axions are a product of a potential plenitude of light axions with different masses (Arvanitaki et al., 2010), known as the "Axiverse". This axiverse is predicted to be populated with axions of masses from 10^{-33}eV to 10^{-10}eV (Arvanitaki et al., 2010), which these axions have masses that should be distributed per decade. A dark matter model with a hierarchy of masses seems not difficult to believe since the standard model of particles follows the same way. Furthermore, some recent works suggested that the recent transition from decelerated to accelerated cosmic expansion is driven by an axion-like quintessence field with a subPlanckian decay constant, postulating them as a possible Dark energy source. Obviously, any observational evidence of such a wide population of axions would reinforce the Sting Theory postulations. Theoretically, the different populations would be responsible for different astrophysical features, being three of the main ones: First, axions with masses between 10^{-33}eV and 4×10^{-28}eV will be responsible for the constant polarization of the CMB, by an angle $\sim 10^{-3}$, quite close to the concluded one by observations $\sim 10^{-2}$ (Wu, 2009; Komatsu et al., 2009). Second, axions with masses from 10^{-28}eV to 10^{-18}eV seem to be a potential candidate for DM suppressing power in small scale(kpcs) density perturbations. Making ultralight axions with masses $\sim 10^{-22}$eV with axion decay constant, fa$\sim 10^{17}$GeV, ideal candidates for the ψDM model. Due to the Uncertainty principle, this kind of axions cannot be confined to a scale smaller than the de Broglie one, so this quantum "pressure" naturally suppresses any gravitational small scale collapse and generates rich structure

on the de Broglie scale (Schive et al., 2014a). Since the axiverse should contain a plethora of string axions with masses homogeneously distributed on a log scale, the existence of multiple steps in the small scale perturbation spectrum is a natural expectation (Arvanitaki et al., 2010). This may naturally generate a universe populated with different DM-dominated galaxies of different axion masses. Finally, axions from 10^{-22}eV to 10^{-10}eV can affect the dynamics, and gravitational wave emission of rapidly rotating astrophysical black holes through the Penrose superradiance process (Arvanitaki et al., 2010).

It has been recently suggested that if dark matter comprises ULAs (ultra-light axions), some DM over density regions should collapse into concentrated gravitationally bound objects of few pcs, known as miniclusters (Hogan & Rees, 1988; Kolb & Tkachev, 1994a, 1993). These miniclusters have already been analyzed in order to define their masses and densities via analytical and numerical N-body simulations (Kolb & Tkachev, 1994b; Zurek et al., 2007), implying a boson mass of 10^{-18}eV for the specific case of Tuc-47 (Emami et al., 2020). However, as we have already pointed out, the most direct observational consequence of these many light axion populations should be the presence of different DM-dominated dwarfs, each dwarf group as a product of a different boson mass. These DM dwarfs should be the product of ULA (ultra-light axion) axions. Moreover, such ULAs seem to be favored directly by string theory to be one of the most abundant axion populations, suggesting that most of the axions originating from the string axiverse would be of the ULA type ($10^{-23.8}$eV to $10^{-20.8}$eV) (Visinelli & Vagnozzi, 2019). Exactly the range that seems to be the candidate to form all the observed galaxies DM halos in the ψDM scenario (Schive et al., 2014a,b, 2016, 2020; Broadhurst et al., 2020; de Martino et al., 2017, 2020b; Pozo et al., 2020; Pozo & others., 2021a). Preliminary works already reinforced such boson value for dwarfs as a result of an observable soliton core mass-radius relation and indicated the existence of at least other two boson subpopulations of $\sim 4 \times 10^{-20}$eV, suggested by the star cluster of Eridanus II, and $\sim 6 \times 10^{-18}$eV proposed by Tucana's 47 clusters.

A significant feature of the Axiverse is that these ultralight axions of masses from 10^{-28}eV to 10^{-18}eV are viable and exciting dark matter candidates. In consequence, it would be interesting to study their possible observational signatures at cosmologically late times in order to see how those imprints could differ from other dark matter candidates; like laboratory searches for axion–photon conversion enhanced by resonance effects (Graham, 2015), or the point that the presence of a background axion population could lead axions decay into photons (Massó & Toldrà, 1997; Grin et al., 2007). Moreover, the presence of micniclusters formed as a consequence of ultra-light axions overdensity regions could imply observational consequences in current or future microlensing experiments, providing us with fundamental evidence of the ψDM dark matter model.

Constraints on this axiverse have already been examined in the context of the ψDM model, to evaluate whether there is evidence of more than one axion population (Luu et al., 2020). This work suggested possible boson masses by analyzing different solitonic dark matter structures in the Milky Way. With a boson mass of

$\sim 10^{-22}$eV already suggested as the primordial one in the galaxy formation and a lighter one of $\sim 10^{-20}$eV derived from the inner density profile of a nuclear star cluster (NSC) of $10^7 M_\odot$. A third possible mass was also discussed (0.5×10^{-18}eV) but with much less convincing data, not string enough as the one for the other two. It is important to remark that they also found that solitons produced by different axions have a negligible effect on each other, enabling the "soliton in soliton" structures in this axiverse scenario. The observed data, as well as the predicted results from the axiverse, where cosmological analyzes expect that the lighter scalar field is likely to have a higher density, suggest bigger densities for the lighter axions, making the axion of $\sim 10^{-22}$eV to be dominant (Luu et al., 2020). Along with this, the observed astrophysical data suggested that apart from the "soliton in soliton" structures, independent structures of the heavier axion of $\sim 10^{-20}$eV seem to be supported, making possible to explain the plenitude of different astrophysical structures as the consequence of a different population of axions. These data also coincided with the previously commented axionic cosmological prediction of the axiverse where the lighter axions should contribute more to the dark matter density, being the ones of $\sim 10^{-22}$eV the primordial ones, followed by $\sim 10^{-20}$eV with a negligible contribution from the heaviest ones of $\sim 10^{-18}$eV. All these results are supported and derived by the number of structures consistent with each axion population (Luu et al., 2020). Moreover, dynamics already show that the conversion from vacuum energy density to dark matter density is earlier for the heavier axion, making the axion density of the heaviest ones to be diluted earlier and, consequently, ending with a lower axion density.

This work firmly proposed after some Jeans-based dynamical calculations that the founded second heavier axion mass of $\sim 10^{-20}$eV was extremely required and consistent to describe the observed small-scale and high-density structures of the "Ultra Faint Galaxies" (UFDs) (Luu et al., 2020). We will show in section 4 that the data (soliton density and dynamical-based calculations) support at least two distinct axions differing by over one order of magnitude in mass. These small dense galaxies, with apparently small σ_{los}, seem quite difficult to be explained for the CDM model, where here are a natural result of the galaxy formation of just an alternative axion mass population. Their small structures, along with their small orbits, have been made to be proposed to be more like nuclear star clusters that have suffered powerful tidal forces, trying to relate them with the observed nuclear clusters found in the inner regions of the milky way, nevertheless even if possible, this axiverse interpretation is able to directly describe them just as a population of galaxies product of a heavier axion mass (Pozo et al., 2023; Luu et al., 2020). The presence of these solitons might be tested in the near future by using the pulsar timing residuals imprinted on millisecond pulsars detected at the Galactic Center (de Martino et al., 2017). Thousand of pulsars are expected to be detected with the SKA, and the presence of them in the center of galaxies, as well as in the nuclear star clusters, will possibly provide indistinguishably imprints like the ones suggested by Luu et al. (2020);" distinctive multi-frequency timing residuals on the respective Compton time scales of these independently oscillating scalar fields, of a few hours and a few months corresponding to $\sim 10^{-20}$eV and $\sim 10^{-22}$eV respectively". Moreover, in ψDM, the coherent oscillations of the field lead to the suppression of the

dark matter small scales structures, as the product of the power spectrum small scale structures cut-off that distinguishes ψDM from CDM could be used to constraint the contribution and abundance as well as the existence of any axion population, as the set scale limit will be a direct result of the de Broglie wavelength that is at the same time established by the axion mass. Depending on the axion mass, this scale can affect observed CMB anisotropies, galaxy clustering, and weak lensing power spectra (Marsh et al., 2013).

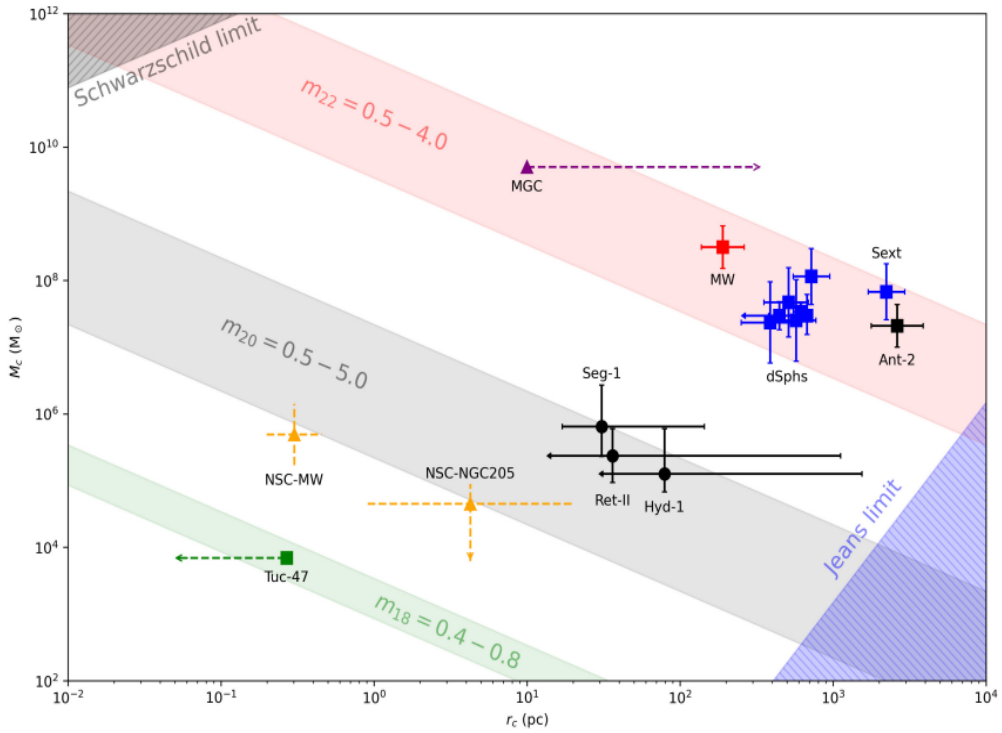

Figure 2.22: Soliton mass Vs. Core radius : Figure from Luu et al. (2020) that directly derives the boson mass for each analyzed astrophysical structure by their expected soliton mass and core size. Notice how each astrophysical structures seem to be part of a product result of different axion masses, with classical dwarfs as the result of a boson mass 0f $\sim 10^{-22}$eV, ultra-faint dwarfs, and nuclear star clusters $\sim 10^{-20}$eV and an extra possible population of $\sim 10^{-18}$eV suggested by the Tuc-47 globular cluster. Each possible axion mass value is represented with the colored shaded bands. Credit Luu et al. (2020).

It is important to me to remark that the existence of the Axiverse would also have important repercussions in the previously explained Ly-α constraints. The existence of many axion populations would imply many different de Broglie sizes and in consequence, many different impacts in the observed Ly-α constraints. Moreover, the proportion of each population in the total axions amount will also be a crucial point to anybody with the intention to do a good constraint, and the lack of knowledge of it will make any study not reliable enough.

2.2 Dwarf Galaxies

Galaxies with stellar masses in the range $10^{4-9}M_{\odot}$ are normally classified as dwarfs (McConnachie, 2012; Javanmardi et al., 2016). These galaxies are mainly divided into two groups: Dwarf spheroidal galaxies(dSph), characterized by their small sizes, low luminosity, little dust, and old stellar population, and elliptical galaxies with very poor recent star formation and even lower amounts of dust, gas, and luminosity. Nevertheless, some new kinds of "dwarfs" (their cataloging is still in debate) have seemed to be detected in recent years. The extremely low in size "ultra-faint galaxies" and the extremely extended ones known as "ultra-diffuse" share an incredibly high lack of stars and luminosity values. As these kinds of galaxies are few in stars and ordinary matter, they are assumed to be dominated by dark matter despite their high-velocity dispersions. Making them the ideal guinea pigs to test DM theories. In this section, we will briefly describe each of these types, noting the different contributions of each one to test ψ DM observationally.

Dwarf galaxies are known to be very dark matter dominated objects with central velocity dispersions of $\sim 10kms^{-1}$ instead of the expected value of $1kms^{-1}$ for self-gravitating systems of the same luminosity and scale radius $\sim$ 100 pc at equilibrium (Mateo, 1998). Even if they can be dwarfs of luminosities of several orders of magnitude of difference, they all show similar velocity dispersions values, suggesting that they are proportionally dominated by similar dark matter distributions (Haslbauer et al., 2019). In the past decades, it has been strongly demonstrated that dwarf galaxies favor central core profiles instead of cusps(Carignan & Freeman, 1988; Carignan, 1989). The first evidence came out in 1988 when the measured HI rotation curve of the dwarf irregular galaxy DDO 154 (Carignan & Freeman, 1988) was best fitted by a cored profile of $\sim$3kpc. In addition, the ultra-faint galaxies show half-light radiuses of a few kpcs that fit better with a core than with a density cuspy profile, leaving all the possible CDM hopes in the effects of the baryonic feedback(Torrealba et al., 2019). In contrast, the ψDM model is able to explain all these dwarfs' characteristics naturally.

2.2.1 Classical dwarf spheroidal (dSph)

Understanding dwarf galaxies' structure and behavior is crucial to for an understanding of the evolution at the low-mass end of the galaxy mass function and the DM properties at small scales. In the Local Group (LG), most dwarfs seem to be dSph, with small sizes compared to their hosts, the Milky Way and Andromeda and masses between 10^9 and $10^{10}M_{\odot}$. With $\sigma_{los} \sim$ 10km/s these poor-gas galaxies have been almost universally claimed to be dominated by DM (Mateo, 1998; Łokas, 2009; Walker et al., 2009). Their vast stellar population diversities have also been recently claimed to be an important test to reinforce the presence of a soliton, where

the called "relaxation" phenomenon should make different observations in each stellar population that are still in test (Bar-Or et al., 2021; Niemeyer, 2020). Moreover, the tidal imprint of the host in these galaxies is also to be detectable, where the ψDM tidal imprints differ from standard CDM, with some recent simulations and observations reinforcing the ψDM predictions (Schive et al., 2020; Du et al., 2018; Pozo et al., 2020; Pozo & others., 2021a). Detailed studies of the internal kinematics and chemical properties of the various morphological types of dwarf galaxies placed in different environments are crucial for identifying similarities and differences between these classes of systems (Kazantzidis et al., 2011), which can then be used to understand their evolutionary paths.

Although the tidal forces from the host could affect the internal dynamics of the galaxies significantly influencing observational results, there are a few confirmed isolated cases in the LG willing to be DM test ideal laboratories. Studying these isolated galaxies will drastically minimize the possible effects of tidal forces in their natural structures, allowing us to fully understand dwarfs' properties, internal dynamics, and the environment's role in their evolution. (Leaman et al., 2013; Kirby et al., 2014). The studies in these dwarfs seem to be the necessary window to resolve the small-scale issues of the ΛCDM paradigm. Tucana, an isolated galaxy whose star formation stopped a long time ago, is one of these examples between others as; Cetus, Leo A, Aquarius, Andromeda XVIII(Gregory et al., 2019; Taibi et al., 2018; Avila-Vergara et al., 2016; Hermosa Muñoz et al., 2017; Kirby et al., 2017)...

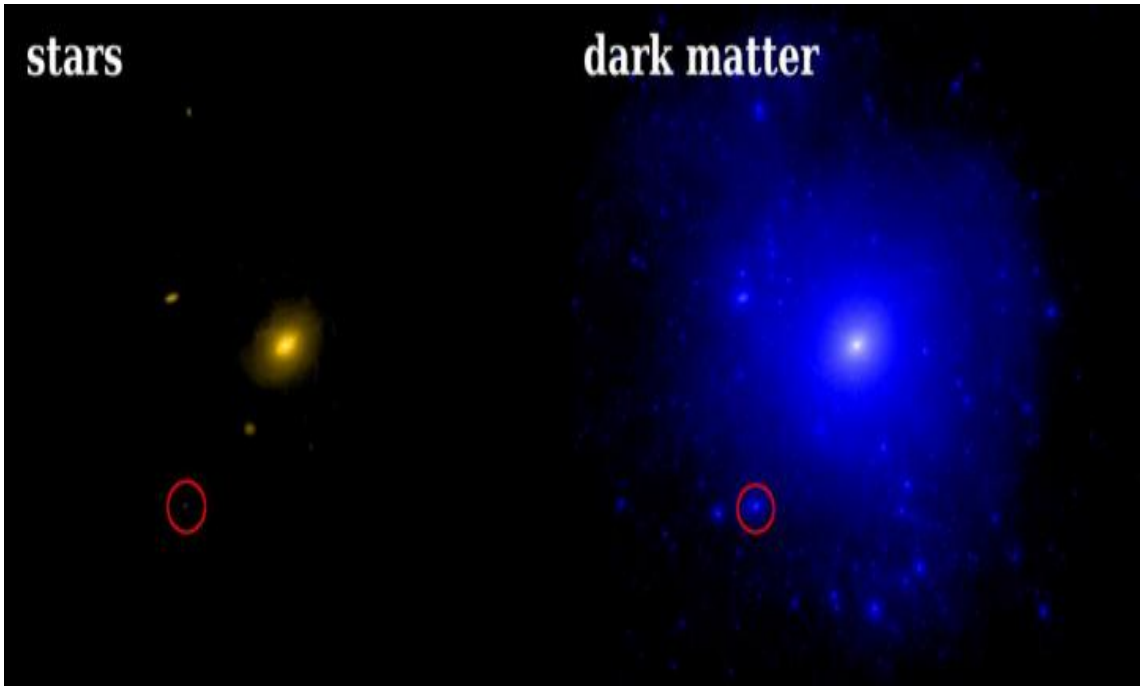

Figure 2.23: Comparation of the observed structure of a dwarf galaxy (left) and the hypothetical DM halo structure of it (right). Credit Wetzel (2016).

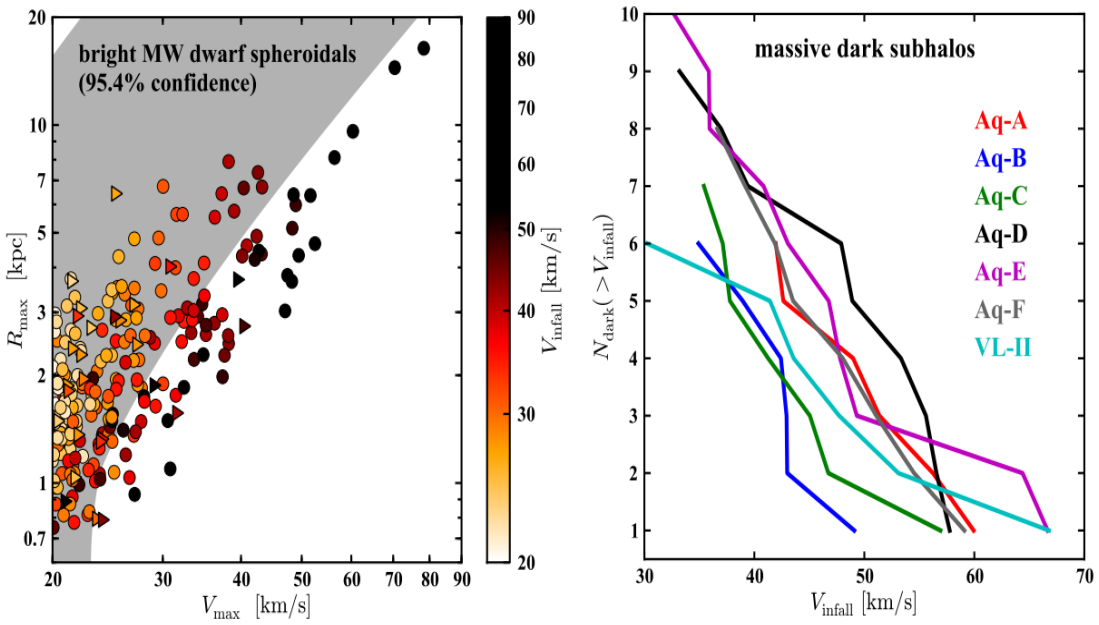

Figure 2.24: TBTF: Experimental and observational evidences to constrain that ΛCDM Milky Way halos are too dense to host any of its bright satellites ($L_V > 10^5 L$). **The left panel:** Simulated different possible halos of different galaxies, circles for Aquarius and triangles for VL-II. The colorized in terms of V_{infall}(peak circular velocities at infall) with a gray shaded area representing the 2σ constrain from the real Milky Way satellites. Notice how there is a high amount of halos that lie beyond the grey area, all of them being too dense to host any of the bright MW dwarf spheroidals. Credit Boylan-Kolchin & Bullock (2011). **The right panel:** Amount of dark halos with bigger V_{infall} values than > 30 km/s; the limited velocity to be consistent with any of the bright MW satellites. Notice how each simulated galaxy has more than six non consistent too dense halos. Credit Boylan-Kolchin & Bullock (2011).

Standard CDM expects galaxies with high density concentrated halos (Navarro & Frenk, 1996) with a central dark matter density $\rho_{DM}(150pc) > 10^8 M kpc^{-3}$ (Read et al., 2018, 2019). The observations in the last two decades had shown the inconsistency of these predictions, with denser values than observed. Being the two main issues the previously explained "cuspy-halo" and "missing satellites" problems. Simulated dark matter halos appear too dense to host the observed dwarf satellites of the Milky Way and Andromeda; a problem referred to as "Too Big to Fail" (TBTF), check figure 2.24 and section 2.1.2. This problem has been represented with some more extended halos than predictions in many of the LG dwarfs (Sohn et al., 2007; Sand & otehrs, 2010; Collins et al., 2019) and with lower density than predicted, like in Andromeda XIX's case (Collins et al., 2021; Ferrero et al., 2012; Caldwell et al., 2017). The inferred masses of most satellite dwarf galaxies within their half-light radii are also inconsistent with this prediction (Read et al., 2006b; Boylan-Kolchin & Bullock, 2011). Even if baryonic physics and environmental effects such as ram pressure, tides (Arraki et al., 2014; Brook et al., 2014), and energy injections from gas and stars Brooks (2013) have been postulated to alleviate the TBTF problem, the non obvious distinction between isolated and orbiting dwarfs seems not to fa-

vor that idea (Kirby et al., 2014). The results show that none of these minimally gravitational-ram pressure affected isolated dwarfs is denser than the densest LG orbiting galaxies, showing no obvious distinction in the velocity dispersion–half-light radius plane from the satellite galaxies of the Milky Way and M31. This is supported by (Kirby et al., 2014) computations, where they focused the TBTF problem in terms of the maximum circular velocity of a subhalo (v_{max}) and its radius when it achieved that circular velocity (r_{max}). Isolated and orbiting galaxies did not distinguish in σ_v, and r_h terms, parameters derived from v_{max} and r_{max} and that can be directly observed. This made them conclude that environmental-baryonic effects seem not to answer the TBTF problem.

In this context, consistency seems to be found with wave dark matter in several aspects, such as the fitting of the phase space distribution of stellar velocities and positions by (Schive et al., 2014a; Chen et al., 2017; Pozo et al., 2020), with results that approximate in good agreement with the soliton mass-halo relation (Schive et al., 2016). The haloes' tidal evolution (Schive et al., 2020; Pozo et al., 2020; Pozo & others., 2021a) and the non-so-dense extended halos Pozo et al. (2020). In summary, wave dark matter shows possible consistent answers to all these questions-issues that CDM cannot. As this is one of the main points of the work, it will be deeper explained in section 4.

2.2.2 Ultra Faint dwarfs (UFD)

Ultra-faint dwarf galaxies (UFDs) are considered the smallest not-failed galaxies in the universe, containing a few hundred to one hundred thousand stars. Due to their small size and luminosity, they repeatedly look like globular clusters. However, UFDs are much more dominated by DM and they have more extended profiles. The combination of the low amount of stars and high quantity of dark matter makes them the most dark matter dominated systems known, enlarging their possibilities to test DM behavior. Although their small size and faint light profile make them still difficult to analyze, requiring much more spectroscopy in the future. UFDs are also some of the oldest systems in the universe, thought to be formed only a few million years after the Big Bang and before the epoch of reionization.

It is now clearly established that these UFDs are also smaller, much less luminous and more metal poor than dwarf spheroidals. Some recent works also postulated that they might be a distinct population in ψDM, arguing to be the product of a different boson mass compared to classical dwarfs (Luu et al., 2020). This result goes in hand with the previously hypothesized natural wide axion population, "Axiverse", as a natural solution of the string theory (Arvanitaki et al., 2010). UFDs like Segue 1, Reticulum II, Carina II, Hydrus 1... seem clear to predict a higher boson mass product of their core-halo relation (Luu et al., 2020), with reasonable halos of$10^{8-9}M_{\odot}$ for Triangulum II and Draco II. These computations required the broadly claimed mass of 10^{-22}eV for dSphs, while the UFDs argued a higher mass

of 10^{-20}eV. This higher mass seems essential to explain their high densities in such small sizes, similar to our results and conclusions in this work, as described in detail in section 4.

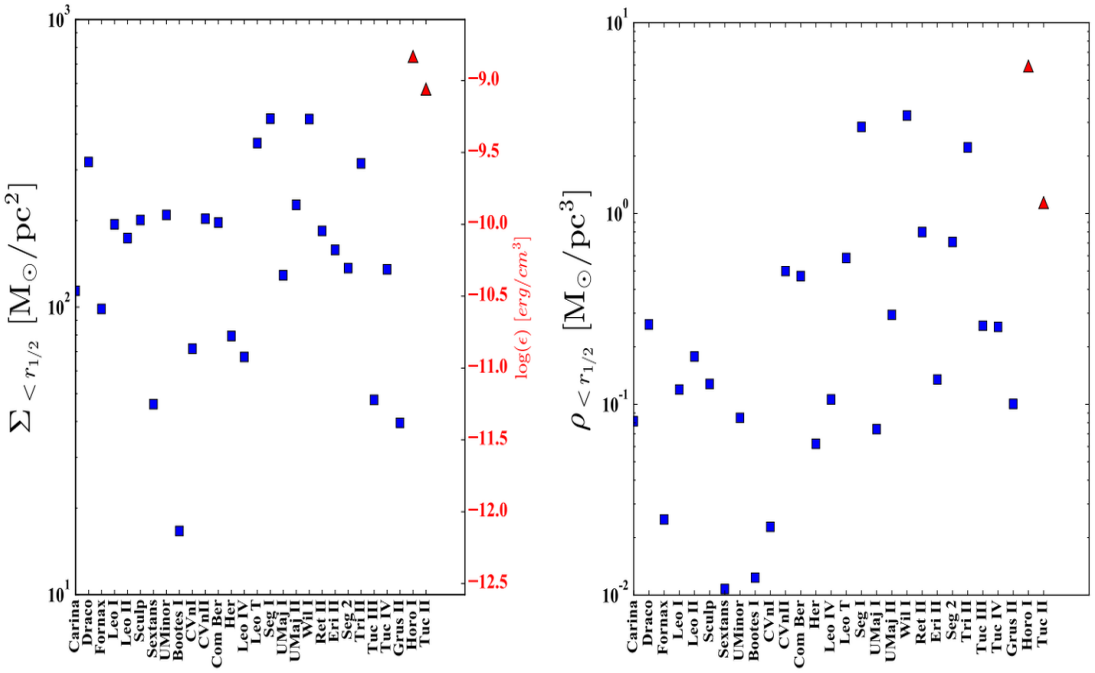

Figure 2.25: "Too-dense-to-be-satellite" problem: Blue squares are galaxies with their formation redshift and halo mass below the MW's line, and the red crosses are galaxies with estimated formation redshift and halo mass at formation close to the MW's assembly line. **The left panel**: Individual galaxy with its surface density within the half-light radius. Notice how the clearly shows the limit with halo masses and formation redshifts inconsistent with being an MW satellite. Credit Safarzadeh & Loeb (2021). **The right panel**: Same as the left panel but with the density within the half-light radius. Credit Safarzadeh & Loeb (2021).

Even if UFDs are expected to be a different group in terms of boson mass, the presence of the main issues of CDM as the "cuspy-core" and the "Too Big to Fail" problems indicate that the may not be very different from dSphs in structural characteristics. The "cuspy-core" problem is also found in these galaxies, with the non-disruption of a stellar cluster in the center of Eridanus II (Contenta et al., 2018), only possible with a cored profile as it was demonstrated for Eridanus I classical dwarf (Schive et al., 2020). At the same time, Tucana II recently showed a more extended DM profile than expected for UFD in the CDM context (Chiti et al., Chiti et al.). Even more, a new kind of CDM problem seems to arise in these galaxies, recently named the " Too-dense-to-be-satellite" problem, highlighted in particular by Tucana II and Horoligium I proportionally dense as MW. With surface densities above mean dark energy cosmic surface density $\sim \Omega_{\Lambda\rho_c c}/H_0 \approx 600 M_\odot/pc^2$ (Safarzadeh & Loeb, 2021). This point makes them simply to be too dense to be explained by standard CDM, with the enclosed density within the half-light radius being unreconcilable with their masses and formation redshifts (Safarzadeh & Loeb,

2021).

2.2.3 Ultra Diffuse galaxies (UDG)

UDG dwarfs are a recently discovered class of galaxies. Their principal characteristic is that they are relatively large in size, up to several Kpc in radius, but with very low surface densities of stars, with median magnitudes of 24 – 26 $mag/arcsec^2$, effective radii r_{eff} = 1.5 kpc – 4.6 kpc and dwarf-like luminosities of $\sim 6 \times 10^7 M_{\odot}$. They were first discovered in the Coma cluster in 2014 (van Dokkum et al., 2015). These new type galaxies seem not to be like the previously discovered low surface brightness galaxies (LSBs) because they do not lie in a star forming, gas-rich disk, but rather the opposite. Visually and structurally, the newly found galaxies resemble dwarf spheroidals. This last point has opened a considerable debate about the origin of UDGs, with three major hypotheses: Possible descendants of "classical" galaxies that have been altered within the cluster tidal field. Alternatively, “tidal dwarfs” systems formed during galaxy interactions and then lost to the cluster potential to exist in a transient, free-floating phase. A third possibility is that they are ancient, remnant systems, perhaps either a species of “peculiar dwarf” or “failed giant,” depending upon their total masses (Beasley et al., 2016). This last point will imply to be one of the most DM dominated systems in the universe, in order to explain their survival efficiency in these cluster environments (van Dokkum et al., 2015).

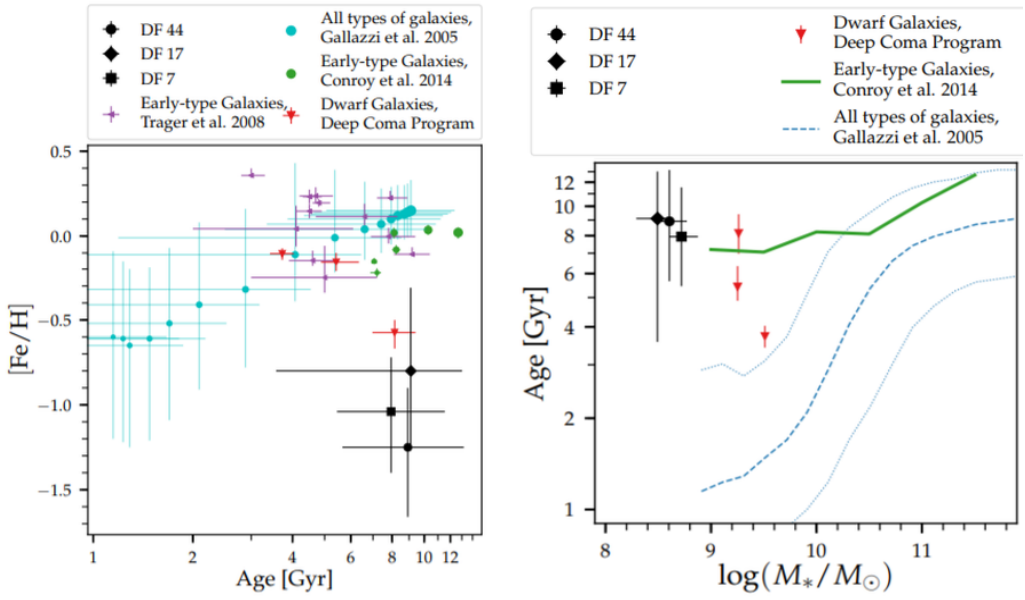

Figure 2.26: Ultra diffuse galaxies whose stellar characteristics clearly differ from other kinds of galaxies, reinforcing the idea of cataloging as a new type.**The left panel:** Stellar median [Fe/H] Vs age. **The right panel:** Stellar mass Vs age. Credit Gu et al. (2018).

The fully dark matter dominated UDG theory has been postulated in many works. One of the recently discovered UDG in the coma cluster, DF 44, seems to reinforce this fully DM dominated idea with a surprisingly large velocity dispersion of 44 km/s for its low stellar mass. Moreover, with a$M_{dyn}(< r_{1/2}) = 0.7^{+0.3}_{-0.2} \times 10^{10} M_{\odot}$ within its deprojected half-light radius of $r_{1/2} = 4.6^{+0.2}_{-0.2}$ kpc, and with a mass-to-light ratio of $M/L_I(< r_{1/2}) = 48^{+12}_{-14} M_{\odot}/L_{\odot}$. With a negligible gas contribution and a stellar mass of $M_* \approx 3 \times 10^8 M_{\odot}$ it was conclude to have a 98%(($M(r < r_{1/2}) - 0.5M_*)/M(r < r_{1/2}) \approx 98\%$) of DM within $r_{1/2}$ (van Dokkum et al., 2016). This would imply that some UDG could rely/exist on halos with baryon fractions below the cosmic average of 1%.

These UDGs dominated galaxies with wide extended halos, apparently contradict the expected concentrate CDM profiles but also the core-halo ψDM relation, as if they rely on halos of $10^{10} M_{\odot}$, the predicted small-concentrate soliton would challenge the observed wide structure. We will find the answer to it in section 4. Nevertheless, there is a special-extreme case of such extended profile, of an also DM dominated galaxy with a surface brightness ∼100 times lower than regular UDGs: Antlia-2. After tracking its stellar motions, it was clearly identified a considerable conflict with CDM, as in this case, the galaxy seems to have a relatively low mass despite its UDG size. Some works suggested that this galaxy would naturally result from a low mass wide soliton that naturally predicted the observed data. This rare case extremely favors the wave dark matter light boson paradigm. As we have already commented, a low mass halo should directly propitiate a wide low-density soliton (Broadhurst et al., 2020). Antlia-2 seems to be such an extreme case that even the ψDM model seems not to explain much wider galaxies, as antlia-2 is already in the lower limit of jeans scale permitted by the uncertainty principle for galaxy formations.

Chapter 3

Methodology

Here we will explain the halo structure of the previously introduced Wave dark matter paradigm in section 2.1.3. We will also highlight the main differences with the NFW cold dark matter halo structure of section 2.1.2. This cold, ψDM non-relativistic Bose-Einstein condensate halo structure was first explained by Schive et al. (2014a), where the main difference with CDM was appreciable at small scales, with gravitationally self-bound solitonic cores inside every galaxy surrounded by extended haloes of interfering density "granules". On large scales, the simulated dark matter distribution is identical, forming connected filaments and collapsed haloes form a large interference network voids (Schive et al., 2014a). The most distinctive ψDM prediction is the formation of a prominent solitonic standing wave at the base of every virialised potential, corresponding to the ground state "within every galaxy" , where an effective pressure matches the self-gravity of the condensate due to the Uncertainty Principle. The solitons found in the simulations have flat cored density profiles that have been shown to accurately match the known time independent solution of the Schrödinger-Poisson equation (Schive et al., 2014a,b, 2016), for which the soliton mass scales inversely with its radius. Furthermore, a scaling relation between the mass of this soliton and its host virial mass has been uncovered by the ψDM simulations, "the core-halo relation", $m_{soliton} \simeq m_{halo}^{1/3}$, such that a more compact dense soliton should be found in more massive galaxies (Schive et al., 2014b) and can be understood from the virial relation (Veltmaat et al., 2018). With denser and more concentrated solitons for more massive galaxies like Milky way galaxies than their own satellites' dwarfs. This core-halo relation seems to be universal in ψDM galaxy profiles with a few reasons that could explain certain breaks of it: Unrelaxed systems (for example, after major mergers), non-isolated systems (galaxies that have suffered high tidal forces from their host), massive halos (where the isothermal assumption may become invalid), non-negligible baryon mass around the center and strong baryonic feedback around the center. It is important to remark that the only free parameter is the boson mass, which we will emphasize in this section (Schive et al., 2014a,b, 2016).

The first simulations in this context have revealed a surprisingly rich wave-like structure with a solitonic standing wave core, surrounded by a halo of interference that is fully modulated on the de Broglie scale (Schive et al., 2014a). The solitonic core corresponds to the ground-state solution of the coupled Schröedinger-Poisson equations, with a cored density profile well-approximated by Schive et al. (2014a,b).

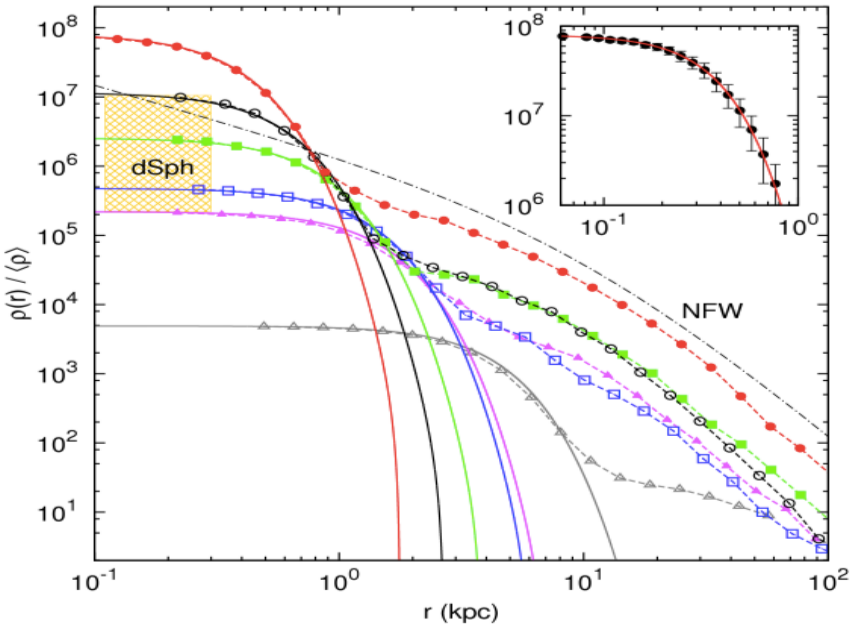

Figure 3.1: Radial density profiles of haloes formed in the ψDM model. Notice how all the galaxy profiles show a clear inner solitonic core (solid line) plus an outer NFW-like halo (dashed line) ψDM. These solitonic cores, which are gravitationally self-bound and appear as additional mass clumps superposed on the NFW profile, are clearly distinct from the cores formed by ψDM and collisional CDM, which truncate the NFW cuspy inner profile at lower values and require an external halo for confinement ψDM. This flat core structure is the main different characteristic from the other DM theories, as warm dark matter and the standard cold dark matter. Credit Schive et al. (2014a).

The simulations also show the soliton core is surrounded by an extended halo of density fluctuations on the de Broglie scale that arise by self interference of the wave function (Schive et al., 2014a) and is "hydrogenic" in the form (Hui, 2020; Vicens et al., 2018). These cellular fluctuations are large, with full density modulation on the de Broglie scale (Schive et al., 2014a) that modulate the amplitude of the Compton frequency oscillation of the coherent bosonic field, allowing a direct detection via pulsar timing (de Martino et al., 2017, 2020b). This extended halo region, when azimuthally averaged, is found to follow the Navarro-Frank-White (NFW) density profile (Navarro & Frenk, 1996; Woo & Chiueh, 2009; Schive et al., 2014a,b).

In a simpler way, the whole wave dark matter halo profile is a consequence of the evolution of the coupled Schröedinger-Poisson equation of section 2.1.3. Dividing the profile into the main two structures: the inner zone will be represented by a soliton (the spherical symmetric non-dispersive ground state solution in the Schröedinger-Poisson equation, below the de Broglie scale, where quantum pressure dominates) that would see his appearance like the NFW profile in the outer halo, represented by these fluctuating density granules resulting from the quantum wave interference, above the de Broglie scale (where gravity dominates and structure formation can

happen, check figure 3.2). It can be appreciated in figure 3.1 that 3D density distribution for Wave-DM has a granular lumpy appearance, which looks like NFW when it is azimuthally averaged the 3D in concentric annuli. This is fundamentally because Wave-DM is "cold". So the outer profiles of galaxy haloes possess a steepening logarithmic slope, similar to the NFW profile of standard CDM (Schive et al., 2014a). It is important to remark that this NFW-like halo profile for the galaxies' outer zone does not imply a central wave-like dark matter + a CDM outer halo profile fusion. However, due to the evolution of the coupled Schröedinger-Poisson equation at regions outside the soliton, the wave-like dark matter will naturally behave as the non-relativistic NFW cold dark matter halo, a product of being both cold. In summary, this certainly does not imply that the outer halo is made of CDM and the inner is wave-DM. It's all Wave-DM, and we can understand that the outer profile of Wave-DM should look like NFW, after averaging, due to the non-relativistic behavior in both cases.

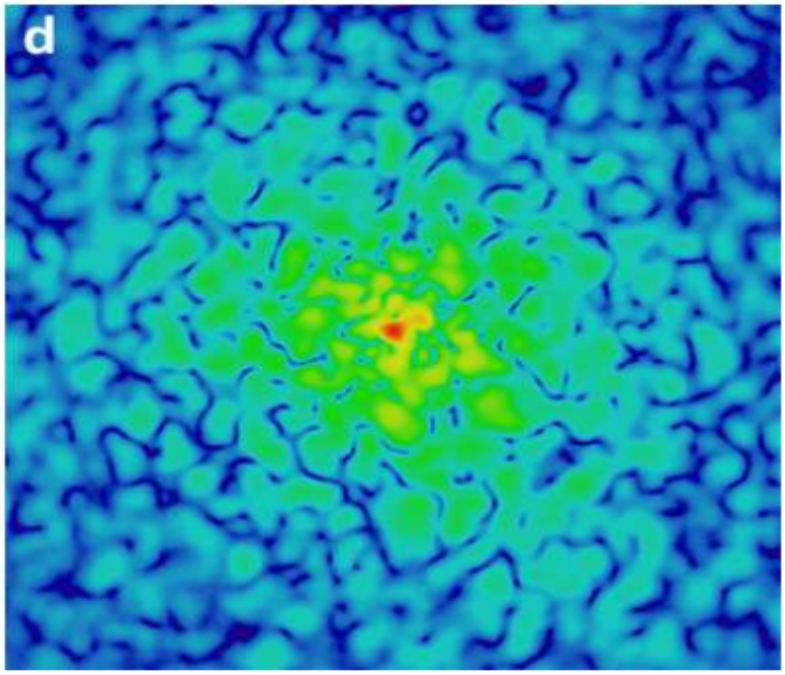

Figure 3.2: ψDM soliton-halo pair. Wave dark matter halo profile as a consequence of the evolution of the coupled Schröedinger-Poisson equations, with the soliton at the center as the ground state solution (below the de Broglie wavelength) and the density granules in the outer halo zone (above the de Broglie wavelength). These fluctuating density granules resulting from the quantum wave interference can be resented by the NFW CDM halo density profile due to their similar behavior, reflecting the non-relativistic nature of condensates beyond the de Broglie scale. Credit Schive et al. (2014b).

We have already pointed out that fluctuating density granules represent this NFW-like wave dark matter halo regime as a result of quantum wave interferences that are directly produced after the formation of many solitons and their subsequent mergers. Figure 3.3 shows this process; whereas solitons merge, they interfere

with quantum mechanics and create waves and interference patterns in the fluid. The support against collapse at small scales is provided by the quantum energy gradient that dominates over the classical kinetic energy. As can be seen, these ψDM soliton-halo pairs are formed after the mergers of many primordial wave dark matter solitons, evolving under the Schrodinger Poisson equations. Forming at the end, a DM matter halo with a solitonic core supported against gravitational collapse thanks to the quantum pressures, and an outer fluctuating density granules interference zone, perfectly described by an asymptotic r^{-3} NFW-like profile. In summary, figure 3.3 shows the formation process of the ψDM soliton-halo pair of figure 3.2. It is important to remark that even if less common, this ψDM core-halo structure can also arise after a large structure's halo formation (see figure 3.4).

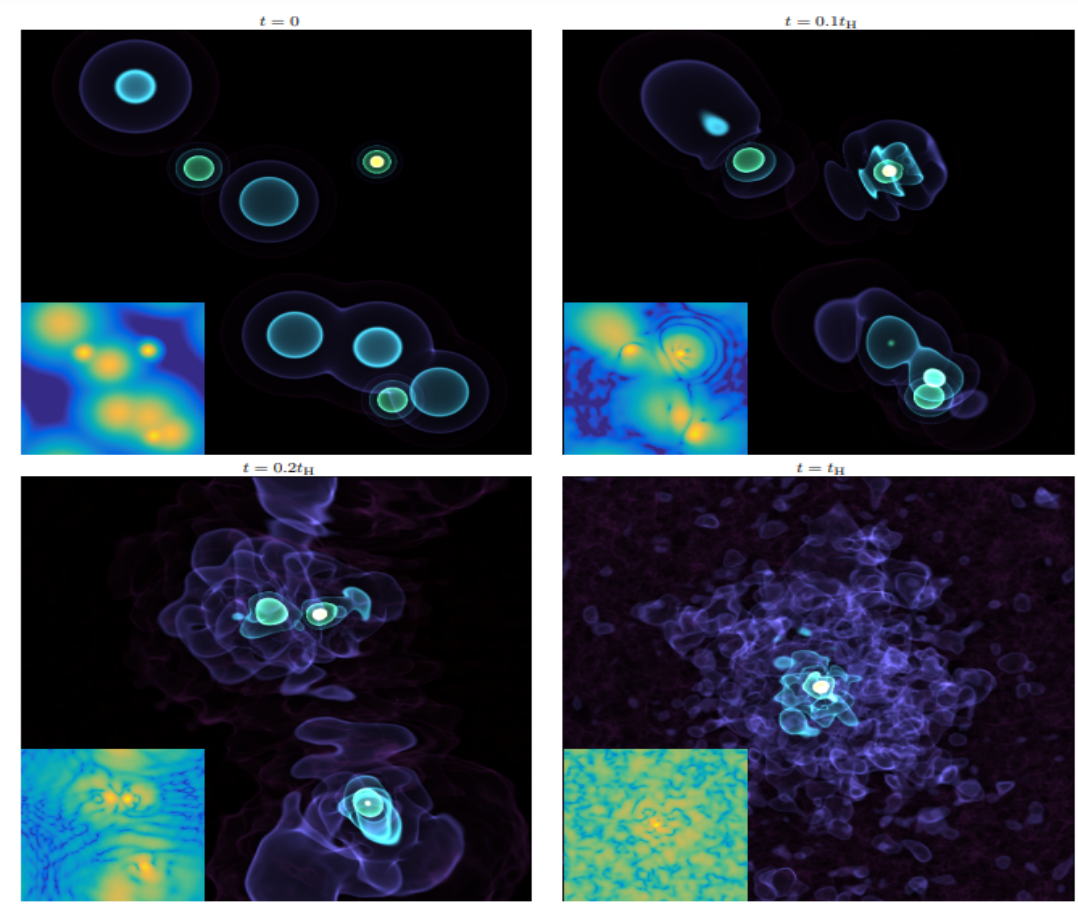

Figure 3.3: Solitons merger process: This figure shows the different phases of the merger of a sort of solitons across time. Notice how the ψDM soliton-halo pair is the final product of these mergers, characterized by the solitonic core. The soliton remains stable and supported against gravitational collapse and turbulence due to the dominance of quantum pressures against classical kinematics. At the same time, an NFW-like interference pattern regime is formed outside the soliton. In contrast, this last one seems to be turbulent due to the comparable quantum potential and classical kinematic energy. Notice how the small panel inside the right-low panel that show the final phase of these isolated solitons mergers, is exactly the ψDM soliton-halo structure represented in figure 3.2. Credit Mocz et al. (2017).

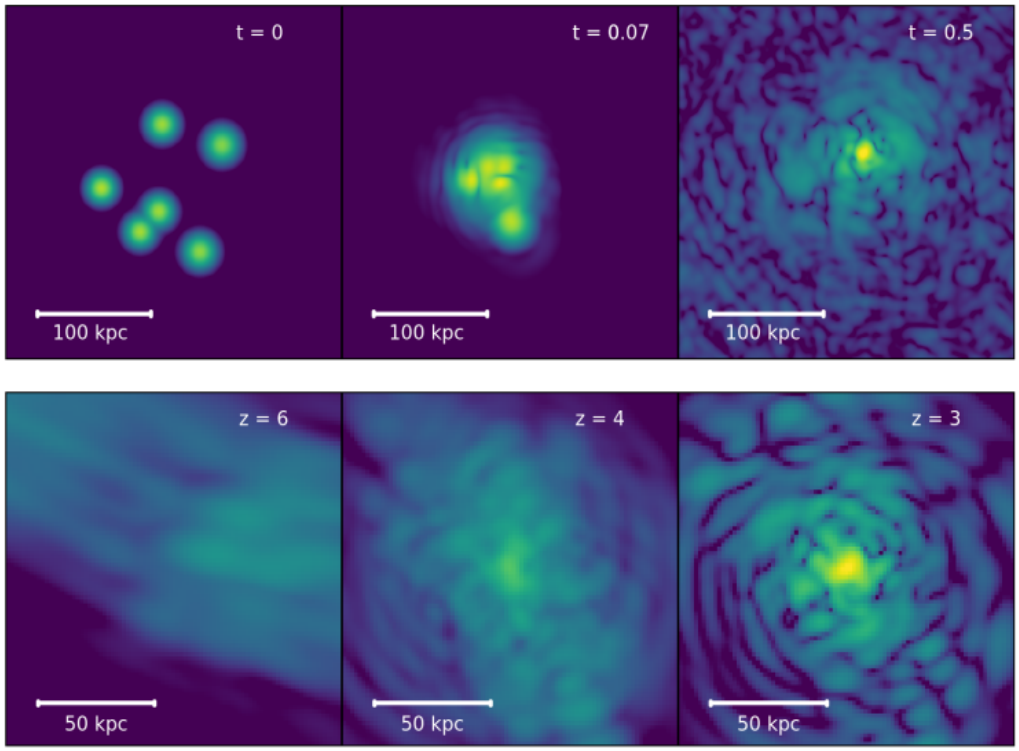

Figure 3.4: Solitons merger process Vs halo formation: This figure compares the time evolution of a core and the respective halo by soliton merger (top row) and a selected halo formation from the large-scale structure simulations by May & Springel (2021) (low row). Notice how for both cases, a stable core–halo structure can always be found at the end of all simulations. Credit Chan (2022).

The typical soliton size after this process is expected to be around 3.5 $\times r_c$ (Mocz et al., 2017; Schive et al., 2014a). However, as this value seems far from always correctly defining the transition point between the soliton and the NFW-like halo, it has not been previously fixed in this work (check equation (3.6), where r_t, the parameter that defines this transition point has not a fixed value). Beyond this transition point, the NFW-like density granules section is obviously found to be turbulent due to its wave interference pattern origin, in contrast to the soliton. The soliton seems to be protected until gravitational collapse at small scales thanks to quantum pressures, where solitons product of bosons with masses around 10^{-22}eV suffer a quantum potential that prevents the collapse below the de Broglie wavelength of few kpcs for such boson mass. Furthermore, this provides the soliton also to be protected against disruptions (being more robust against tidal forces than the halo, as we will see it later in section 3.4) and turbulent perturbations, which should start after the transition point, in the NFW-like halo regime (r^{-3}), where classical kinetic energies become comparable to the quantum pressures (Mocz et al., 2017). This quantum nature and turbulent r^{-3} NFW-like regime outer the solitons also explain the interference pattern of the cosmic web inside the ψDM context, where such turbulences are the product of the interference pattern created outside the soliton during the mergers, where the quantum pressure is not big enough to dominate the classical kinematic energy. Finally, his NFW-like halo regime is expected to evaporate (not bounded anymore to the soliton) after the system reaches

virial equilibrium, leaving the central soliton alone (Mocz et al., 2017).

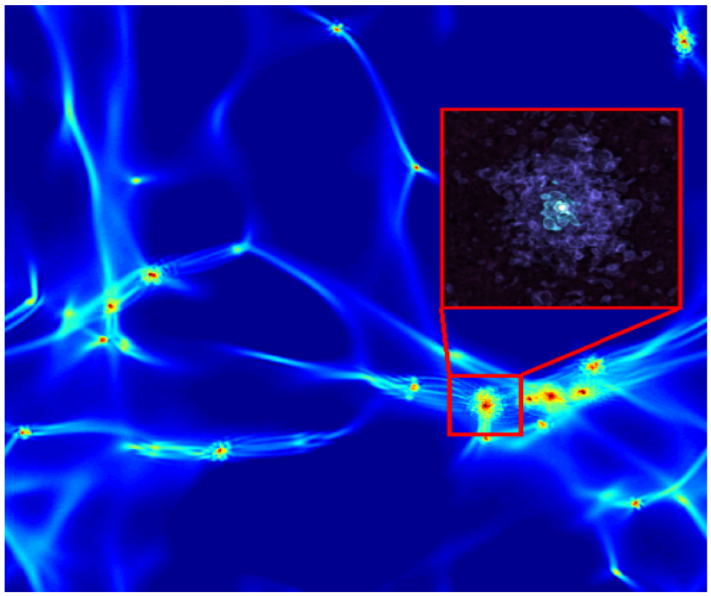

Figure 3.5: Combination of figures 2.10 , 3.2 and 3.3: In this figure we can see the location ψDM soliton-halo pair (figure 3.2) inside the large scale ψDM cosmic web (figure 2.10). Credit Mocz et al. (2020).

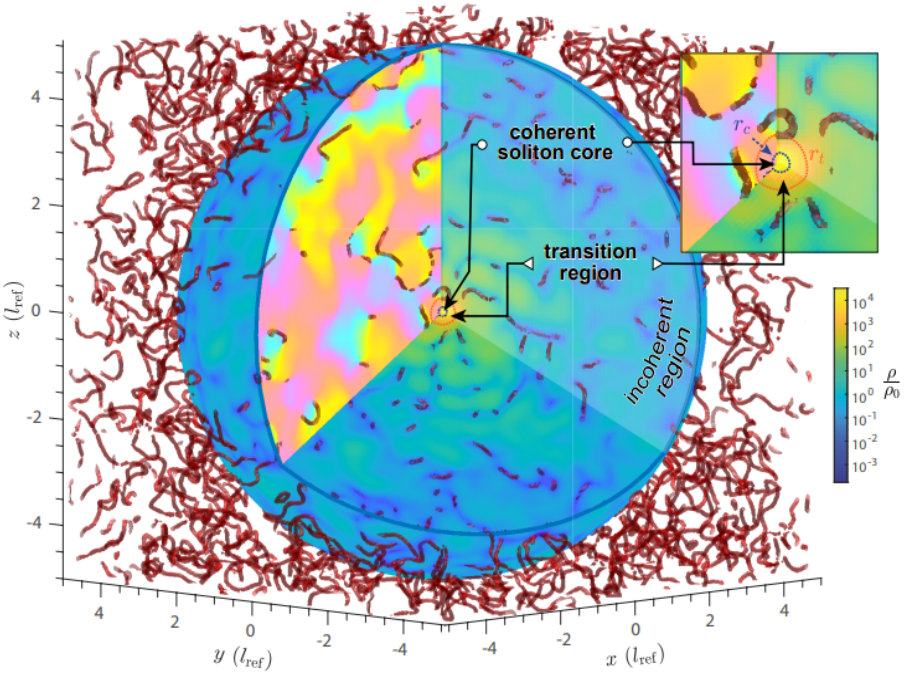

Figure 3.6: Structure of a ψDM halo: Visual representation of a ψDM halo with a soliton of r_c radius in the center and a clear representation of the expected transition point marked with a red circle of r_t radius. A color bar has been added to represent the different density values. The pink-blue-yellow zone and the red filaments are not of interest for this work. Credit Liu et al. (2022).

3.1 The Wave Dark Matter Halo

Ultralight bosons, such as Axions, explored in relation dark matter (Widrow & Kaiser, 1993; Hu et al., 2000) in their simplest version, without self-interaction, the boson mass is the only free parameter, which if sufficiently light means the de-Broglie wavelength exceeds the mean free path set by the density of dark matter, so these bosons can satisfy the ground state condition for a Bose-Einstein condensate described by the coupled Schröedinger-Poisson equation, that in comoving coordinates reads:

$$\left[i\frac{\partial}{\partial\tau}+\frac{\nabla^2}{2}-aV\right]\psi=0\,, \tag{3.1}$$

$$\nabla^2 V=4\pi(|\psi|^2-1)\,. \tag{3.2}$$

Here ψ is the wave function, V is the gravitation potential and a is the cosmological scale factor. The system is normalized to the time scale $d\tau=\chi^{1/2}a^{-2}dt$, and to the scale length $\xi=\chi^{1/4}(m_B/\hbar)^{1/2}\mathbf{x}$, where $\chi=\frac{3}{2}H_0^2\Omega_0$ where Ω_0 is the current density parameter (Widrow & Kaiser, 1993).

Recently, it has proved possible with advanced GPU computing to make reliable, high dynamic range cosmological simulations that solve the above equations, (Schive et al., 2014a; Schwabe et al., 2016; Mocz et al., 2017; May & Springel, 2021) that evolve to produce large scale structures indistinguishable from CDM, but with virialized halos characterized by a solitonic core in the ground state that naturally explains the dark matter dominated cores of dwarf spheroidal galaxies (Schive et al., 2014b). Another, important feature arising from simulations is that the central soliton is surrounded by an extended halo with a “granular" texture on the de-Broglie scale, due to interference of excited states, but which when azimuthally averaged follows closely the Navarro-Frank-White (NFW) density profile (Navarro & Frenk, 1996; Woo & Chiueh, 2009; Schive et al., 2014a,b).

The fitting formula for the density profile of the solitonic core in a ψDM halo is obtained from cosmological simulations (Schive et al., 2014a,b):

$$\rho_c(r)\sim\frac{1.9\ a^{-1}(m_\psi/10^{-23}\ \mathrm{eV})^{-2}(r_c/\mathrm{kpc})^{-4}}{[1+9.1\times10^{-2}(r/r_c)^2]^8}\ M_\odot\mathrm{pc}^{-3}. \tag{3.3}$$

where the values of the constants are: $c_1=1.9$, $c_2=10^{-23}$, $c_3=9.1\times10^{-2}$; m_ψ is the boson mass and r_c is the solitonic core radius. The latter scales with the product of the galaxy mass and boson mass, obeying the following scaling relation which has been derived from our simulations (Schive et al., 2014b):

$$r_c=1.6\left(\frac{10^{-22}}{m_\psi}eV\right)a^{1/2}\left(\frac{\zeta(z)}{\zeta(0)}\right)^{-1/6}\left(\frac{M_h}{10^9M_\odot}\right)^{-1/3}kpc \tag{3.4}$$

Which simulations show scales as halo mass (Schive et al., 2014b) in the following way:

$$r_c \propto m_\psi^{-1} M_{halo}^{-1/3} \,. \tag{3.5}$$

Where $a = 1/(1+z)$. Beyond the soliton, at radii larger than a transition scale (r_t), the simulations also reveal the halo is approximately NFW in form, presumably reflecting the non-relativistic nature of condensates beyond the de Broglie scale, and therefore the total density profile can be written as:

$$\rho_{DM}(r) = \begin{cases} \rho_c(r) & \text{if} \quad r < r_t, \\ \dfrac{\rho_0}{\frac{r}{r_s}\left(1+\frac{r}{r_s}\right)^2} & \text{otherwise}, \end{cases} \tag{3.6}$$

where ρ_0 is chosen such that the inner solitonic profile matches the outer NFW-like profile at approximately $\simeq 2r_c$, and r_s is the scale radius.

In detail, the scale radius of the solitonic solution, which represents the ground state of the Schröedinger-Poisson equation, is related to the size of the halo through the uncertainty principle. From cosmological simulations, the latter is found to hold non-locally, relating a local property with a global one (for more details we refer to (Schive et al., 2014b)).

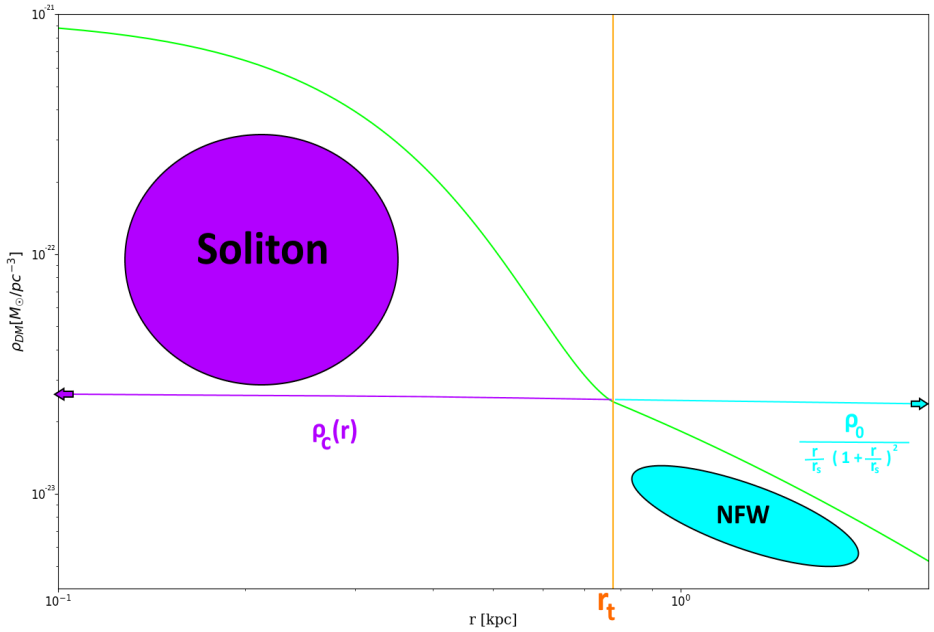

Figure 3.7: ψDM soliton-halo profile. Simple graphical representation of equation (3.6). The transition point (vertical solid orange line), differs the two main behaviors of ψDM, solitonic core below the de Broglie scale, and NFW like halo beyond it. The green solid line shows the 3D $\rho_{DM}(r)$ profile.

3.2 Dynamical Model of Galaxies in Wave Dark Matter Halo

The classical dwarf galaxies are known to be dominated by DM, and so the stars are treated as tracer particles (Gregory et al., 2019; McConnachie & Irwin, 2006; McConnachie et al., 2006; Kang & Ricotti, 2019) moving in the gravitational potential generated by DM halo density distribution.

In this context, assuming that the dwarf galaxies contain one or more pressure-supported stellar populations in dynamical equilibrium tracing the underlying dark matter gravitational potential, the dynamical mass distribution $M_{dyn}(r)$, which accounts for both the stellar and the dark matter distribution, is related to the stellar distribution through the Jeans equation, from which the velocity dispersion profile can be predicted by solving this spherically symmetric Jeans equation:

$$\frac{d(\rho_*(r)\sigma_r^2(r))}{dr} = -\rho_*(r)\frac{GM_{DM}(r)}{r^2} - 2\beta\frac{\rho_*(r)\sigma_r^2(r)}{r}, \tag{3.7}$$

where $M_{DM}(r)$ is the mass DM halo obtained by integrating the spherically symmetric density profile in Eq. (3.6), β is the orbital velocity anisotropy parameter of the stellar component (see Binney & Tremaine 2008J. & S. (2008), Equation (4.61))

$$\beta = 1 - \frac{\sigma_t^2}{\sigma_r^2}. \tag{3.8}$$

And $\rho_*(r)$ is the stellar density distribution defined by the standard Plummer profile for the stellar population:

$$\rho_*(r) = \frac{3M_*}{4\pi r_{half}}\left(1 + \frac{r^2}{r_{half}^2}\right)^{-\frac{5}{2}}. \tag{3.9}$$

Here, r_{half} is the half-light radius, and M_* is the stellar mass.

Thus, the gravitational potential is given by:

$$d\Phi_{DM}(r) = G\frac{M_{DM}(r)}{r^2}dr\,, \tag{3.10}$$

with a boundary condition $\Phi_{DM}(\infty) = 0$, and the mass enclosed in a sphere of radius r is computed as follows

$$M_{DM}(r) = 4\pi\int_0^r x^2\rho_{DM}(x)dx\,. \tag{3.11}$$

Finally, to directly compare our predicted dispersion velocity profile with the observations, we have to project the solution of the Jeans equation along the line of sight as follows:

$$\sigma^2_{los}(R) = \frac{2}{\Sigma(R)} \int_R^\infty \left(1 - \beta \frac{R^2}{r^2}\right) \frac{\sigma_r^2(r)\rho_*(r)}{(r^2 - R^2)^{1/2}} r dr \tag{3.12}$$

where

$$\Sigma(R) = 2 \int_R^\infty \rho_*(r)(r^2 - R^2)^{-1/2} r dr \,. \tag{3.13}$$

Here we simply assume that the stellar mass is negligible compared to the dark matter, given their high mass-to-light ratios, when testing dark matter models. Many of the Milky Way's dwarf galaxies' projected velocity dispersion profiles have been successfully fitted using a Markov Chain Monte Carlo method (Walker et al., 2009), being able to reproduce the kinematic data with both, cuspy and core density distribution. With no statistical evidence favoring one model over the other. Nevertheless, the Jeans model is affected by a degeneracy between β and the total halo mass (J. & S., 2008), giving unambiguous results about the dark matter parameters values. Two ways have been postulated in order to prevent or at least ameliorate the effects of this degeneracy: Information from multiple stellar populations (Walker & Peñarrubia, 2011; Zhu et al., 2016a,b), or higher velocity moments (Łokas & Mamon, 2003). Additional information about stellar populations would help to control the degeneracy but would not improve the constraints of the dark matter parameters. On the other hand, higher velocity moments seem to be more appropriate if proper motion measurements are available (Read & Steger, 2017; Webb & Vesperini, 2018). Fornax and Sculptor are good examples of it, where using kinematic data of their well known two distinct stellar population was enough to remove the degeneracy (Walker & Peñarrubia, 2011; Battaglia et al., 2008). Even if this result favored cored profiles, results from LSB (Hayashi et al., 2004) and late-type dwarf galaxies (van den Bosch & Swaters, 2001) seemed to be more consistent with cuspy ones.

3.3 Stars trace dark matter

Galaxies with low velocity dispersions $\lesssim 15$ km/s, indicating small masses, are classed as "dwarfs" with half of the stars detected typically within only $r_{1/2} \simeq 0.3$ kpc. So it is surprising that several low mass dwarfs are now known to possess large halos of stars and dark matter extending to over several kpcs, defying the dwarf definition. This includes two spectroscopically detected halos that are dynamically dominated by dark matter around the Tucana II and AndXXI dwarf spheroidal galaxies (Chiti et al., Chiti et al.; Collins et al., 2021). This adds to the case of

Crater II, a dwarf that extends to over 3 kpcs despite its very low velocity dispersion of $\simeq 3$ km/s and also the "ghostly" Antlia II of extremely low surface brightness extending over 4 kpcs with a dispersion of 6 km/s, discovered serendipitously using GAIA satellite proper motions (Torrealba et al., 2016; Collins et al., 2021). Such "large dwarfs" are at odds with the compact, high concentration profiles predicted for low mass galaxies in N-body simulations of standard heavy particle dark matter of cold Dark Matter (CDM), where dwarfs are predicted to have the highest internal density of dark matter of any galaxy, reflecting the relatively high universal mean density at earlier times when dwarf galaxies were first formed. In this CDM context, the extended halos of dwarfs have been qualitatively attributed to tidal effects induced by the Milky Way, or Andromeda (Torrealba et al., 2019; Collins et al., 2021; Chiti et al., Chiti et al.), based on simulations that show stars may be periodically stripped or shocked near pericenter to beyond the tidal radius, generating halo-like extensions of enhanced velocity dispersion, whereas the outer velocity dispersions observed in most dwarf halos appear to be significantly lower than in their cores (Wilkinson et al., 2004; Fabrizio, 2016; Collins et al., 2021). Strong tidal effects are expected for only a minority of orbiting dwarfs on eccentric orbits with small pericenters and so it is important to examine the generality of stellar halos to determine whether such halos are atypical or perhaps a common structural component of dwarf galaxies. Two such cases of the Milky Way dwarfs are definitively established to be in the process of being tidally stripped, namely the Sagittarius and Tucana III dwarfs which show opposing pairs of tidal arms (Li et al., 2018; Newby et al., 2013), representing only $\simeq 5\%$ of the dwarfs orbiting the Milky Way and both of these dwarfs have relatively small orbits.

In this context, we examine whether stars do trace dark matter for ψDM profiles. In particular, we test for the presence of a dense central soliton within galaxies and its imprint in the stellar profiles. Calculating the effect of such soliton on the stellar profile as a function of galactocentric radius. One of the key points is to identify the same core-halo relation explained in section 3.1 and figure 3.7, with the predicted substantial drop outside the soliton compared with the inside imprint and the change of regime between the soliton and the NFW-like halo.

In summary, we examine the following profile predictions:

1. Dark matter simulations as a Bose-Einstein condensate predict large halos surrounding a soliton core with a marked density transition at the core radius (Schive et al., 2014a,b).

2. Most relevant stellar profiles models, as Plummer and King, emphasize the cored shape of stellar density profiles (Plummer, 1911; V., 2016). Reveling an apparent similarity with ψDM profiles, where the central density also provides a core (Schive et al., 2014a,b):

   Both models have a mathematical expression to describe their rapid falloff of the density at large radii. More precisely, the point where the surface density

drops to half of its central value, is called the core radius. Just the same as equation (3.4), making us think that should represent the same physical characteristic, the product in this case of the more protagonist gravitational potential of the wave dark matter profile, making his imprint on the stars.

Plummer's model core radius (Plummer, 1911):

$$r_c = a\sqrt{\sqrt{2} - 1} \sim 0.64a \tag{3.14}$$

Where "a" for clusters and galaxies is the half-light radius, r_{half}, this model postulates a proportional core/half-light radius relation, being the core radius a bit smaller. Something that we will corroborate and reinforce in our results (See section 4.3).

King's model core radius King (1962); V. (2016):

$$r_c = \sqrt{\frac{9\sigma^2}{4\pi G\rho_0}} \tag{3.15}$$

Check pages 36-51 of V. (2016) and King (1962) for a detailed explanation.

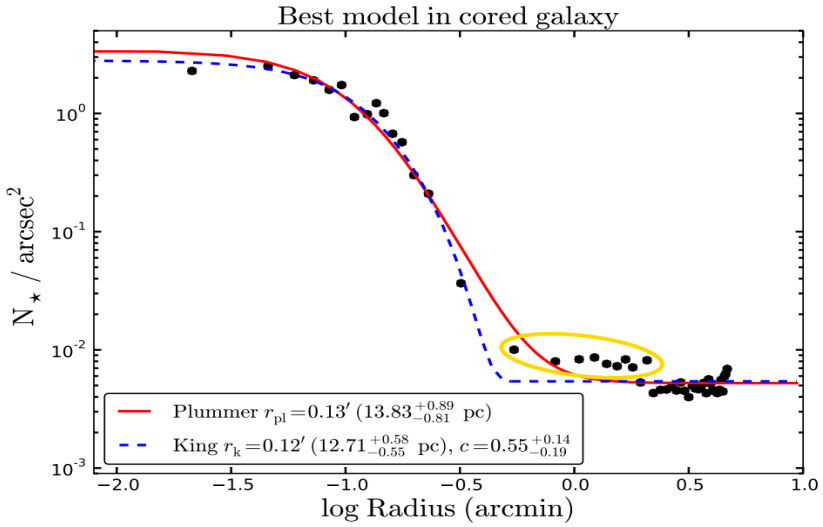

Figure 3.8: Plummer and King's profiles applied to Eridanus II's surface brightness profile. Notice the flat Central profile, coinciding with the soliton's prediction. Take into account how these two profiles rapidly fall to zero (here averaged to the background value) after describing the core, unable to describe the group of data points in the outer zone of the profile (yellow circle). Credit Contenta et al. (2018).

3. Most nearby classical dwarf galaxies are now known to be surrounded by large halos of stars extending to over 2kpc (Chiti et al., Chiti et al.; Collins et al.,

2021; Gregory et al., 2019; McConnachie & Irwin, 2006; McConnachie et al., 2006)

4. Clear transitions are also evident for most classical dwarfs that orbit the Milky Way, with pronounced amplitudes indicating significant tidal stripping as anticipated in ψDM simulations of orbiting dwarfs (Schive et al., 2020). Here we identify this predicted transition at a radius of $\sim$1 kpc in the stellar profiles of dwarfs.

5. The shallow slope of the observed halos accurately matches the tidal stripping simulation, something that we will extend in the results section.

   These first five points make us indirectly detect the ψDM imprint in the stellar profiles of the galaxies.

6. Notice that the stellar density profile, $\rho_*(r)$, is one of the "ingredients" of eq.(3.7), making the assumption that stars trace DM. Moreover, the well-accepted Jeans equation, realizes that the DM potential dominates in these dwarfs galaxies, assuming that stars' dynamics are dominated and traced by DM. So why not also assume that imprint, in stellar density profiles?

   A possible imprint of the soliton in the velocity dispersion profile will be analyzed in section 4.

7. As already commented in point 6 of list 2.1.3, simulations from (Mocz et al., 2019, 2020) show a very different behavior of baryonic matter in ψDM compared to CDM and WDM. In CDM, baryons follow DM imprint on scales larger than the filtering scale (the characteristic distance on which pressure acts), whereas on smaller scales, the gas is diffused by pressure. This does not happen in ψDM and WDM, where the filtering scale is below the cutoff scale of the initial power spectrum, vanishing pressure's effect. Making ψDM/WDM filaments able to collect gas along with their structure compared to the visible fragmentation that can be appreciated in figure 2.15. In summary, Mocz et al. (2019) simulations clearly show how gas profile traces ψDM while stars appear to be potential "detectable smoking-gun signatures of ψDM". These simulations also contradict the possible effect of baryons on the central dark matter structure, arguing that DM should dominate baryons. Moreover, even if supernova feedback and photo-heating of the UV background during reionization may influence the distribution of gas and stars, the ψDM/WDM filaments are dense enough to be entirely lit up by the first generation of stars even in the presence of sub-grid models for baryonic feedback. This main difference between CDM and ψDM where gas and stars should follow DM imprint also in the filaments should be only appreciable at high redshifts (potentially detectable by the James Webb Space Telescope (JWST)). As in lower redshifts, gravity should break these structures, bounding stars in more spherical objects (Mocz et al., 2019). Nevertheless, even at these low redshifts, stars

should be less concentrated in spherical objects than in CDM, with a still potential imprint of these past "full star-filled filaments", still conserving some stars. Something that could explain these observed extensive stellar halos represented in figure 3.9. These possible evidences probing that stars trace DM in ψDM (Mocz et al., 2019, 2020) have been already widely represented in this work in point 6, previous section, but we will try to sort them out here again:

(a) The filaments should endure for more time (should be appreciable at much lower redshifts) in ψDM, as the earlier formation of the first halos in CDM should start breaking these filaments earlier due to gravitational attraction. Moreover, the longer life of these filaments in wave dark matter will favor the formation of much more stars inside these filaments, making a great difference in the location and extension of stellar profiles in CDM and ψDM galaxies, as well as making baryonic objects look "fuzzier"/more smoothed than in CDM (Mocz et al., 2019, 2020), postulating them as excellent DM tracers in ψDM

(b) The global star formation in ψDM/WDM will occur quite later due to the delayed halo formation(product o the small scale structure cut-off), being at z$\sim$13, while in CDM will start at z $\sim$35. The star formation rate seems to be also smaller in ψDM/WDM, decreasing the possible disturbances of baryonic feedback, like supernovas, increasing the possibilities of stars being tracers of DM

(c) The simulations already proved that the baryonic gas is a good tracer of the dark matter density in the initial formation phases (Mocz et al., 2019, 2020). Making gas also follow the gravitational potential at large scales, limiting shock and cooling to unimportant roles in the ψDM context. In consequence, this initial suppression of the power spectrum limits the minimum dark matter halos that can form, making the baryonic objects look more smoothed and more homogenously distributed alongside the halos and filaments, being in good agreement with the dark matter density profile and therefore, tracing it (Mocz et al., 2019, 2020)

(d) The time where baryons should welly trace DM in WDM/ψDM, should endure from z=127 to z$\sim$10, where baryons show the same lack of power at large frequencies(small scales) compared to CDM (due to the initial power spectrum cut-off). However, after the first halo formations and the starting fragmentation of the filaments, baryons should also start feeling their own pressure, making their distribution not exactly to dark matter ones, but still partially tracking it (Mocz et al., 2019, 2020). The point why baryons really trace DM and still be imperfect tracers of DM at z=7 and later on is shown in figure 2.16, where simulations by Mocz et al. (2020) showed that the ratio between gas and dark matter is closer to unity at low frequencies(small values of "k"), than for CDM, showing a smoother distribution of the dark matter. Being also one that stays closer to unity along the frequencies.

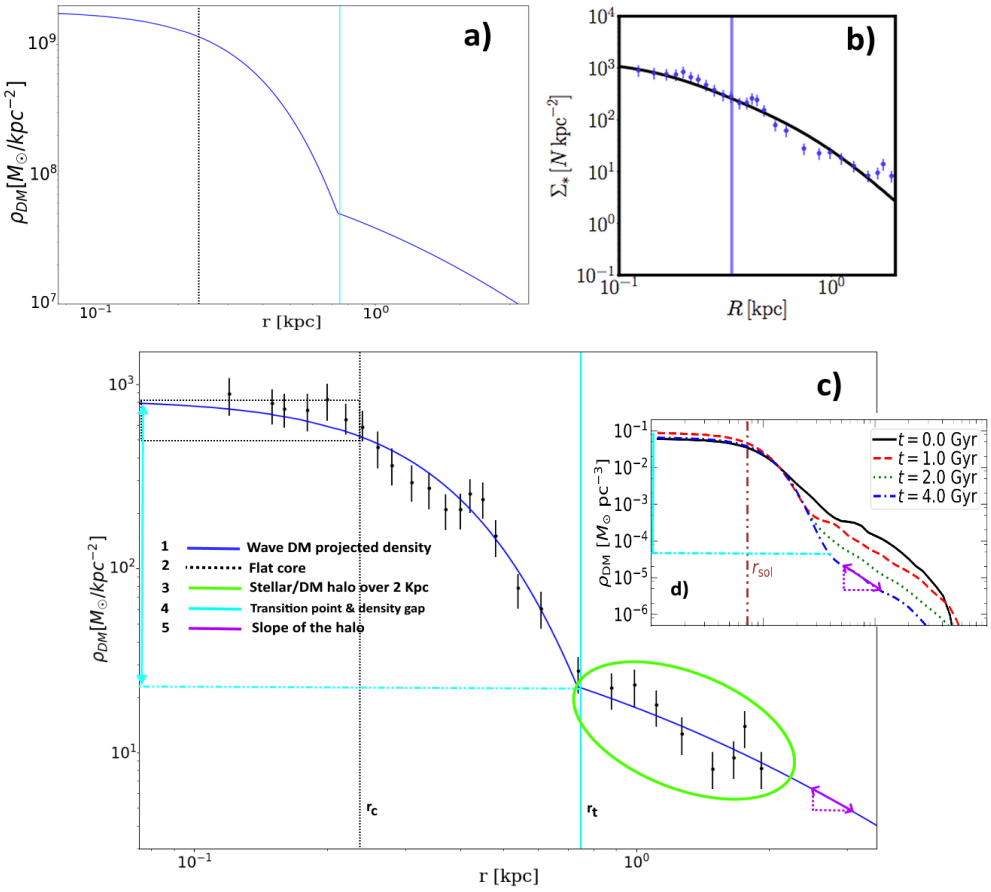

Figure 3.9: Graphical representation of the first five points that favor stars trace dark matter. Panel a: ψDM projected density profile (solid blue line). The vertical dashed lines represent the point where the surface density drops to half of its central value, the core radius. At the same time, the solid vertical cyan line shows the transition point from the solitonic regime to the outer halo. **Panel b:** Stellar radial profile of the isolated Tucana dwarf galaxy Gregory et al. (2019). Notice how the value of the DM density from panel "a" is much higher than the hypothetical mass that this stellar density profile will show, assuming that his gravitational potential would be negligible compared to DM's. **Panel d**: Simulation of a dwarf galaxy after suffering tidal forces in a ψDM context Schive et al. (2020). **Panel c**: Normalization of panels "a" and "b" in order to compare the DM profile with the stellar density. Notice how they match exceptionally well and how this makes sense with the arguments that stars trace dark matter (point 1). The stellar profile follows the flat core that ψDM reproduces (point 2), while the stars seem to expand over two kpc, contradicting the expected concentrated halos from CDM (point 3). The stars clearly seem to show the exact change of regime from soliton to halo, at r_t. At the same time, the density gap from the peak to this point seems to be higher for tidally stripped galaxies, coinciding with the independent simulations from Schive et al. (2020) (point 4). The slope of the stellar haloes seems to coincide with the simulations from Schive et al. (2020) (point 5, Notice that here panel "c" represents the density in 2D and panel "d" in 3D, so the slope comparison must be made in the exact dimensions for both). All these points will be deeper explained in section 4, especially 4 and 5.

(e) The distribution of gas and stars was clearly seen to have a cuspy profile for WDM/CDM, while in ψDM, stars seem to develop the solitonic core shape (Mocz et al., 2019)

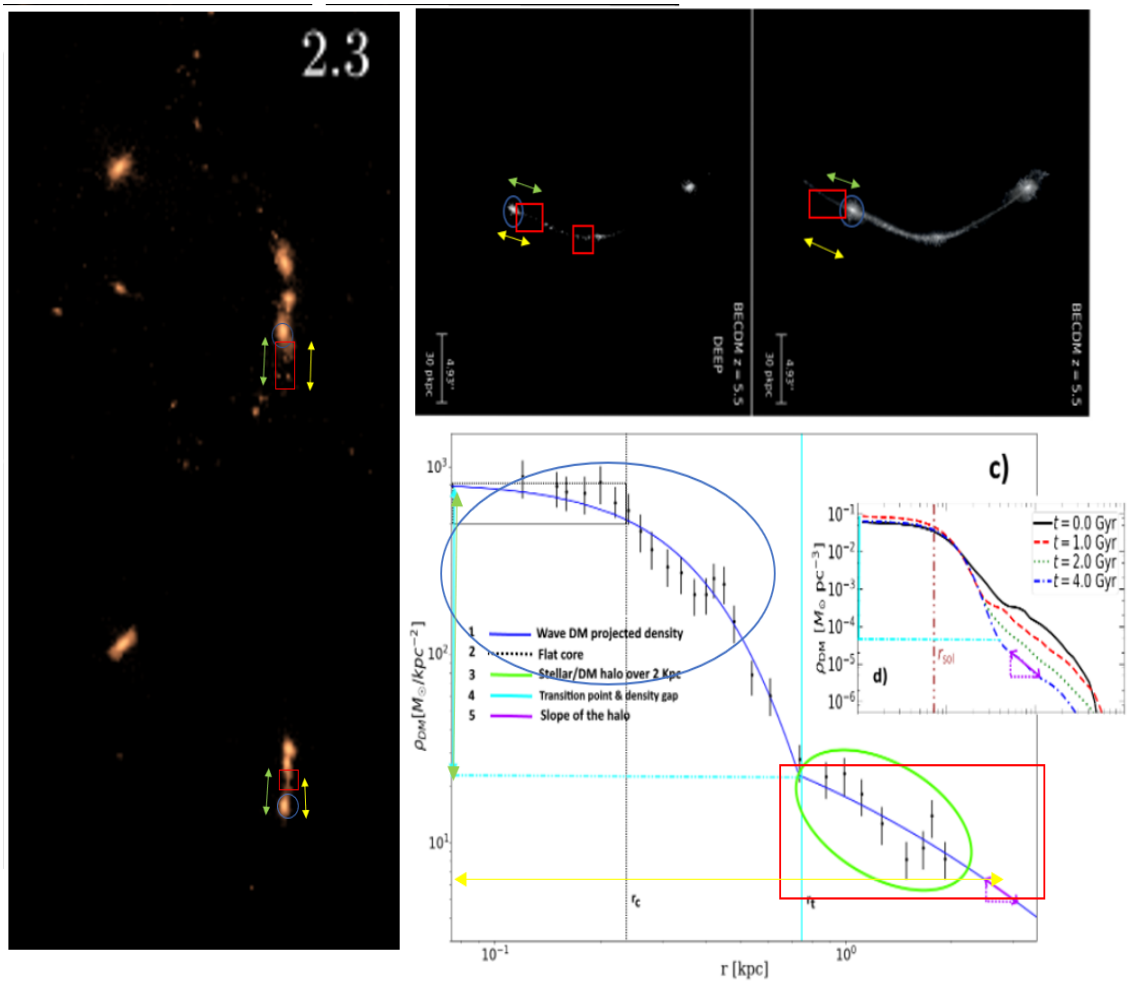

Figure 3.10: Possible correlation of the actual dwarfs' galaxies stellar profiles with the cosmological evolution of them in ψDM scenario.. Strategy to analyze if the actual stellar profiles of dwarfs still show imprints of their past cosmological strictures inside the hypothesis that stars trace dark matter, summing the arguments that have constructed figure 3.9 with the ones of figure 2.17. 1) Solitonic shape of stars in the center of every halo (blue circle). 2) Location of extended stars outside the center as remnants of past stars born in the filaments (red square). 3) Check if the density fall between the halo and the filament remnants coincides with the density fall between the core and the NFW halo regime of the dwarfs' stellar profiles (Green line). 4) Check if the distance/size where the transition point (r_t) is located and the final locations of stars at the NFW-like regime coincide (Yellow line). Credit Mocz et al. (2020).

(f) By z∼6, just half of the stars per unit volume are formed in low mass halos, indicating that they will be more embedded to DM due to their smaller own pressure and feedback. This lack of start at such redshift also could indicate that the last stars formed in the filaments will be formed

late enough to still see some of them in an extensive, distant position compared to the ones concentrated in the halo center (check figure 2.17). With filaments finally being accreted into the haloes, but much more later than in CDM, with still some baryonic objects, primordially starts, in a more extensive position and distant to the core as the imprint of these past stars full-filled filaments.

Is important to remark that the half-light radius of stars is not necessarily a guide to the soliton radius - its not likely to be larger but may be significantly smaller depending on how the gas that formed the stars cooled in the DM halo, whereas the radius to which the dispersion velocity profile remains approximately constant is likely close to the soliton radius. The equilibrium between gas and DM in the ψDM context and subsequent relaxation and heating by the de Broglie scale fluctuations and soliton oscillation and also whether disk formation dominates star formation or the infall of stars to form an extended halo are open questions in this context that simulations will clarify.

Figure 3.9 shows a graphical combination of how all the listed points above (which suggest that start could trace dark matter) could be tested in the following section 4.

The ψDM stellar profile

The classical dwarf galaxies are known to be dominated by DM, and so the stars are treated as tracer particles (Gregory et al., 2019; McConnachie & Irwin, 2006; McConnachie et al., 2006; Kang & Ricotti, 2019) moving in the gravitational potential generated by DM halo density distribution. In order to apply this idea that stars trace DM to the stellar density model, $\rho_*(r)$ from equation (3.9) has to be modified to a ψDM approximation, being the stellar density distribution defined by the soliton's wave dark matter imprint:

$$\rho_*(r) = \begin{cases} \rho_{1*}(r) & \text{if} \quad r < r_t, \\ \frac{\rho_{02*}}{\frac{r}{r_{s*}}\left(1+\frac{r}{r_{s*}}\right)^2} & \text{otherwise}, \end{cases} \tag{3.16}$$

where

$$\rho_{1*}(r) = \frac{\rho_{0*}}{[1 + 9.1 \times 10^{-2}(r/r_c)^2]^8} \; N_* \mathrm{kpc}^{-3} \tag{3.17}$$

Here, r_{s*} is the 3D scale radius of the stellar halo corresponding to ρ_{0*} the central stellar density, ρ_{02*} is the normalization of ρ_{0*} at the transition radius and the transition radius, r_t, is the point where the soliton structure ends and the halo begins at the juncture of the core and halo profiles.

3.4 Tidal stripping in Wave dark matter scenario

Many satellites dwarf galaxies of a bigger host have to deal with tidal forces due to their host's more considerable gravitational potential. Here we will try to introduce the already explained tidal imprints in wave dark matter scenarios and the way to compute them. We study tidal stripping of wave dark matter cores using simulations of the Schröedinger-Poisson equations and analyze the dynamics of tidal disruption highlighting the differences with standard cold dark matter. Our methodology and assumptions are almost based on these two previous works: Du et al. (2018), and Schive et al. (2020).

As well as in other DM scenarios, the ψDM galaxies see their masses "eaten" by the bigger host that are orbiting. Both regimes, core (Du et al., 2018) and halo (Schive et al., 2020) seem to see their mass lost due to these tidal forces, but not in an identical way and proportion. We will first concentrate on what happens to the soliton:

1. **Soliton-core**: Due to its wave behavior, when the soliton sees its mass lost, it is transformed to a more elliptical shape, from its original more spherical one (Du et al., 2018). Moreover, as a natural consequence of ψDM paradigm, a less massive soliton means a less dense and wider one. This is because one of the main characteristics of the soliton is to see its core inversely scaled with its mass (Eq. (3.4) and Eq. (3.5)). Before explaining the exact process of the solitonic stripping, we must take into account this assumption made by Du et al. (2018) about the effect of NFW-like halos of ψDM on the soliton stripping process: "Under the assumption that the incoherent matter in FDM subhalos with an NFW-like density profile behaves similarly to CDM, their solitonic cores will be stripped clean after a certain number of orbits and exposed to tidal forces."

   As the mass outside the tidal radius is removed by the host, due to the reason that we have already pointed out, the core should relax into a new ground state with less mass and a wider core. In the process, mass is transferred through the tidal radius and subsequently stripped away. Resulting in a continuous mass loss, being tidally locked with a continuous ellipticity increasing before being disrupted (Here, we can see one of the main differences between wave dark matter and CDM stripping scenarios, as in CDM this process is not enough to disrupt the satellite totally). When the other parts of the satellite are totally stripped, the remnant core is no longer in virial equilibrium, needing to convert its extra kinetical energy to potential one, in order to recover the equilibrium. This is the main physical phenomenon apart from the direct ψDM relation between mass and core size, which explains why the resulting shape has a larger characteristic radius and decreased density. Finally, once the soliton's density drops below 4.5 times the average density of the host,

seeing its tidal radius becomes smaller than its core radius, it should become unstable, getting totally stripped (Du et al., 2018).

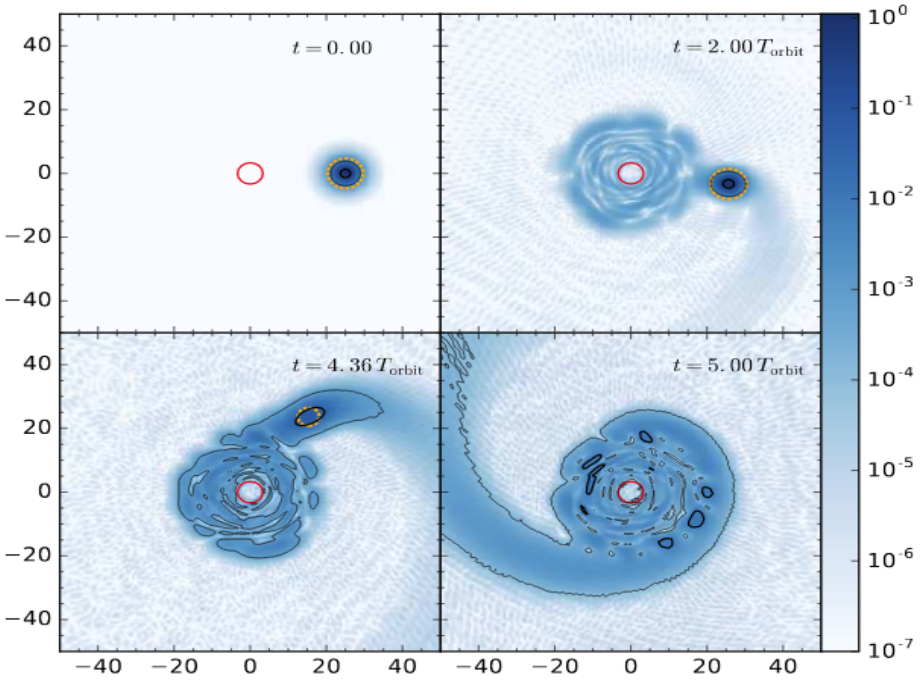

Figure 3.11: As can be seen, the core loses mass gradually but since the gravitational time scale is smaller than the mass loss time scale, it quickly relaxes to a new soliton state with a lower central density (upper-right plot). At t= 4.36Torbit (lower-left plot), the tidal radius is comparable to the core radius. Afterward, in less than one orbit, the core is totally disrupted and leaves only a long tail behind (lower-right plot). Credit Du et al. (2018).

These are the two main distinct scenarios-methods used by Du et al. (2018) to describe and explain tidal mass-loss of a solitonic core orbiting inside a host halo:

• Classic= A satellite halo orbiting the host halo loses its mass due to the tidal force of the host halo, i.e. the tidal stripping effect. Considering a satellite orbiting its host with synchronous rotation, i.e. the angular velocity of self-rotation equals the orbital angular velocity, the tidal radius can be calculated from classical Newtonian dynamics

• Tunneling approximation= tidal stripping of ψDM halos is treated quantum-mechanically by adding a spherical tidal potential to the Schröedinger equation. The authors propose that mass inside the tidal radius can be stripped insufficiently long time due to tunneling. Moreover, as the solitonic core loses some of its mass and becomes less dense, it is increasingly vulnerable to tidal forces. The mass loss rate is obtained from the imaginary part of the (complex) energy eigenvalue E (which only depends on the density ratio between

the central density of the soliton ψc and the average density of the host within the orbital radius). Since both tidal and gravitational potentials are taken to be time independent, so is the tidal radius. Consequently, the mass loss is fully characterized by the decreasing amplitude of the wave function.

Below we mathematically describe different effects of tidal stripping including the mass-loss and core enlargement.

We first calculate the relation between M_h(halo mass) and M_c (core mass) using Eq. (3.3) until the core radius, as indicated in Eq (3.6). After that, the core mass-loss rate is inferred for each orbit with the following formula (Du et al., 2018):

$$d(M_c(t))/dt = -2 \times M_c(t) e^{a[\frac{3\mu(M_c(t))}{2\gamma}]^2 + b[\frac{3\mu(M_c(t))}{2\gamma}] + c}, \tag{3.18}$$

With the best fitting parameters' values: (a,b,c)$\equiv$(5.89794 10^{-5}, -8.72733 10^{-2}, 1.6774), γ, the effect of the centrifugal force owing to synchronous rotation of the orbiting satellite, assuming it to be a rigid body, fixed to 3/2 for a soliton (Du et al., 2018) and μ, the density ratio between the central density of the soliton ρ_c and the average density of the host within the orbital radius ρ_{host}, $\mu \equiv \rho_c/\rho_{host}$ (Du et al., 2018). Nevertheless, μ must be recalculated across the orbits due to the core density loss along each orbit:

$$\mu = 4.38 \times 10^{10} m_\psi^6 M_c^4 d^3 m_{host}^{-1}, \tag{3.19}$$

2. **Halo**: More recent simulations from Schive et al. (2020) seem to predict a more stable and robust soliton than halo against tidal forces. In this ψDM model with a soliton in the center and an outer NFW-like halo regime, tidal forces seem to affect the halo more and quicker, as its mass is easier stripped than the soliton's mass. These simulations emphasize the importance of the self-gravity of the soliton as it clearly offers him a more robust defense against tidal forces compared to the NFW-like halo regime. The main observable imprint of tidal forces in this core's more robust scenario is a clear density gap (check out point 4 of section 3.3 and figure 3.9) increment. Even in cases where tidal forces are not strong enough to remove mass from the soliton, check figure 3.12.

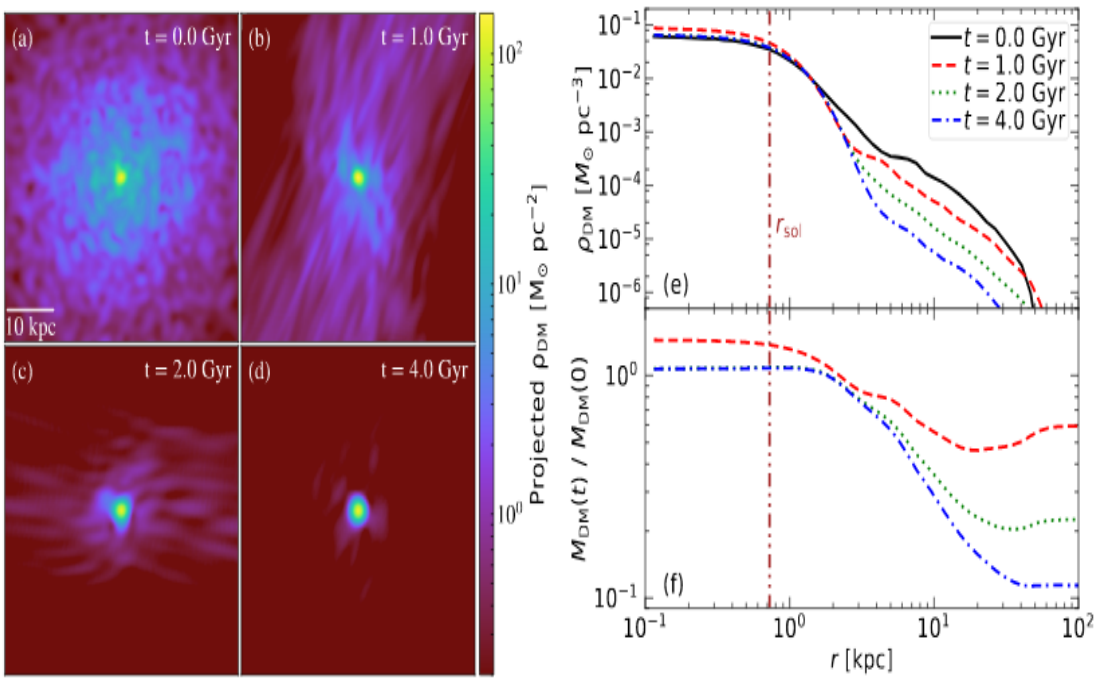

Figure 3.12: This plot shows how the halo regime of Eridanus II is easier removed by Milky's tidal field, while the soliton can maintain almost intact.**The left panel:** Projected dark matter density. We can see how the galaxy's halo is almost removed after 4Gyr of tidal forces while the soliton remains almost there. **The right upper panel:**Dark matter density profiles. Notice how the soliton (central) dark matter maintains equal across the Gyrs while the halo shows its bigger weakness to tidal forces losing density. This density gap between the core and the halo,Δ_{C-H}, and its connections with tidal forces will be deeper analyzed in section 4.2. Credit Schive et al. (2020).

One clear observational evidence of this core robustness in contraposition to the weakness of the halo against tidal forces was detected after analyzing the stellar cluster of Eridanus II (Schive et al., 2020). Eridanus II is a tidally affected dwarf galaxy orbiting the Milky Way. This galaxy has a star cluster in its central area, which survival clearly defies ψDM soliton behavior, which random walk (product of its wave behavior) should disrupt the cluster in less than 1 Gyr. Nevertheless, Schive et al. (2020) already demonstrated with his simulations the more significant weakness of the halo against tidal forces, leaving the relatively dense soliton intact, and directly declining the soliton random walk. Softening it and delaying clusters disruption to 5 Gyrs (check figure 3.13). Allowing the star cluster to survive time much longer within the soliton due to a substantial halo removal.

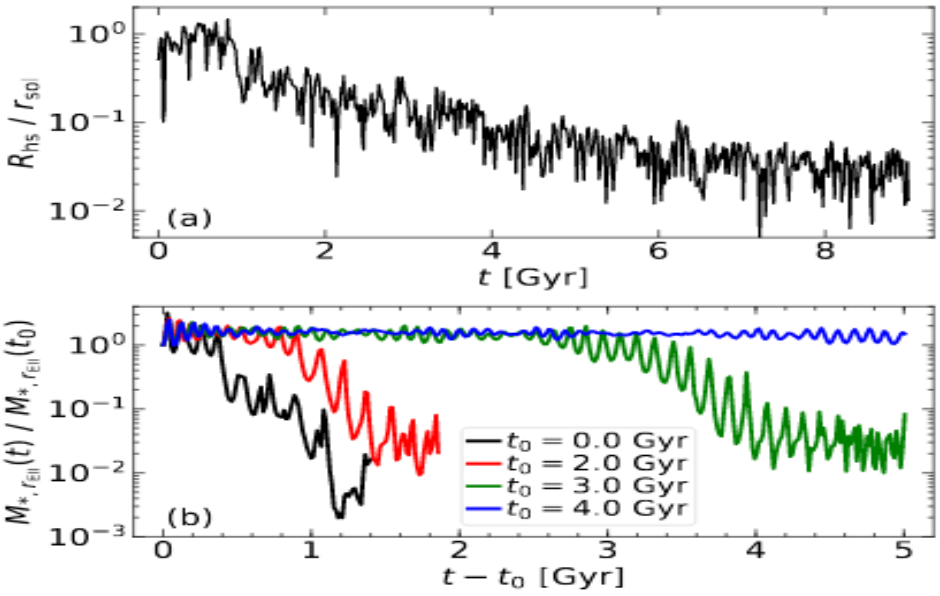

Figure 3.13: This plot shows how the Milky Way's tidal field affects a soliton's random walk. With an original soliton random walk (black line), the star cluster will trace the soliton trying to follow its random motion. Because of the soliton's random motion, the expected characteristical separation between the star cluster and the soliton will be $\sim r_c$. In this isolated scenario, the tidal field suffered by the cluster due to that characteristical separation will disrupt the cluster in ∼1Gyr. Nevertheless, these simulations predict that the soliton's random motion becomes smaller as the halo is tidally stripped, increasing the cluster's survival time to 5Gyrs. Credit Schive et al. (2020).

3.5 Stars as test particles uniting the Uncertainty Principle with the Axiverse

Until recently the classical "dwarf spheroidal" (dSph) galaxies were recognised as the lightest type of galaxy, with masses of $10^{9-10} M_\odot$ comprised mainly of dark matter. But the previously presented distinct new class of smaller and denser "ultra faint" dwarfs (UFD's) has been uncovered in recent surveys, with masses of only $10^{7-8} M_\odot$ that are also dominated by dark matter. This bimodality amongst low mass galaxies contrasts with the scale free continuity expected for galaxies formed under gravity, as in the standard Cold Dark Matter (CDM) model of collisionless particles.

Our results show (below in section 4.4) that the dSph and UFD dwarfs follow parallel, inverse relations between their core sizes, r_c and stellar velocity dispersions, σ, such that the cores are larger for dwarfs of lower velocity disper-

sion within each class, quite the opposite of standard expectations where larger galaxies should be more massive. This behavior is predicted for dark matter as a Bose-Einstein condensate because the Uncertainty Principle linking position and momentum dictates $r_c \times \sigma$ is set by Planks constant, h requiring an inverse relation between r_c and σ as observed. We use this relation for each class of dwarf to derive the boson mass, m_b directly via $m_b = h/r_c\sigma$, differing by a factor of ten between both galaxy populations in m_b. This light boson interpretation is independently reinforced by the presence of the prominent central soliton cores, explained in section 3.1 and 3.3, visible for the dSph and UFD dwarfs that differ in scale by a factor of 10 in radius. This soliton core is also seen in terms of the core density, ρ_c which follows the predicted steep relation $\rho_c \propto r_c^{-4}$, for both the dSph and UFD dwarfs, required by the Uncertainty Principle. This relation is easily extracted from the solitonic core equations (see equations (3.4) and (3.5), which corresponds to the ground-state solution of the coupled Schröedinger-Poisson equations, with a cored density profile well-approximated by Schive et al. (2014a,b)) and the fact that the core mass scales as $\sigma^2 r_c$, giving us the opportunity to describe density in the ψDM scenario by the following relation:

$$\rho_c \propto (\sigma/r_c)^2 \tag{3.20}$$

Taking into account the inverse soliton core mass vs. radio relation required by the uncertainty principle ($M_c \propto 1/r_c$) and that the soliton's density is equal to its mass divided by its volume ($\rho_c = M_c/r_c^3$), we got the wanted relation:

$$\rho_c \propto r_c^{-4} \tag{3.21}$$

A condensate of Bose-Einstein is revealed when a boson gas is cooled to temperatures near absolute zero, this DM version of a bose-einstein condensate is assumed to be "born in the ground state", rather than cooling down into the ground state. In this context, the bosons would occupy the lowest energy-quantum state, at which point microscopic quantum mechanical phenomena, particularly wavefunction interference, become apparent macroscopically. An ideal Bose gas is a collection of non-interacting N bosonic particles. Following the laws of quantum mechanics, these particles have a wave nature that the de Broglie wavelength can characterize;

$$\lambda_B = \frac{h}{p} \tag{3.22}$$

and which can be used to obtain the de Broglie thermal wavelength for ideal gases with massive particles:

$$\lambda_{BT} = \frac{h}{\sqrt{3mk_BT}} \tag{3.23}$$

Where m is the particle's mass, T is the temperature, h Planck's constant, and k_B is Boltzmann's constant. At high temperatures, when λ_{BT} is smaller than the distance between particles, their thermal movement dominates the gas properties as localizable particles. But while the temperature decreases, λ_{BT} increases to values more significant than the distances between the particles, arising their wave behavior. In this situation, the different matter waves overlap, coordinating their state and producing the Bose-Einstein condensate. A single wave function defines the entire system as a "super-paricle". At his point, all de particles are in the smaller quantum-energy state, being identical. As all of them share the same quantum state and have the same minimum energy, they become indistinguishable from each other, behaving as a single super-particle. More precisely as a "coherent wave function" in our ψDM, where all bosons in the ground state coherently oscillate together as one wave function. In summary, in a coherent Bose-Einstein condensate, all bosons would "wave together" due to being in the identical ground state. This was formalised by Gross-Pitaevskii's wave function (Gross, 1961), making us possible to describe the collective behavior of bosons in a condensate with the Schröedinger equation (Eq.(3.1)).

In this scenario, we can consider the condensate as one single particle, where the de Broglie wavelength of such "super-particle" would correspond to the total size of the condensate, of the soliton in this case. Making us make a possible relation with the Uncertainty principle:

$$\Delta x \Delta p \geq \frac{\hbar}{2} \tag{3.24}$$

Where Δx, the position dispersion, can be replaced by the soliton's size (equivalent to the de Broglie wavelength$\simeq 2\times r_c$) and Δp, the dispersion of the lineal momentum (p=m$\times$v), where "v" can be replaced with the corresponding velocity dispersion value (Eq.(3.12)) in the soliton, equivalent to the one of the bosons in a system in a dynamical equilibrium where stars are dominated by the higher potential of the dark matter. In summary, in this ψDM context, where self-gravity balances the effective pressure from the Uncertainty Principle, we could relate the size of the soliton (almost defined by the de Broglie wavelength($\simeq 2\times r_c$)) with the momentum product of the dominant dark matter potential, represented by the observed velocity dispersion(equivalent to the motion of the bosons if they will behave as macroscopic particles) of the stars and the mass of the boson corresponding to the de Broglie wavelength of such astronomical structure (Eq.(3.24)). The point why the mass of the lineal momentum would correspond to the boson's one is obvious; simply

cause the boson mass is the value that sets the size of the de Brogile wavelength and in consequence of the soliton's size, defining the value of Δx as well. The point why the dispersion velocity is meaningful to determine the Δp, is a more complicated statement. First of all, as we are talking about spheroidal and not circular galaxies, the velocity dispersion will be the most representative direct observable value of the dominant potential, DM's. So the observed velocity dispersion of the stars is a direct product of the soliton's dominant gravitational potential. Secondly, as stars and bosons are supposed to be at the same temperature(as particles moving with a certain velocity in a system, not their internal own temperature), both should have the same velocity dispersion giving us the opportunity to use the stars' velocity as an accurate representation of bosons'. The last point to clarify here is that the bosons due to being in a BE condensate, should all be represented by a single one, so no dispersion velocity would exist between them. So how can we use stars' dispersion velocity as a synonym of theirs? The answer relies on the fact that both, stars and bosons are dominated by the soliton's potential and that the stars are just simply showing the bosons' exact behavior but on the macroscopic scale, in other words, stars are showing us how bosons would behave in case of being macroscopic particles. Stars and bosons are behaving in the same way, but this exact behavior is differently represented in macro and micro scales. What we are observing is how particle behavior would be represented in the macro and the micro scales for the same quantum phenomenon.

All these points, allow us to determine the mass that corresponds to the astronomically relevant de Broglie wavelength, the boson mass:

$$m_\psi \simeq \frac{h}{8\pi r_c \sigma_{los}} \tag{3.25}$$

Chapter 4

Results & Conclusions

This section will explain all the results we obtained for this work. First of all, in section 4.1, we will show the efficiency of ψDM model to fit the observable dynamical data of the previously introduced classical dwarfs (section 2.2.1) and ultra-diffuse galaxies (section 2.2.3). As a result of the already explained methodology for it in section 3.2. Secondly, we will show all the analyses done to the observable stellar profiles of the local group's dwarfs that reinforce the idea of stars tracing dark matter (section 3.3). Thirdly, we will present all the simulations made in a ψDM paradigm towards tidal stripping in order to validate the arguments of section 3.4. Finally, we will focus again on the stellar observable data of these local dwarfs and ultra-faint galaxies of sections 2.2.1 and 2.2.2 respectively, to favor the theory of a wide range of axion masses, previously introduced as the concept of the "axiverse", in section 2.1.6. Each result section will have a small script to explain the working method, motivation, and final results and conclusions concisely.

4.1 Wave DM modeling in classical dwarfs and UDG (Paper 1)

As we have previously commented in this work, dark matter as a Bose-Einstein condensate, such as the axionic scalar field particles of String Theory, can explain the coldness of dark matter on large scales. Pioneering simulations in this context predict a rich wave-like structure, with a ground state soliton core in every galaxy surrounded by a halo of excited states that interfere on the de Broglie scale. This de Broglie scale is largest for low mass galaxies as momentum is lower, providing a simple explanation for the wide cores of dwarf spheroidal galaxies. Here we extend these "wave dark matter" (ψDM) predictions to the newly discovered class of "Ultra Diffuse Galaxies" (UDG) that resemble dwarf spheroidal galaxies but with more extended stellar profiles. Currently, the best studied example, DF44, has a uniform velocity dispersion of $\simeq$ 33km/s, extending to at least 3 kpcs, that we show is reproduced by our ψDM simulations with a soliton radius of $\simeq$ 0.5 kpc. In the

ψDM context, we show the relatively flat dispersion profile of DF44 lies between massive galaxies with compact dense solitons, as may be present in the Milky Way on a scale of 100pc and lower mass galaxies where the velocity dispersion declines centrally within a wide, low density soliton, like Antlia II, of radius 3 kpc.

Here, we compare our wave-DM predictions for the newly discovered class of UDG galaxies, in particular for DF44 the currently best-studied example, in the Coma Cluster. It was discovered with the pioneering Dragon Fly multi-beam telescope, built for the purpose of reaching unprecedentedly low surface brightness in ground based surveys (Abraham & van Dokkum, 2014). The extended stellar profiles of these UDG galaxies and their low surface brightness seem to challenge models of galaxy formation in standard CDM where large tidal forces and ram pressure stripping, or high rotation dark halos have been proposed by Liao et al. (2019) and Tremmel (2020) and even stars formed in outflows by Di Cintio et al. (2017). These ideas are hotly debated and hard to extend to the discoveries of isolated examples of UDGs some of which show modest ongoing star formation and also extended HI.

We also compare DF44 with wave-DM profiles fitted to other well-studied galaxies of higher and lower mass, for which extended velocity dispersions have been measured. In sections 3.1 and 3.2 we describe our baseline model consisting of the solitonic core plus a NFW-like outer profile; and in section 4.1.1 we compare our predictions to the dataset of the Dragon Fly 44 dwarf galaxy, together with other newly discovered dwarf galaxies. We also show the self-consistency of our baseline model for explaining the dispersion profile of those galaxies. Throughout the section, we assume a standard cosmology (Collaboration et al., 2016).

Gas outflows have been appealed to for flattening the central DM density profile of dwarf galaxies in the context of CDM, with increasingly detailed modeling to help capture the complexities of supernova-driven outflows powered by repeated bursts of star formation, (Navarro & Frenk, 1996; Gelato & Sommer-Larsen, 1999; Binney et al., 2001; Gnedin & Zhao, 2002; Mo & Mao, 2004; Read & Gilmore, 2005; Mashchenko et al., 2006, 2008), and also dynamical friction of inflowing clumped baryons with repeated outflows (El-Zant & Shlosman, 2001; Weinberg & Katz, 2002; Tonini et al., 2006; Romano-Díaz et al., 2009; Goerdt et al., 2010; Cole et al., 2011). The formation of large cores is now questioned in the latest detailed high resolution simulations by Bose et al. (2019) indicating the gravitational coupling between gas outflows and the central DM profile may not be sufficient to significantly modify the central DM profile, with confirmation by Benítez-Llambay et al. (2019) who emphasise that only the high gas density regime is relevant for core formation in the CDM context, requiring frequently repeated outflows with gas continuing to dominate the central potential for Gyrs.

4.1.1 Minimal Wave-Dark-Matter Radial Profile Comparison

Here we first compare the measured velocity dispersion and light profile of DF44 with Wave-DM with the minimum number of parameters that are consistent with the findings from our simulations and then subsequently we allow a wider range of soliton and halo mass to allow comparison with previous work for more general conclusions.

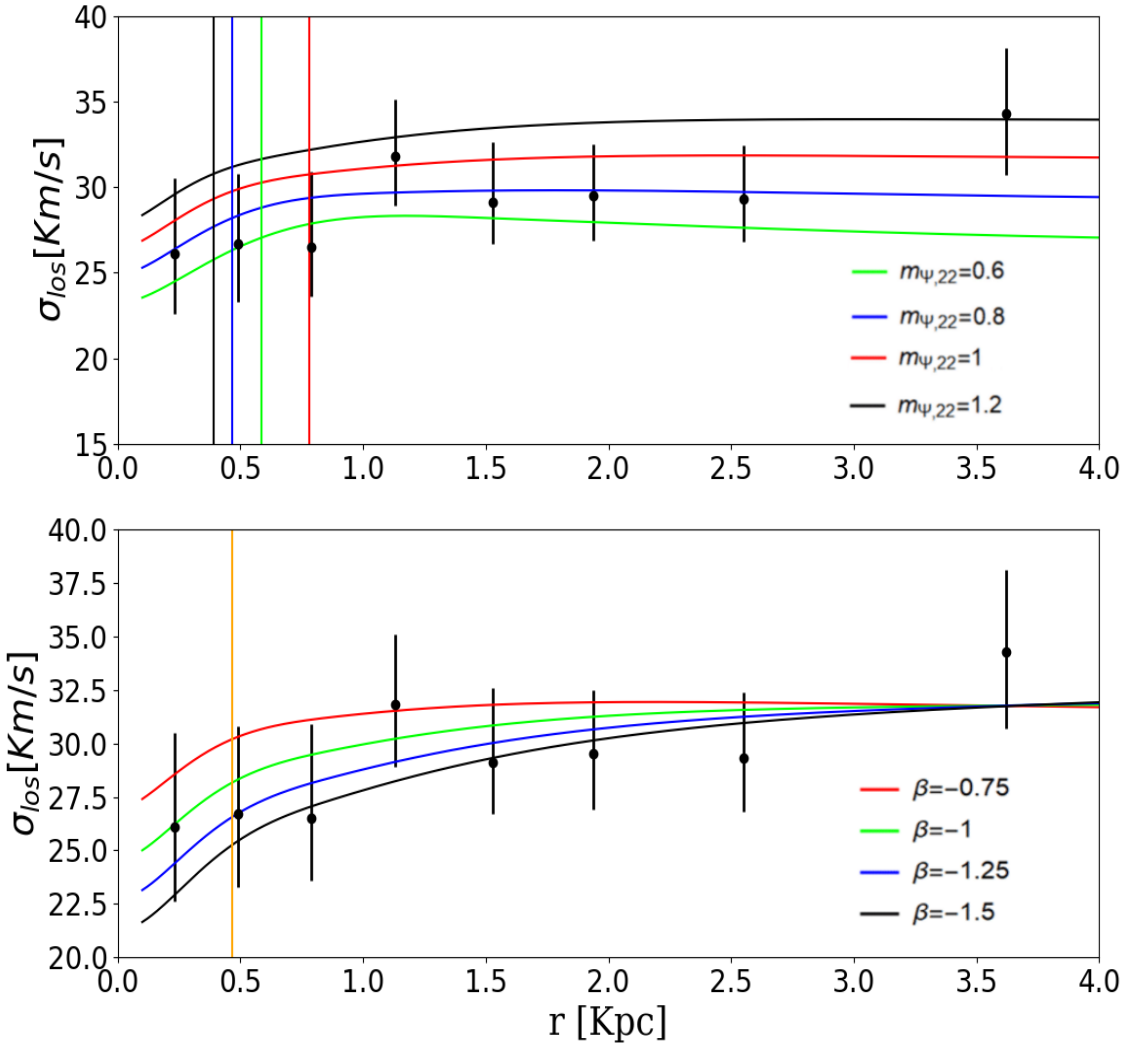

Figure 4.1: The figure shows the acceptable range of predicted velocity dispersion profiles comparison with DF44 for our minimal model, where the soliton scale is determined by the halo mass and the boson mass. We vary boson mass in the upper panel, setting $\beta = -0.8$ and in the lower panel we set the boson mass to $m_\psi = 10^{-22}$ eV and vary β according to the legend. This show that a light boson mass in the above range, with modestly negative β, produces acceptable reduced χ^2.

For our minimal model profiles, we solve the spherically symmetric Jeans equation, described above, Eq. (3.7), subject to a total mass of $4 \times 10^{10} M_{\odot}$, which is the dynamical mass estimated by van Dokkum et al. (2019b) for this galaxy adopting the virial estimate commonly used for dwarf spheroidal galaxies (Walker et al., 2009). We also adopt the commonly used Plummer 'profile for the stellar profile and match it the measured half-light projected radius of 4.6 kpc measured for DF44 (van Dokkum et al., 2019b).

For our minimal model adopt the soliton–halo mass scaling relation of Eq. (3.5) discovered in the ψDM simulations (Schive et al., 2014b). This provides the scale of the soliton for a fixed total halo mass. The ψDM simulations have also shown that the NFW form provides a good azimuthal description of the granular ψDM halos outside the soliton core. Hence we may fix the scale length of the NFW profile, r_s, to provide the total mass computed with our model for a given choice of concentration we set $r_s = 8$ kpc. All values are summarized in Table 4.2.

This comparison shows simply that the general level of velocity dispersion measured for DF44 of $\simeq 30\ km/s$ is consistent with the widely favored boson mass from similar analyses of dwarf spheroidal galaxies $\simeq 10^{-22}$ eV, for which the observed absence of any central rise in the velocity dispersion favors a predominance of tangential over radial dispersion. We can also see that for a larger choice of boson mass of 1.2×10^{-22} eV, a larger value of β can be tolerated. This contrasts with the significantly larger mean boson mass of $\simeq 3 \times 10^{-22}$ eV, highlighted by Wasserman et al. (2019) in a recent analysis of DF44, but is consistent with the lower end of their 95% range of 1.2×10^{-22} eV.

Acceptable minimal model profiles for DF44 are shown in Figure 4.1 for several illustrative values for the minimal set of parameters listed in Table 4.2, varying the boson mass and the velocity anisotropy parameter. These profiles have reduced χ^2 values near unity, consistent with the measured dispersion profile of DF44 for its observed large half light radius and virial mass estimate. In the upper panel of Figure 4.1 we vary the boson mass in the range $[0.6, 1.2] \times 10^{-22}$ eV, setting $\beta = -0.8$ on the basis of the analysis in (van Dokkum et al., 2019b). In the bottom panel, we do the opposite by setting $m_{\psi} = 10^{-22}$ eV and varying the anisotropy parameter in the range $[-0.75, -1.5]$. In both cases, the wave-like DM is able acceptably reproduce to the dispersion velocity profile out to $r \sim 3$ kpc and even outsider for lower panel profiles.

4.1.2 Comparison of the velocity profile of DF44 with other low and intermediate mass Galaxies

Here we place the velocity profile of DF44 in the wider context of dwarf galaxy

profiles for the ψDM framework, spanning the full range of lower masses appropriate for dwarf galaxies. We compare our minimal model with the velocity dispersion profile of representative well studied low mass galaxies whose halo mass and half-light radius span the ranges from $\sim 10^9 M_\odot$ to $\sim 5 \times 10^{10} M_\odot$ and from ~ 0.8 kpc to ~ 5 kpc, respectively. Since our minimal model must assume a halo mass to compute the corresponding solitonic profile, Eq. (3.5), we take care to check that the predicted total mass from our model is compatible within the errors with the total mass estimates from observations.

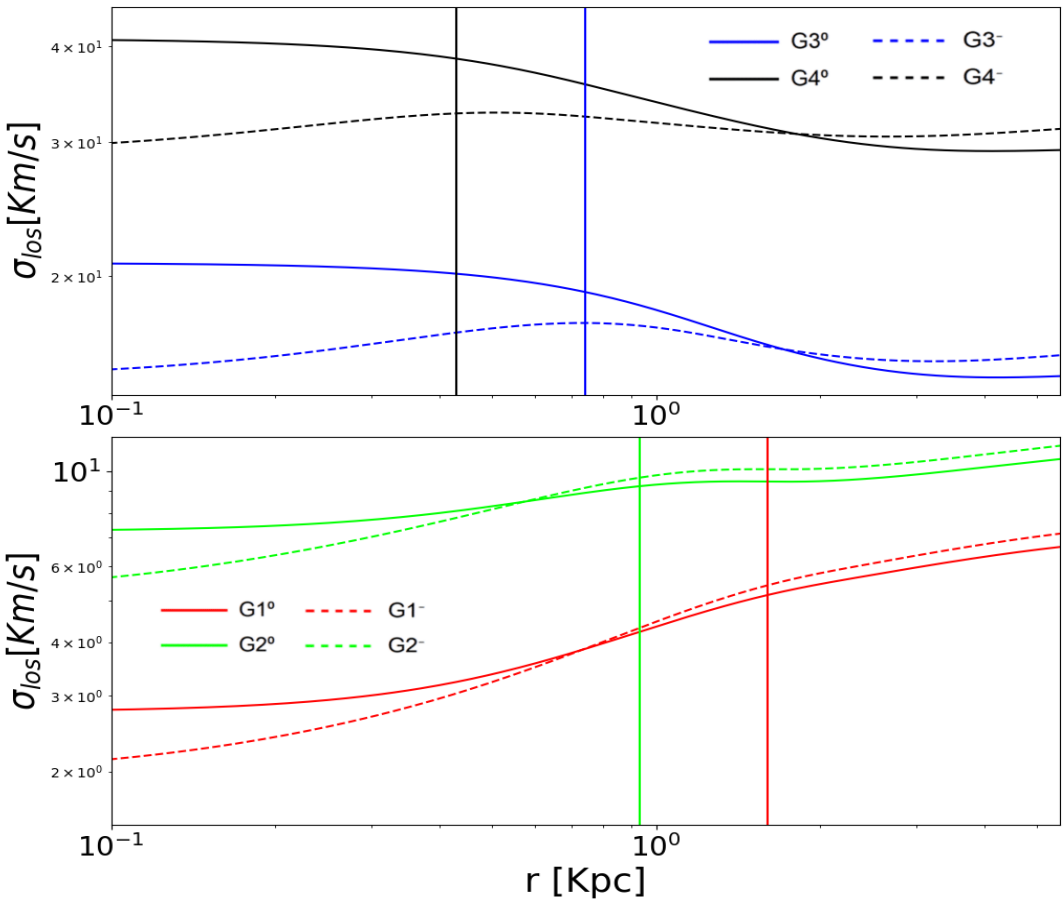

Figure 4.2: In this figure, we show model solutions for all model galaxies listed in Table 4.1 to highlight the transitional feature in the radial profile from the soliton to the NFW-like halo. Solid lines represent solution of the isotropic Jeans equation ($\beta = 0$), while dashed lines indicates the predicted dispersion profiles for negative values of β. For a better visualization, we plot the galaxies with higher mass in the upper panel, while the remaining galaxies are shown in the lower panel.

In Figure 4.2 shows illustrative velocity dispersion profiles for a range of ψDM mass profiles highlighting the transition from the soliton core to the outer NFW-like outer profile (Schive et al., 2014a,b; Vicens et al., 2018). The velocity dispersion profiles are listed in Table 4.1, and cover one order of magnitude in the total mass starting from $10^9 M_\odot$ and for different choices for the extent of the stellar profile, and for each model profile compare two representative values of $\beta = [0.0, -0.5]$ to

Model	M_{halo} ($10^{10} M_\odot$)	r_{sol} (kpc)	r_{half} (kpc)	M_* ($10^7 M_\odot$)	r_s (kpc)	β
$G1^0$	0.1	1.6	0.6	0.3	8.5	0.0
$G1^-$						-0.5
$G2^0$	0.5	0.94	0.6	0.3	10.5	0.0
$G2^-$						-0.5
$G3^0$	1.0	0.74	2.5	3.0	9.0	0.0
$G3^-$						-0.5
$G4^0$	5.0	0.43	2.5	3.0	7.5	0.0
$G4^-$						-0.5

Table 4.1: Values of the parameters used to construct the velocity dispersion profile of a set of *simulated* dwarf galaxies [G1,G2,G3,G4] for two values of the anisotropy parameter. We also vary here the Plummer scale radius for the stars, which allows for a range in "depth" that the stars may occupy in 3D, given by the half light radius.

show the effect of the transition in a family of physical systems representing dwarf galaxies. Solid and dashed lines depict in Fig. 4.2 for each system, our predicted dispersion profile for β is set to 0.0, and -0.5, respectively.

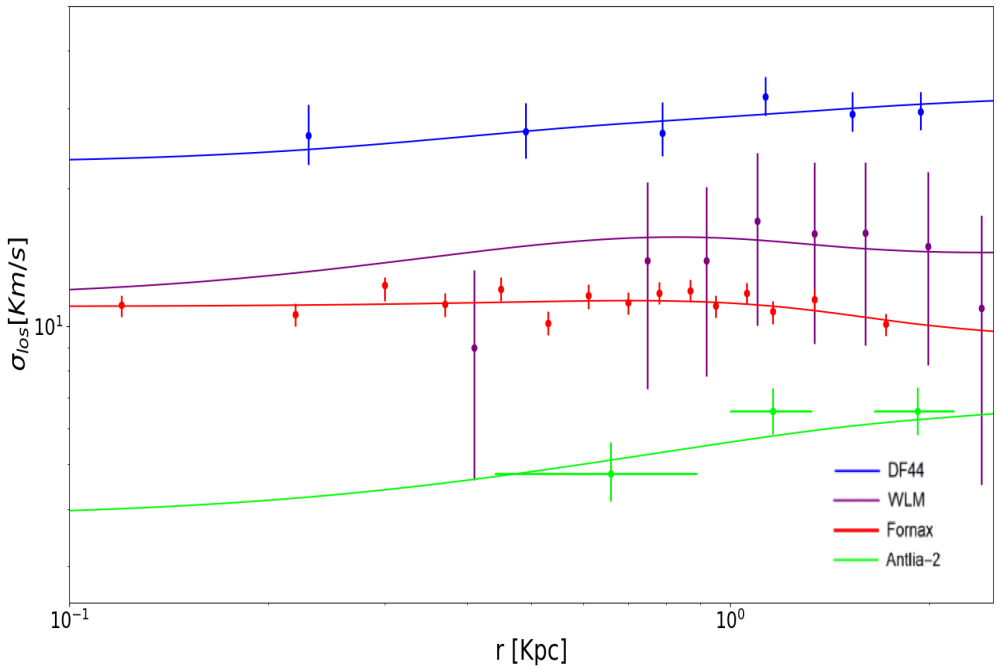

Figure 4.3: Comparison of the observed velocity dispersion profiles with the predictions, for all galaxies listed in Table 4.2.

Galaxies	m_ψ (10^{-22} eV)	$M_{halo,obs}$ ($10^9 M_\odot$)	r_{sol} (kpc)	r_s (kpc)	r_{half} (kpc)	$M(r<r_{half}),_{obs}$ ($10^7 M_\odot$)	$M(r<r_{half}),_{th}$ ($10^7 M_\odot$)	β	χ^2_{red}	Refs.
DF44	1	40	0.47	8	4.6 ± 0.2	390 ± 50	300	-1.25	0.87	(van Dokkum et al., 2019b)
WLM	1	10	0.74	7	1.66 ± 0.49	43 ± 3	25	-0.75	0.82	(Leaman et al., 2013)
Fornax	1	7	0.84	4	0.85	6.1-8	6.57	0.0	1.21	(Mashchenko, 2015)
Antlia II	1	1	1.6	7	2.9 ± 0.3	5.5 ± 2.2	9.75	-0.75	1.34	(Torrealba et al., 2019)

Table 4.2: Observed and estimated magnitudes of the dwarfs galaxies.

Finally, in Figure 4.3, we apply our model to the dwarf galaxies listed in Table 4.2, together with the reduced chi-square. We have aimed to illustrate the family of predicted profile shapes to see how of the velocity profile of DF44 may fit in. It can be seen that the relatively flat profile DF44 appears to be continuous with the lower mass galaxies shown here, including Fornax, and Antila II (Schive et al., 2014b; Broadhurst et al., 2020) that span the dSph regime and for which we have previously derived boson masses. We have added the more massive, well studied "transition" galaxy, WLM for broader mass coverage. Note, we don't intend to be exhaustive here in this comparison as this would require an understanding of the transformative role of tidal effects which are important for most nearby dwarf galaxies orbiting the major local group galaxies, as we have recently shown in Pozo et al. (2020). Our results show that the minimal model is able to provide a good fit of these dwarf galaxies, where we vary the whole set of parameters, namely (M_{halo}, r_s, β). For all galaxies, we also compute the total mass within the half-light radius to ensure that it matches the observations. All results are listed in Table 4.2.

4.1.3 Pure NFW profile.

Here we consider a pure NFW profile for a range of relatively high concentration parameter, c, appropriate for relatively low mass galaxies like DF44, ranging over $20 < c < 40$, guided by the mass-concentration relation and its inherent dispersion derived from CDM simulations.

Generically of course a centrally rising dispersion profile is predicted for NFW profiles, shown in Figure 4.4 (and Table 4.3 labeled as NFW_1 and NFW_2) as expected given the inherently cuspy density profile of CDM, but is quite unlike the flat profile observed for DF44. A better match DF44 requires a negative anisotropy parameter, with $\beta < -1$ as shown in Figure 4.4 (and Table 4.3 labeled as NFW_3, NFW_4 and NFW_5) in order to more than counter the CDM cusp. The NFW_5 model has a concentration parameter has been set to the best NFW fit obtained by Torrealba et al. (2019), while β is the same as explored by van Dokkum et al. (2019b) and this is marginally acceptable with $\beta = -1.25$, in terms of the velocity dispersion profile. However, the scale length predicted for this model $r_s = 3.6$ kpc is smaller than the measured half light radius of DF44, therefore appearing to be unreasonable, and this is generally the case for the other solutions we have explored here and listed in Table 4.3, as generically the cooling of gas required to form stars is not

expected to produce a stellar distribution that is more concentrated than the dark matter halo as both stars and DM particles behave as test particles. Furthermore, any subsequent "heating" that may have occurred through interactions subsequent to formation may be expected to affect collisionless stars and dark matter equally.

Profiles	M_{halo} ($10^9 M_\odot$)	r_s (kpc)	c	β
NFW_1	10	2.89	15	0
NFW_2	8	2.01	20	0
NFW_3	40	4.59	15	-2
NFW_4	40	3.44	20	-3
NFW_5	20	3.64	15	-1.25

Table 4.3: DragonFly 44 NFW predicted profiles

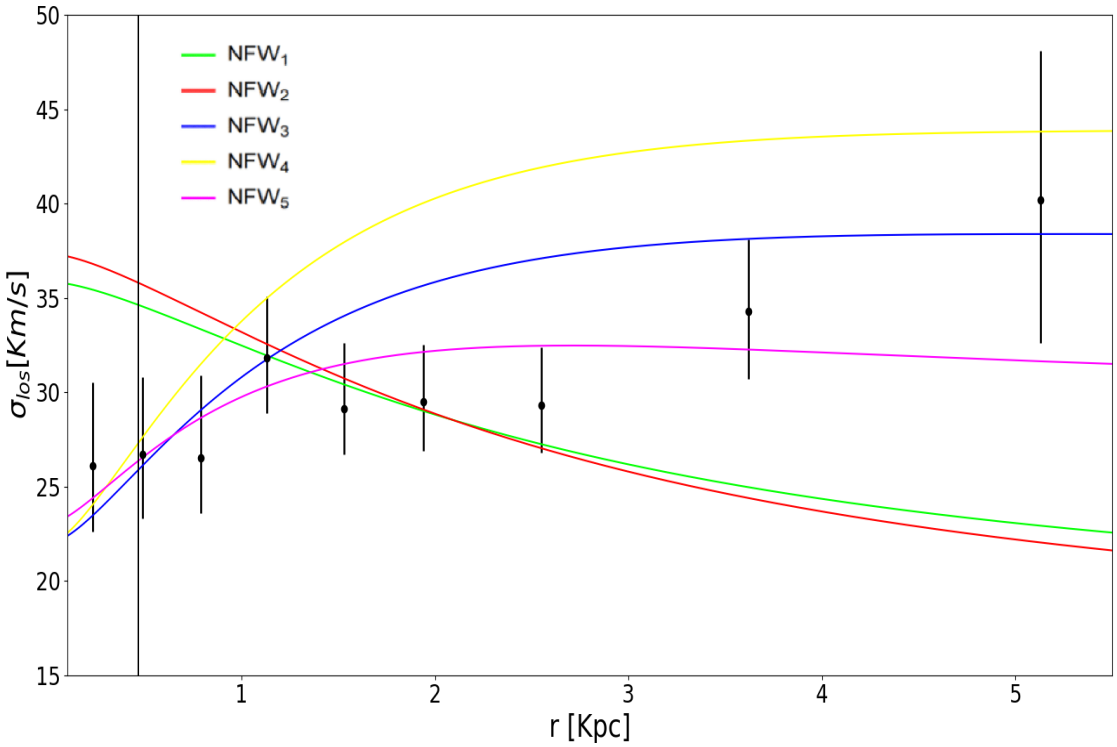

Figure 4.4: Result of the best pure NFW fits for DF44 listed in table 4.3.The black vertical line is the limit of the calculated soliton for the wave DM profile.

4.1.4 Generalised Wave-Dark-Matter profile fitting

Here we explore a fuller range of parameters that does not rely on the "standard" dynamical mass advocated by Walker et al. (2009) for simple stellar systems, since this may not be fully appropriate for the Wave-DM model that we examine here,

but has been calibrated in the context of CDM simulations.

For this purpose, we have constructed an MCMC multi-parameter scheme that we compare with the dynamical data and observed scale length for DF44, which we link through the Jeans analysis outlined earlier. In addition to the parameters of the minimal model above, we allow the halo mass to be free and some freedom in "transition radius" between the central soliton and outer NFW halo components given by ϵ below that is consistent with the spread found in the first simulations (Schive et al., 2014a).

Wide uniform priors are adopted for the above model:

$$-0.5 < \log_{10}(m_\psi) < 2.5; \tag{4.1}$$
$$1 < \log_{10}(r_{sol}) < 4; \tag{4.2}$$
$$-1 < -\log_{10}(1-\beta) < 1; \tag{4.3}$$
$$2 < \epsilon < 3.5. \tag{4.4}$$

Note, here we have let the matching radius between the soliton and the NFW halo vary over a range of scale, where $r_{\rm trans} = \epsilon r_{sol}$, implied by the inherent spread found in the simulations.

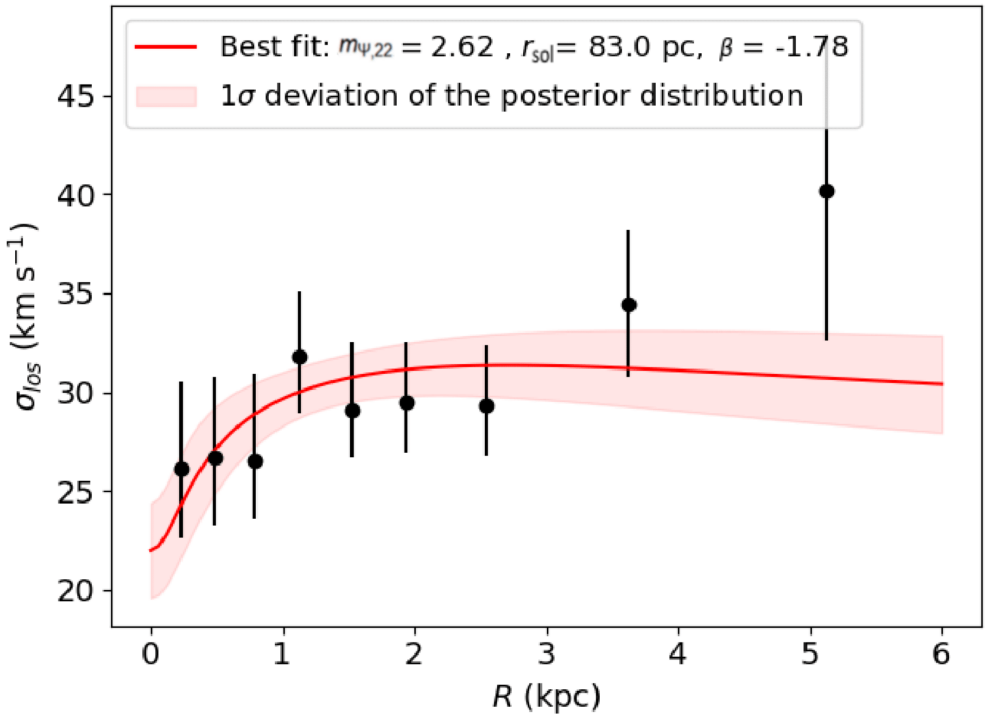

Figure 4.5: The best fit soliton + NFW model and its one-sigma deviation is calculated by randomly sampling from the distributions of velocity dispersion at each radius.. Corner plot in the appendix , Figure 4.64.

The best fit velocity dispersion curve of the above model is shown in Figure 4.5, together with the 1-σ uncertainty. The preferred value is of the core radius of this

model is $\simeq 100$ pc, which is quite small compared to the size of DF44 (~ 4.6 kpc). The preferred halo mass, $1.5^{+3.5}_{-0.7} \times 10^{11} M_{\odot}$, is several times larger than the dynamical mass adopted earlier of $4 \times 10^{10} M_{\odot}$ for our minimal model and the best fitting soliton mass is lower in relation to the halo mass, only 2% of the halo mass and hence this model is essentially a pure NFW profile with a relatively large tangential anisotropy $\beta \simeq -2$ that counters the inherent NFW cusp, lowering the central velocity dispersion as shown in Figure 4.5. This halo dominated solution is very similar in terms of halo mass and velocity anisotropy to our best fitting pure NFW profile, NFW_5 described in section 4.1.3.

This halo dominated ψDM solution has a somewhat higher favored boson mass than we derived in section 4.1.2 for our minimal model, but with a sizeable uncertainty: $m_{\psi} = 2.1^{4.9}_{-1.3} \times 10^{-22} eV$. This value of the boson mass is compatible with that obtained by Wasserman et al. (2019) for their independent MCMC analysis of DF44 and also agrees with their relatively large negative value of β. Hence, this higher mass soliton for both the boson mass and the halo mass may be less physically compelling than the minimal model solution we found earlier, for which the reduced χ^2 is certainly acceptable, and for which the soliton is wider so that a relatively less extreme value of β is required (Luu et al., 2020; Kang et al., 2020; Łokas et al., 2005a; Klimentowski et al., 2007).

Summary & Conclusions

1. **Motivation**:

   Test ψDM model efficiency for stellar dynamics in classical dwarfs and the recently discovered UDGs, whiches such extended profiles seem to contradict CDM expectations.

2. **Methodology**:

   Step 1: Use the observable σ value to compute a consistent wave dark matter halo as described in section 3.1.

   Step 2: Apply the corresponding potential of the computed wave dark matter halo to Equation (3.7) in order to get the value of the projected velocity dispersion of Equation (3.12) and compare it with the observational profile.

3. **Results**:

   Result 1: Figure 4.1 shows the efficiency of wave dark matter to reproduce the observable data with a boson mass of $\sim 10^{-22}$eV.

   Result 2: Figure 4.3 clarifies how the ψDM model can reproduce observed velocity dispersion profiles of all kinds of galaxies; UDG(DF44), Intermediate galaxy (WLM), classical dwarf (Fornax), and ghostly galaxy (Antlia-2). While table 4.2 shows the consistency of the wave dark matter profile values with the theoretical ones.

Result 3: Even if Figure 4.4 shows how some NFW model is able to fit well the observed profile, the attached anisotropy (β) and scale radius (r_s) values of them, listed in table 4.3, seem unreasonable.

4. **Conclusions**:

   Conclusion 1: Here we have been particularly interested in whether this class of galaxy may have implications for the newly appreciated "Wave-Dark-Matter" interpretation of DM, because of the distinctive density profiles found in the first cosmological simulations in this context that predict a rich wave-like structure in the non-linear regime with collapsed halos that should contain solitonic standing wave core of dark bosonic matter at the center surrounded by a wide halo of excited states that are fully modulated in density on the de Broglie scale (Schive et al., 2014a,a, 2016)

   Conclusion 2: We have shown that this distinctive Wave-DM profile can account for the puzzling combination of the large radius of DF44 and its shallow, low velocity dispersion profile predicted for intermediate mass halos, of approximately $\simeq 4 \times 10^{10} M_{\odot}$ with a soliton radius of $\simeq 400pc$, this is several times more massive than typical dwarf spheroidal galaxies in the local group neighbourhood for which Wave-DM profiles fitted typically have masses of a few $\times 10^9 M_{odot}$ with a soliton radius of $\simeq 700pc$ (Schive et al., 2014a; Chen et al., 2017).

   Conclusion 3: Regarding the NFW profile, our Jeans analysis has explored the range of concentrations, $10 < c < 20$, predicted by ΛCDM simulations for dwarf galaxies and we have examined the scale length of the Plummer profile used to model the projected star profile for comparison with the measured half light radius of 4.6Kpc for DF44. We firstly adopted the pure NFW halo and isotropic stellar orbits, $\beta = 0$, which produced a centrally rising velocity dispersion, that is at odds with the flat profile of DF44, as shown in Figure 4.3, irrespective of the halo mass. To help flatten the dispersion profile we extend our Jeans analysis to large negative values of β, larger than used for ψDM profile and this reverses the predicted velocity dispersion profile, more like the data, as shown in Figure 4.3, for the profiles with $\beta < 0$. To reproduce the large observed stellar half light radius, 4.6kpc requires a high halo mass with a larger mean velocity dispersion as shown as the NFW_4 profile in Figure 4.3. A reasonable compromise can be found by either lowering the concentration allowing a lower halo mass, given by the NFW_5 solution listed in Table 4.3, and shown in Figure 4.4, for which the DM scale length is only 30% smaller than the stellar profile, or by enhancing the velocity anisotropy with the NFW_3 solution where the scale length matches the observations with $\beta = -2$. Thus one may conclude that in order to obtain a reasonable fit to DF44 that it is possible to reverse the inherent tendency for a centrally rising profile to match the observed centrally declining profile by invoking sizeable radial velocity anisotropy.

   Conclusion 4: We conclude that the NFW is in some significant tension with DF44, but is not firmly excluded provided the relatively large tangential velocity dispersion anisotropy can be deemed reasonable for a NFW halo sufficient to explain the relatively large half light radius scale. Core formation

by outflows may help to lower the central dispersion though if this requires repeated outflows of recycled gas for a lasting dark core(Pontzen & Governato, 2012), including UDG galaxies (Freundlich et al., 2020) and a minimum level of star formation (Bose et al., 2019; Benítez-Llambay et al., 2019; Dutton et al., 2020)this may conflict with the old age and rather low stellar metallicity estimated for DF44(van Dokkum et al., 2019b). The advantage of ψDM is that it supplies an inherently large core without the need for transformative outflows.

Conclusion 5: This consistency we find for DF44 with ψDM is important as it extends the viability of this form of wave-like DM beyond the dSph class for which clear agreement has been claimed with the wide solitonic cores predicted for this lower mass class of galaxy. The Milky Way provides more evidence of this possibility, as a dense, dark central mass of $10^9 M_\odot$ has been uncovered (Portail et al., 2017) from the centrally rising dispersion profile of bulge stars that appears in excellent agreement with the expectation of ψDM for a boson mass of $\simeq 10^{-22} eV$ (de Martino et al., 2020a).

4.2 Dwarfs' Wave DM core-halo structure (Paper 2)

Galaxies with low velocity dispersions $\lesssim$ 15 km/s, indicating small masses, are classed as "dwarfs" with half of the stars detected typically within only $r_{1/2} \simeq 0.3$ kpc (Check section 2.2.1 for more info). So it is surprising that several low mass dwarfs are now known to posses large halos of stars and dark matter extending to over several kpc, defying the dwarf definition. This includes two spectroscopically detected halos that are dynamically dominated by dark matter around the Tucana II and AndXXI dwarf spheroidal galaxies (Chiti et al., Chiti et al.; Collins et al., 2021). This adds to the case of Crater II, a dwarf that extends to over 3 kpc despite its very low velocity dispersion of $\simeq$ 3 km/s and also the "ghostly" Antlia II of extremely low surface brightness extending over 4 kpc with a dispersion of 6 km/s, discovered serendipitously using GAIA satellite proper motions(Torrealba et al., 2016; Collins et al., 2021). Such "large dwarfs" are at odds with the compact, high concentration profiles predicted for low mass galaxies in N-body simulations of standard heavy particle dark matter of cold Dark Matter (CDM), where dwarfs are predicted to have the highest internal density of dark matter of any galaxy, reflecting the relatively high Universal mean density at earlier times when dwarf galaxies were first formed. In this CDM context, the extended halos of dwarfs have been qualitatively attributed to tidal effects induced by the Milky Way, or Andromeda(Torrealba et al., 2019; Collins et al., 2021; Chiti et al., Chiti et al.), based on simulations that show stars may be periodically stripped or shocked near pericenter to beyond the tidal radius, generating halo-like extensions of enhanced velocity dispersion, whereas the

outer velocity dispersions observed in most dwarf halos appear to be significantly lower than in their cores (Wilkinson et al., 2004; Fabrizio, 2016; Collins et al., 2021). Strong tidal effects are expected for only a minority of orbiting dwarfs on eccentric orbits with small pericenters and so it is important to examine the generality of stellar halos to determine whether such halos are atypical or perhaps a common structural component of dwarf galaxies. Two such cases of the Milky Way dwarfs are definitively established to be in the process of being tidally stripped, namely the Sagittarius and Tucana III dwarfs which show opposing pairs of tidal arms(Li et al., 2018; Newby et al., 2013), representing only $\simeq 5\%$ of the dwarfs orbiting the Milky Way and both of these dwarfs have relatively small orbits.

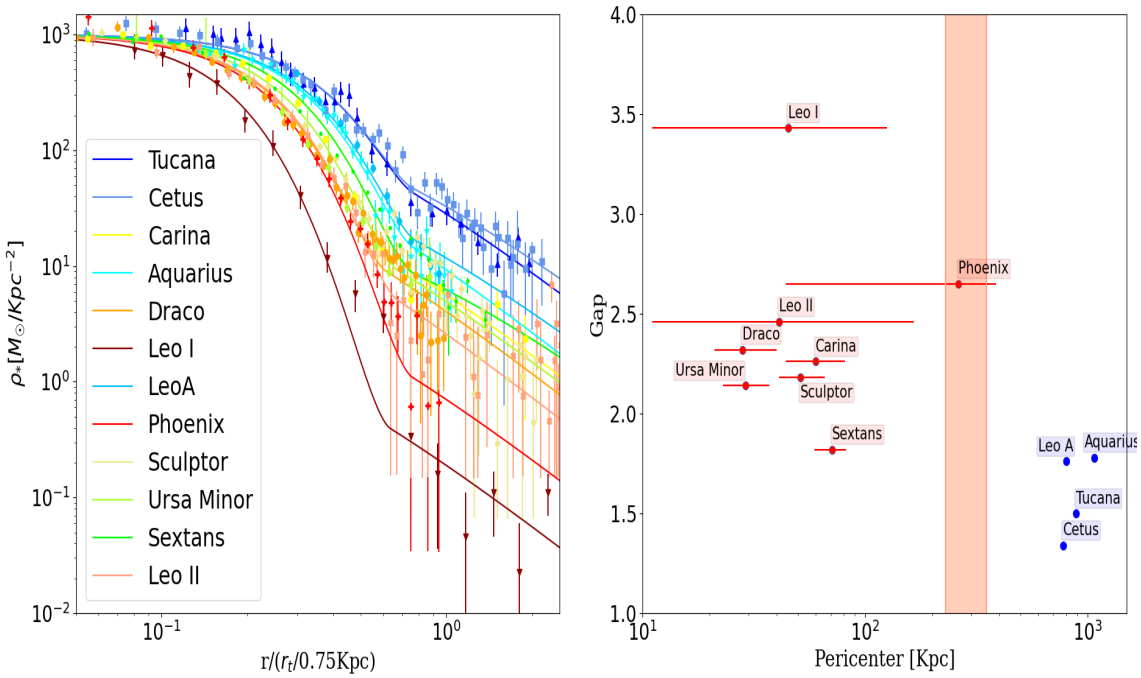

Figure 4.6: Stellar profiles of classical dwarfs orbiting the Milky Way and also the four well known "isolated" dwarfs that lie beyond in the Local Group (all listed in Table 1), and rescaled by their measured transition radius, revealing these profiles have a common core-halo form that is more pronounced for the orbiting dwarfs (redder colors) for which the halo density is generally lower than the "isolated" dwarfs (bluer profiles). **The right hand panel** compares the change in stellar density, or "gap", between the core and halo against the pericenter radius estimated from GAIA proper motions, showing the isolated dwarfs beyond the Milky Way (blue points) have generally smaller transition amplitudes compared to most of the orbiting dwarfs (red points).

Here we examine the outer profiles of all known classical dwarf spheroidal galaxies (dSph) in the local neighborhood, where stars can be individually counted to large radius, so the entire stellar profile can be traced free of surface brightness limitations. We start with the best studied "isolated" dwarfs lying beyond the virial radius of the Milky Way, and understood not to have interacted tidally with the major members of the Local group (Gregory et al., 2019; Fraternali et al., 2009;

Taibi et al., 2018; Kirby et al., 2017). These isolated dwarfs include Cetus, Tucana, Aquarius and Leo A, which have small velocity dispersions $\simeq$ 10 km/s and old spheroidal stellar populations. Their stellar profiles are shown in Figure 4.7, where their large radial extents are visible to over $\simeq$ 2 kpc (Gregory et al., 2019; McConnachie & Irwin, 2006; McConnachie et al., 2006). It is also apparent from Figure 4.7 that the stellar halos of these dwarfs extend radially from a well defined core, with a clear transition in density between the core and the halo. The core is reasonably well fitted by the standard Plummer profile in each dwarf (red curve in Figure 4.7), but falls well short in the halo region beyond a transition radius indicated in Figure 4.7 (vertical orange band). Reinforcing observations the assumption of section 3.3.

We now turn to the well studied classical dwarf galaxies orbiting the Milky Way. For these, detections of stars at surprisingly large radius beyond the estimated tidal radiusIrwin & Hatzidimitriou (1995) and originally termed "..'extra tidal stars' - for convenience..." (Irwin & Hatzidimitriou, 1995). Subsequently, such stars have been assumed to be tidally stripped, motivated by simulations where temporary extensions can be generated for dwarfs on rather radial orbits. However, the predicted enhancement of the velocity dispersion for stripped in the simulations may conflict with the observations, as reduced velocity dispersions are found at large radius (Wilkinson et al., 2004). In Figure 4.6 we compare the deepest, wide-field profiles for the classical dwarfs, for which a general core-halo structure is seen extending beyond $\simeq$ 1.0 kpc, with very similar outer profile gradients that are relatively shallow and extend well beyond the standard Plummer profile. Distinct cores are also evident, with a clear density transition between the core to the halo visible in most cases, (individual fits shown in Figure 4.11, and fitted parameters listed in Table 4.4). In Figure 4.8_{left} we scale the stellar profiles by their individually fitted core radius, which reveals more clearly the distinctive core-halo profile, with relatively larger density transitions seen for these orbiting dwarfs (red data, Figure 4.8_{right}) than the mean isolated dwarf profile (blue data, Figure 4.8_{right}). The observed profiles are seen to be very similar within the core region, below the mean transition radius of 0.75kpc, whereas at larger radius the profile vary by two orders of magnitude, but with similar gradients.

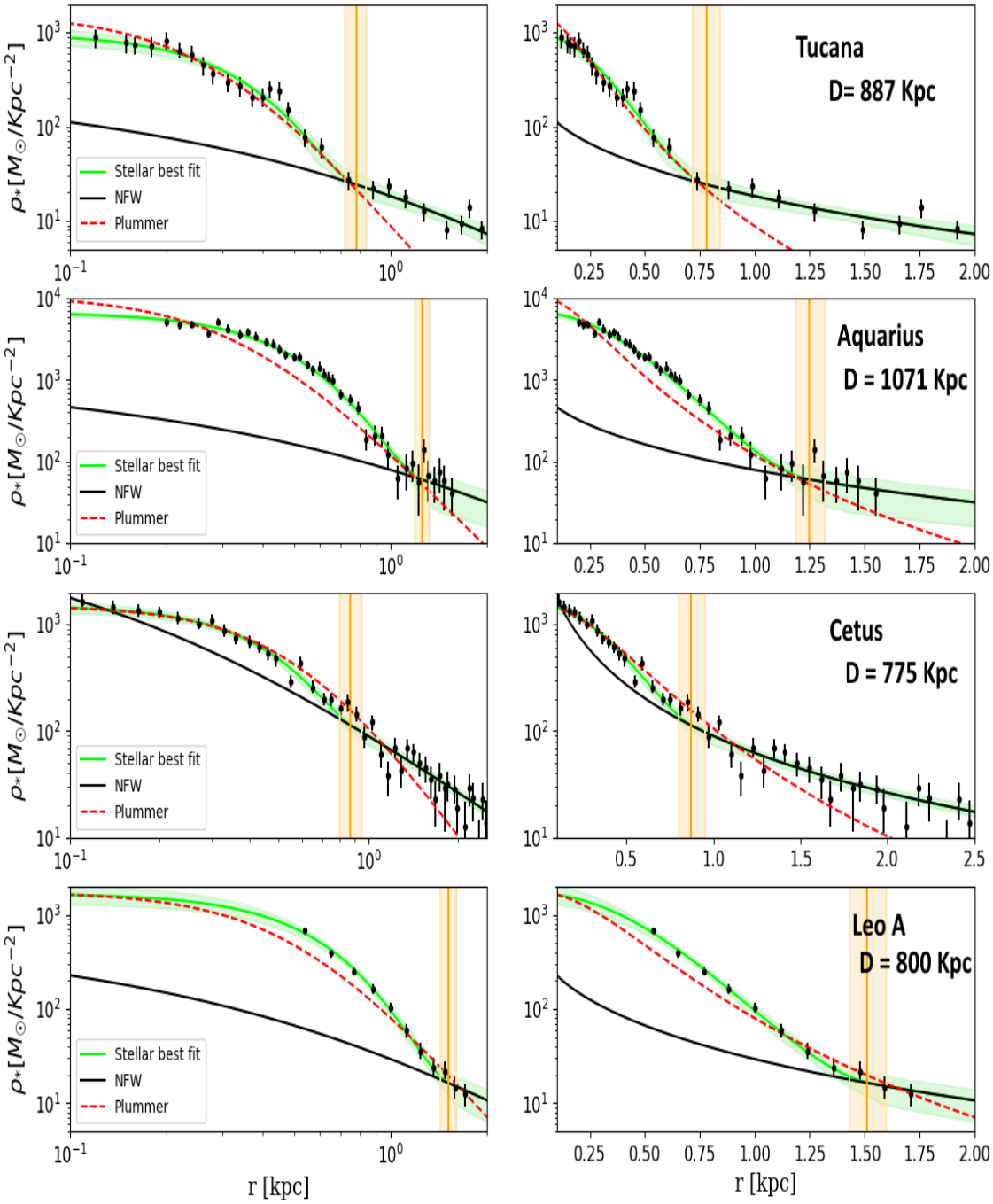

Figure 4.7: Isolated Dwarf Galaxies: This figure shows the star count profiles versus dwarf galaxy radius for the well studied "isolated" dwarf galaxies in the local group, lying outside the virial radius of the Milky Way. (In the right panels D shows the distance from the Milky Way galaxy center.) Each dwarf galaxy has an extended halo of stars stretching to $\simeq 2$ kpc and most evident on the linear scale of left hand panel. Cores are also evident on a scale < 1 kpc in each dwarf. A standard Plummer profile (red curve) is seen to fit approximately the core region but falls well short at large radius. Our predictions for light boson dark matter, ψDM, are shown in green, where the distinctive soliton profile provides and excellent fit to the observed cores with the surrounded halo of excited states that average azimuthally to an approximately NFW-like profile beyond the soliton radius. The observed cores are excellent agreement with the predicted soliton, best seen on a log scale in the right panels, and the predicted ψDM halo (grey curve) is also seen to match well the observed halos, including the characteristic density drop of about a factor of $\simeq 30$ predicted by ψDM between the prominent core and tenuous halo at a radius $\simeq 1$ kpc indicated by vertical orange band. The best fit MCMC profile parameters are tabulated in the appendix.

We define a transition gap to quantify the change in density between the core and the halo; $\Delta_{C-H} = \log \rho_C/\rho_H$, where ρ_C is the asymptotic central core stellar density, and shown in Figure 4.6_{right}. The value of the gap is generally larger for the orbiting dwarfs than the isolated dwarfs, with $\Delta_{C-H} > 2.0$, see Figure 4.6_{right}. The largest core-halo transition is found for Leo I, with $\Delta_{C-H} \simeq 3.5$ (Figure 4.6_{right}) and so it is interesting that although Leo I is relatively distant now at 250 kpc, its orbital pericenter is now established by the GAIA satellite to be only $\simeq 50$ kpc, moving on an eccentric orbit (see table 4.4) where tidal stripping is enhanced during close approaches Sohn et al. (2007). Tidal effects are also claimed for Ursa Minor (Martínez-Delgado et al., 2001), Sculptor (Walker & Peñarrubia, 2011; Amorisco & Evans, 2012) and Carina dwarfs (Battaglia et al., 2012b).

The core-halo structure we have uncovered here is a general feature of these classical dwarfs and far from expected for standard CDM, where low mass galaxies should be concentrated and core-less, with no inherent density transition. A fair fit to the inner region is provided by the Plummer profile, standard in Jeans analysis, but clearly does not extend into the halos. Expectations of small sizes and high concentrations for low mass galaxies are conditioned by CDM simulations, however a physically very different explanation for dark matter as light bosons is now understood to naturally form wide cores and extended diffuse halos. This is seen in the first simulations of dark matter (DM) as a Bose-Einstein condensate(Schive et al., 2014a,b; Schwabe et al., 2016) revealing unanticipated, rich wave-like structure on the de Broglie scale, described simply by a coupled Schröedinger-Poisson equation for the mean field behavior under self-gravity, hence the term ψDM. Condensates are inherently non-relativistic and hence ψDM behaves as "cold" dark matter on large scales, exceeding the de Broglie wavelength, where it is statistically indistinguishable from CDM, as demonstrated in the first simulations (Schive et al., 2014a). Several unique predictions are now established for ψDM, including a dark core within each galaxy that follows the soliton solution of the Schröedinger-Poisson equation (see methods) with a radius, r_{sol}, set by the de Broglie wavelength and also that this core radius should be largest in lower mass galaxies, m_{gal}, of lower momentum, scaling as: $r_{sol} \propto m_{gal}^{-1/3}$ as predicted by Schive et al. (2014b)Schive et al. (2014b) and verified in independent simulations, (Schwabe et al., 2016; Niemeyer, 2020; Mocz et al., 2017; Veltmaat et al., 2020; Hui et al., 2020).

The predicted soliton profile has been shown to match well the Fornax dwarf, for which the dynamical data extends beyond the core radius allowing a determination of the boson mass of $m_\psi \simeq 10^{-22}$eV (Schive et al., 2014a) and this supported by Jean's analyses of other classical dwarfs (Chen et al., 2017).

Here we examine the unique prediction that the density of ψDM should transition sharply between the soliton core and the surrounding halo, as the soliton forms a prominent core that contrasts by over an order of magnitude in density above the halo. This transition is predicted to be distinct even though observations are made in projection, because the soliton core is close to a Gaussian and hence its sharp 3D boundary is preserved in 2D at the core radius. It is important to appreciate this prominent core is quite unlike the behaviour of smooth cores employed, where the

core is continuous in density with the halo. In contrast, the ψDM core is a stable standing wave that is a gravitationally self-reinforcing (Schive et al., 2014b) with a pronounced overdensity predicted to be about > 30 times denser than the surrounding halo in the case of low mass galaxies relevant here, of $\simeq 10^{10} M_{\odot}$ (see Figures 1 & 2 of Schive et al. (2014b)). It is also clear that the soliton core is relatively stable to tidal stripping compared to the halo, as shown in recent simulations of dwarf galaxies orbiting the Milky Way (Schive et al., 2020) as the soliton by nature is self reinforcing. The halo comprises excited de Broglie scale waves that fully modulate the density but is seen in the simulations to average azimuthally to an approximately Navarro-Frenk-White (NFW), reflecting the cold, non-relativistic nature of the condensate on scales exceeding the de Broglie wavelength (Schive et al., 2016).

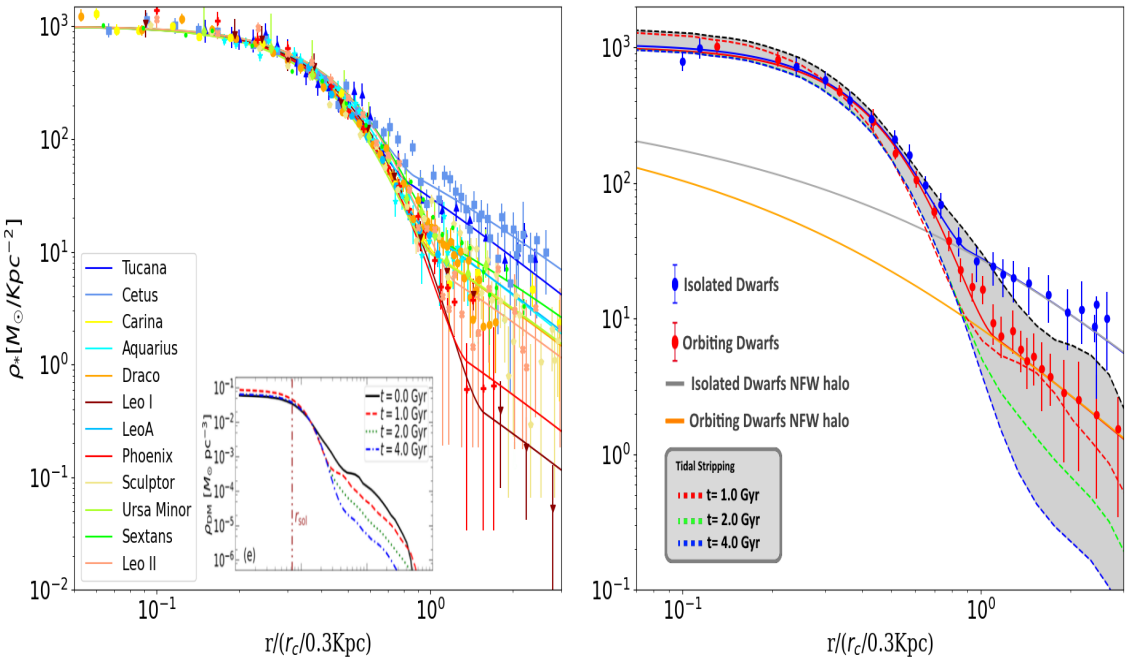

Figure 4.8: **The left hand panel** compares all the dwarf profiles scaled by their individual best fitting core radius. The profiles are very similar in the core region, differing in the extended halo region relative to the core, with the isolated galaxies (bluer colors), having denser halos than the orbiting dwarfs (redder colors). **The right hand panel** shows the projected simulation profiles for ψDM by Schive et al. (2020), where little dependence on the degree of tidal stripping is predicted for the core region, in contrast to the halo region bracketed in grey where stripping is significant. The duration of stripping is indicated by the legend and also shown in the inset of the left hand panel spanning 1-4Gyrs, and matching well the observed range of halo profiles. Note, the simulations predict the halo slope is relatively shallow and fairly independent of the degree of stripping, in good agreement with the mean halo profile of the isolated dwarfs (blue data) and the orbiting dwarfs (red data points) including the larger core-halo transition of the orbiting dwarfs. The NFW profile fits to the halos are also shown and can be seen to fall well below the prominent cores.

We first perform MCMC based ψDM profile fits to the isolated dwarfs, shown in Figure 4.7. The shape of the soliton core profile is fully characterised by the core radius, r_c. For the halo we fit an NFW profile with scale radius r_{s*} and normalization ρ_{o*}. The only other free parameter we require is the transition radius, r_t, defining the radius of the density transition between the soliton and NFW profile which we vary within a prior range indicated by the ψDM simulations, of $2-4\times r_c$ (see Method's section 3.3), with the best parameters and uncertainties listed in Table 4.4 and in Figures 4.67, 4.68, 4.69 and 4.70.

We now compare the ψDM model with the orbiting dwarfs, with new ψDM simulations that quantify the effect of tidal stripping of a dwarf galaxy orbiting within a Milky Way sized halo, shown in Figure 4.8_{right}. The main effect of tidal stripping is to strip the relatively tenuous halo, thereby enhancing the density transition at the core-halo radius, providing a natural explanation for the generally larger "mass gap" of the orbiting dwarfs compared to the isolated dwarfs, plotted in Figure 4.6_{right}. In detail, the family of profiles for the orbiting dwarfs in seen in Figure 4.8_{right} to span the predicted range when tidal stripping is included, spanning several Gyrs, as can be seen in Figure 4.8_{left}. The Sextans dwarf galaxy has a core-halo transition that is intermediate between orbiting and isolated dwarfs, with an extensive core-halo structure and a transition gap of $\Delta_{C-H}\simeq 1.8$ (Figure 4.6_{right}), suggesting that Sextans is less tidally stripped than the other orbiting dwarfs, a conclusion supported by the undisturbed morphology and simple internal dynamics noted for Sextans (Roderick et al., 2016; Okamoto et al., 2017), indicating Sextans may have become bound to the Milky Way relatively recently.

Galaxy	r_c (kpc)	r_t (kpc)	r_{s*} (kpc)	Gap(Log) Δ_{C-H}	Distance (kpc)	Pericenter (kpc)	σ_{los} (km/s)	Ref -
Aquarius	$0.35^{+0.01}_{-0.01}$	$1.25^{+0.07}_{-0.06}$	$1.05^{+0.82}_{-0.64}$	1.78	1071	-	-	-
Cetus	$0.36^{+0.02}_{-0.02}$	$0.87^{+0.08}_{-0.07}$	$0.24^{+0.14}_{-0.06}$	1.34	775	-	-	-
Tucana	$0.25^{+0.01}_{-0.01}$	$0.78^{+0.06}_{-0.06}$	$1.05^{+0.90}_{-0.57}$	1.5	887	-	$13.3^{+2.7}_{-2.3}$	(Gregory et al., 2019)
Leo A	$0.43^{+0.02}_{-0.02}$	$1.51^{+0.09}_{-0.08}$	$0.73^{+0.49}_{-0.47}$	1.76	800	-	-	-
Sextans	$0.48^{+0.01}_{-0.01}$	$1.31^{+0.05}_{-0.06}$	$1.61^{+0.51}_{-0.49}$	1.82	90	71^{+11}_{-12}	$7.0^{+1.3}_{-1.3}$	(Cicuéndez & Battaglia, 2018)
Phoenix	$0.28^{+0.05}_{-0.06}$	$1.27^{+0.01}_{-0.01}$	$1.10^{+0.54}_{-0.55}$	3.44	415	263^{+126}_{-219}	$9.3^{+0.7}_{-0.7}$	(Zaggia et al., 2011)
Leo I	$0.24^{+0.01}_{-0.01}$	$1.30^{+0.08}_{-0.08}$	$1.75^{+0.78}_{-0.96}$	3.43	250	45^{+80}_{-34}	$9.2^{+1.2}_{-1.2}$	(Koch et al., 2007b)
Draco	$0.17^{+0.01}_{-0.01}$	$0.56^{+0.02}_{-0.02}$	$0.1^{+0.09}_{-0.05}$	2.32	80	28^{+12}_{-7}	$9.1^{+1.2}_{-1.2}$	(Łokas et al., 2005a)
Carina	$0.21^{+0.01}_{-0.01}$	$0.81^{+0.04}_{-0.04}$	$1.17^{+0.51}_{-0.61}$	2.26	101	60^{+21}_{-16}	-	-
Sculptor	$0.20^{+0.01}_{-0.01}$	$0.72^{+0.07}_{-0.07}$	$0.12^{+0.25}_{-0.09}$	2.18	80	51^{+15}_{-10}	$9.2^{+1.4}_{-1.4}$	(Walker et al., 2009)
Ursa Minor	$0.28^{+0.01}_{-0.01}$	$0.96^{+0.05}_{-0.04}$	$0.52^{+0.90}_{-0.40}$	2.14	66	29^{+8}_{-6}	$9.5^{+1.2}_{-1.2}$	(Walker et al., 2009)
Leo II	$0.14^{+0.01}_{-0.01}$	$0.60^{+0.03}_{-0.03}$	$1.34^{+0.42}_{-0.55}$	2.45	210	45^{+121}_{-30}	$6.6^{+0.7}_{-0.7}$	(Walker et al., 2009)

Table 4.4: Observations and ψDM profile fits. Column 1: Dwarf galaxy colour coded as in figure 2b, Column 2: Core radius r_c, Column 3: Transition point r_t, Column 4: Stellar scale radius r_{s*}, Column 5: Gap Δ_{C-H}, Column 6: Distances from Milky Way center & Column 7: Pericenter determined from GAIA Fritz et al. (2018), Column 8: Mean dispersion velocity σ_{los} from McConnachie & Venn (2020), Column 9: References of the profiles of figure 4.10.

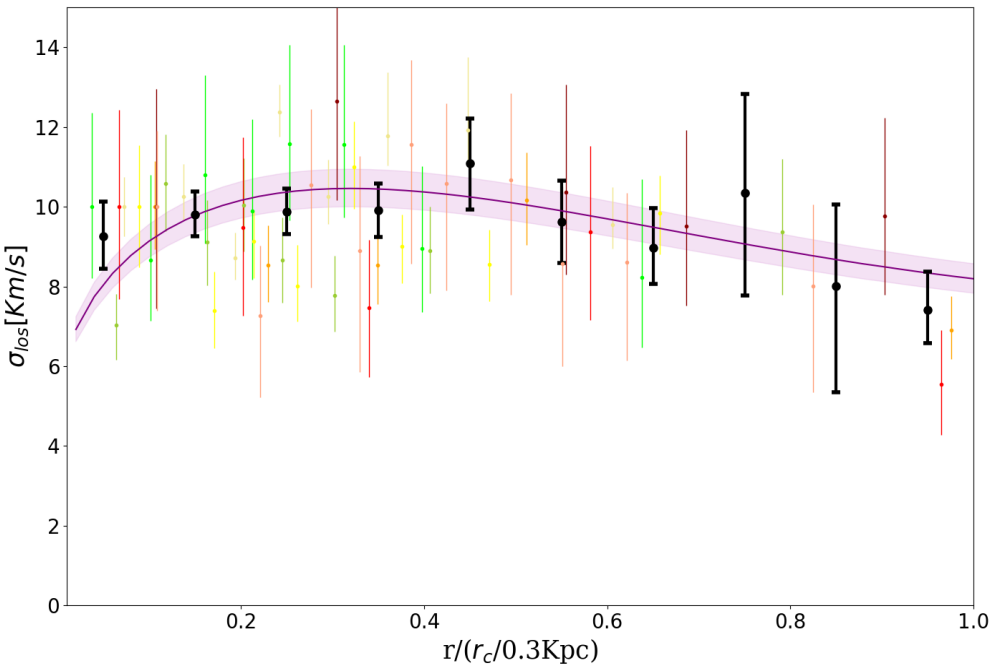

Figure 4.9: Comparison of the predicted mean velocity dispersion of the ψDM profile (purple model curve), with the mean observed velocity dispersion shown as black data points with errors averaged over the eight dwarfs with well resolved dynamical data, in units of the core radius from fitting the star counts (listed in Table 4.4). The individual dispersion data are also shown for each dwarf, (coloured in the same way as Figures 4.6 & 4.8) and normalised to the mean level for this comparison, demonstrating the dwarfs follow the general form expected for ψDM, peaking near the observed mean core radius of $\simeq$ 0.3 kpc, and then declining into the lower density halo. The mean level of the dispersion at the peak is 10 km/s and together with the mean core radius of 0.3 kpc may be used to obtain an approximate boson mass, via eq. 3.4 to $\simeq 1.5 \times 10^{-22}$eV, for a mean formation redshift of z=6.

We now make an independent, dynamical consistency check of our ψDM fitted stellar profile fits above, using the well resolved velocity dispersion profiles available for most of the classical dwarfs, by inputting our bestfit ψDM density profile for each dwarfs into the Jeans equation (see section 3.2) to predict the corresponding velocity dispersion profile for comparison with the data for each dwarf. The form of these predicted velocity dispersion profiles should peak just beyond the core radius and then decline into the lower density halo, as shown in Figure 4.10, where consistency is evident in each case, both in terms of the form of the profile and in terms of the stellar core radius (vertical lines in Figure 4.10). The amplitude of the dispersion profiles peaks at a mean level of $\simeq$ 10 km/s and together with the mean core radius of $\simeq 0.3kpc$ provides an estimate of the boson mass of $1.3 - 1.7 \times 10^{-22}$eV (see appendix) as indicated by the spread in the model curves in Figures 4.9 and 4.10. This is similar to the boson mass from other dynamical studies for these classical dwarfs for ψDM (Schive et al., 2014a; Chan et al., 2020; Broadhurst et al., 2020), and for the intermediate mass galaxy DF44 (Pozo et al., 2020) and also consistent with the boson mass estimate for the claimed soliton core within the Milky Way of $\simeq$ 100pc, which is smaller than for dwarf galaxies estimated here, reflecting the

inverse momentum dependence of the de Broglie scale (Schive et al., 2014b).

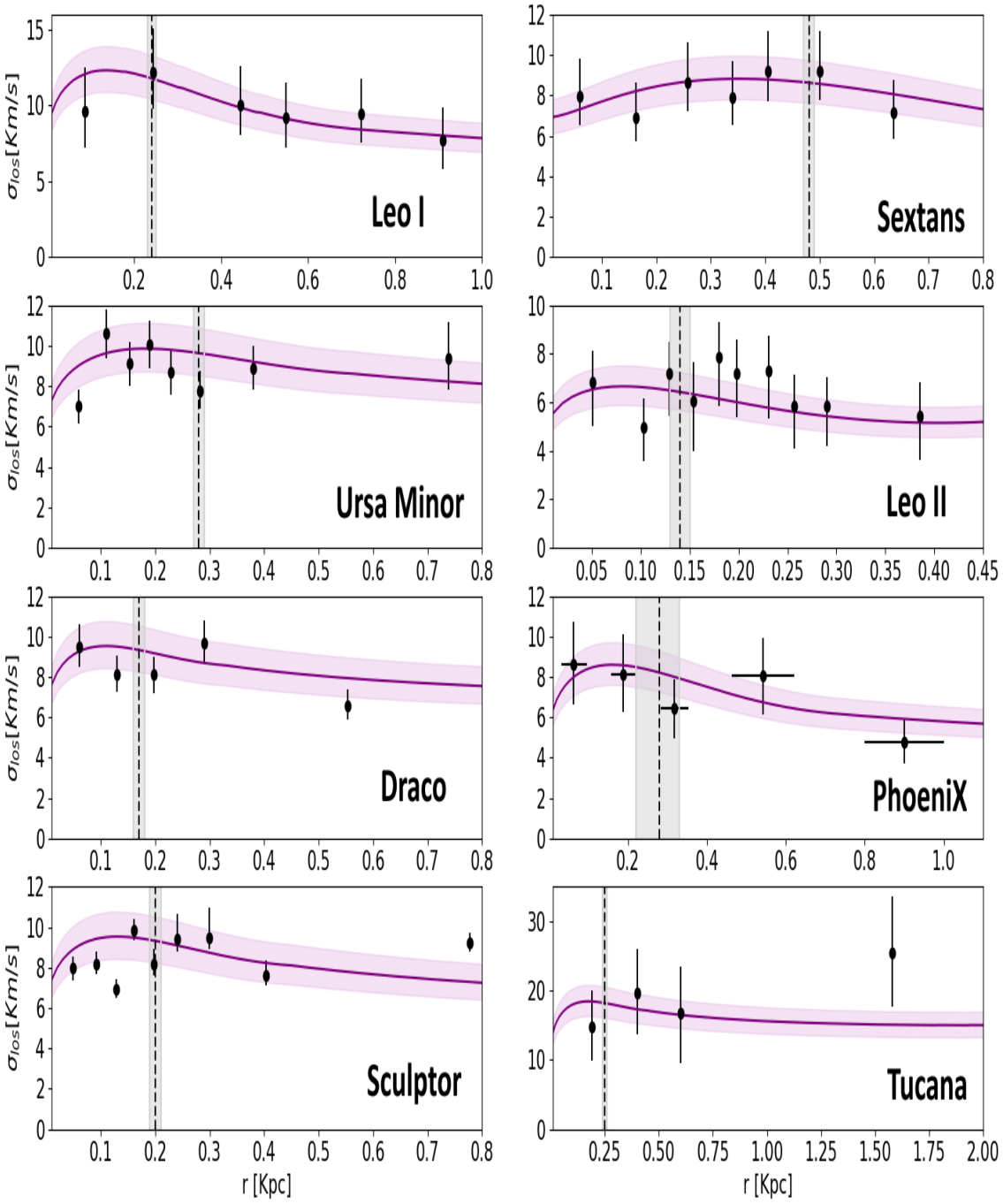

Figure 4.10: Comparison of the well measured dispersion profiles (black data points) of the classical dwarfs, with the ψDM model fit obtained from the stellar profiles with our MCMC analysis above (purple curves), indicating good consistency in general with the characteristic ψDM dispersion profile that can be seen to peaks near the core radius in each case, indicated by the vertical band (listed in Table 1). The range of model profiles shown spans the range of boson mass of $1.3 - 1.7 \times 10^{-22}$eV, and assumes a modest fixed anisotropy parameter, β = -0.5

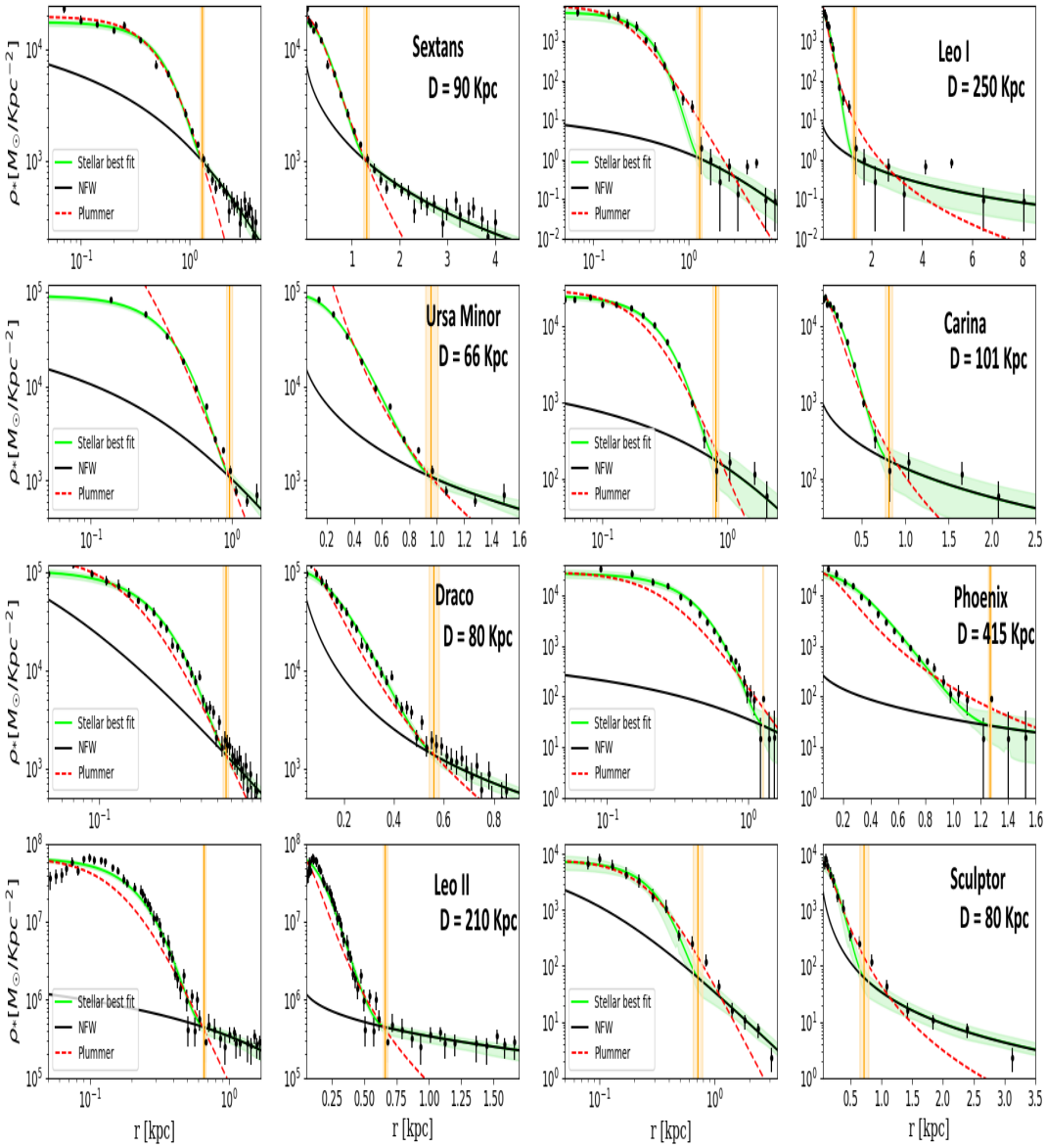

Figure 4.11: Stellar density profiles of orbiting dwarf galaxies listed on table 4.4. The green profile shows the 95% uncertainty on the fitted profile obtained from the MCMC simulation. with the model transition radius r_t and uncertainty marked as the vertical orange bar, separating the core and halo regions. Notice the highly extended halos for Carina, Leo I, Sculptor, Sextans and Leo II were after subtracting the background level, stars can be detected to even 8kpc in the case of Leo I. The red dashed line represents the standard Plummer profile with the r_{half} of each galaxy as the only free parameter, observe how is not sufficiently pronounced for almost all the galaxies in contrast to the soliton. References for the data are: Tucana (Gregory et al., 2019), Cetus (McConnachie & Irwin, 2006), Leo A (Kang & Ricotti, 2019) , Aquarius (McConnachie et al., 2006), Carina Frinchaboy et al. (2012), Ursa Minor (Martínez-Delgado et al., 2001), Leo I (Sohn et al., 2007), Leo II (Moskowitz & Walker, 2020), Phoenix (Battaglia et al., 2012a), Sculptor (Frinchaboy et al., 2012), Sextans (Okamoto et al., 2017) and Draco (Wilkinson et al., 2004)).

Summary & Conclusions

1. **Motivation**:

   Motivation 1: All the explained points in section 3.3 assume that stars trace dark matter in a ψDM context.

   Motivation 2: Working with the assumption that stars trace dark matter; NFW is inefficient to describe the density profile in the center due to its cuspy profile. At the same time, Plummer and king profiles cannot describe the outsider extended stellar halos due to their rapid fall of the density at large radiuses. Therefore they cant also explain the different observed $\Delta_{C-H} = \log \rho_C/\rho_H$, a product of tidal iterations.

2. **Methodology**:

   Step 1: Establish a selection criterion for the galaxies, only analyzing galaxies with two main characteristics; stellar cores from 150 to 500 pc and with $\sigma \sim$ 10 km/s. They are divided between isolated and orbiting to emphasize the excellent source that isolated galaxies should be due to not suffering tidal forces and supposedly being in their natural conditions. Orbiting should be the ones inside Milky Way's virial radius, 230-350 kpc, marked by a vertical shaded region in the right panel of figure 4.6.

   Step 2: Fit our best ψDM stellar profile (section 3.3) to the observed stellar profile of the galaxy in order to quantify the core radius size (r_c) and the transition point (r_t) between the soliton and the NFW-like halo (represented in Figure 4.69). With this wave dark matter profile, we will also quantify the density gap between the core and the halo, observed in the stellar profile, $\Delta_{C-H} = \log \rho_C/\rho_H$.

   Step 3: Normalize all the different galaxy profiles to compare the different density gaps ($\Delta_{C-H} = \log \rho_C/\rho_H$).

   Step 4: Apply the used wave dark matter profile of the first step to check his consistency with the observable dynamical data, calculating the projected velocity dispersion by equations (3.7) and (3.12).

3. **Results**:

   Result 1: Compute all the ψDM profiles that fit well with each individual stellar profile with equations (3.16) and (3.17) of section 3.3 with a fixed boson mass of 1.5×10^{22}eV. The correspond value of r_c, product of equations (3.17) and (3.4) will give us the core size of the galaxy while the observed regime change will give us the value of r_t, equation (3.16) (Results in table 4.4). The selected value of m_ψ is only motivated by previous works that recommend such value to get reliable halo masses of $10^{9-10}M_\odot$. **Notice that the selected boson mass will not provide different r_c and r_t values, as these are direct results of the stellar profile shape. So the assumption of different boson masses and halo masses combinations will always**

provide the same r_c and r_t values for a certain stellar profile. Check figures 4.7 and 4.11 to see how the stellar profiles follow the wave dark matter imprint in the soliton and NFW-like imprint in the halo, being the transition point (set by de Broglie wavelength) equal for stars and DM.

Result 2: Figure 4.6 shows an apparent correlation between the density gap ($\Delta_{C-H} = \log \rho_C/\rho_H$) and the possible tidal iterations suffered by the galaxies, where the isolated galaxies show a smaller gap, check figure 4.6. This seems to be reinforced by the independent simulations from (Schive et al., 2020) where the core seems to be most robust against tidal forces while the halo gets easier stripped (More explanations in section 3.4), something that matches accurately with the observable data, see figure 4.8.

Result 3: Figure 4.10 clarifies how the ψDM model is able to reproduce observed velocity dispersion profiles of all these dwarfs, isolated and orbiting.

4. **Conclusions**:

   Conclusion 1: Here we find large halos are a general feature of the well known dwarfs orbiting the Milky Way and also for the isolated dwarfs in the Local Group. These large halos of stars and dark matter around some of the lowest mass galaxies defy CDM expectations that dwarf galaxies should be small and dense.

   Conclusion 2: These halos are seen to surround a dense core within each dwarf, with a clear density transition visible between the core and the halo at a radius of $\simeq$ 1.0kpc. This common core-halo structure is hard to understand for standard heavy particle dark matter where featureless, concentrated profiles are predicted, whereas dark matter as a Bose-Einstein condensate, ψDM, naturally accounts for the observed profiles, predicting a dense soliton core in every galaxy surrounded by a tenuous halo of interfering waves. We show that the stellar profiles are accurately fitted by the core-halo structure of ψDM, with only one free parameter, the boson mass.

   Conclusion 3: The case we have made here for common core-halo structure, with consistency found between the stellar profiles and dynamics in the context of ψDM, implies stars trace well the dark matter in dwarf spheroidal galaxies. In summary, dark matter comprised of light bosons, such as the axions generic in String Theory, provides a compelling solution for the structure of dwarf galaxies with stars that simply trace the dark matter profile of a Bose-Einstein condensate.

   Conclusion 4: The observed different density gaps ($\Delta_{C-H} = \log \rho_C/\rho_H$) and the almost invariable stellar density profiles in the core region suggest that the halo is much weaker to tidal forces than the soliton. This point highly remarks the sturdiness of the soliton and will explain why stripped galaxies still show a core structure, in contradiction to CDM expectations.

   Conclusion 5: We also find independent consistency with the stellar velocity dispersions measured in these dwarf galaxies, which peak at the core radius and fall in the halo, at a level consistent with a boson mass of $\simeq 1.5 \times 10^{-22}$ eV.

4.3 Crater II and Classical dwarfs with tidally stretched Wave Dark Matter (Paper 3)

A surprising diversity of dwarf galaxies has been steadily uncovered over the past decade, with many "ultra faint dwarfs" (Moskowitz & Walker, 2020; Mutlu-Pakdil et al., 2018; Muñoz et al., 2018; Koposov et al., 2015) that are much smaller and denser than the well studied class of dwarf spheroidal galaxies (dSph), and other "ghostly" dwarfs of very low surface brightness that are large and lower in density. The aptly named "feeble giant", Crater II, has been particularly puzzling, with its dwarf-like velocity dispersion of only $\simeq 3$ km/s (Torrealba et al., 2016; Caldwell et al., 2017) and large size, over $\simeq 2$ kpc, that strains the dwarf definition in terms of size. Despite the low velocity dispersion, the mass-to-light ratio of Crater II is large, $M/L \simeq 30$ (Caldwell et al., 2017; Ji et al., 2021; Sanders et al., 2018) and appears to have a shallow, cored profile (Ji et al., 2021; Sanders et al., 2018) and an old, but not ancient stellar population, dated to $\simeq 10$ Gyrs (Torrealba et al., 2016; Caldwell et al., 2017), resembling in these respects the common class of dwarf Spheroidal galaxy (dSph) for which dark matter dominated cores are commonly claimed. However, both the stellar surface brightness and the velocity dispersion of Crater II are both much lower than the typical dSph dwarfs.

Here we determine whether this predicted momentum dependence of ψDM can account for the relatively unusual properties of Crater II, given that its relatively wide core and low-velocity dispersion relative to the classical dSphs seems to support this possibility qualitatively. Similarly, it has been proposed that an ultra-light boson of $m_\psi c^2 = (0.6 - 1.4) \times 10^{-22}$ eV accounts for the large size and modest velocity dispersion stars within Antlia II, consistent with boson mass estimates for more massive dwarf galaxies with smaller dark cores (Schive et al., 2014a) and places Antlia II close to the lower limiting Jeans scale for galaxy formation permitted by the Uncertainty Principle for this very light boson mass. New spectroscopy data has revealed that Antlia II has a systematic velocity gradient that is comparable with its velocity dispersion (Ji et al., 2021) indicating that it has suffered tidal elongation or possibly rotating, at least in the outskirts where the sign change of the velocity gradient is apparent (Ji et al., 2021). The tidal field of Crater II is also thought to have had a significant effect given the small pericenter that is now established for Crater II in the latest 'Gaia' based analysis (Ji et al., 2021), though it does not show any clear evidence for a velocity gradient nor visible elongation along its orbit, unlike the case of Antlia II where tidal effects appear more evident (Ji et al., 2021). Moreover, the range of core-to-halo variation predicted by this simulation has been shown to match well the family of profiles of dSph galaxies, indicating most are stripped at some level relative to the more distant "isolated" dSphs (Pozo et al., 2020).

The effect of tidal stripping in ψDM has been examined recently by Schive et al. (2020); Du et al. (2018) demonstrating the resilience of the soliton, which is self-reinforcing so that halo is stripped first, with an abrupt disruption of the soliton

predicted to follow if significant tidal stripping of the soliton follows (Du et al., 2018). A steady loss of the halo is found in the ψDM simulation of (Schive et al., 2020), for a typical dwarf of $10^9 M_\odot$, following a circular orbit of $\simeq$ 200 kpc in a Milky Way sized halo, showing that the halo density drops relative to the soliton over several Gyrs with little change in the slope of the density profile of the halo.

This behavior has been recently claimed to bracket the range of profiles found for dwarf spheroidal galaxies, which are observed to follow the predicted form with a clear core and halo structure seen in all the stellar profiles of the classical dwarf spheroidal galaxies (Pozo et al., 2020), and this is also supported by the generally lower level of the velocity dispersion seen in the halo relative to the core as predicted for ψDM (Pozo et al., 2020). This phenomenon is reinforced by (Schive et al., 2020) as he already found that tidal stripping increases the density contrast between the core and the halo, as the halo is relatively easily stripped compared to the core and as mass outside the tidal radius is stripped, the core should relax, becoming less massive and hence more extended, obeying the uncertainty principle. With increased stripping such that the tidal radius becomes similar in size to the core radius, the core will be disrupted, perhaps rather abruptly, leaving just extended tails (Du et al., 2018). A recent dedicated ψDM simulation that explores the properties of the Eridanus II dwarf, shows that under steady modest stripping the core remains stable as the halo is reduced in density, leading to an enhanced contrast over time between the relatively dense core and the tenuous surrounding halo (Schive et al., 2020), and the range of core-to-halo variation predicted by this simulation has been shown to match well the family of profiles of dSph galaxies indicating most are stripped at some level, relative to the more distant “isolated" dSphs (Pozo et al., 2020).

Here we focus on the "ghostly" dwarf galaxy, Crater II, found recently to be orbiting the Milky Way at a radius of 117 kpc currently (Torrealba et al., 2016), with a half-light radius of 1.1 kpc and with a relatively small pericenter, so that that significant tidal stripping is assumed to be likely, perhaps resulting in 90% reduction in its mass, with the possible presence of tidal distortion seen (Ji et al., 2021), consistent with the most recent 'Gaia' based pericenter estimate of only 18^{+14}_{-10} kpc (Fritz et al., 2018; Battaglia et al., 2022), well within the measured virial radius of the MW halo (Sanders et al., 2018).

4.3.1 Crater II's Modeling Results

The unusually large, “feeble dwarf" galaxy Crater II, with its small velocity dispersion, $\simeq$ 3 km/s, defies expectations that low mass galaxies should be small and dense. In this scenario, we try to define its unusual properties in the context of “Wave Dark Matter", combining the latest stellar and velocity dispersion profiles for Crater II, finding a prominent dark core of radius $\simeq 0.71^{+0.09}_{-0.08}$ kpc, surrounded by a low density halo, with a visible transition between the core and the halo. This observed behavior is very similar to the distinctive core-halo profile structure of dark

matter as a Bose-Einstein condensate, ψDM, where the ground state forms a prominent soliton core, surrounded by a tenuous halo of interfering waves, with a marked density transition predicted between the soliton and the halo. Crater II conforms well to this distinctive ψDM prediction, with consistency found between its large core and low velocity dispersion for a boson mass of $m_\psi c^2 \simeq (1.5 \pm 0.3) \times 10^{-22}$ eV. Similar core-halo structure is also apparent in most dwarf spheroidal galaxies (dSph), but with typically smaller cores, $\simeq 0.25$ kpc and higher velocity dispersions, $\simeq 9$km/s. We argue that Crater II may have been a more typical dSph dwarf that has lost most of its halo mass to tidal stripping in the context of ψDM, resulting in a factor 3 reduction in velocity dispersion causing a threefold expansion of the soliton core, following the inverse scaling between velocity and de Broglie wavelength required by the Uncertainty Principle. This tidal origin for Crater II is supported by its small pericenter of $\simeq 20$ kpc, now established by 'Gaia', implying significant tidal stripping by the Milky Way.

This behavior we have now established holds generally for the well studied dSph galaxies which all fit well the soliton core profile and with extended halos (Pozo et al., 2020). This behavior may be taken to imply simply that the stars trace the dark matter, as may be expected approximately in dark matter dominated galaxies of spheroidal morphology. Note also that the soliton form is closely similar to the standardly adopted Plummer form widely used to model dSph galaxies, where it fits well to several times the core radius but falls well short of the extended stellar halos now commonly found (Torrealba et al., 2019; Chiti et al., Chiti et al.; Collins et al., 2021; Pozo et al., 2020).

We now apply the wave dark matter paradigm (section 3.1 and 3.2) to the newly measured dispersion profile of Crater II dwarf galaxy, discovered by Torrealba et al. (2016) and some ideal ψDM cases. This unusual galaxy was identified in imaging data of the VST ATLAS survey and seemed to be located at $\simeq$120 kpc from the sun. Designed to search for extended low-surface-brightness emission (Torrealba et al., 2016). The galaxy Crater II is one of the most extensive examples of these low mass dwarfs, with a half-light radius ~ 1.08 kpc, and one with the lowest surface brightness dwarfs, similar to cases like Tuc II, Tuc IV, and UMa II. Its stellar velocity dispersion profile has recently been measured with deep spectroscopy by Caldwell et al. (2017). Its stellar velocity dispersion profile has recently been measured with deep spectroscopy by Caldwell et al. (2017) and found to be unusually low with a surprisingly low mean value of only 2.7km/s traced to over 1kpc shown in 4.12 where we see the data is consistent with the characteristic ψDM σ form which peaks at the soliton radius and declines into the halo (see figure 4.12).

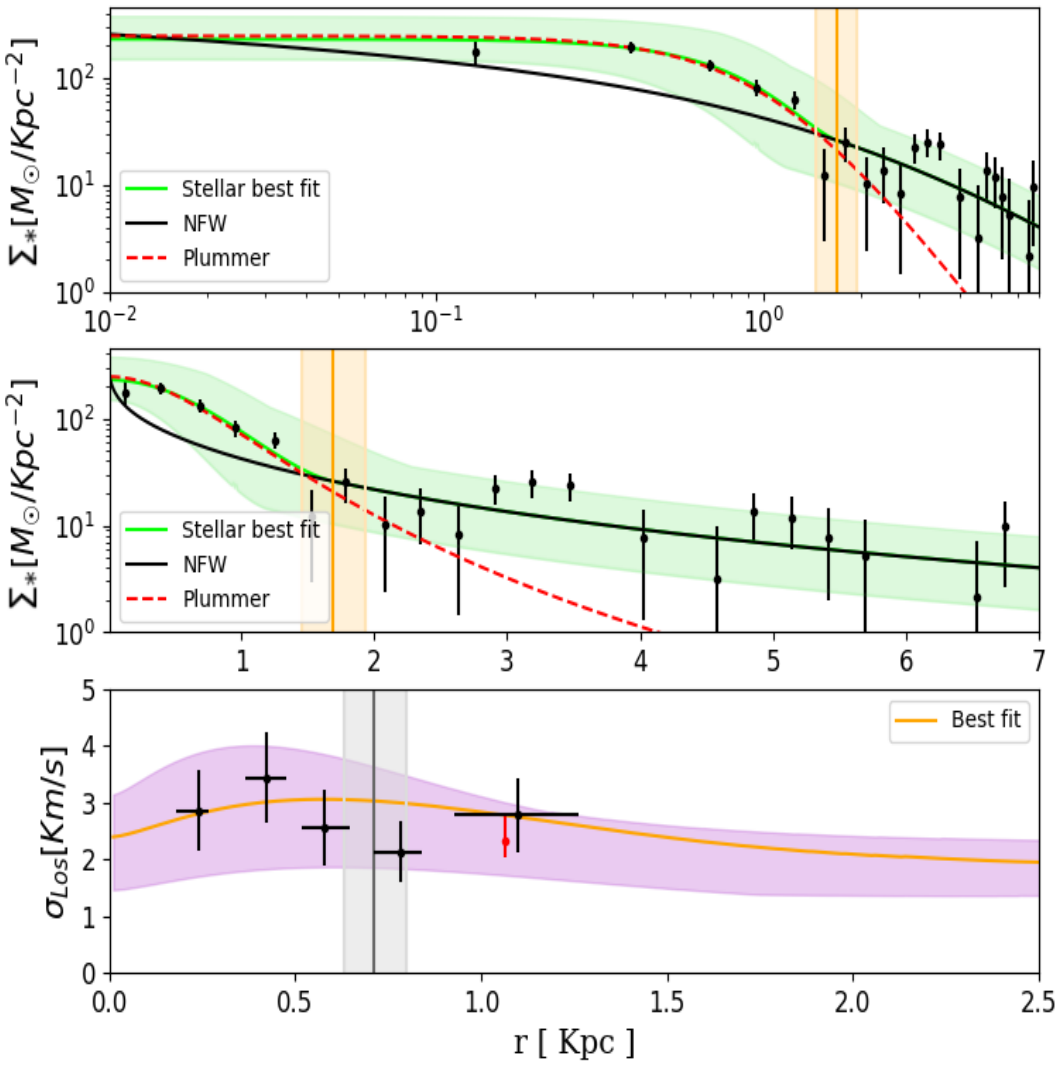

Figure 4.12: Stellar and velocity dispersion profiles of Crater II compared with ψDM. **Upper panel**: The data points are the star counts of Crater II rebinned from Torrealba et al. (2016), after applying background subtraction based on their asymptotic limit (red curve in Figure 5 of (Torrealba et al., 2016)), compared to the ψDM profile shown as the green shaded area, representing the 2σ range of the posterior distribution of profiles, including the soliton core and the outer halo approximate by the NFW form. The apparent excess at ∼3kpc seems to be a product of possible contamination by background galaxies (Torrealba et al., 2016). A standard Plummer profile is also shown, which is very similar to the soliton form but underpredicts the observations outside the core. The orange vertical shaded area indicts the transition radius of the ψDM core. **Middle panel**: this shows the same comparison as the upper panel, but on a linear scale, so the extent of the halo can be appreciated better. **Lower panel**: The data points are the velocity dispersion measurements from Caldwell et al. (2017) which are compared to the predicted velocity dispersion for Crater II corresponding to the stellar profile fits to the star counts in the upper and central panels for the 2σ range of the MCMC fits (see Fig.4.65 for details). The vertical grey shaded area indicates the stellar core radius and uncertainty from the above-stellar profile.

Galaxy	r_c (kpc)	r_t (kpc)	$M(r<r_h)$ ($10^6 M_\odot$)	$M(r<r_h)_{,obs}$ ($10^6 M_\odot$)	M_h ($10^8 M_\odot$)	$*_{age,obs}$ Gyr	$[Fe/H], obs$	Refs
Crater II	$0.71^{+0.09}_{-0.08}$	$1.68^{+0.25}_{-0.23}$	$7.17^{+12.83}_{-4.56}$	$4.4^{+1.2}_{-0.9}$	$2.93^{+2.99}_{-1.44}$	~ 10	$-1.98^{+0.1}_{-0.1}$	Caldwell(2017)

Table 4.5: Observations and ψDM profile fits. Column 1: Dwarf galaxy name, Column 2: Core radius r_c, Column 3: Transition radius r_t, Column 4: Dynamical mass $M(r < r_h)$, Column 5: Observed dynamical mass $M(r < r_h)_{,obs}$, Column 6: Halo Mass M_h, Column 7: Observed Stellar age, Column 8: Observed mean stellar metallicity, Column 9: References of the observed data.

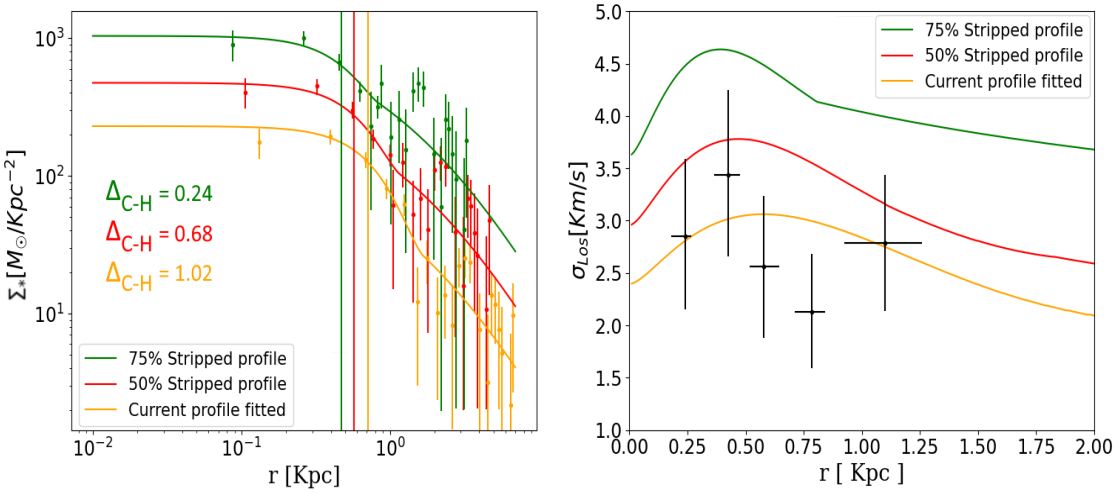

Figure 4.13: Evolution of the density and velocity dispersion profiles predicted for Crater II. **The left panel**: Possible evolution of Crater II's stellar profile in a ψDM context, with the measure profile shown in orange, whereas the red and the green represent previous less stripped profiles with 50% and 75% more mass. Notice how the profile becomes "stretched" with a broader core (marked by the vertical lines) and a bigger density gap between the core and the halo (larger Δ_{C-H}). **The right panel**: Evolution of the velocity dispersion profile due to tidal stripping corresponding to the same epochs as the left panel. The peak of the dispersion moves to larger radius as stripping increases, following the expansion of the core, and the distinction in velocity between the core and the halo diminishes.

Here we compare the measured velocity dispersion and the stellar profile of Crater II with ψDM. We fit the data with the following free parameters; the core radius r_c of the soliton profile given by Eq.(3.17), the transition radius r_t between the core and the halo, the central 3D stellar density ρ_{0*} and the 3D scale radius of the stellar halo r_{s*} describing the scale radius of the NFW-like halo that we infer from fitting to the outer stellar profile beyond the transition radius. Note that the boson mass is fixed, with a value of 1.5×10^{-22} eV, consistent with our previous dynamical work on dwarf galaxies in the context of ψDM (Schive et al., 2014a,b; Broadhurst et al., 2020; Pozo et al., 2020).

In generating our model profiles, we solve the spherically symmetric Jeans equa-

tion, described above, Eq. (3.7), subject to a total mass for Crater II of $2.93^{+2.99}_{-1.44} \times 10^8 M_\odot$, that we obtain from fitting the core radius size (Eq.(3.17)) in the stellar profile data with a fixed boson mass of 1.5×10^{-22} eV, which is consistent with the dynamical mass estimated by Caldwell et al. (2017) (see table (4.5) .The transition radius, r_t, is expected to be two or three times larger than the core radius in simulations of ψDM (Schive et al., 2014a,b), which we show below is consistent with $r_t \sim 2.4 r_c$ that we derive here for Crater II.

The results are listed in table (4.5), and figure (4.12) shows the self-consistency of these data in both stellar and kinematic profiles. The transition radius, r_t at which the profile changes from being dominated by the halo rather than the soliton is marked with a vertical orange line in Figure (4.12). The green and purple shadowed areas represent the 2σ range, respectively. The comparison shown in Figure (4.12) between the models and the data represents a consistency check, where we simply employ the Jeans equations in making predictions for the velocity dispersion profile (purple model band in lower panel of Figure (4.12) when inputting the set of core+halo profiles that acceptably fit the stellar profile data (green model band Figure (4.12) and subject to a constraint on the total galaxy mass set by the mean level of velocity dispersion of about 3km/s. Note, the limited precision of the velocity dispersion data does not yet warrant a classic combined Jeans analysis.

Figure (4.13) shows our predicted evolution of the stellar profile of Crater II as well as the change in the velocity dispersion profile for two choices of galaxy mass and spanning a mass loss of up to 50%. As a consequence of continued core mass loss (Du et al., 2018), a widening of the core is induced, described by Eq. (3.4). It is important to point out how both densities of core and halo seem to decrease, with the halo changes more strongly over time, in good agreement with the halo's greater weakness against tidal forces (Schive et al., 2020). This tidally induced mass loss results in a reduction of the velocity dispersion while widening the core so that the dispersion profile has a less pronounced peak that shifts the larger radius, reflecting the widening core as tidal stripping proceeds as seen in Fig.4.16 for the parameters of Crater II. This is in line with the simulations of Fu et al. (2019) where prolonged tidal stripping should produce a drop in the mean velocity dispersion in conjunction with a half-light radius increasing (Fattahi et al., 2018; Sanders et al., 2018; Torrealba et al., 2019).

We conclude that the extended core size of $r_c \simeq 0.71$ kpc of Crater II is the product of its low halo mass($\simeq 10^8$) and significant tidal stripping of the halo have have occurred which is natural in the ψDM context, while CDM struggles to explain the observed combination of low-velocity dispersion and large radius (Fattahi et al., 2018). Moreover, Fig.4.12 clearly shows how a cuspy NFW profile is unable to explain the stellar density and kinematic behavior in the core, under the assumption that stars trace the dark matter. We also note that we have not adopted the commonly used Plummer profile for the stellar profile, preferring instead the soliton form that fits well the stellar profile of Crater II (Eq. (3.16)).

4.3.2 Ideal dwarfs' Modeling Results

Here we predict the tidal evolution of dwarf galaxy profiles in the context of ψDM. Figure (4.15) shows how the soliton core mass should decrease with time over several Gyrs, according to Eq.(3.18). The soliton profile remains unchanged until it becomes stripped, then the core relaxes into a softer profile during this process, (see figures (4.15) and (4.14). This right hand panel of Figure (4.15) shows the soliton becoming wider, indicated by the difference between thick and dashed lines of the same color, due to the halo mass loss described by Eq(3.4) and at the same time the amplitude of the density gap and the transition radius can be seen to increase as the halo is stripped. Similar behaviour is noticeable in the recent ψDM simulations of Schive et al. (2020), where tidal stripping has been approximated for the orbiting dwarf Eridanus II.

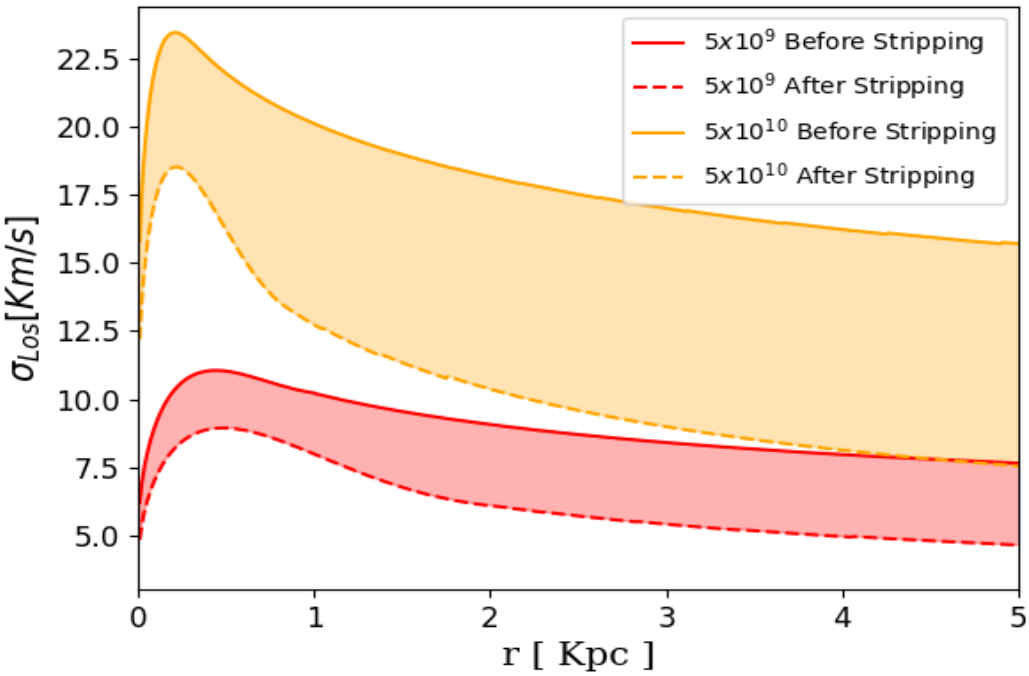

Figure 4.14: Velocity dispersion profile evolution for two tidally evolved profiles of different galaxy mass spanning the classical dwarf range, as in figure 4.15. Notice how the core is more evident in the dispersion profile for the more concentrated, massive soliton, indicated by the orange profile, compared to the softer core-halo transition for the less massive dwarf indicated by the red profile.

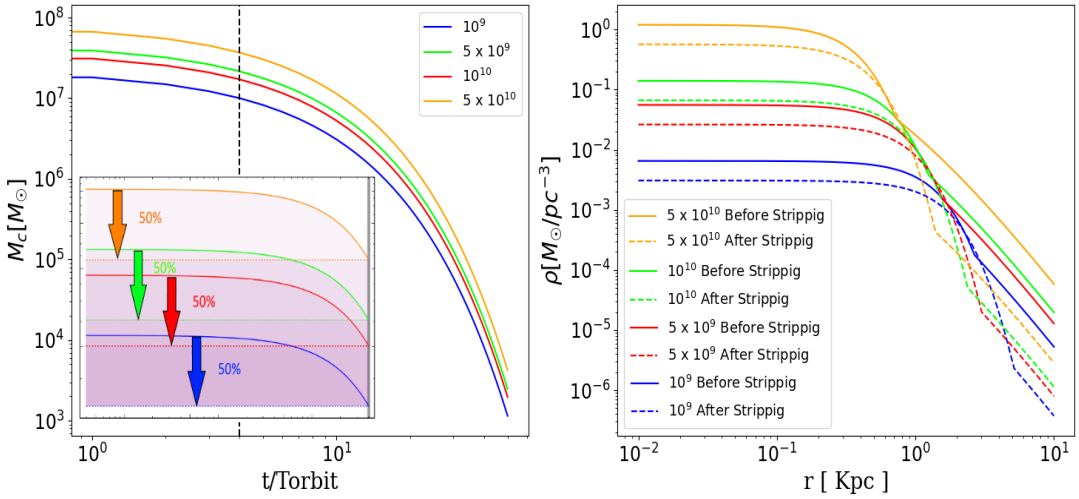

Figure 4.15: The evolution of Four typical dSph ψDM density profiles predicted for orbits within the Milky Way, with a constant density ratio of; μ=50. **The left panel**: Core mass loss of the four profiles. The vertical dashed line marks four orbits. The small panel shows in detail the profiles after each has lost 50% of the total mass to steady tidal stripping after the first four orbits. **The right panel**:Tidal evolution of the ψDM density profiles. The thick lines represent the original profiles before the stripping process, while the dashed lines represent their situation after four orbits. Notice how in all the cases, the core becomes extended due to losing mass as the transition radius increases.

Figure (4.14) shows illustrative velocity dispersion profiles for a range of ψDM mass profiles highlighting the transition from the soliton core to the outer NFW-like outer profile (Schive et al., 2014a,b; Vicens et al., 2018). The velocity dispersion profiles are listed in the right upper panel and cover one order of magnitude in the total mass starting from $5 \times 10^9 M_\odot$ to $5 \times 10^{10} M_\odot$. Solid and dashed lines differentiate the original ideal isolated profile from the stripped one for each system. In terms of the Jeans based calculation of the dispersion profile, the choice of β is not very important, affecting the velocity dispersion well within the core, where it rises (or falls) sharply for a positive (or negative) value of beta and remains flat if isothermal. The data appear to favor a mildly negative value for β as the dispersion of the innermost bin is lower than the mean, though quite uncertain, as can be seen in Figure (4.12) (lower panel), consistent with our adopted $\beta = -0.5$ and this is similar to the value chosen by Caldwell et al. (2017) for modeling dwarf spheroidals, to counter the rising dispersion profile that would otherwise result from the "cusp" of an NFW profile. The main influence on the velocity dispersion profile is from the presence of the soliton core, rather than the choice of β, because the soliton is dense relative to the halo (by a factor of about 30), generating a peaked form at about the core radius, as can be seen in Figure (4.14) and also in figure (4.12).

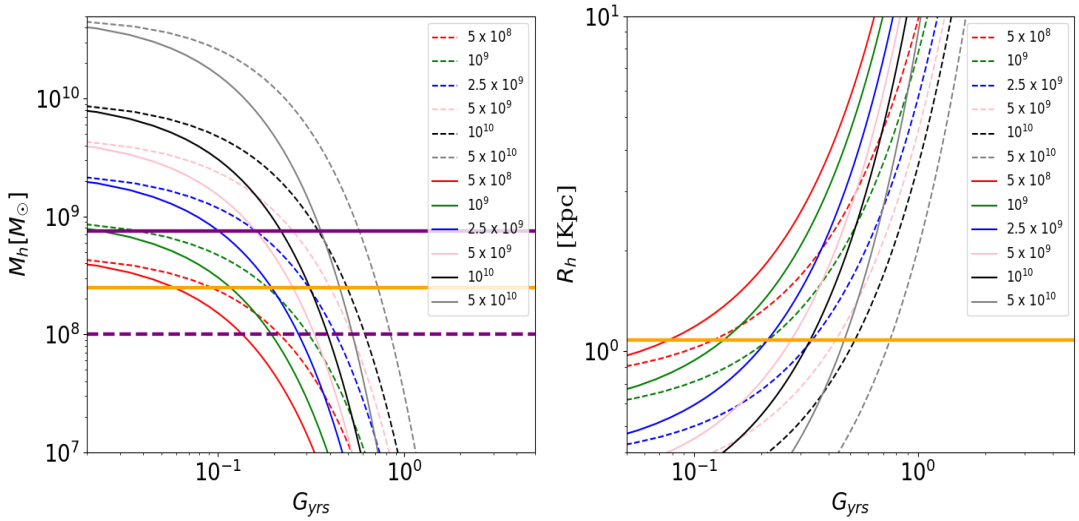

Figure 4.16: Evolution of mass and r_{half} radius due to tidal stripping. The thick solid and dashed lines are with a Milky way host of 5×10^{12} $M_\odot$ and 10^{12} $M_\odot$, respectively. **The left panel**: Total mass loss evolution predicted for Crater II in the ψDM context. The orange horizontal line represents the best fit mass of Crater II (see figure 4.12 and table 4.5). The solid and dashed purple horizontal lines indicate the maximum and minimum allowed masses of Crater II from our analysis, corresponding limiting purple contours of Figure 4.12. **The right panel**: Predicted evolution of the r_{half} radius growth for Crater II, in a ψDM context. The orange horizontal line represents Crater II's actual r_{half}.

Summary & Conclusions

1. **Motivation**:

   Motivation 1: Examination of Crater II and other "large" dwarfs in the context of ψDM.

   Motivation 2: Compute the general tidal imprints of dwarf galaxies in ψDM context, such as the core widening and the decrement of the velocity dispersion. This was also analyzed to reinforce the theory that Crater's actual profile could be explained as a natural product of a typical dwarf after suffering tidal forces in the ψDM scenario.

2. **Methodology**:

   Note*:For ψDM, the core and halo are coupled, with the ground state soliton surrounded by the halos of excited states. A Core-halo relationship has been established in the simulations, with more massive solitons formed in more massive halos that are denser because of the higher momentum. Mass loss by

tidal forces readily strips the tenuous halo (Schive et al., 2020) and, in turn, is expected to affect the soliton via the core-halo relation, but in a smaller proportion (Du et al., 2018).

In order to explain Crater's actual profile:

Step 1: Fit our best ψDM stellar profile (section 3.3) to the observed stellar profile of Crater II in order to quantify the core radius size (r_c) and the transition point (r_t) between the soliton and the NFW-like halo (represented in Figure 4.12). With this wave dark matter profile, we will also quantify the density gap between the core and the halo, observed in the stellar profile, $\Delta_{C-H} = \log \rho_C/\rho_H$.

Step 2: Apply the used wave dark matter profile of the first step to check his consistency with the observable dynamical data, calculating the projected velocity dispersion by equations (3.7) and (3.12).

In order to understand the tidal forces imprints in a ψDM galaxy:

Step 1: Analyze the consequences in the DM density profiles of some ideal dwarf galaxies after suffering a mass loss with a constant density ratio of; μ=50. Eq. (3.18).

Step 2: Calculate the corresponding velocity dispersion profiles with equations (3.7) and (3.12).

3. **Results**:

For Crater II:

Result 1: We show how ψDM model can welly represent Crater's actual observable expanded core as a product of a total halo mass of $2.93^{+2.99}_{-1.44} \times 10^8 M_\odot$. Moreover, that total mass and an acceptable value of the formation redshift (check Schive et al. (2014b)) fit the velocity profile of Crater's stars well. See figure 4.12.

Result 2: As the computed total halo mass of the galaxy of the order of $\sim 10^8 M_\odot$ is small for a typical dwarf galaxy, we directly calculated the possible past situation of Crater II (Figure 4.13). We show a possible solution where a less tidally affected Crater II, which relatively less of his mass being stripped(More or less with double mass that actually), should show a much concentrated and massive soliton of $\sim r_c = 0.4$kpc with a higher $\sigma_{los} \sim 4.5$km/s. Values that fit pretty well with a low mass typical dwarf, indicating that Crater II naturally fits with a ψDM tidally stripped galaxy, where the core widening and velocity dispersion decrement are a natural process.

For ideal dwarfs that have suffered tidal forces in a ψDM context:

Result 1: We show that in a ψDM enough strong tidal context, typical dwarfs seem to see both soliton and halo partially removed in terms of mass, being the imprints much more visible for the halo due to its more considerable weakness. The soliton sees its core enlarged due to the mass loss while the density gap between the halo and the core highly increases due to the bigger halo mass loss

rate (figure 4.15). All this has a direct repercussion on the velocity dispersion profile, where its mean values decrease (figure 4.14).

Result 2: An approximate proportionality between r_c and the observed half light radius, r_h, for local dSph galaxies in Pozo et al. (2020), of about $\simeq$ 1.3. This r_h/r_c ratio was also been pointed out by Lazar et al. (2020); Schive et al. (2014a,b). So as well as computing the mass loss due to tidal stripping using Eq (3.18), we continuously increment r_c by updating the mass-loss in Eq. (3.3). Finally, we use the above ratio between r_c and r_h to increment r_h across the orbits (see the righthand panel of Fig.4.16). The enlargement of r_t, (extracted from the simulations made by Schive et al. (2020), where it is defined in which ratio should the transition radius of a Milky way's satellite dwarf galaxy increase due to Milky Way's tidal forces: "The halo surrounding the central soliton is found to be vulnerable to tidal disruption; the density at r $> r_t$ decreases by more than an order of magnitude after $\sim$ 2 Gyr") will explain the observed Δ_{C-H}(density drop between the core and the halo, $\Delta_{C-H} = \log \rho_C/\rho_H$, where ρ_C is the asymptotic central core stellar density and ρ_H is the stellar density at the transition radius(r_t)) changes in the halo of the galaxies.

4. **Conclusions**:

   Conclusion 1: We have shown that Crater II can be readily understood in the context of dark matter as a Bose-Einstein condensate by comparison with the profiles of galaxies generated in ψDM simulations (Schive et al., 2020), especially if tidal stripping is included.

   Conclusion 2: It should be emphasized that the simulations also make clear that there is a marked transition between the core and the halo, and we can see that Crater II does possess a well-defined core with such a visible transition in its stellar profile at a radius of $\simeq$ 0.7kpc, shown in Figure 4.12, and this is despite the relatively low surface brightness of Crater II, for which the star counts are much lower than typical well-studied dSph galaxies. The existence of this core is also supported by the velocity dispersion profile of Crater II, which we have shown is consistent with being peaked at about the stellar core radius, as we have shown is predicted for ψDM in Figures 4.15 & 4.14.

   Conclusion 3: We have also pointed out that the observed stellar profile behavior of Crater II is continuous with the distinctive core-halo structure that appears to be a general feature of the classical dSph galaxies, established in the previous subsection 4.2, where we found that essentially all the well studied dSph galaxies have a prominent stellar core that accurately matches the unique soliton form, and also that the velocity dispersion profiles of these dSph galaxies generally peak near the stellar core radius and are lower in the halo. However, despite this qualitative similarity between Crater II and the dSph class, there is a clear difference in that the dSphs are about a factor three smaller, with a mean core radius of $\simeq$ 0.25Kpc, compared to $\simeq$ 0.7kpc for Crater II, and also in terms of the characteristic velocity dispersion which is about three times greater for the dSphs, with a mean level of $8-12$km/s compared to only 2.7km/s for Crater II significantly higher than Crater II, and

also of course, as the name "feeble giant" suggests, Crater II is relatively more extended and of unusually low surface brightness than typical dSph galaxies (Torrealba et al., 2016).

Conclusions 4: Our analysis of Crater II has examined the possibility that tidal stripping in the context of WaveDM may account for the rather extreme properties of this dwarf galaxy, with its relatively large size and low velocity dispersion. In support of this we show the stellar profile of the Crater II (upper panel Figure 4.15) is well fitted by a soliton core plus a shallow NFW halo and that this combined profile, which is generic to WaveDM, is consistent with the extended, shallow, velocity dispersion profile of Crater II, (lower panel Figure 4.15) where the low mean level of velocity dispersion of $\simeq 3$km/s corresponds to a total galaxy mass of about $3 \times 10^8 M_\odot$. The consistency we find here may indicate that the stellar core and DM core are similar in scale, though this is by no means conclusive at the currently limited precision of the dispersion profile and relies on some extent the level of velocity anisotropy assumed, but may imply the stars behave essentially as tracer particles within the dark matter dominated potential. Detailed hydrodynamical simulations of gas and star formation within dwarf galaxy haloes will be required for a more definitive exploration of this relationship between stars and DM, which must include the relaxation effects understood to be significant in randomly deflecting stars orbiting through the de Broglie scale density fluctuations predicted for WaveDM halos (Schive et al., 2014a) and proposed as possible explanation for the increasing scale height of disk stars in the Milky Way with stellar age, by Church et al. (2019), and Bar-Or et al. (2019). For now, we content ourselves with the largely qualitative conclusion that tidal stripping of a DM dominated dwarf galaxy in the context of Wave DM can plausibly result in the unusual properties of Crater II, with an expansion of its soliton core in response to stripping of its DM halo, an effect that follows fundamentally from the Uncertainty Principle for WaveDM.

Conclusion 5: We have been able to understand these differences in the context of ψDM, as the possible consequence of tidal stripping. It is now understood that Crater II has a small pericenter within the Milk Way, so that tidal stripping should be significant and this we have shown provides an interpretation of Crater II as a stripped dSph galaxy. This possibility follows directly from considering how the soliton expands as the halo mass is stripped away, as proposed by Du et al. (2018) that is implied by the existence of a relatively clear relationship established in the ψDM simulations between the mass of a galaxy and the soliton core, which may act together with the strict inverse relationship required for a soliton (by the Uncertainty Principle), such that as galaxy mass is reduced by tidal stripping, the momentum associated with the soliton ground state is also lower and hence the soliton expands as the de Broglie Wavelength is larger following the inverse soliton mass-radius relation, with a reduce soliton density and hence lower velocity dispersion. We may conclude that in order for Crater II to have originated as a typical dSph, its core has expanded by approximately a factor of 2-3, and hence the core mass was 2-3 times higher and hence initially, the total mass would have been $\simeq 10 - 30\times$ larger, assuming the core-halo mass scaling relation scaling is

followed, i.e. $m_{sol} \propto m_{gal}^{1/3}$. We can come to the same quantitative conclusion by comparing the velocity dispersion $\simeq$ 3km/s of Crater II, which also differs by a factor of 3 with the typical $8-10$km/s peak dispersion for the dSph's. This agreement is quite compelling for the ψDM interpretation as this factor difference would not be expected, whereas for ψDM it is a requirement as the uncertainty principle dictates that the soliton obeys $r_{sol}\sigma_{sol}$=$h/8\pi m_{\psi}$, (taking $2r_{sol}$ as the width of the soliton wave packet) providing an approximate boson mass of $2.51^{+0.68}_{-0.51} \times 10^{-22}$eV, and because σ_{sol} and r_{sol} vary inversely with a fixed product, this boson mass estimate is expected to be independent of tidal evolution, in the absence of extreme tidal disruption that may deform the soliton (Du et al., 2018). This value of m_{ψ} is consistent with estimates for the cores of classical dSph galaxies, $\simeq 1-2\times10^{-22}$eV (Chen et al., 2017), and thus Crater II quantitatively reinforces the light boson solution for dark matter.

4.4 Dwarfs and multiple Axion species (Paper 4)

Here we test these unique soliton predictions, examining all well resolved Local Group dwarf galaxies orbiting Andromeda and the Milky Way, using their star count profiles and velocity dispersion profiles (as in section 4.2). We first plot the reported the half-light radius, R_h against the standard dynamical measure of density, within this radius, $M(< R_h) \propto \sigma^2 R_h$, so the central density scales to order unity dimensionless constant α, as $4\pi G\rho_h = \alpha\sigma^2/R_h^2$. This is plotted in Figure 4.17 (left panel) and color coded by stellar luminosity, revealing two steep parallel relations with UFD galaxies following a relatively small and dense track compared to the dSph dwarfs. Both classes of dwarf show a similar, surprisingly negative correlation, towards lower density and larger radius for UDF and dSph dwarfs shown in Figure 4.17.

The presence of prominent cores can be seen clearly in the star count profiles of the UDF and dSph dwarfs, in Figure 4.19, when averaged within each class of dwarf, with an obvious difference in scale between the UFD and dSph galaxies of about a factor of 10 in radius. Individually, these cores are also evident in deep images available in most cases (all individual fits are below in subsection 4.4.1) and are "prominent", meaning the core density rises well above the surrounding "halo" by a factor of 30 in density for both classes of dwarf seen in Figure 4.19. The stellar cores are similar to the commonly adopted Plummer profile (red curve Figure 4.19) but more accurately match the soliton form of ψDM in the ground state, despite the inherent parameter free form of the soliton profile, with the boson mass as the only free parameter for ψDM setting just the soliton radius. Furthermore, we also see extended halos around these solitons as a general feature, extending to Kpc scales in agreement with recent discoveries of halos around two well studied dwarfs (Chiti et al., Chiti et al.; Collins et al., 2021). Such extended halos are inherent to ψDM composed of excited states, above the ground state soliton as shown NFW form, as predicted by the ψDM simulations (Schive et al., 2014a), reflecting the inherently

non-relativistic nature of ψDM. Averaged to the core-halo structure of all dSph and UDF dwarfs are shown in figure 4.19 showing very tight agreement, with all individual profiles shown at the end of the section, demonstrating the generality of this cor-halo behavior for all well studied dwarfs, including a typically sharp density transition between the core and the halo seen in Figure 4.19 and for most individual dwarf profiles, indicated as vertical orange bands.

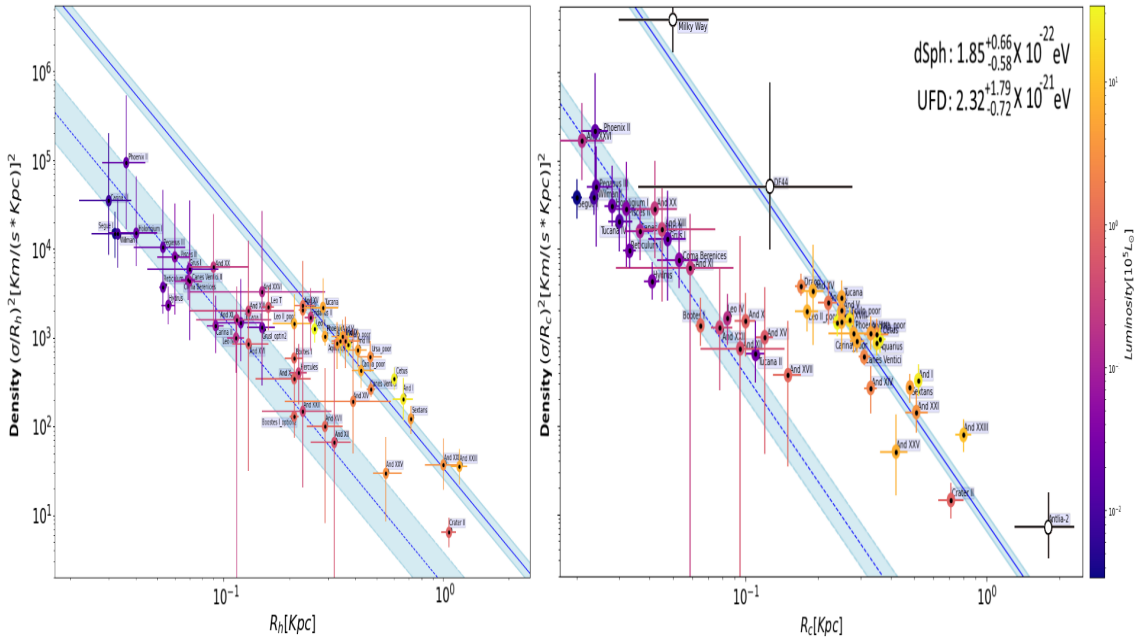

Figure 4.17: Left panel: Density vs. half-light radius. Here we plot central density, $(\sigma/R_h)^2$ for each local dwarf (named on plot) reported by many groups(see Supplement) and these are color coded by luminosity revealing a clear distinction between the UFD and dSph classes, forming two parallel power-law fits shown in blue. **Right panel: Density vs. core radius** Here we plot density within our fitted core radius for each dwarf, $(\sigma/R_c)^2$, using the soliton form for the core (see Supplement for all individual dwarf fits to ψDM and Plummer profiles) which results in sharper parallel relations between the UDF and dSph dwarfs and a good fit to the slope, $d\log\rho_c/d\log R_c = -4$, for the time independent soliton solution of the Schröedinger-Poisson relation, where the higher the soliton mass the narrower the core. We have added to this the core densities reported Milky Way, DF44 and Antlia-2 and seen to be consistent with the lighter boson, in common with the dSph class.

This agreement with the core-halo profile of ψDM is striking and we can now plot the core density versus radius relation for the soliton radius measured individually for all the dwarfs shown in Figure 4.17 where we also use the velocity dispersion measured within that radius. Two parallel relations become more apparent now in Figure 4.17, right panel, for the UFG and dSPh dwarfs respectively in terms of $\rho_c \propto \sigma^2/R_c^2$. A steep slope of $\rho_{sol} \propto R_{sol}^{-4}$ is predicted for ψDM because in addition to the volume dependence, R_{sol}^{-3} dependence, there is an inherent inverse scaling of the soliton radius with soliton mass, $M_{sol} \propto 1/R_{sol}$, given by the time independent,

soliton, solution of the Schröedinger-Poisson coupled equation (and verified by the ψDM simulations (Schive et al., 2014a,b)) so $\sigma^2/R_h^2 = \beta^2(\hbar/m_b)^2/R_h^4$, where β is order unity dimensionless scaling given by the Uncertainty Principle, $\hbar = m_b \sigma R_h$, resulting in a slope of $d\log\rho_{sol}/d\log R_{sol} = -4$, for ψDM, which is clearly consistent the data in Figure 4.17 (right panel) for both the UFD and dSPh galaxies, thereby accounting naturally the otherwise puzzling trend that the large cores within each class of dwarf have lower velocity dispersions. Note too the "feeble giant" dwarf, Crater II, falls on this relation, as do estimates of the core radius of the Milky Way and the ultra diffuse low mass galaxy DF44, of 80pc and 220pc respectively (de Martino et al., 2020b; Pozo & others., 2021a). Note too, this core density-radius relation is unaffected by tidal stripping, (inferred to have affected significantly Crater II and Antlia II with small pericenter orbits about the Milky Way, see section 4.3) as the stability of the soliton requires that it always follows the inverse mass-radius relation set by the boson mass, so that a stripped galaxy may move down the core density-radius relation but will not depart from it until the soliton is catastrophically destroyed by tidal forces (Veltmaat et al., 2018).

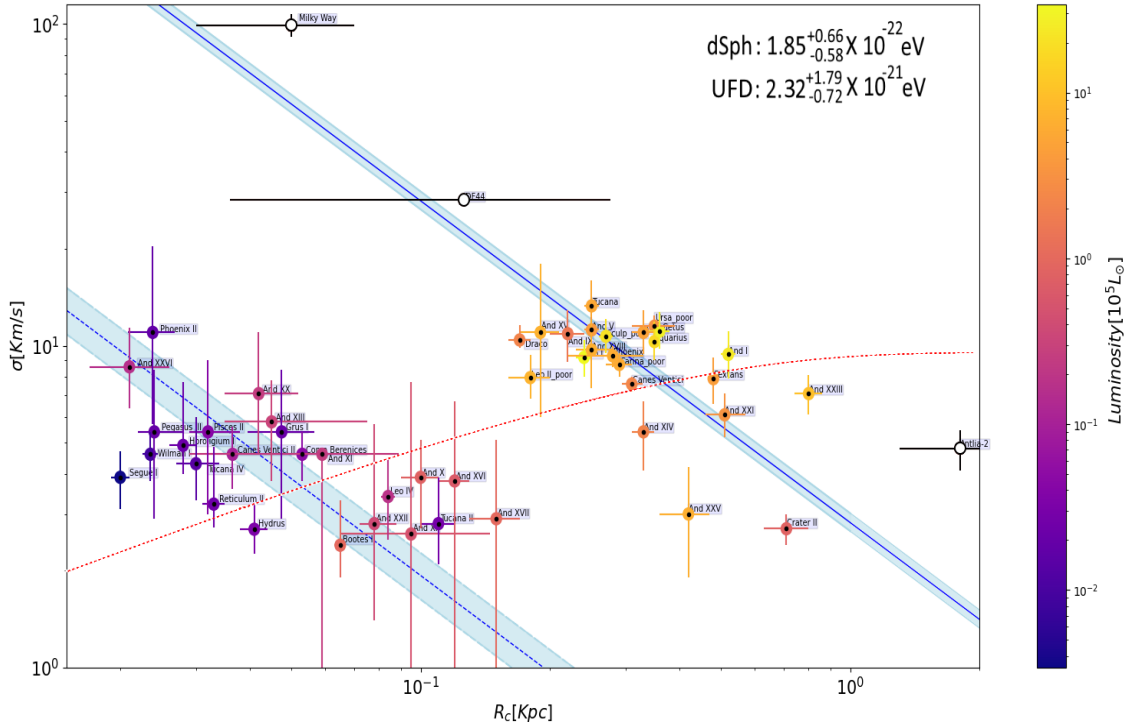

Figure 4.18: Velocity dispersion vs. core radius. Here we simply plot the observed velocity dispersion against core radius for all dSph and UDF dwarfs and compare them with the inverse relation required by the Uncertainty Principle, indicated by the best fit red lines to the UFD and dSPh dwarfs separately, with the corresponding boson masses derived from the normalization shown in the legend. Also shown is the CDM related prediction (Walker et al., 2009) as thin red curve, where galaxies with NFW profiles are larger with increasing mass and hence the opposite of ψDM.

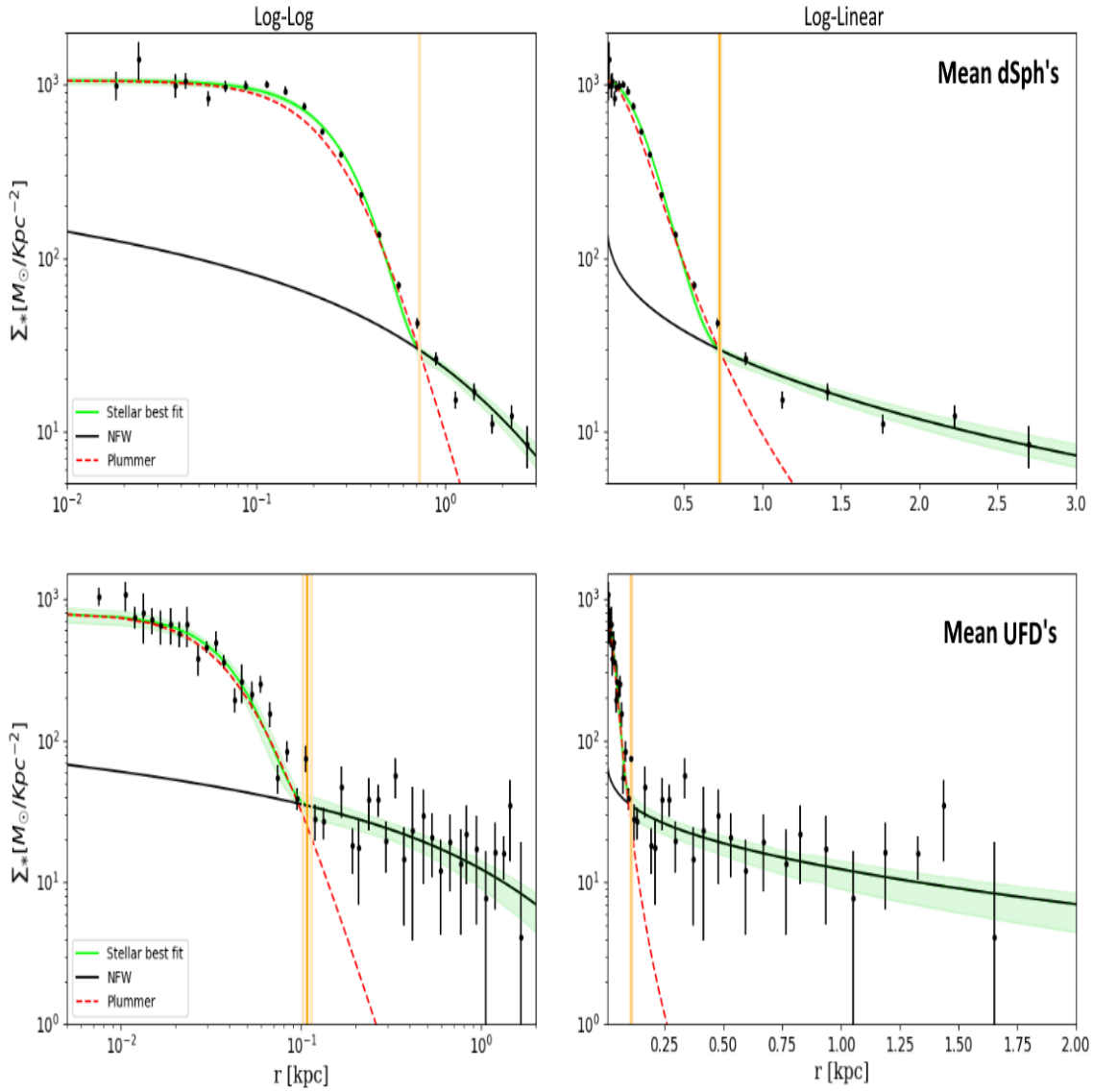

Figure 4.19: Top panel: Dwarf Spheroidal Galaxies Mean star count profile, after scaling to the mean core radius of all dSph dwarfs, listed in table 4.7. The cores of both dSPh are prominent relative to the halo that extends to several times the core radius. A standard Plummer profile (red dashed curve) fits approximately the core region but falls well short at large radius, whereas the ψDM profile with its inherent core-halo structure provides an accurate fit to the core from the soliton component and to the halo when averaged azimuthally over the excited states that approximate the NFW form. The form of the soliton profile has only one free parameter, the boson mass, m_b that sets the scale radius of the soliton. The sharp drop in density visible between the core and the halo, by a factor of $\simeq 30$ is characteristic of ψDM at a transition radius marked by vertical orange band. The best fit MCMC profile parameters are tabulated in table 4.7. **Lower panel: Ultra Faint Dwarfs** Mean profile averaged over all resolved profiles of Ultra Faint dwarfs, listed in table 4.8. The predicted ψDM core-halo structure is also evident for ultra faint dwarfs, including a marked transition in density between the core (marked in orange), with best fit MCMC profile parameters tabulated in table 4.8.

Finally, we test directly for the role of the Uncertainty Principle to see if the inverse scaling is present between σ_c and r_c from the commutability of momentum and position required for the soliton. In Figure 4.18 we see this inverse relationship is indeed supported by both the UFD and dSph dwarfs, in parallel, which is quite the opposite of the positive correlation predicted for CDM (Walker et al., 2009) where more massive dwarfs are larger. This agreement means we can roughly estimate the boson mass for both the UFD and dSPh classes from the normalization between the core momentum $m_b\sigma_c$ and the width of the soliton standing wave so, $m_b = \hbar/2R_c\sigma_c$, fitted in Figure (4.17), obtaining $m_b = 2.27^{+1.79}_{-0.65} \times 10^{-21}$eV for the UFD's and $m_b = 1.85^{+0.66}_{-0.58} \times 10^{-22}$eV for the dSph's, differing by an order of magnitude. This simple estimate using the Uncertainty Principle may be compared to individual Jeans analysis of dSph dwarfs (Chen et al., 2017), where a similar range of boson mass and core radius is derived dynamically for several dSph with high quality profiles, in the range $0.9 - 2.8 \times 10^{-22}$eV. This estimate assumes stars are test particles (see section 3.5 for a deeper explanation) so the 3D velocity dispersion associated with the soliton wave function, where only the radial mode of kinetic energy $< KE >_r$ is present, means in 1D we have $r_c\sigma = 0.5(\hbar/m)$, as adopted in our estimate. Core masses of constant density scale as $\rho_c \propto (\sigma/r_c)^2$ and in the context of ψDM there is also an inverse relationship between soliton core mass and solton radius relation required by the non-linear solution to the Schröedinger-Poisson equation (**?**) so the soliton's density scales more steeply than the volume with radius, i.e. $\rho_c \propto r_c^{-4}$. The radius of the soliton is given approximately by the de Broglie wavelength $\lambda_B = \frac{h}{p}$, following from the Uncertainty principle $\Delta x \Delta p \geq \frac{\hbar}{2}$, where Δx, the position dispersion given by the soliton width, $2\times r_c$, and the dispersion in momentum Δp, given approximately by $m_b\sigma$, the product of the boson mass and the velocity dispersion of stars as tracer particles of the dominant DM potential. This allows us to determine the boson mass that corresponds to the de Broglie wavelength, $m_\psi \simeq \hbar/4r_c\sigma_{los}$. The simulations also show the soliton core is surrounded by an extended halo of density fluctuations on the de Broglie scale that arise by self interference of the wave function (Schive et al., 2014a) and is "hydrogenic" in form (Hui, 2020; Vicens et al., 2018). These cellular fluctuations are large, with full density modulation on the de Broglie scale (Schive et al., 2014a) that modulate the amplitude of the Compton frequency oscillation of the coherent bosonic field, allowing a direct detection via pulsar timing (de Martino et al., 2017, 2020b).

More precise absolute boson masses may need to rely on simulations as it is now clear that stellar orbit scattering by soliton oscillation modes affects the evolution of stellar orbits within the soliton. We emphasise that irrespective of absolute values, Figure 4.18 indicates there is an order of magnitude difference in boson mass between UFD and dSph dwarfs. Furthermore, this conclusion is supported independently by the dwarfs associated with the Milky Way and with Andromeda, prefixed by "And" in Figures 4.17 & 4.18, for which we find indistinguishable core density relations and bosons masses, as listed in Table 4.6, thus reinforcing the generality of our two boson solution for local dwarf galaxies.

Combinations	r_c (kpc)	r_t (kpc)	N_{gal}	m_ψ 10^{-22}eV
$dSph_{Both}$	$0.21^{+0.003}_{-0.003}$	$0.71^{+0.021}_{-0.021}$	23	$1.85^{+0.66}_{-0.58}$
UFD_{Both}	$0.033^{+0.002}_{-0.002}$	$0.11^{+0.006}_{-0.006}$	21	$23.21^{+17.91}_{-7.23}$
$dSph_{MilkyWay}$	$0.22^{+0.003}_{-0.003}$	$0.75^{+0.022}_{-0.023}$	13	$1.85^{+0.66}_{-0.58}$
$dSph_{Andromeda}$	$0.26^{+0.007}_{-0.006}$	$0.82^{+0.032}_{-0.028}$	10	$1.86^{+0.45}_{-0.53}$
$UFD_{MilkyWay}$	$0.032^{+0.002}_{-0.002}$	$0.093^{+0.008}_{-0.007}$	12	$31.36^{+12.39}_{-11.57}$
$UFD_{Andromeda}$	$0.042^{+0.002}_{-0.002}$	$0.14^{+0.008}_{-0.008}$	9	$17.83^{+4.31}_{-6.73}$

Table 4.6: Profile parameters for dwarfs associated with the Milky Way and Andromeda. Column 1: Dwarf CLass, Column 2: Core radius r_c, Column 3: Core-Halo transition radius r_t, Column 4: Number of galaxies N_{gal}, Column 5: Boson mass m_ψ.

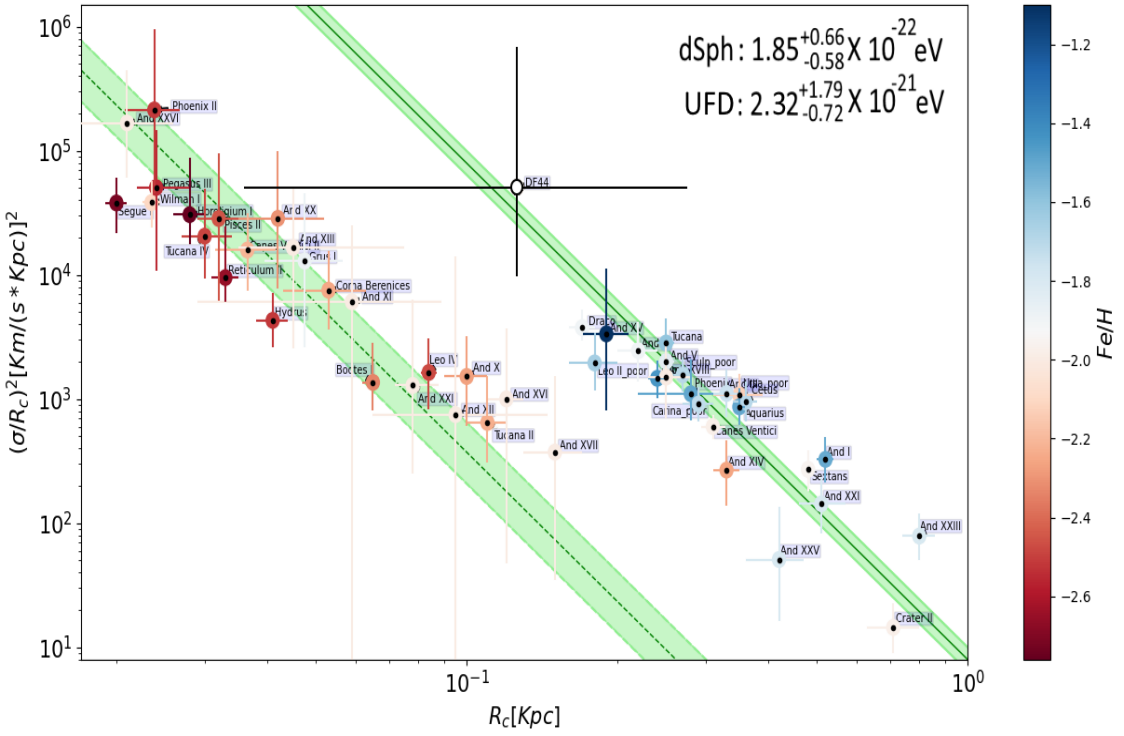

Figure 4.20: DM density vs. Core radius. Expansion of the left panel of figure 4.17 but now with the color representing metallicity. Notice how the Ultra-faint galaxies are systematically more poor-metal that the dSph class, supporting the empirical distinction (based on luminosity) of two classes of dwarf galaxy.

Our two boson solution for dwarf galaxies may point to the "Axiverse" scenario generic to string Theory (Arvanitaki et al., 2010), where in general terms a wide spectrum of axion-like scalar fields is predicted with a discrete mass spectrum spanning many decades in mass, with approximately one axion per decade. In this context we may infer that the proportion of the Universal DM in a higher mass boson may be approximately ∼3% compared to the lighter boson, given the factor 10 mass difference we find, as the higher mass axion enters the horizon earlier and

is redshifted to lower density ahead of lower mass axion (Luu et al., 2020). Our two boson conclusion improves the viability of this String Theory solution for DM raised in relation to the existence of UFD galaxies (Mohammadtaher & Spergel, 2020) and may relieve tension with ψDM based on excessive variance of the of the Ly-forest (Armengaud et al., 2017), though gas outflows and early AGN heating must also be expected to enhance the forest variance above ideal DM simulation based predictions at some level, as too may an initially "extreme" angle scalar field for ψDM (Hsu & Chiueh, 2021). We can also now anticipate constraints on this two boson solution from JWST, where early galaxy formation related to the subdominant, heavier boson will be governed by the dominant density field of the lighter boson and hence strongly biassed, favoring the formation of UFD dwarfs in groups and clusters. Alternatively, JWST may reveal that dwarf galaxies are physically continuous at early times, as expected for scale free CDM, implying subsequent evolutionary processes are responsible for the physical distinction between UDF and dSph dwarfs seen today.

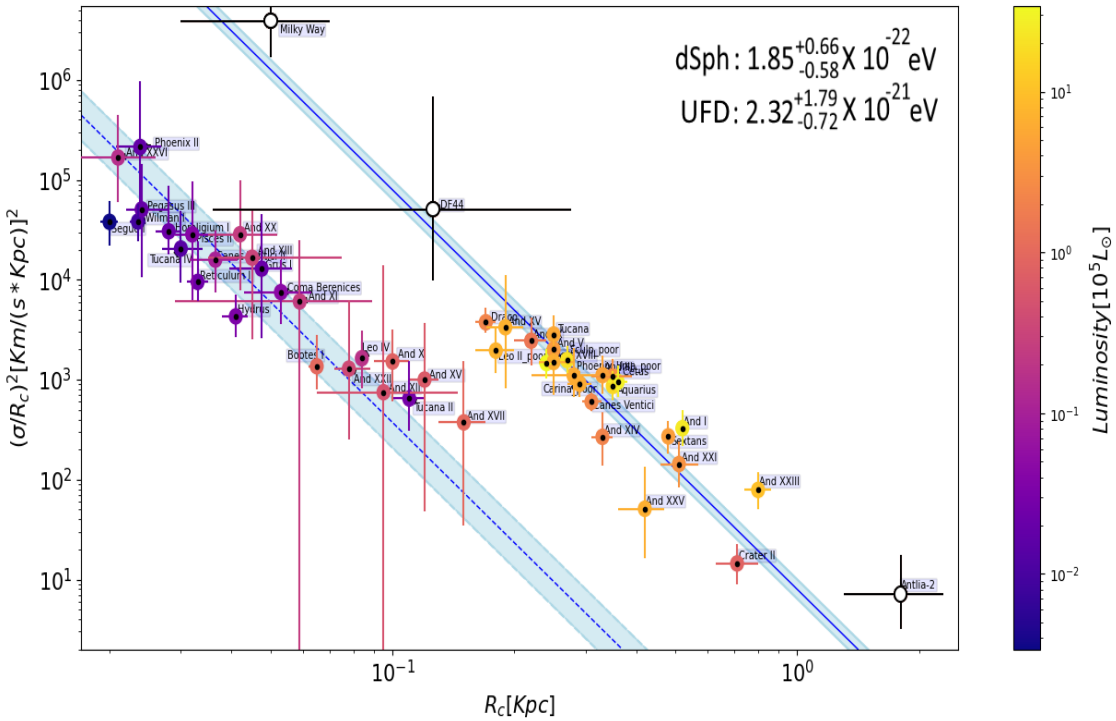

Figure 4.21: DM density vs Half-light radius. Expansion of the right panel of Fig.4.17 .

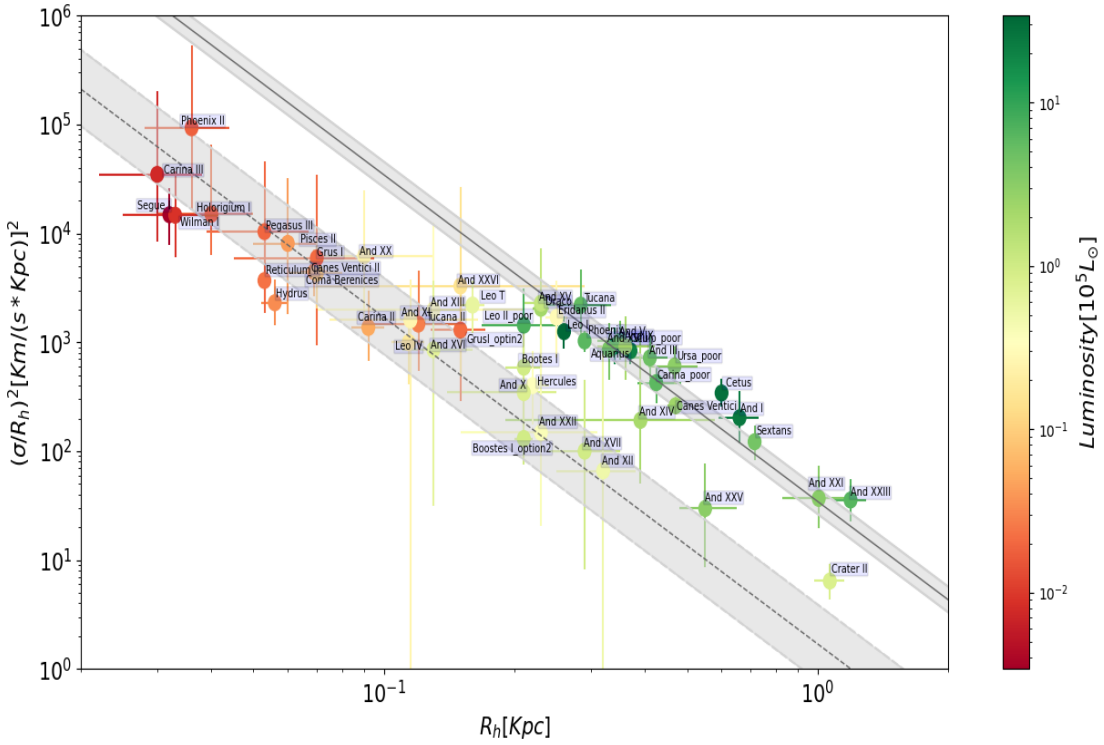

Figure 4.22: DM density vs Half-light radius. Expansion of the left panel of Fig.4.17 .

4.4.1 Individual ψDM core-halo structures

Here we show all the stellar density profiles of a comprehensive sample of dSph and UFD dwarfs that we compare with the generic ψDM core-halo profile of section 3.3 (Equation 3.16), as in section 4.2. As can be seen in all the figures of sections 4.4.1 and 2.2.2, these dwarfs do appear to have a distinctive common form, similar core-halo structure predicted for ψDM. The cores accurately conform to the unique soliton form in all cases where the star counts are deep, and also the azimuthally averaged outer at larger radius is well fitted by the NFW profile as predicted for ψDM (Schive et al., 2014a). These core and halo regimes are distinct because the core is prominent in density above the halo, with the orange vertical line in the plots marking the transition radius. The figures make clear that this profile behavior is similar for dwarfs orbiting Andromeda's and the Milky Way, that are classified as either "ultra-faint" or "dwarf Spheroidal". The extension of these NFW-like stellar halos is traceable in some dwarfs to over 2 kpc in radius, whereas the cores are typically 0.5kpc for the dSPh's and an order of magnitude smaller on average for the UFD's, 0.05 kpc.

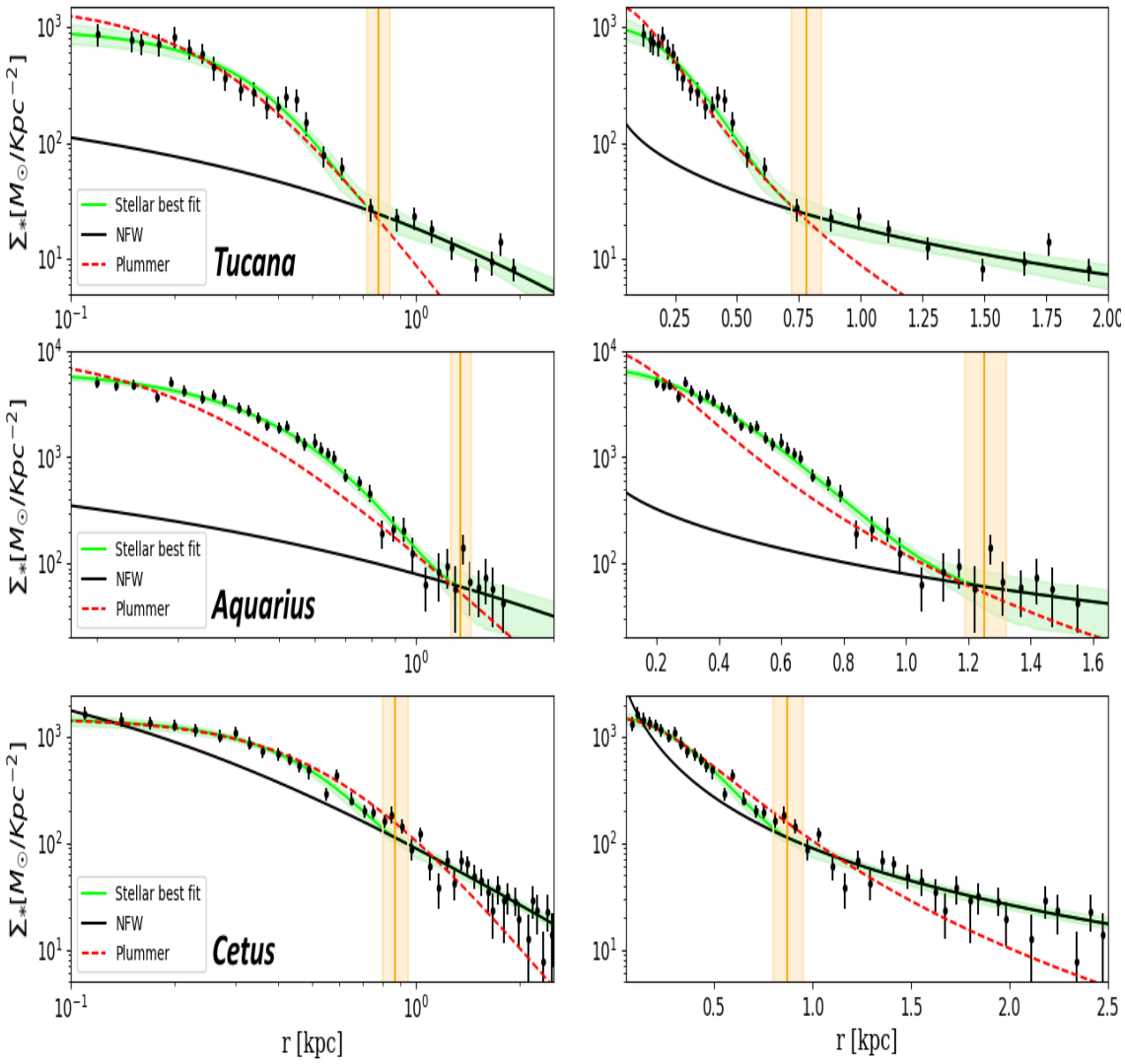

Figure 4.23: Dwarf Spheroidal Galaxies: This figure shows the star count profiles versus dwarf galaxy radius for the well studied dSph dwarf galaxies in the local group, listed in table 4.7. An extended halo of stars is visible in most cases, stretching to $\simeq$ 2 kpc and most evident on the linear scale of left hand panel. Prominent cores are also evident on a scale $<$ 1 kpc in each dwarf. A standard Plummer profile (red dashed curve) is seen to fit approximately the core region but falls well short at large radius. Our predictions for the dSph class ($\simeq 10^{-22}eV$) for ψDM are shown in green, where the distinctive soliton profile provides and excellent fit to the observed cores and the surrounding halo of excited states that average azimuthally to an approximately NFW-like profile beyond the soliton radius. The accuracy of the core fit to the soliton, is best seen on a log scale in the right panels, with linear scale of the left shows the extent of the halo, including the characteristic density drop of about a factor of $\simeq$ 30 predicted by ψDM between the prominent core and tenuous halo at a radius $\simeq$ 1 kpc indicated by vertical orange band. The best fit MCMC profile parameters are tabulated in the supplement and references to the data in this figure are:Tucana (Gregory et al., 2019), Cetus(McConnachie & Irwin, 2006) and Aquarius (McConnachie et al., 2006)

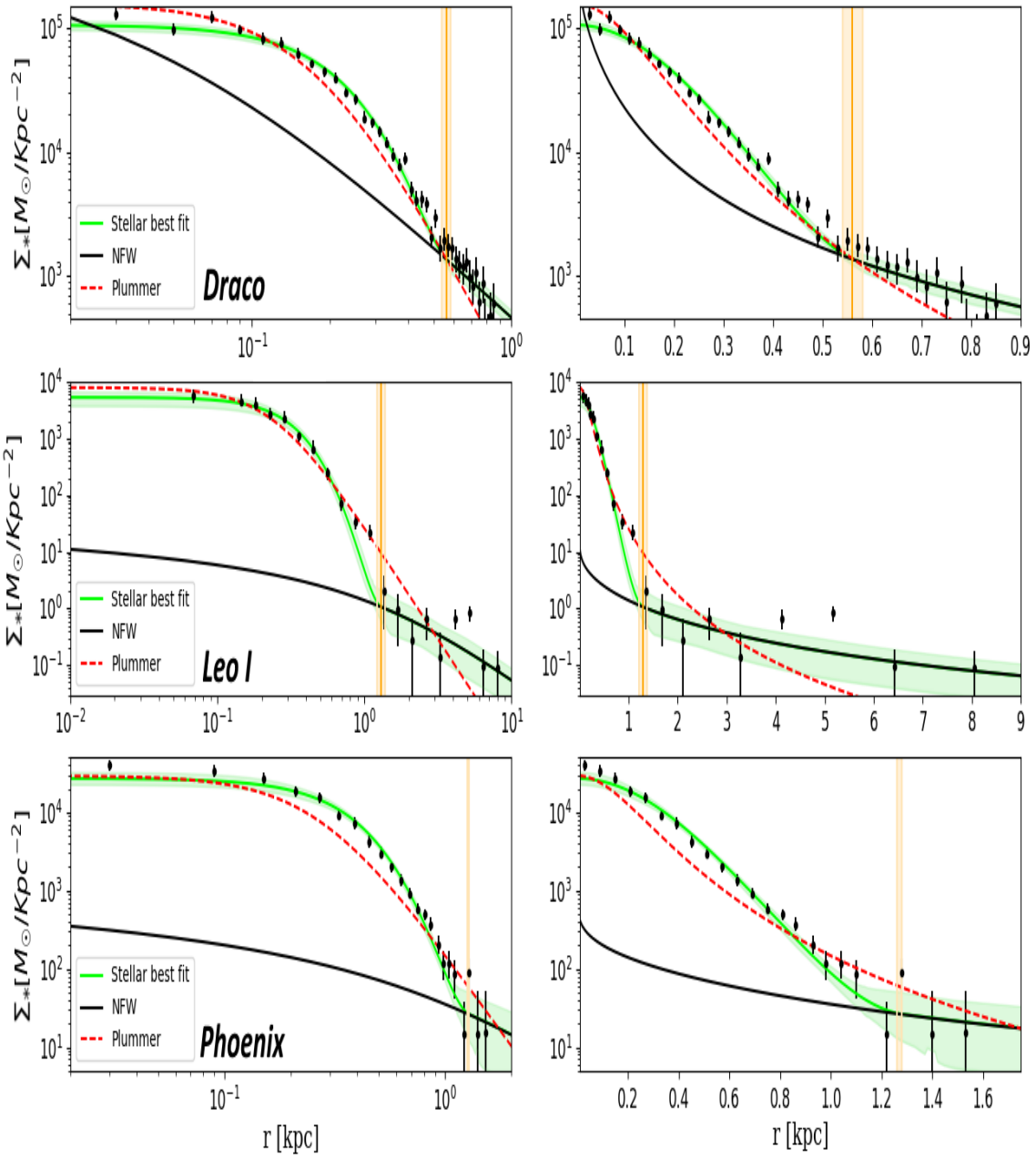

Figure 4.24: Dwarf Spheroidal Galaxies: Same as figure 4.23 for three more dSPh galaxies and references to the data are: Draco (Wilkinson et al., 2004), Leo I (Sohn et al., 2007) and Phoenix (Battaglia et al., 2012a)

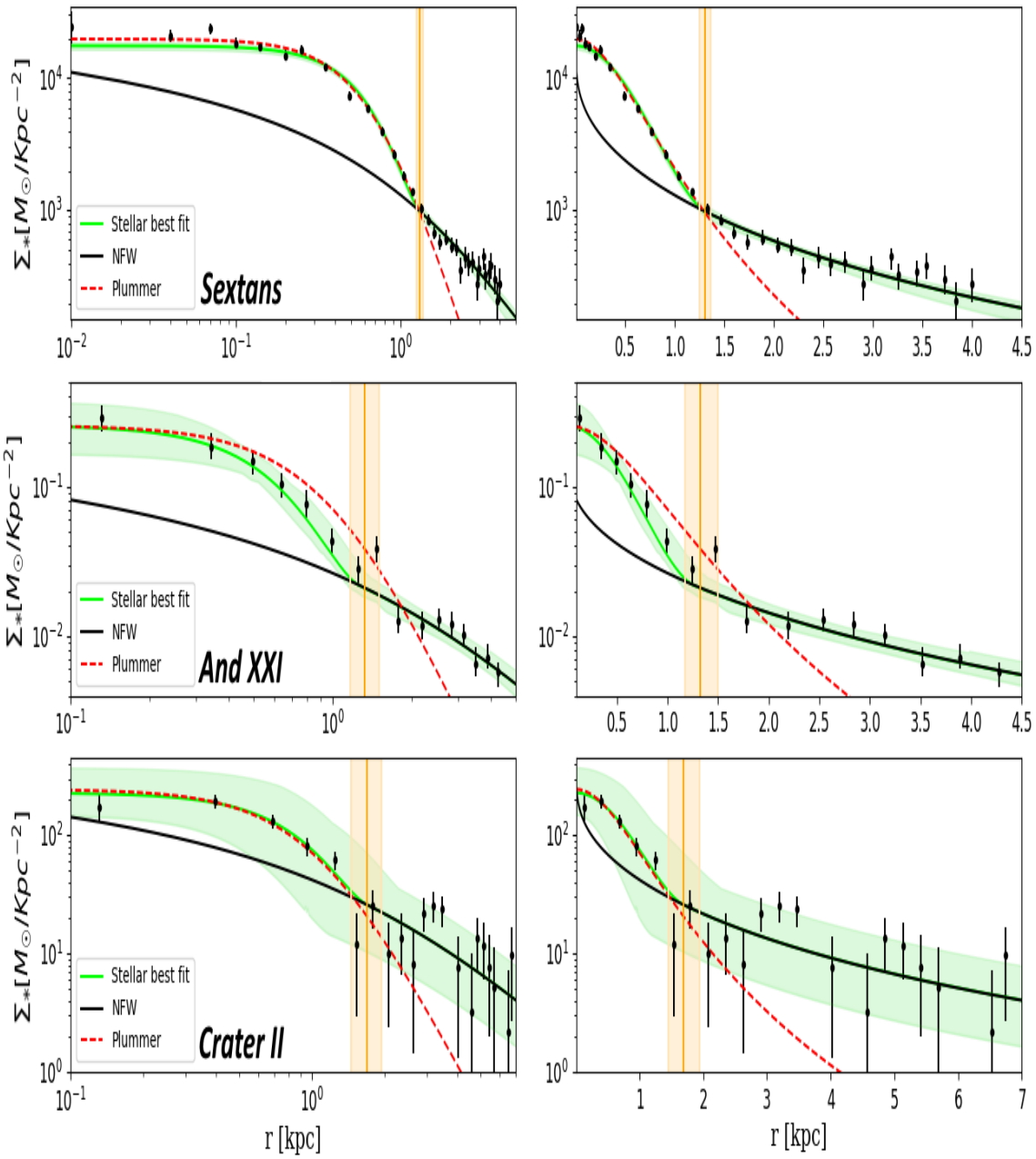

Figure 4.25: Dwarf Spheroidal Galaxies: Same as figure 4.23 with references for the data: Sextans (Okamoto et al., 2017), Andromeda XXI (Collins et al., 2021) and Crater II (Torrealba et al., 2016). It is important to point out that Andromeda XXI shows the same ψDM core-halo structure as dSph satellites of the Milky Way, reinforcing his "universality" of this profile for dwarfs.

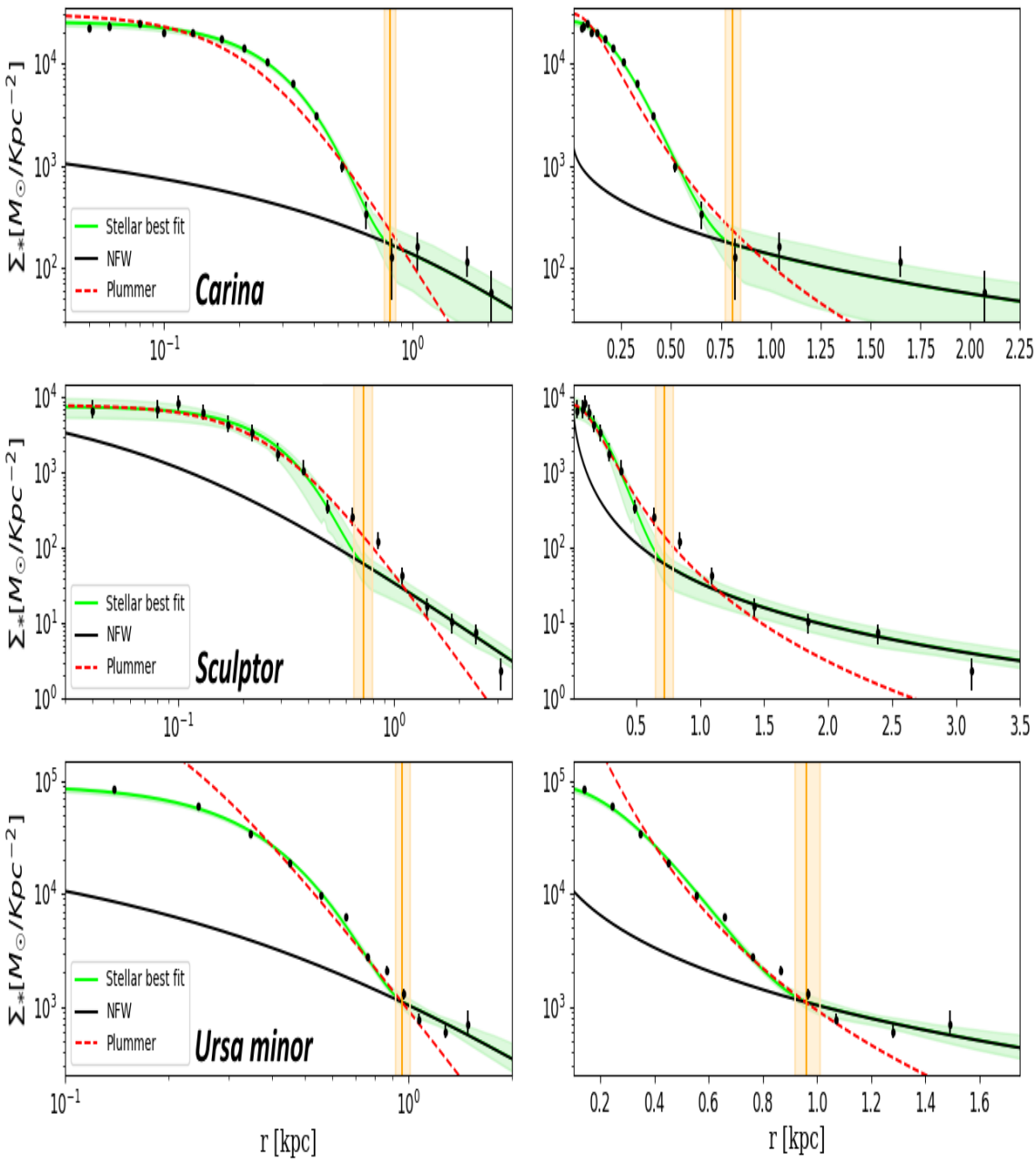

Figure 4.26: Dwarf Spheroidal Galaxies: Same as figure 4.23 for three more galaxies. References for the data are:Carina (Frinchaboy et al., 2012), Sculptor (Frinchaboy et al., 2012) and Ursa Minor (Martínez-Delgado et al., 2001).

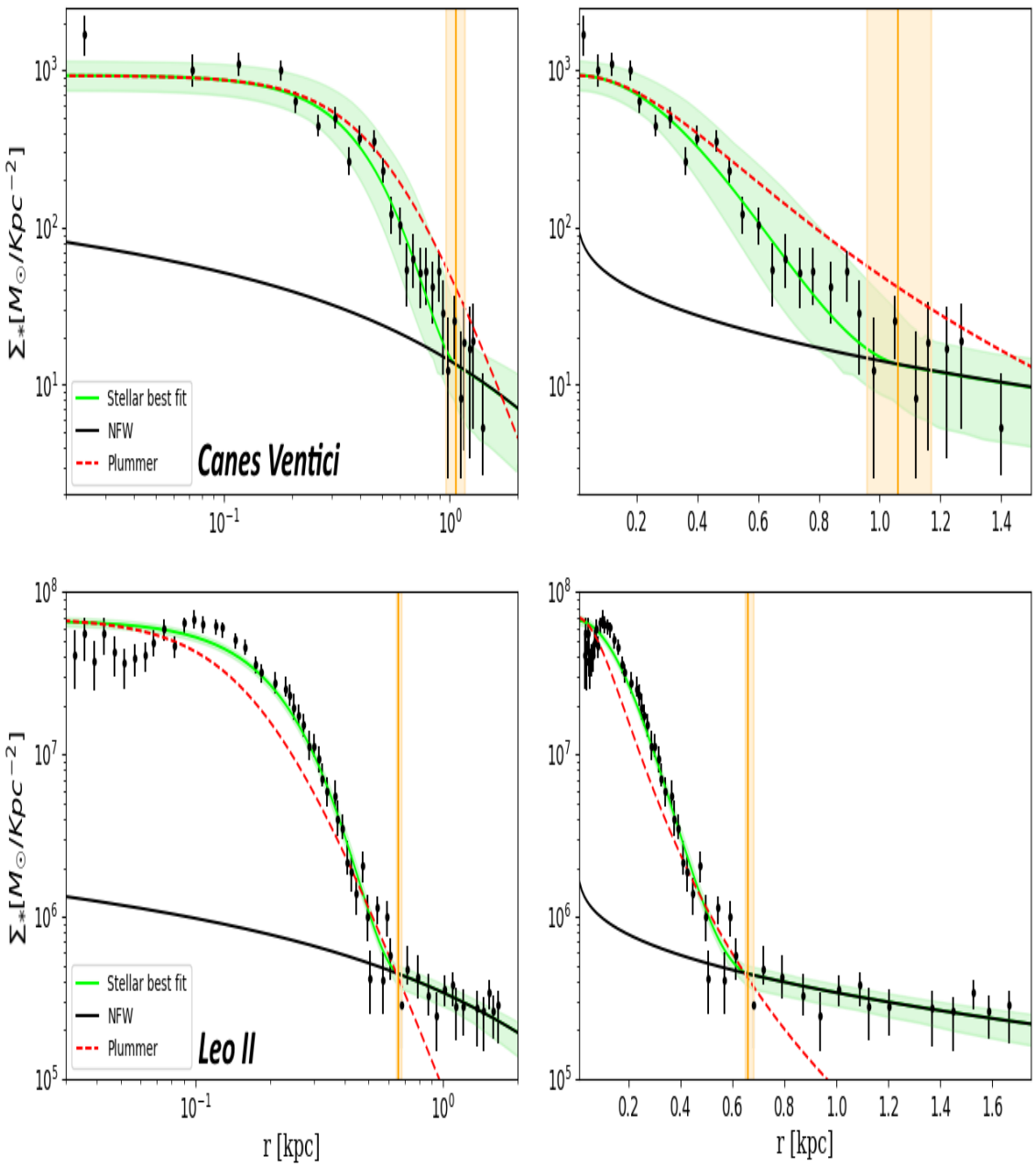

Figure 4.27: Dwarf Spheroidal Galaxies: Same as figure 4.23 but with three more galaxies. References for the data are: Canes Ventici (Zucker et al., 2006b) and Leo II (Moskowitz & Walker, 2020).

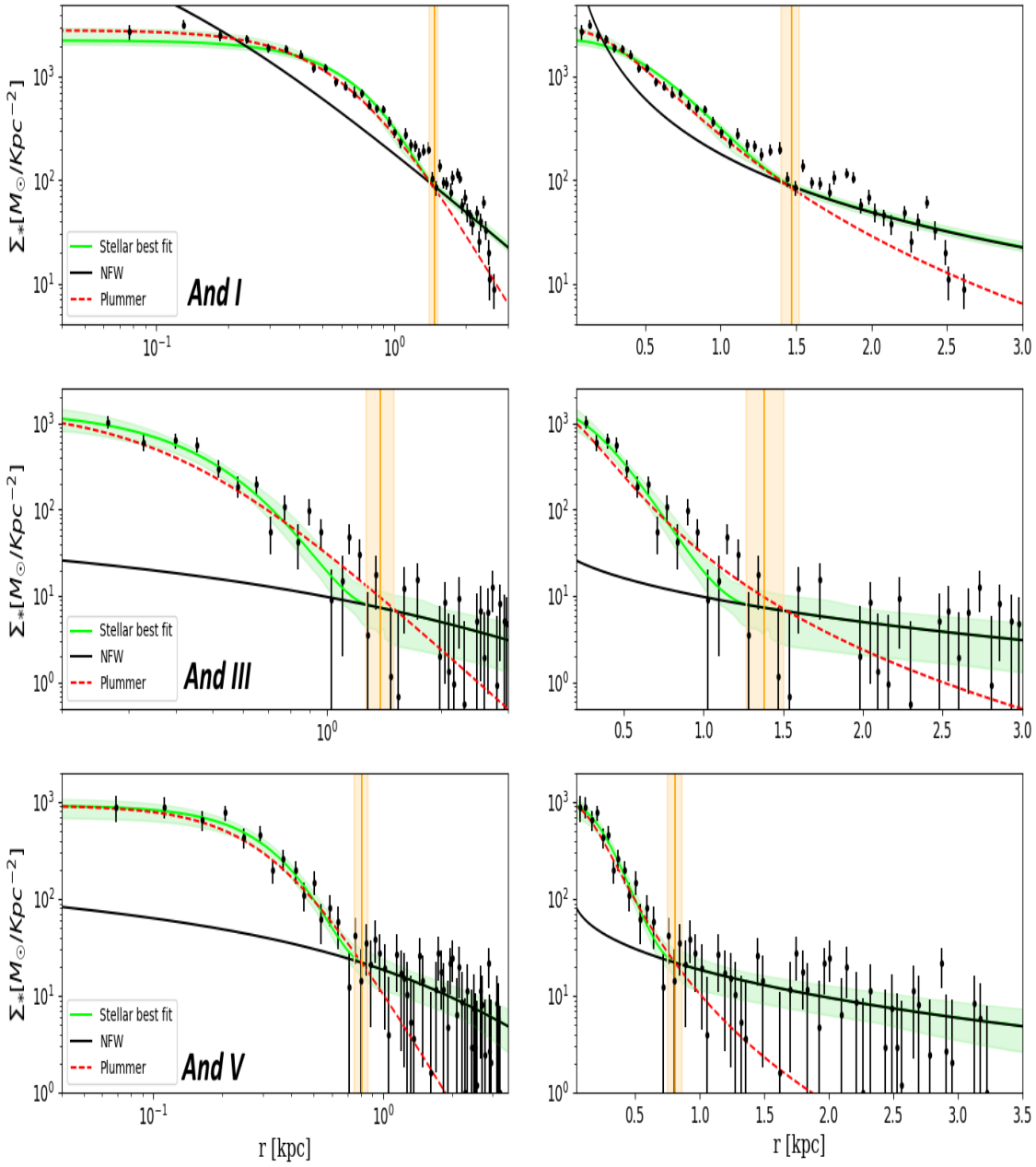

Figure 4.28: Dwarf Spheroidal Galaxies: Same as figure 4.23 but with three more galaxies. It is important to point out how these Andromeda galaxies show the same ψDM core-halo structure as UDF galaxies in the Milky Way, reinforcing the universality of the ψDM profile for dwarfs. References to the data are: Andromeda I (Saremi et al., 2020) , Andromeda III (Martin et al., 2016) and Andromeda V (Martin et al., 2016).

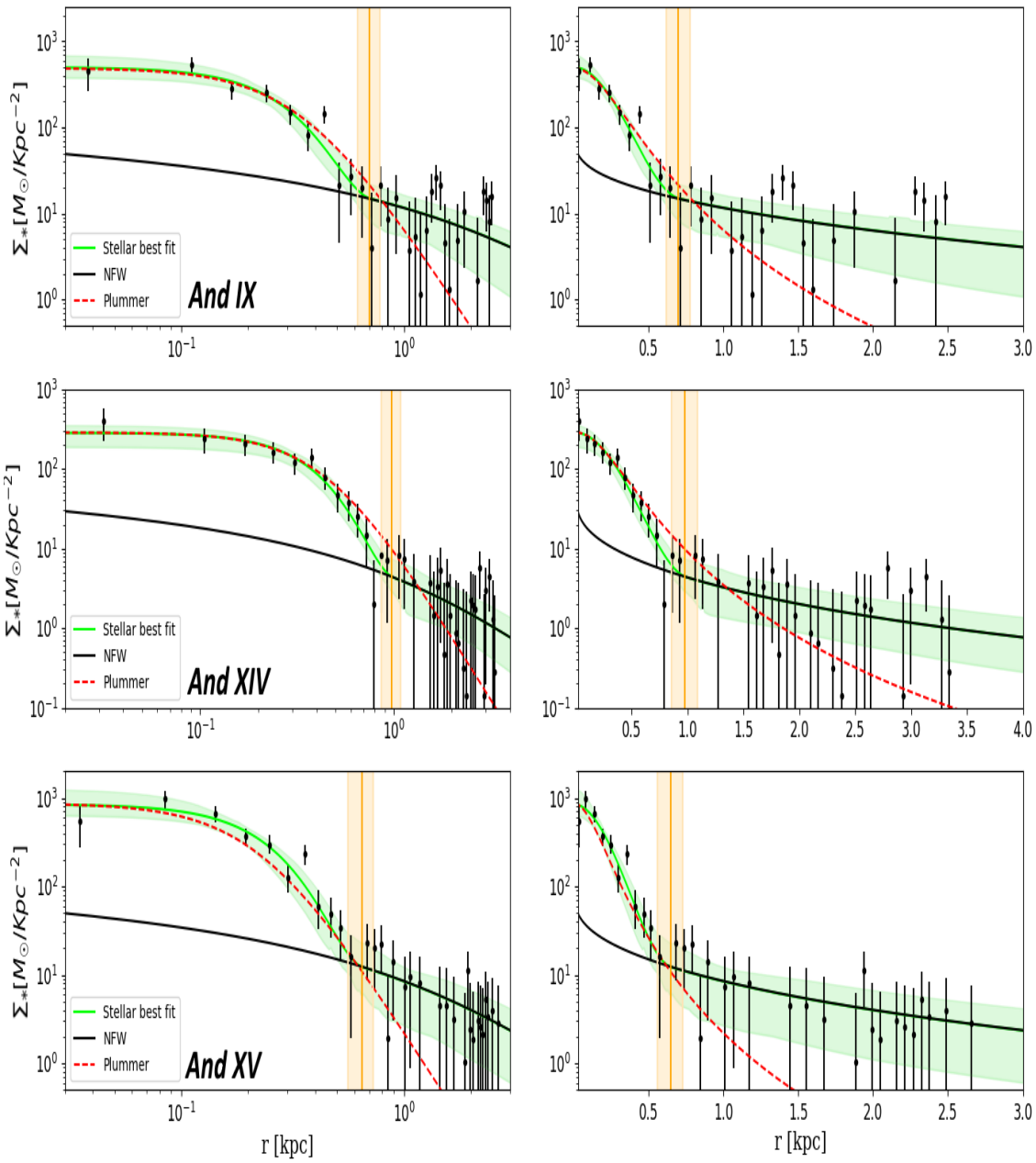

Figure 4.29: Dwarf Spheroidal Galaxies: Same as figure 4.23 but with three more galaxies. References to the data are: Andromeda IX (Martin et al., 2016), Andromeda XIV (Martin et al., 2016) and Andromeda XV (Martin et al., 2016).

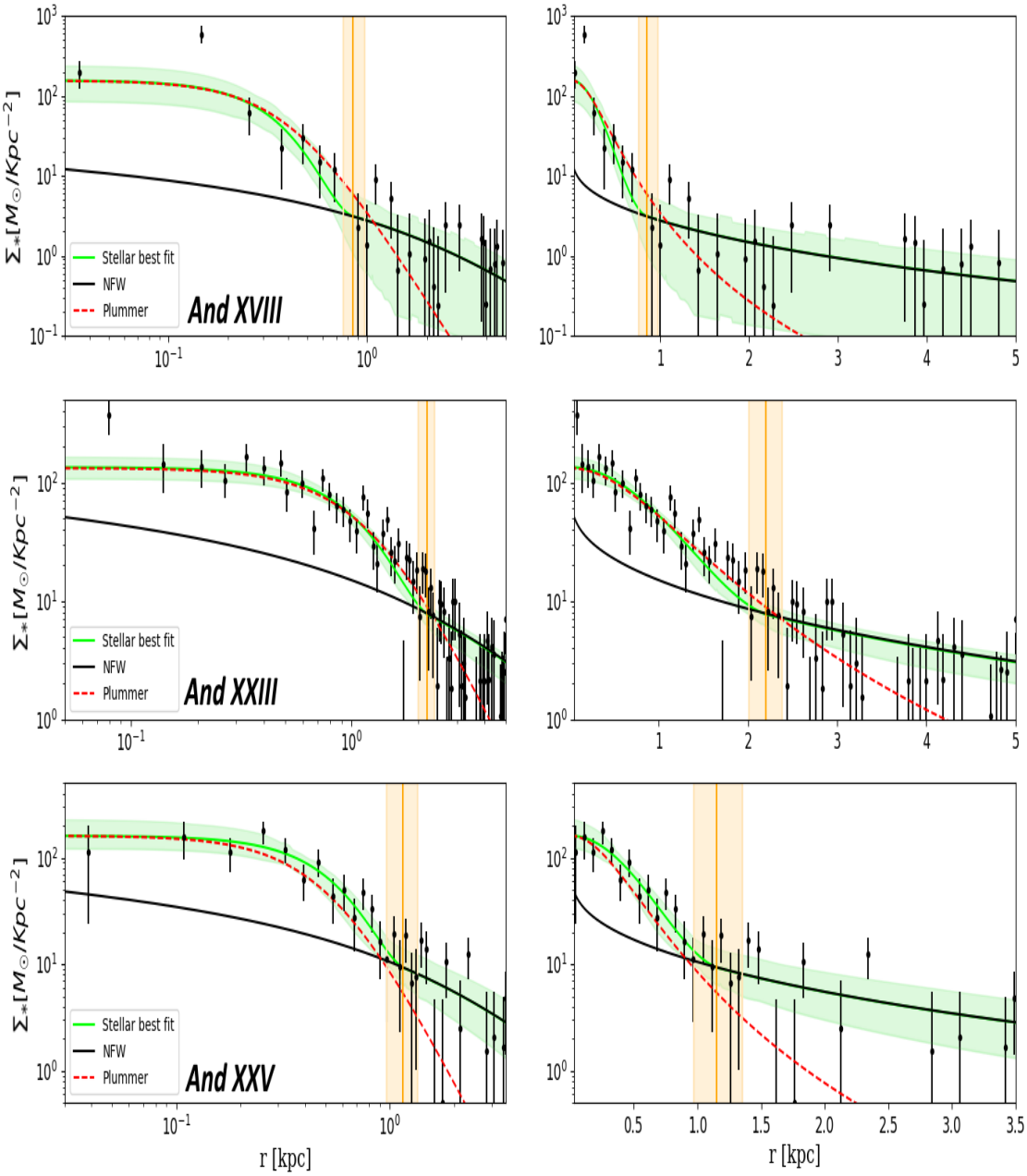

Figure 4.30: Dwarf Spheroidal Galaxies: Same as figure 4.23 but with three more galaxies. References to the data are: Andromeda XVIII (Martin et al., 2016), Andromeda XXIII (Martin et al., 2016) and Andromeda XXV (Martin et al., 2016).

Galaxy	r_c (kpc)	r_t (kpc)	r_{s*} (kpc)	$\sigma_{los,obs}$ (km/s)	$r_{half,obs}$ (kpc)	L_{obs} ($10^5 L_\odot$)	[Fe/H],obs
Tucana	$0.25^{+0.01}_{-0.01}$	$0.78^{+0.06}_{-0.06}$	$1.05^{+0.50}_{-0.57}$	$13.3^{+2.7}_{-2.3}$(Gregory et al., 2019)	$0.284^{+0.05}_{-0.05}$(Gregory et al., 2019)	5.5(Gregory et al., 2019)	∼-1.6(Taibi et al., 2020)
Cetus	$0.36^{+0.02}_{-0.02}$	$0.87^{+0.08}_{-0.07}$	$0.24^{+0.14}_{-0.06}$	$11.1^{+1.6}_{-1.3}$(Taibi et al., 2018)	$0.6^{+0.01}_{-0.01}$(Taibi et al., 2018)	28^{+8}_{-8}(Taibi et al., 2018)	∼-1.7(Taibi et al., 2018)
Aquarius	$0.35^{+0.01}_{-0.01}$	$1.25^{+0.07}_{-0.06}$	$1.05^{+0.82}_{-0.64}$	$10.3^{+1.6}_{-1.3}$(Hermosa Muñoz et al., 2017)	$0.34^{+0.01}_{-0.01}$(Hermosa Muñoz et al., 2017)	17(Kirby et al., 2017)	∼-1.5(Kirby et al., 2017)
Draco	$0.17^{+0.01}_{-0.01}$	$0.56^{+0.02}_{-0.02}$	$0.1^{+0.09}_{-0.05}$	$11^{+2.1}_{-1.5}$(Massari et al., 2020)	$0.23^{+0.01}_{-0.01}$ (McConnachie & Venn, 2020)	2.2(Łokas et al., 2005a)	∼-1.9(Aparicio et al., 2001)
Leo I	$0.24^{+0.01}_{-0.01}$	$1.30^{+0.08}_{-0.08}$	$1.75^{+0.78}_{-0.96}$	$9.2^{+1.2}_{-1.2}$(McConnachie & Venn, 2020)	$0.26^{+0.01}_{-0.01}$(Battaglia et al., 2022)	34^{+11}_{-11}(Koch et al., 2007b)	∼-1.45 (McConnachie & Venn, 2020)
Phoenix	$0.28^{+0.05}_{-0.06}$	$1.27^{+0.01}_{-0.01}$	$1.1^{+0.54}_{-0.55}$	$9.3^{+0.7}_{-0.7}$(McConnachie & Venn, 2020)	$0.29^{+0.01}_{-0.01}$(McConnachie & Venn, 2020)	6.2(Held et al., 1999)	∼-1.5(McConnachie & Venn, 2020)
Canes Venitici	$0.308^{+0.019}_{-0.018}$	$1.06^{+0.11}_{-0.10}$	$2.29^{+1.77}_{-1.35}$	$7.6^{+0.4}_{-0.4}$(McConnachie & Venn, 2020)	$0.47^{+0.02}_{-0.02}$(McConnachie & Venn, 2020)	2.3(C. et al., 2020)	$-1.98^{+0.01}_{-0.01}$(McConnachie & Venn, 2020)
Sextans	$0.48^{+0.01}_{-0.01}$	$1.31^{+0.05}_{-0.06}$	$1.61^{+0.51}_{-0.49}$	$7.9^{+1.3}_{-1.3}$(McConnachie & Venn, 2020)	$0.715^{+0.01}_{-0.01}$(Okamoto et al., 2017)	$4.37^{+1.69}_{-1.69}$(Battaglia, 2011)	∼-1.95(McConnachie & Venn, 2020)
Crater II	$0.71^{+0.09}_{-0.08}$	$1.68^{+0.25}_{-0.23}$	2.6^{+}_{-}	$2.7^{+0.3}_{-0.3}$(Caldwell et al., 2017)	$1.066^{+0.084}_{-0.084}$(Caldwell et al., 2017)	0.83(Caldwell et al., 2017)	$-1.98^{+0.1}_{-0.1}$(Caldwell et al., 2017)
Leo II	$0.17^{+0.01}_{-0.01}$	$0.66^{+0.02}_{-0.01}$	$3.76^{+0.79}_{-1.07}$	$7.4^{+0.4}_{-0.4}$(Battaglia et al., 2022)	$0.191^{+0.02}_{-0.02}$(Moskowitz & Walker, 2020)	7.4^{+2}_{-2}(Koch et al., 2007a)	∼-1.65(McConnachie & Venn, 2020)
Carina	$0.21^{+0.01}_{-0.01}$	$0.81^{+0.04}_{-0.04}$	$1.17^{+0.51}_{-0.61}$	$6.6^{+1.2}_{-1.2}$(McConnachie & Venn, 2020)	$0.424^{+0.06}_{-0.04}$(Hayashi et al., 2018)	5.9(de Boer et al., 2014)	$-1.72^{+0.01}_{-0.01}$(McConnachie & Venn, 2020)
Ursa Minor	$0.28^{+0.01}_{-0.01}$	$0.96^{+0.05}_{-0.04}$	$0.52^{+0.9}_{-0.4}$	$11.5^{+0.9}_{-0.8}$(Pace et al., 2020)	$0.4675^{+0.06}_{-0.06}$(Pace et al., 2020)	3(Carrera et al., 2002)	∼-2.13 (McConnachie & Venn, 2020)
Sculptor	$0.21^{+0.01}_{-0.01}$	$0.72^{+0.07}_{-0.07}$	$0.12^{+0.25}_{-0.09}$	$10.1^{+0.3}_{-0.3}$(Battaglia et al., 2022)	$0.289^{+0.01}_{-0.01}$(Battaglia et al., 2022)	$20.3^{+7.9}_{-7.9}$(Bettinelli et al., 2019)	∼-1.45(McConnachie & Venn, 2020)
And I	$0.52^{+0.02}_{-0.02}$	$1.47^{+0.05}_{-0.07}$	$0.13^{+0.05}_{-0.02}$	$9.4^{+1.7}_{-1.5}$(Kirby et al., 2001)	$0.66^{+0.07}_{-0.07}$(Collins et al., 2013)	$23.98^{+0.57}_{-0.54}$(Martin et al., 2016)	$-1.51^{+0.02}_{-0.02}$ (Kirby et al., 2001)
And III	$0.33^{+0.02}_{-0.02}$	$1.38^{+0.12}_{-0.11}$	$2.53^{+1.56}_{-0.89}$	$11.0^{+1.9}_{-1.6}$(Kirby et al., 2001)	$0.41^{+0.04}_{-0.04}$(Martin et al., 2016)	$4.78^{+0.11}_{-0.11}$(Martin et al., 2016)	$-1.75^{+0.01}_{-0.01}$ (Kirby et al., 2001)
And V	$0.25^{+0.01}_{-0.01}$	$0.81^{+0.05}_{-0.06}$	$2.59^{+1.47}_{-1.37}$	$11.2^{+1.1}_{-1.0}$(Kirby et al., 2001)	$0.35^{+0.04}_{-0.04}$(Martin et al., 2016)	$4.07^{+0.10}_{-0.09}$(Martin et al., 2016)	$-1.84^{+0.03}_{-0.03}$ (Kirby et al., 2001)
And IX	$0.22^{+0.02}_{-0.02}$	$0.70^{+0.08}_{-0.08}$	$3.22^{+1.15}_{-1.46}$	$10.9^{+2.0}_{-2.0}$(Alexander et al., 2017)	$0.36^{+0.06}_{-0.05}$(Martin et al., 2016)	$1.99^{+0.52}_{-0.41}$(Alexander et al., 2017)	$-1.90^{+0.60}_{-0.60}$ (Collins et al., 2013)
And XIV	$0.33^{+0.02}_{-0.02}$	$0.98^{+0.11}_{-0.12}$	$1.77^{+1.83}_{-1.10}$	$5.4^{+1.3}_{-1.3}$(Jason et al., 2010)	$0.39^{+0.19}_{-0.20}$(Collins et al., 2013)	$1.99^{+0.52}_{-0.41}$(Alexander et al., 2017)	∼
And XV	$0.19^{+0.02}_{-0.02}$	$0.65^{+0.08}_{-0.09}$	$1.88^{+1.81}_{-1.24}$	$11.0^{+7.0}_{-5.0}$(McConnachie, 2012)	$0.23^{+0.03}_{-0.02}$(Collins et al., 2013)	$1.25^{+0.74}_{-0.25}$(Alexander et al., 2017)	∼ −1.1 (Collins et al., 2013)
And XVIII	$0.25^{+0.03}_{-0.02}$	$0.85^{+0.12}_{-0.09}$	$2.99^{+1.27}_{-1.49}$	$9.7^{+2.3}_{-2.3}$(McGaugh & Milgrom, 2013b)	$0.33^{+0.02}_{-0.02}$(Collins et al., 2013)	$3.98^{+2.32}_{-1.47}$(McGaugh & Milgrom, 2013b)	$-1.80^{+0.50}_{-0.50}$ (Collins et al., 2013)
And XXI	$0.51^{+0.06}_{-0.05}$	$1.32^{+0.18}_{-0.15}$	3.16^{+}_{-}	$6.1^{+1}_{-0.9}$(Collins et al., 2021)	$1.005^{+0.175}_{-0.175}$(Collins et al., 2021)	$3.2^{+0.8}_{-0.7}$(Collins et al., 2021)	∼-1.8 (Collins et al., 2021)
And XXIII	$0.80^{+0.06}_{-0.06}$	$2.20^{+0.18}_{-0.19}$	$3.92^{+0.70}_{-1.35}$	$7.1^{+1.0}_{-1.0}$(Alexander et al., 2017)	$1.19^{+0.10}_{-0.10}$(Collins et al., 2013)	$6.30^{+1.04}_{-1.29}$(Alexander et al., 2017)	$-1.80^{+0.20}_{-0.20}$ (Collins et al., 2013)
And XXV	$0.42^{+0.05}_{-0.06}$	$1.15^{+0.20}_{-0.18}$	$2.79^{+1.30}_{-1.18}$	$3.0^{+1.2}_{-1.1}$(Alexander et al., 2017)	$0.55^{+0.10}_{-0.07}$(Martin et al., 2016)	$3.16^{+0.82}_{-0.65}$(Alexander et al., 2017)	$-1.80^{+0.50}_{-0.50}$(Collins et al., 2013)

Table 4.7: Observations and ψDM profile fits for Dwarf Spheroidal galaxies. Column 1: Dwarf galaxy name, Column 2: Core radius r_c, Column 3: Transition point r_t, Column 4: Stellar scale radius r_{s*}, Column 5: Observable projected velocity dispersion $\sigma_{los,obs}$, Column 6: Observable half-light radius $r_{half,obs}$, Column 7: Observable luminosity L_{obs}, Column 8: Observable metallicity. We exclude the centrally younger more metal rich stellar populations found in some of these dwarfs (that may be due to later gas infall) adopting the metal-poor stellar and velocity dispersion profiles of Leo II, Carina, Ursa Minor, and Sculptor, with mean velocity disperison respectively of $\sigma_{los,poor,obs}$ (km/s): $7.96^{+1.39}_{-1.1}$ (Spencer et al., 2017), $8.75^{+0.75}_{-0.75}$ (Wilkinson et al., 2006; Fabrizio, 2016), $11.5^{+0.9}_{-0.8}$ (Pace et al., 2020) and $10.7^{+1.4}_{-1.2}$ (Chen et al., 2017).

4.4.2 Ultra-Faint Dwarf Galaxies

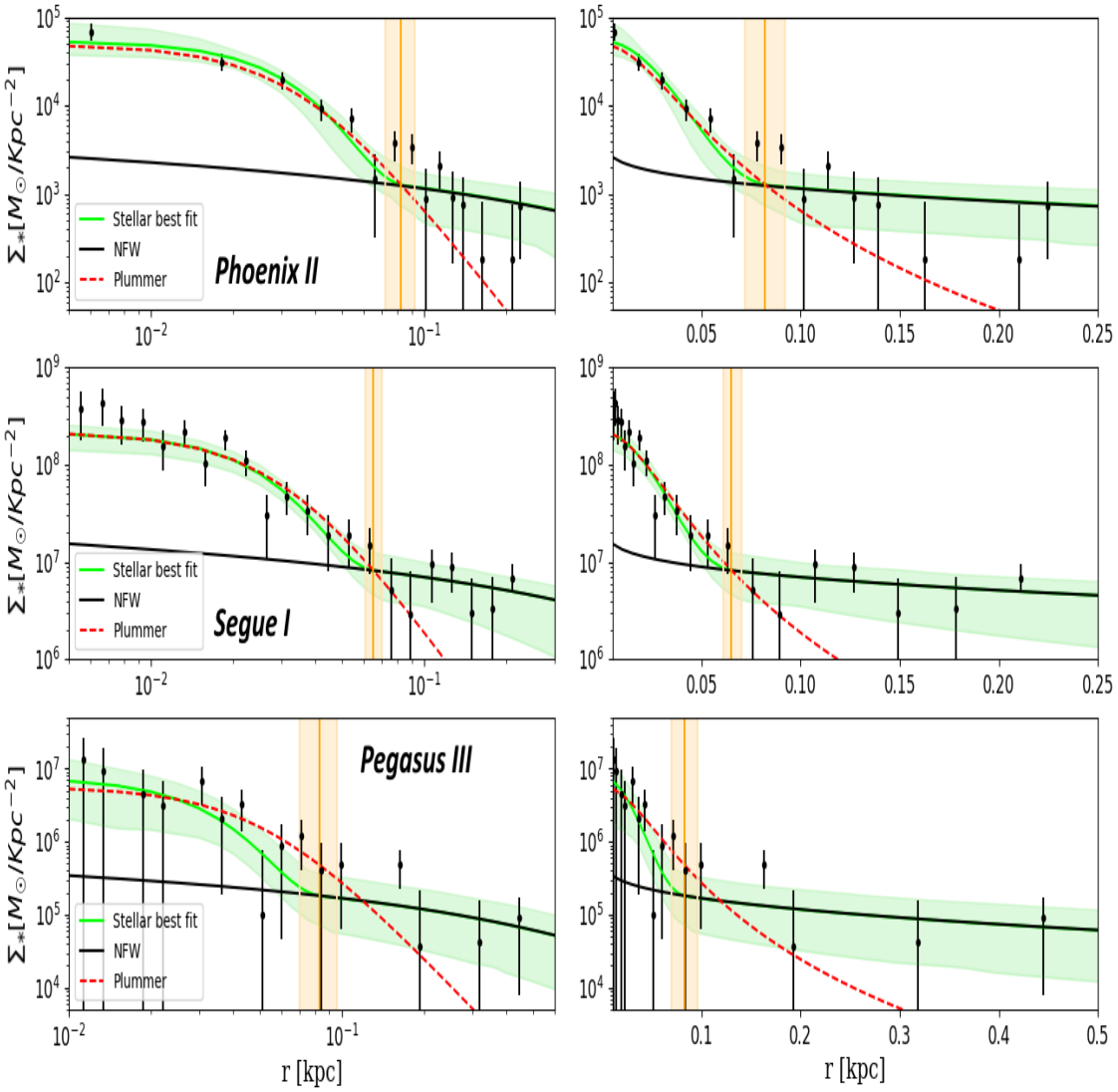

Figure 4.31: Ultra Faint Dwarfs: This figure shows the star count profiles versus dwarf galaxy radius for the "ultra-faint" dwarf galaxies in the local group, listed in table 4.8. Many UDF dwarfs appear to show clear evidence of extended halos stretching to $\simeq 0.5$ kpc, most evident for on the linear scale of the left hand panel. Cores are also evident on a scale < 0.1 kpc in these UDF dwarfs. A standard Plummer profile (red dashed curve) is seen to fit approximately the core region but falls well short at large radius. The soliton profile is normalised to the mean boson mass that we estimate for these dwarfs, $\simeq 10^{-21}eV$) and shown in green, where the distinctive soliton profile provides and excellent fit to the observed cores with the surrounded halo of excited states that average azimuthally to an approximately NFW-like profile beyond the soliton radius. The cores agree well with the predicted form of the soliton profile, as best seen on a log scale in the right panels. The best fit MCMC profile parameters are tabulated in the supplement.References for the data are: Phoenix II (Mutlu-Pakdil et al., 2018), Segue I (Moskowitz & Walker, 2020) and Pegasus III (Moskowitz & Walker, 2020)

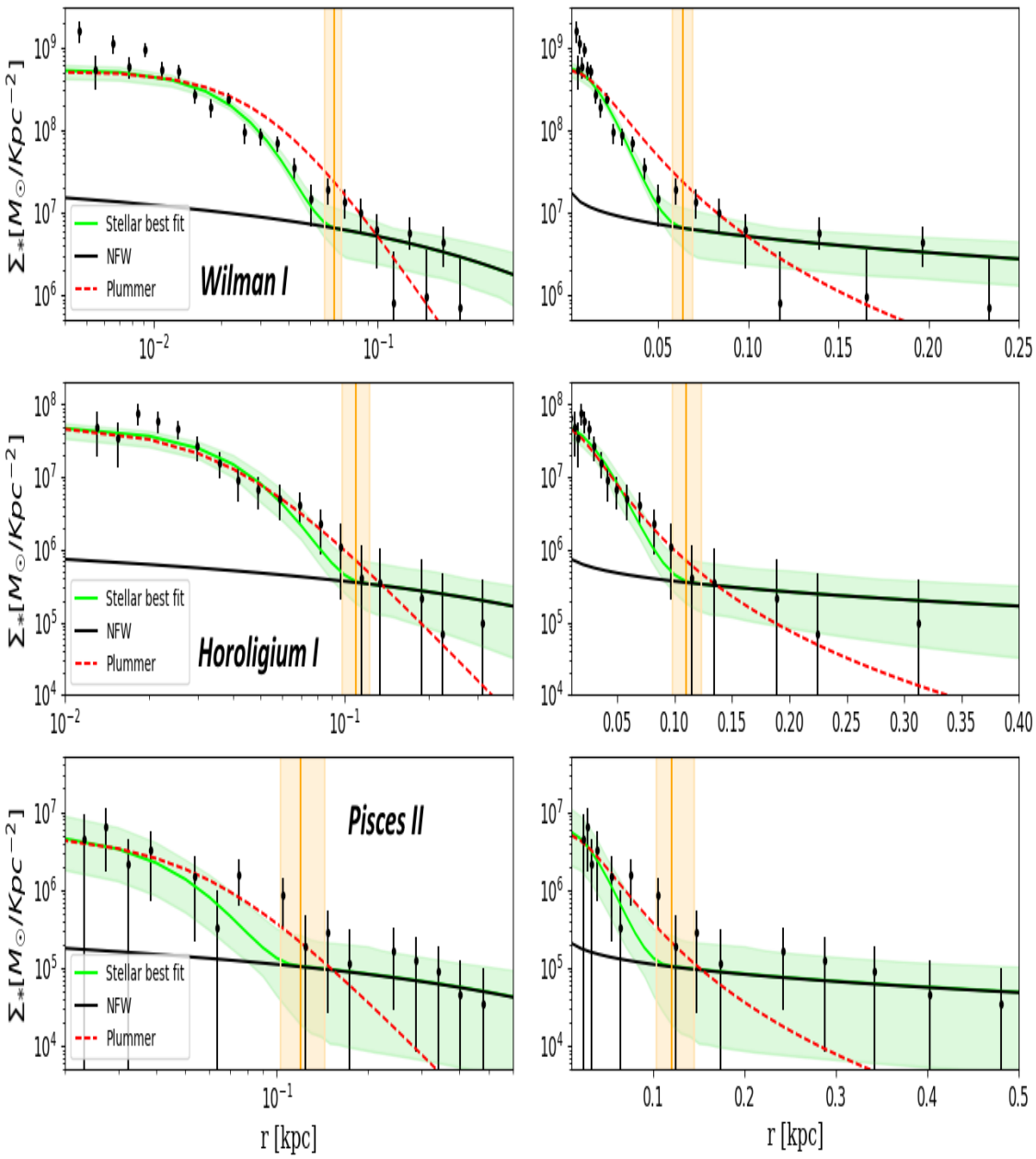

Figure 4.32: Ultra Faint Dwarf Galaxies: Same as figure 4.28 but with three more galaxies. References to the data are: Wilman I (Moskowitz & Walker, 2020), Horoligium I (Moskowitz & Walker, 2020) and Pisces II (Moskowitz & Walker, 2020).

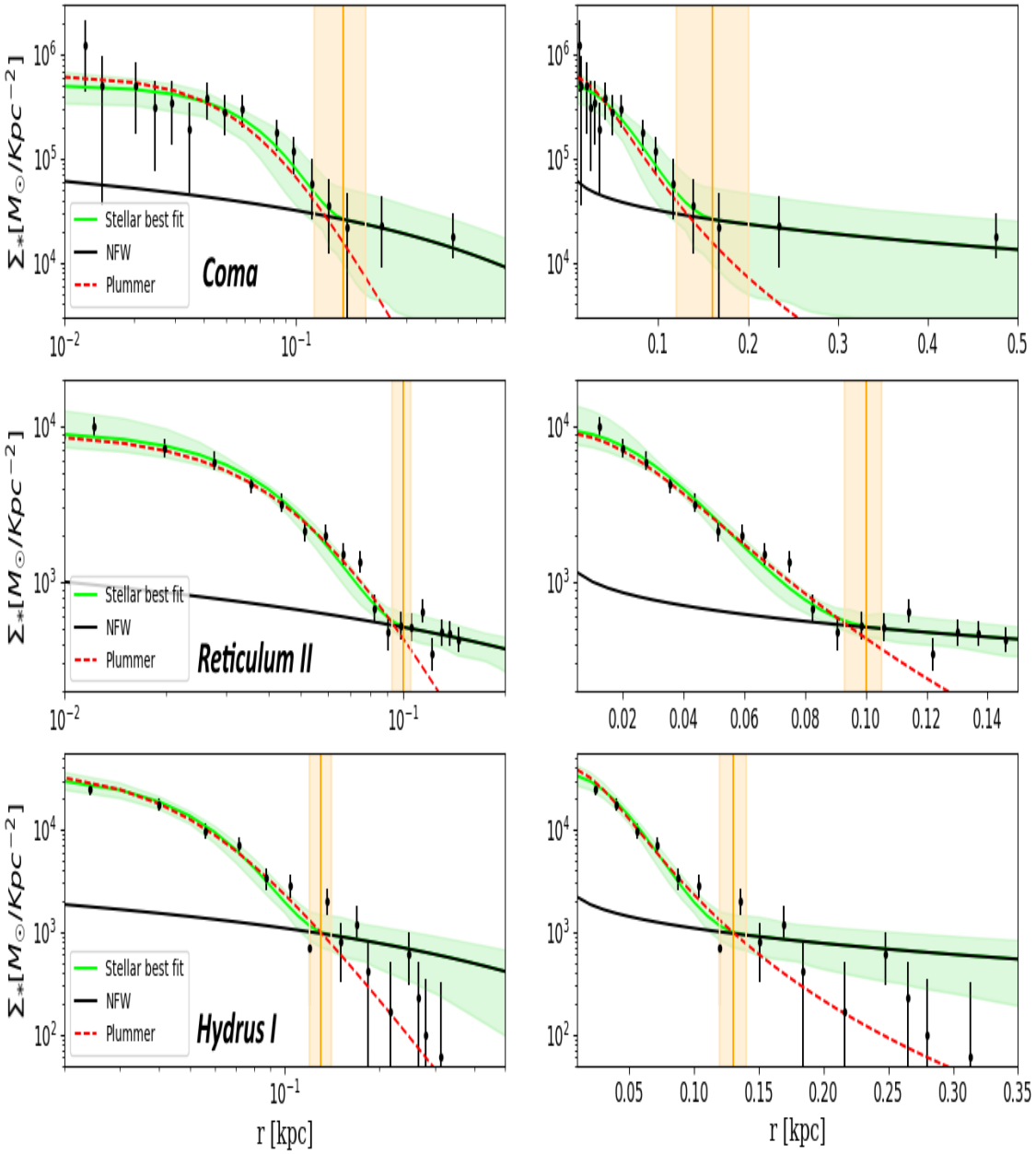

Figure 4.33: Ultra Faint Dwarf Galaxies: Same as figure 4.28 but with three more galaxies. References to the data are: Coma Berenices (Moskowitz & Walker, 2020), Reticulum II (Koposov et al., 2015) and Hydrus I (Koposov et al., 2018).

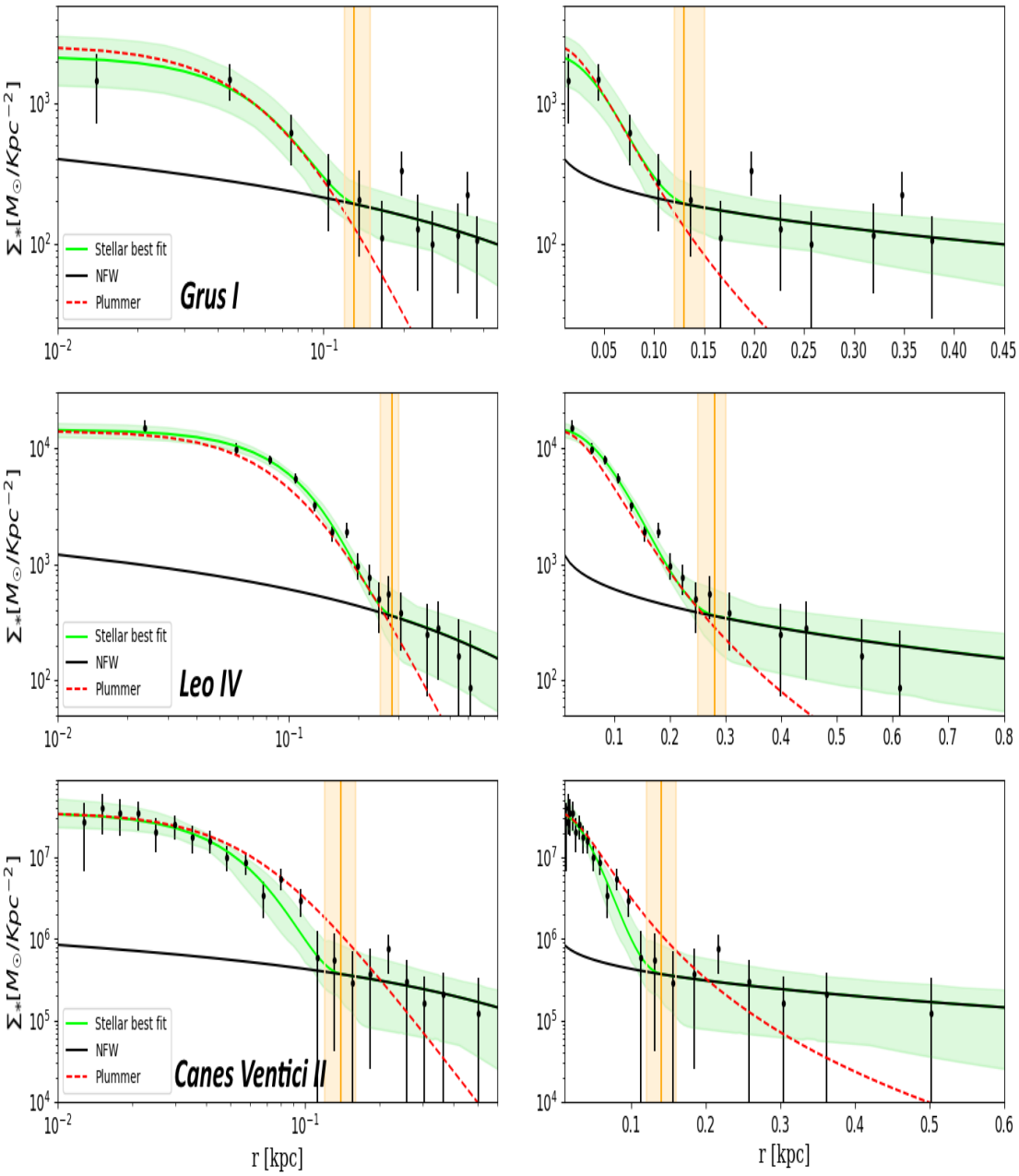

Figure 4.34: Ultra Faint Dwarf Galaxies: Same as figure 4.28 but with three more galaxies. References to the data are: Grus I (Koposov et al., 2018), Leo IV (Okamoto et al., 2012) and Canes Ventici II (Koposov et al., 2018).

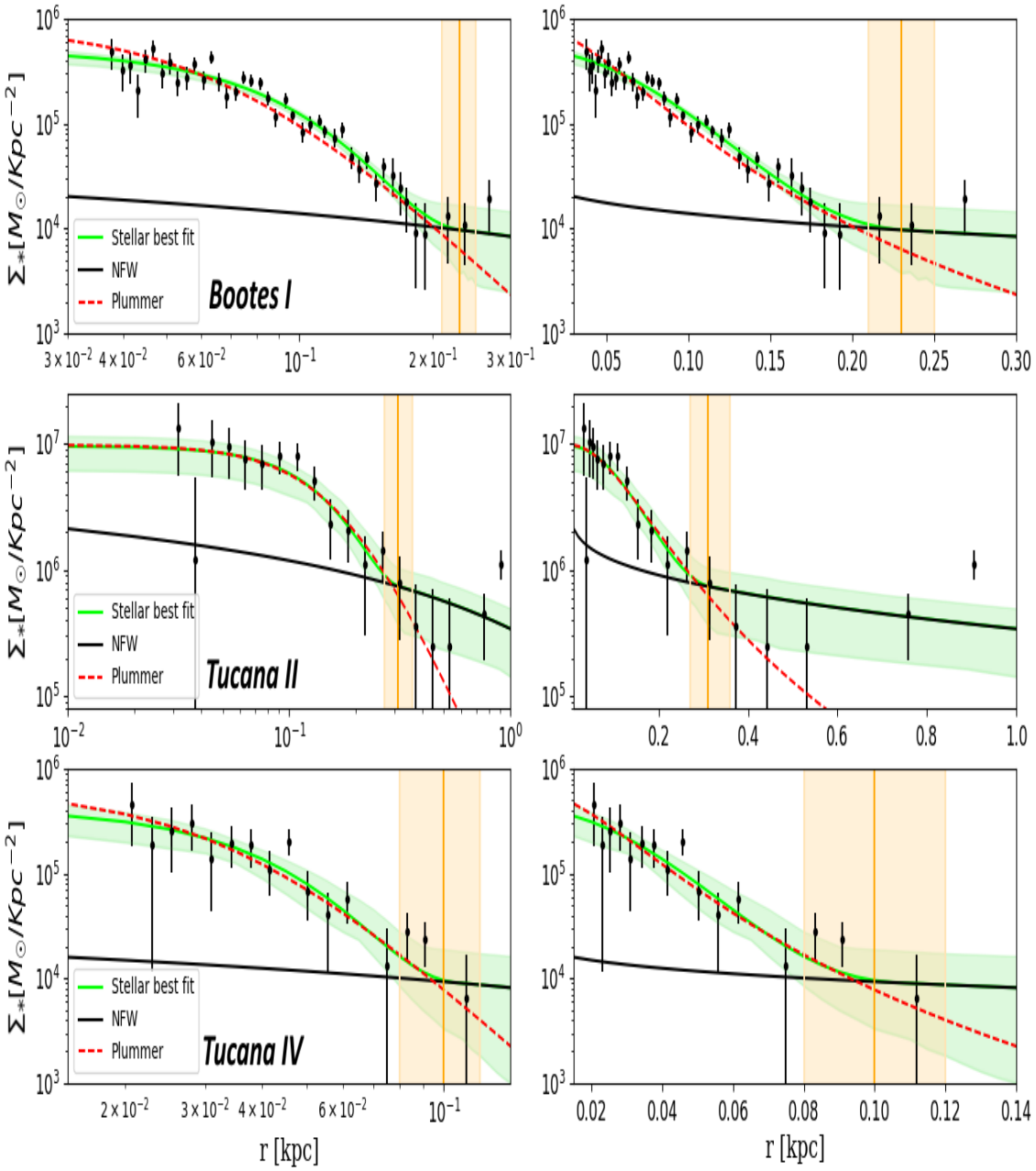

Figure 4.35: Ultra Faint Dwarf Galaxies: Same as figure 4.28 but with three more galaxies. References to the data are: Bootes I (Moskowitz & Walker, 2020), Tucana II (Chiti et al., 2022) and Tucana IV (Moskowitz & Walker, 2020). Note, a surprisingly extended halo of stars and dark matter of 1kpc in extent has been claimed for Tucana II by Chiti et al Chiti et al. (Chiti et al.)

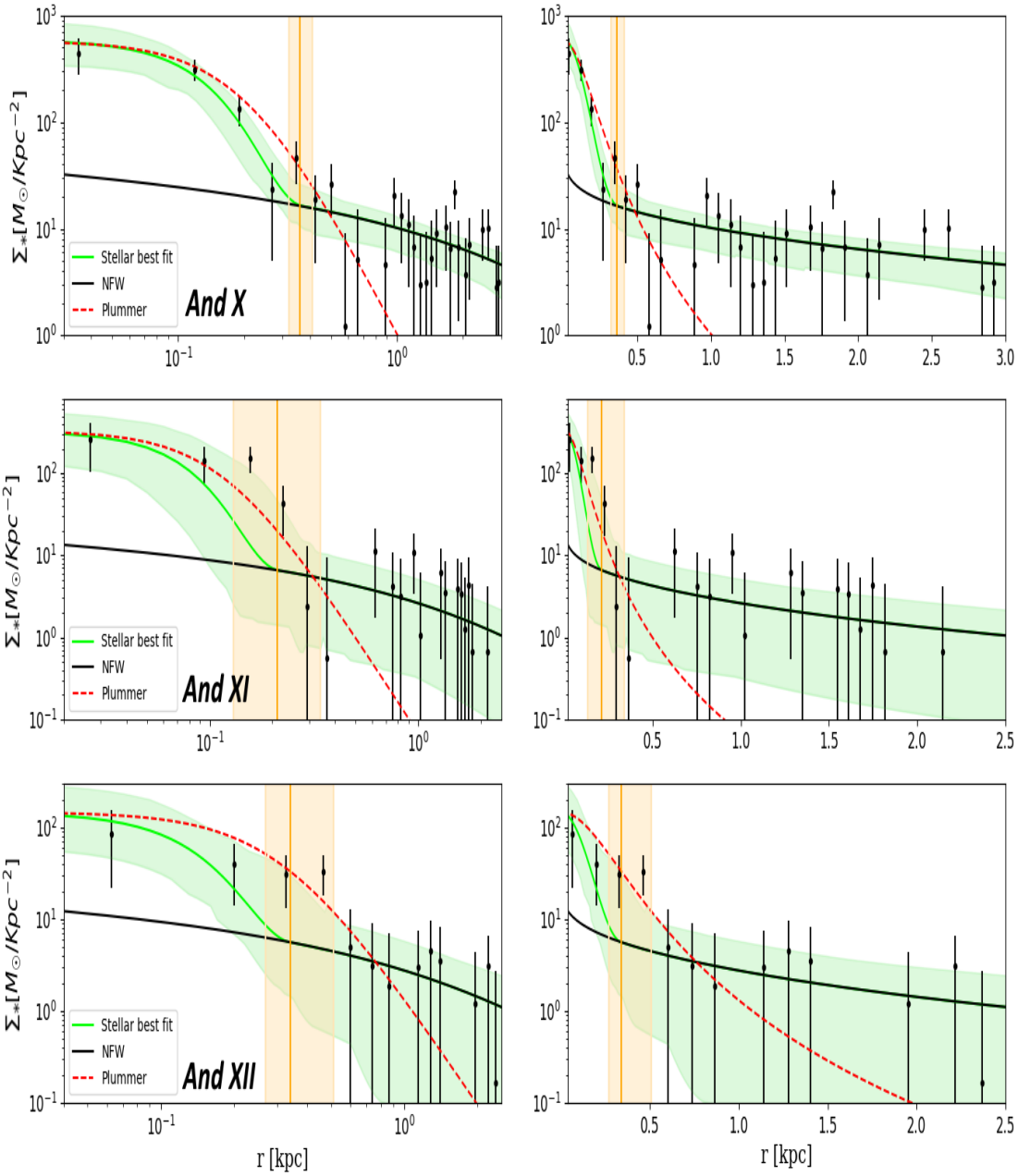

Figure 4.36: Ultra Faint Dwarf Galaxies: Same as figure 4.28 but with three more galaxies. References for the data are: Andromeda X (Martin et al., 2016), Andromeda XI (Martin et al., 2016) and Andromeda XII (Martin et al., 2016).

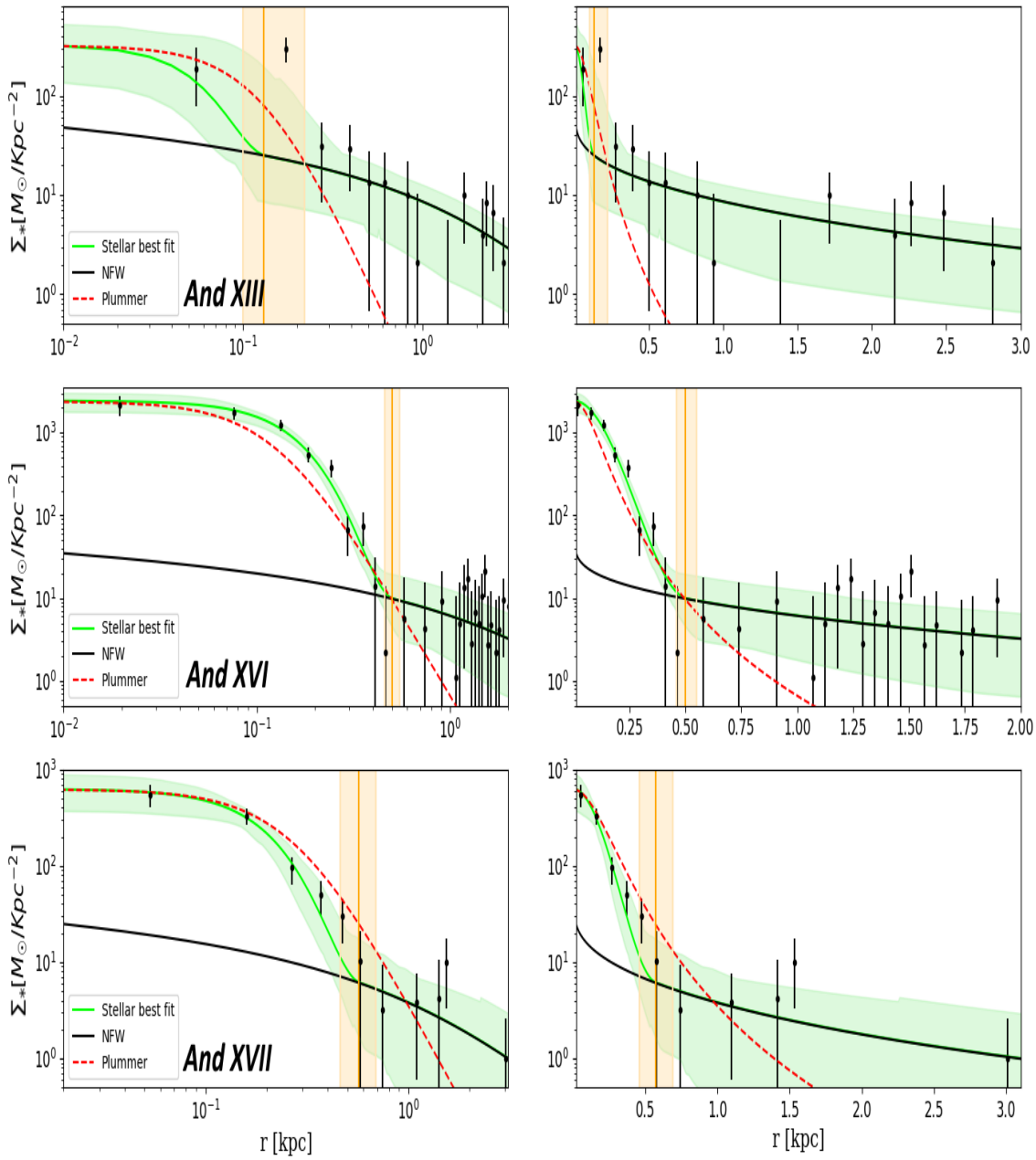

Figure 4.37: Ultra Faint Dwarf Galaxies: Same as figure 4.28 but with three more galaxies. References for the data are: Andromeda XIII (Martin et al., 2016), Andromeda XVI (Martin et al., 2016) and Andromeda XVII (Irwin et al., 2008).

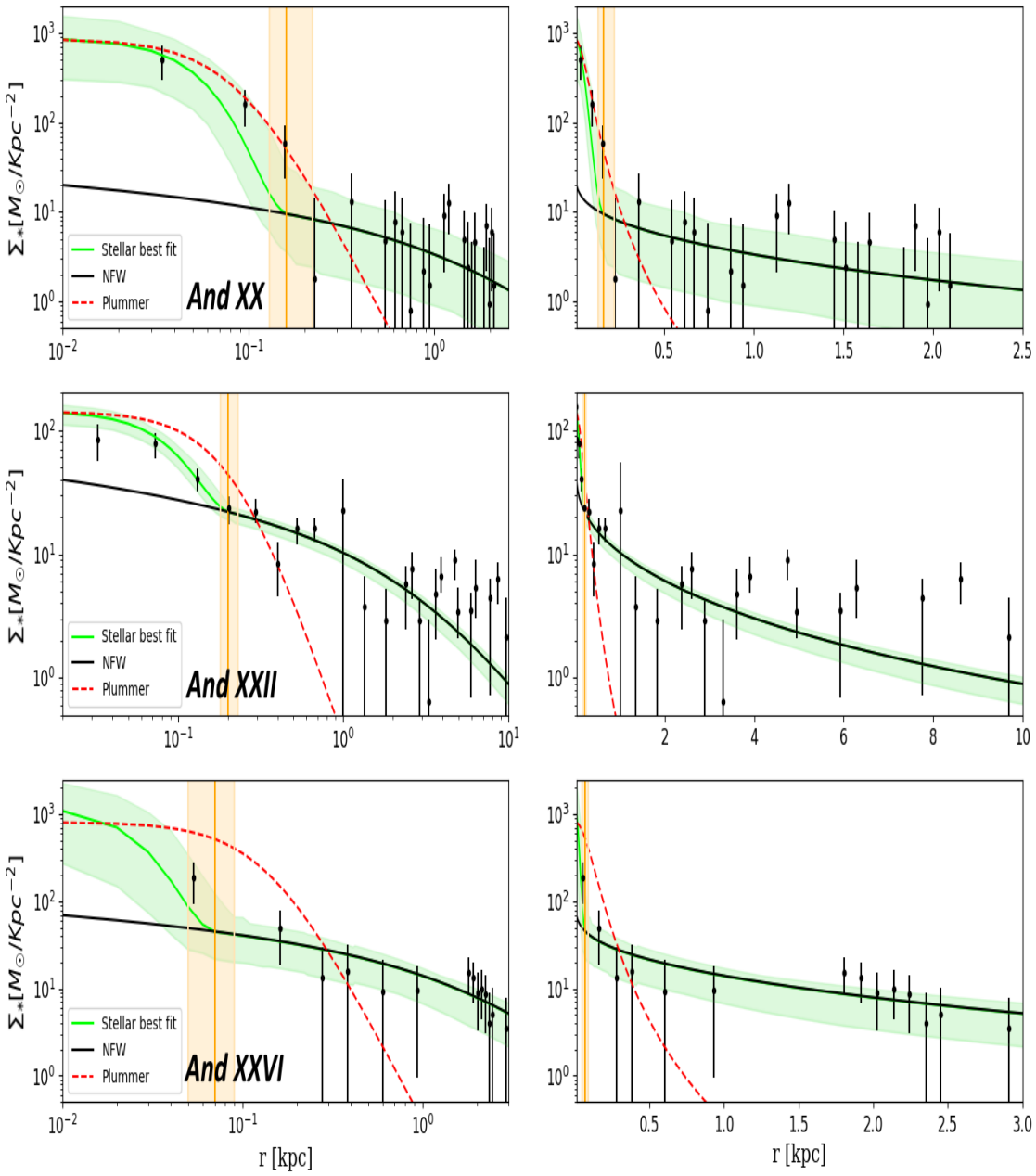

Figure 4.38: Ultra Faint Dwarf Galaxies: Same as figure 4.28 but with three more galaxies. References for the data are: Andromeda XX (Martin et al., 2016), Andromeda XXII (Chapman et al., 2013) and Andromeda XXVI (Martin et al., 2016).

Galaxy	r_c (kpc)	r_t (kpc)	r_{s*} (kpc)	σ_{los} (km/s)	$r_{half,obs}$ (kpc)	L,obs ($10^3 L_\odot$)	[Fe/H],obs
Phoenix II	$0.024^{+0.003}_{-0.003}$	$0.082^{+0.01}_{-0.01}$	$1.37^{+1.17}_{-1.10}$	$11^{+9.40}_{-5.3}$(Battaglia et al., 2022)	$0.036^{+0.008}_{-0.008}$(Battaglia et al., 2022)	$1.79^{+1.41}_{-0.79}$(Muñoz et al., 2018)	$-2.51^{+0.19}_{-0.17}$(Battaglia et al., 2022)
Segue I	$0.020^{+0.001}_{-0.001}$	$0.065^{+0.005}_{-0.004}$	$1.59^{+0.81}_{-0.77}$	$3.9^{+0.8}_{-0.8}$(McConnachie & Venn, 2020)	$0.032^{+0.003}_{-0.003}$(McConnachie & Venn, 2020)	$0.28^{+0.27}_{-0.14}$(Muñoz et al., 2018)	$-2.72^{+0.4}_{-0.4}$(McConnachie & Venn, 2020)
Pegasus III	$0.024^{+0.004}_{-0.002}$	$0.083^{+0.013}_{-0.013}$	$1.16^{+1.10}_{-0.76}$	$5.4^{+3}_{-2.5}$(Battaglia et al., 2022)	$0.053^{+0.014}_{-0.014}$(Battaglia et al., 2022)	1.96(Kim et al., 2016)	$-2.55^{+0.15}_{-0.15}$(Battaglia et al., 2022)
Wilman I	$0.0235^{+0.001}_{-0.001}$	$0.064^{+0.005}_{-0.006}$	$0.64^{+1.21}_{-0.44}$	$4^{+0.8}_{-0.8}$(Battaglia et al., 2022)	$0.033^{+0.008}_{-0.008}$(Battaglia et al., 2022)	$0.87^{+0.86}_{-0.43}$(Muñoz et al., 2018)	∼-2.1(Battaglia et al., 2022)
Horoligium I	$0.028^{+0.002}_{-0.002}$	$0.11^{+0.013}_{-0.012}$	$1.29^{+1.01}_{-0.87}$	$4.9^{+2.8}_{-0.9}$(Battaglia et al., 2022)	$0.041^{+0.01}_{-0.01}$(Battaglia et al., 2022)	$2.24^{+1.51}_{-0.90}$(Muñoz et al., 2018)	$-2.76^{+0.10}_{-0.10}$(Battaglia et al., 2022)
Pisces II	$0.032^{+0.006}_{-0.003}$	$0.12^{+0.024}_{-0.017}$	$1.85^{+1.30}_{-1.19}$	$5.4^{+3.6}_{-2.4}$(Battaglia et al., 2022)	$0.062^{+0.01}_{-0.01}$(Battaglia et al., 2022)	$4.16^{+1.76}_{-1.22}$(Muñoz et al., 2018)	$-2.45^{+0.07}_{-0.07}$(Battaglia et al., 2022)
Coma Berenices	$0.053^{+0.010}_{-0.011}$	$0.16^{+0.04}_{-0.04}$	$1.67^{+0.79}_{-0.90}$	$4.6^{+0.8}_{-0.8}$(Battaglia et al., 2022)	$0.069^{+0.005}_{-0.005}$(Battaglia et al., 2022)	$4.81^{+1.24}_{-0.99}$ (Muñoz et al., 2018)	$-2.25^{+0.05}_{-0.05}$(Battaglia et al., 2022)
Reticulum II	$0.0333^{+0.002}_{-0.002}$	$0.10^{+0.005}_{-0.007}$	$1.48^{+1.04}_{-0.85}$	$3.22^{+1.64}_{-0.49}$(McConnachie & Venn, 2020)	$0.053^{+0.002}_{-0.002}$(McConnachie & Venn, 2020)	$2.36^{+0.2}_{-0.2}$ (Simon et al., 2015)	$-2.65^{+0.07}_{-0.07}$(Simon et al., 2015)
Hydrus	$0.041^{+0.003}_{-0.003}$	$0.13^{+0.01}_{-0.01}$	$1.27^{+1.01}_{-0.87}$	$2.69^{+0.51}_{-0.43}$(McConnachie & Venn, 2020)	$0.056^{+0.004}_{-0.004}$(McConnachie & Venn, 2020)	3.38(Koposov et al., 2018)	$-2.59^{+0.09}_{-0.09}$(Koposov et al., 2018)
Grus I	$0.0475^{+0.009}_{-0.008}$	$0.13^{+0.02}_{-0.01}$	$1.79^{+0.72}_{-0.76}$	$5.4^{+3}_{-2.5}$(Battaglia et al., 2022)	$0.070^{+0.025}_{-0.025}$(McConnachie & Venn, 2020)	$2.10^{+1.51}_{-0.88}$(Muñoz et al., 2018)	$-1.88^{+0.09}_{-0.03}$(Battaglia et al., 2022)
Leo IV	$0.084^{+0.003}_{-0.003}$	$0.28^{+0.02}_{-0.03}$	$1.34^{+1.42}_{-0.34}$	$3.4^{+1.3}_{-0.9}$(Jenkins, 2021)	$0.114^{+0.01}_{-0.01}$(Jenkins, 2021)	18^{+8}_{-8}(Blaña et al., 2021)	$-2.48^{+0.16}_{-0.13}$(Jenkins, 2021)
Canes Venitici II	$0.037^{+0.005}_{-0.005}$	$0.14^{+0.02}_{-0.02}$	$1.39^{+0.99}_{-0.93}$	$4.6^{+1.0}_{-1.0}$(Battaglia et al., 2022)	$0.07^{+0.01}_{-0.01}$(Muñoz et al., 2018)	$10.46^{+3.05}_{-3.05}$(Muñoz et al., 2018)	$-2.21^{+0.05}_{-0.05}$(McConnachie & Venn, 2020)
Bootes I	$0.065^{+0.002}_{-0.003}$	$0.23^{+0.02}_{-0.02}$	$1.86^{+0.73}_{-1.03}$	$2.4^{+0.9}_{-0.5}$(Battaglia et al., 2022)	$0.22^{+0.01}_{-0.01}$(Battaglia et al., 2022)	$21.78^{+5.64}_{-4.48}$(Muñoz et al., 2018)	$-2.34^{+0.05}_{-0.05}$(Jenkins, 2021)
Tucana II	$0.11^{+0.01}_{-0.01}$	$0.31^{+0.05}_{-0.04}$	$2.45^{+0.98}_{-1.09}$	$2.8^{+1.2}_{-0.7}$(Chiti et al., 2022)	$0.12^{+0.03}_{-0.03}$(Chiti et al., 2022)	∼2.83(Muñoz et al., 2018)	∼-2.7(Chiti et al., Chiti et al.)
Tucana IV	$0.030^{+0.004}_{-0.003}$	$0.10^{+0.02}_{-0.02}$	$1.90^{+1.31}_{-1.21}$	$4.3^{+1.7}_{-1.0}$(Battaglia et al., 2022)	$0.11^{+0.011}_{-0.009}$(Moskowitz & Walker, 2020)	$1.40^{+0.60}_{-0.30}$(Simon et al., 2020)	$-2.49^{+0.15}_{-0.16}$(Battaglia et al., 2022)
Leo V*	$0.021^{+0.002}_{-0.001}$	$0.076^{+0.007}_{-0.007}$	$1.61^{+1.50}_{-1.16}$	$3.7^{+2.3}_{-1.4}$(McConnachie & Venn, 2020)	$0.055^{+0.02}_{-0.02}$(Battaglia et al., 2022)	$4.92^{+1.93}_{-1.39}$(Muñoz et al., 2018)	$-2.28^{+0.15}_{-0.16}$(Battaglia et al., 2022)
And X	$0.10^{+0.01}_{-0.01}$	$0.36^{+0.05}_{-0.04}$	$6.18^{+2.47}_{-2.87}$	$3.9^{+1.2}_{-1.2}$(McGaugh & Milgrom, 2013a)	$0.21^{+0.04}_{-0.07}$(Martin et al., 2016)	$79.43^{+20.57}_{-16.}$(Martin et al., 2016)	$-2.27^{+0.03}_{-0.03}$(Collins et al., 2013)
And XI	$0.059^{+0.03}_{-0.02}$	$0.21^{+0.13}_{-0.08}$	$2.67^{+1.43}_{-1.44}$	≤ 4.6(Putman et al., 2021)	$0.12^{+0.05}_{-0.04}$(Martin et al., 2016)	$25.12^{+14.69}_{-9.28}$(Martin et al., 2016)	$-2.0^{+0.20}_{-0.20}$(Collins et al., 2013)
And XII	$0.10^{+0.05}_{-0.02}$	$0.34^{+0.17}_{-0.07}$	$2.62^{+1.37}_{-1.33}$	$2.6^{+5.1}_{-2.6}$(McGaugh & Milgrom, 2013a)	$0.32^{+0.06}_{-0.07}$(Collins et al., 2013)	$50.12^{+29.31}_{-18.50}$(Martin et al., 2016)	$-2.0^{+0.2}_{-0.2}$(Collins et al., 2013)
And XIII	$0.045^{+0.03}_{-0.01}$	$0.13^{+0.09}_{-0.03}$	$2.96^{+1.21}_{-1.28}$	$5.8^{+2.0}_{-2.0}$(McGaugh & Milgrom, 2013a)	$0.13^{+0.08}_{-0.06}$(Martin et al., 2016)	$31.62^{+18.50}_{-15.77}$(Martin et al., 2016)	$-2.0^{+0.16}_{-0.13}$(Collins et al., 2013)
And XVI	$0.12^{+0.01}_{-0.01}$	$0.50^{+0.05}_{-0.04}$	$2.84^{+1.34}_{-1.57}$	$3.8^{+2.9}_{-2.9}$(McGaugh & Milgrom, 2013a)	$0.13^{+0.03}_{-0.02}$(Martin et al., 2016)	$63.09^{+16.34}_{-12.97}$(Martin et al., 2016)	$-2.0^{+0.5}_{-0.5}$(Collins et al., 2013)
And XVII	$0.15^{+0.02}_{-0.02}$	$0.57^{+0.12}_{-0.11}$	$1.84^{+1.54}_{-1.25}$	$2.9^{+2.2}_{-1.9}$(McGaugh & Milgrom, 2013b)	$0.29^{+0.06}_{-0.05}$(Martin et al., 2016)	$100.00^{+25.89}_{-20.57}$(Martin et al., 2016)	~ -2.0(Collins et al., 2013)
And XX	$0.042^{+0.01}_{-0.007}$	$0.16^{+0.06}_{-0.03}$	$2.64^{+1.48}_{-1.27}$	$7.1^{+3.9}_{-2.5}$(McGaugh & Milgrom, 2013b)	$0.09^{+0.04}_{-0.02}$(Martin et al., 2016)	$25.12^{+14.69}_{-9.27}$(Martin et al., 2016)	$-2.3^{+0.5}_{-0.5}$(Collins et al., 2013)
And XXII	$0.078^{+0.01}_{-0.006}$	$0.20^{+0.03}_{-0.02}$	$4.57^{+0.31}_{-0.47}$	$2.8^{+2.9}_{-1.4}$(McGaugh & Milgrom, 2013b)	$0.23^{+0.08}_{-0.08}$(Martin et al., 2016)	$39.81^{+23.29}_{-19.86}$(Martin et al., 2016)	$-1.85^{+0.10}_{-0.10}$(Collins et al., 2013)
And XXVI	$0.021^{+0.005}_{-0.004}$	$0.07^{+0.02}_{-0.02}$	$3.65^{+0.86}_{-1.19}$	$8.6^{+2.8}_{-2.2}$(McGaugh & Milgrom, 2013b)	$0.15^{+0.14}_{-0.08}$(Martin et al., 2016)	$15.85^{+24.00}_{-9.57}$(Martin et al., 2016)	$-1.9^{+0.20}_{-0.20}$(Collins et al., 2013)

Table 4.8: Observations and ψDM profile fits to ultra faint dwarf galaxies. Column 1: UFD name, Column 2: Core radius r_c, Column 3: Transition point r_t, Column 4: Stellar scale radius r_{s*}, Column 5: Observable projected velocity dispersion $\sigma_{los,obs}$, Column 6: Observable half-light radius $r_{half,obs}$, Column 7: Observable luminosity L_{obs}, Column 8: Observable age, Column 9: Observable metallicity. Note: Leo V has recently been suggested not to be a galaxy.

In this point we analyse separately the Milky Way's and Andromeda's satellites independently to see whether there is any difference in core-halo structure (visible in figures 4.39 and 4.43) or in the density vs. core radius trend (visible in figures 4.40 and 4.44).

4.4.3 Milky Way

Milky way's galaxies alone.

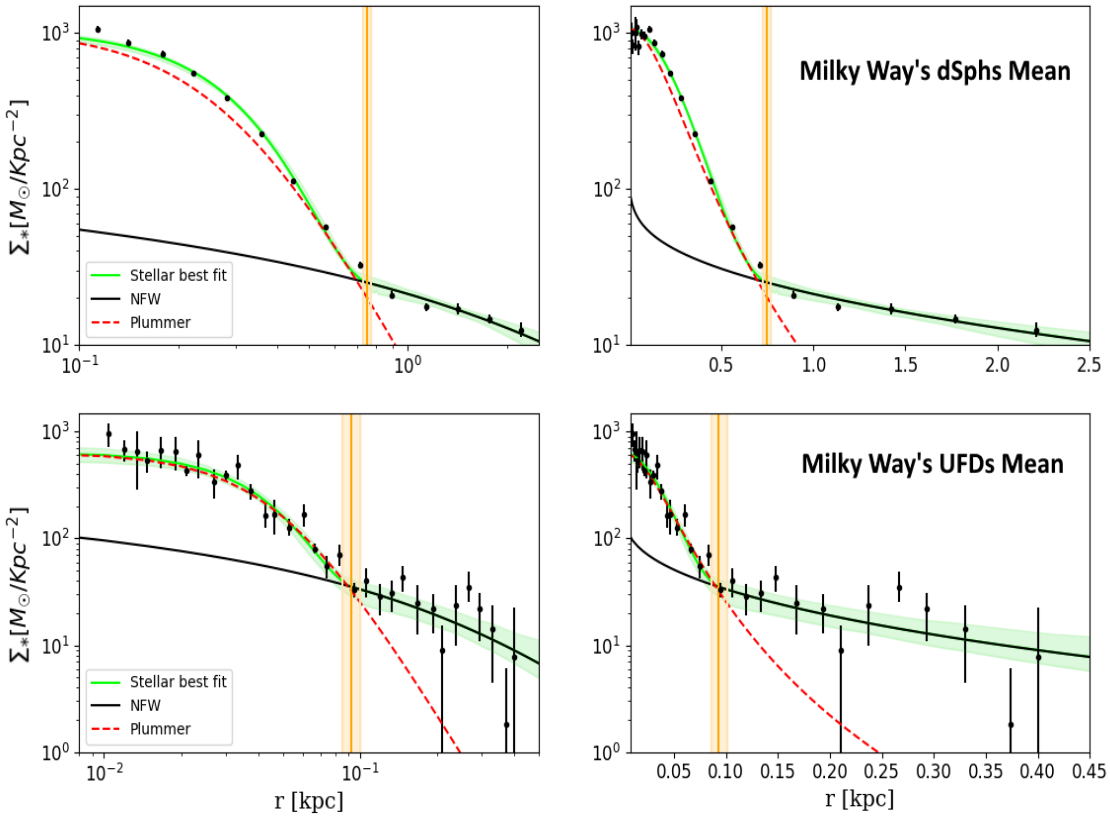

Figure 4.39: Like Figure 4.19 but just for Milky Way's satellites.

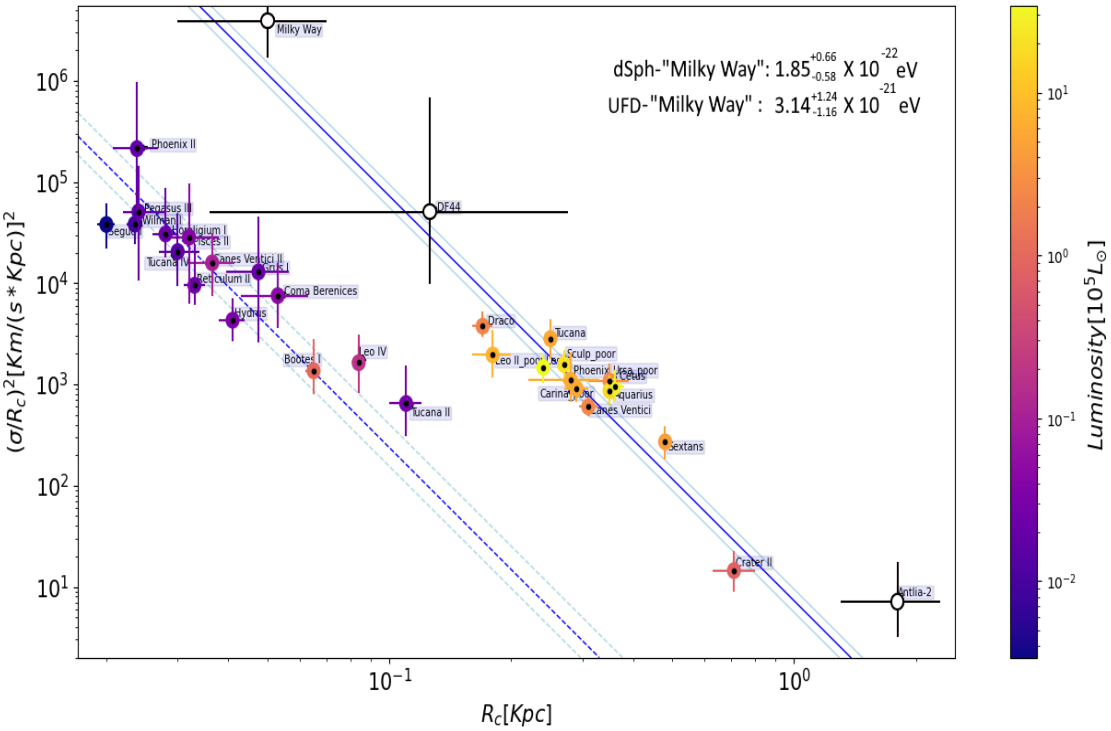

Figure 4.40: **DM density Vs Core radius**. Like Figure 4.17_{right} just for Milky Way's satellites.

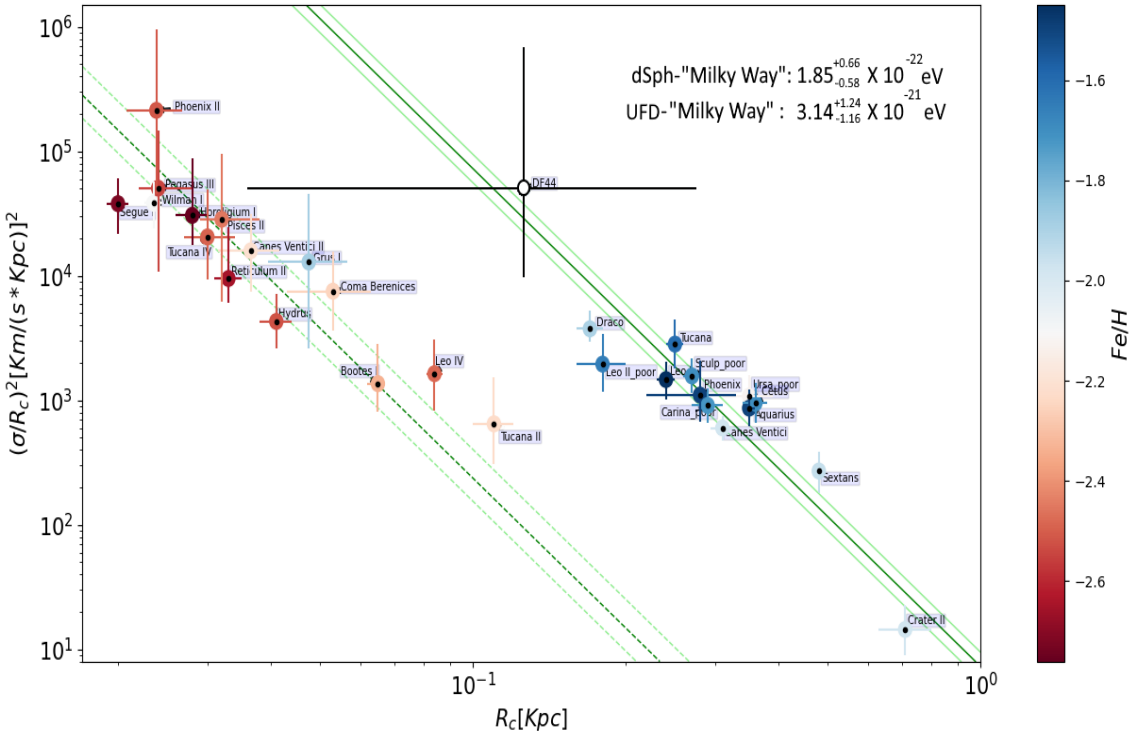

Figure 4.41: DM density Vs Core radius. Like Figure 4.20 but just for Milky Way's satellites.

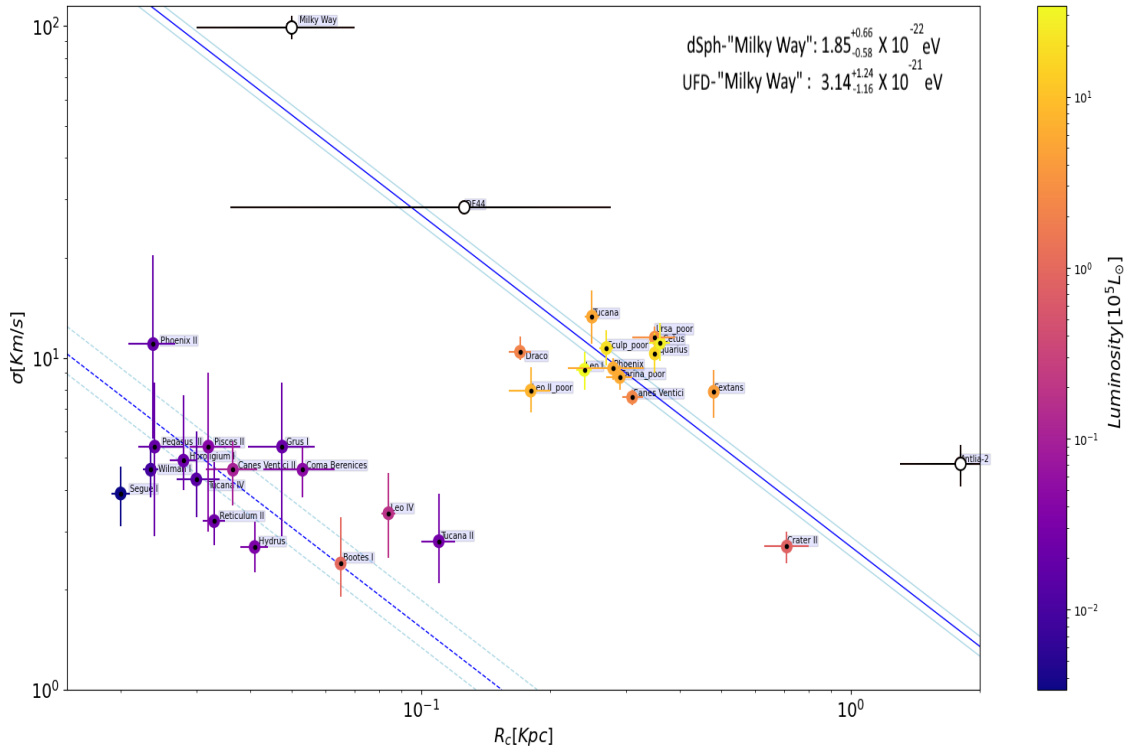

Figure 4.42: Velocity dispersion Vs Core radius. Like Figure 4.18 but just for Milky Way's satellites.

4.4.4 Andromeda

Andromeda's galaxies alone.

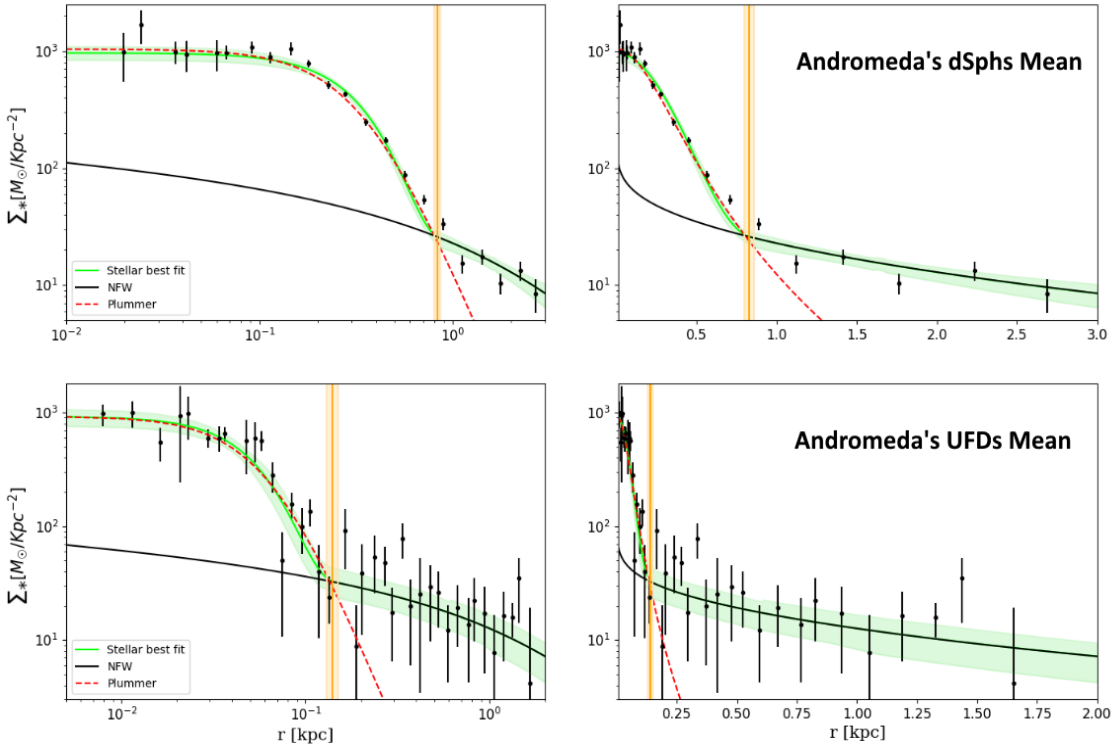

Figure 4.43: Like Figure 4.19 but just for Andromeda's satellites.

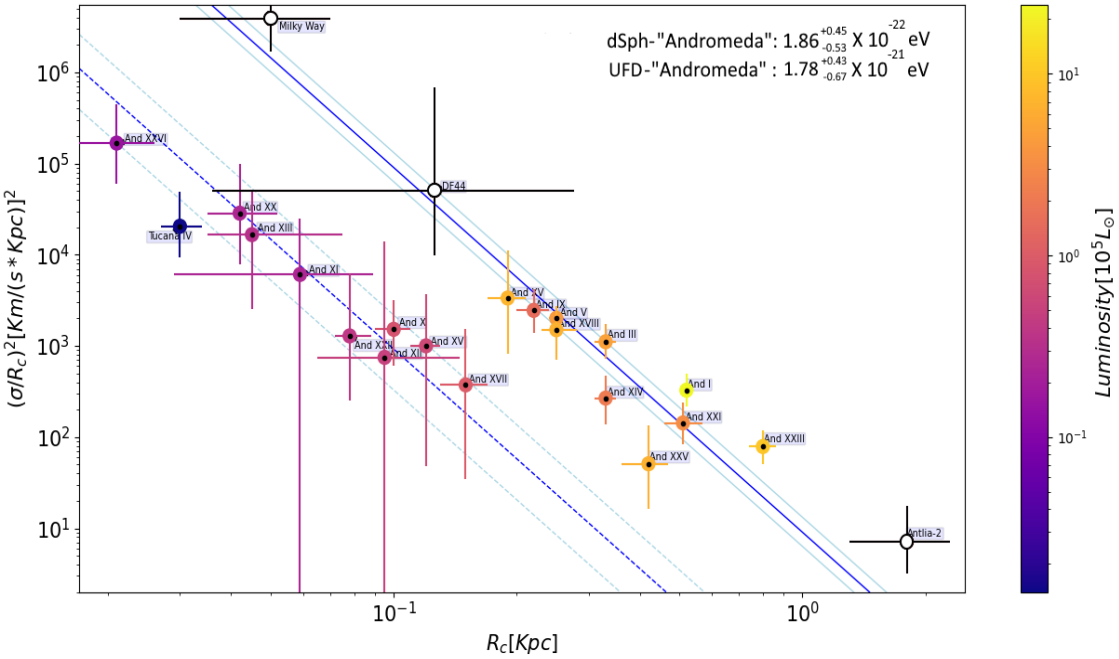

Figure 4.44: **DM density Vs Core radius**. Like Figure 4.17_{right} but just for Andromeda's satellites.

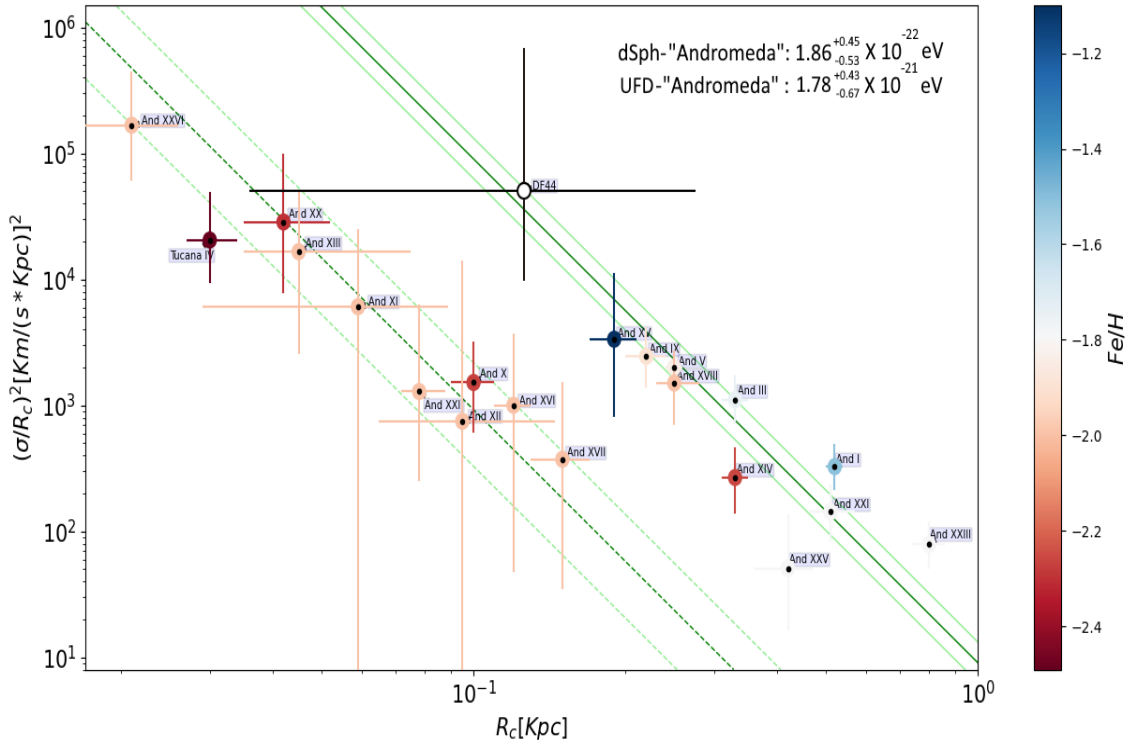

Figure 4.45: DM density Vs Core radius. Like Figure 4.44 but with the metallicities.

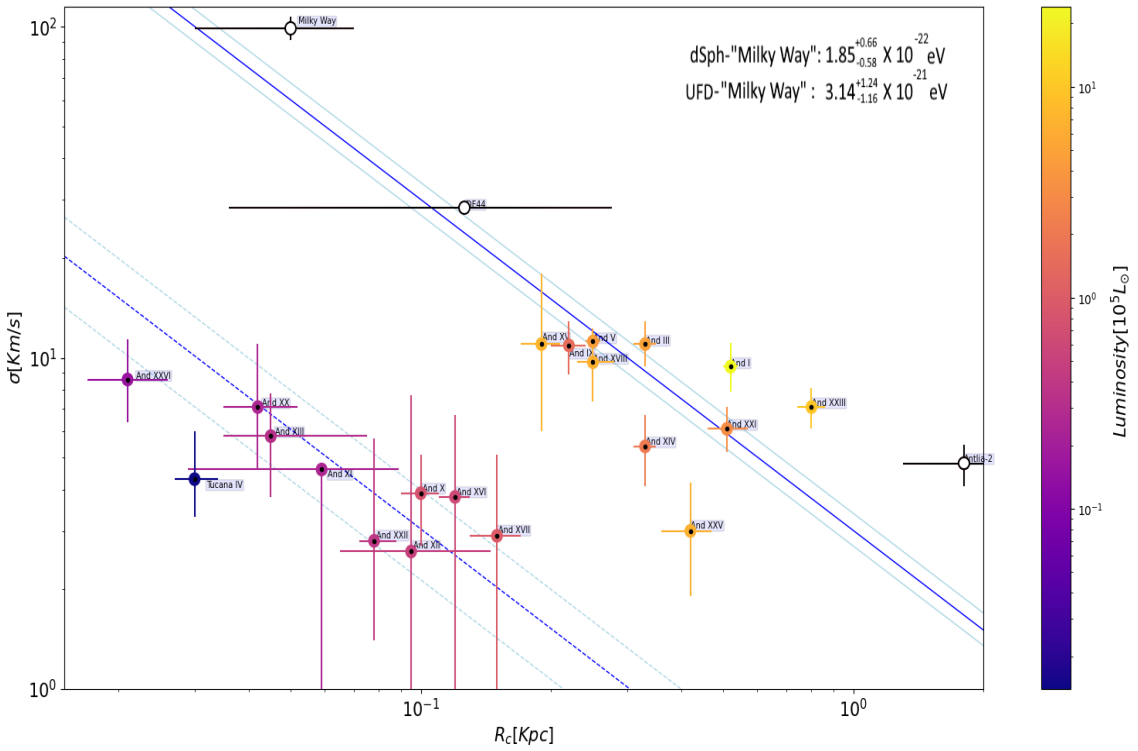

Figure 4.46: Velocity dispersion Vs Core radius. Like Figure 4.18 but just for Andromeda's satellites.

Summary & Conclusions

1. **Motivation**:

   Motivation 1: Expand the observed core-halo structures in section 4.2 to the rest of the Local Group dwarfs, including the UFDs. With the objective of demonstrating its universality among all dwarfs(only dwarfs cause are the most dominated DM systems) independently to their host/location or size/class.

   Motivation 2: Contrasts with the scale free continuity expected for galaxies formed under gravity, as in the standard Cold Dark Matter (CDM) model of collisionless particles. Confirm that the dSph and UFD dwarfs follow inverse relations between their core sizes, r_c and stellar velocity dispersions, σ, such that the cores are larger for dwarfs of lower velocity dispersion within each class, quite the opposite of standard expectations where larger galaxies should be more massive. Furthermore, confirm the uncovered scaling relation between the mass of the soliton and its host virial mass by the ψDM simulations, $m_{soliton} \simeq m_{halo}^{1/3}$, such that a more compact dense soliton should be found in more massive galaxies (Schive et al., 2014b), following from the virial relation (Veltmaat et al., 2018).

   Motivation 3: Test this inverse soliton density-radius relation for the first time, which should follow the predicted steep relation $\rho_c \propto r_c^{-4}$, for both the dSph and UFD dwarfs, required by the Uncertainty Principle.

   Motivation 4: Examine for the first time the Uncertainty Principle in this context, examining the velocity dispersion of stars within the soliton and the soliton radius which must be inversely related, $m_{sol} \propto 1/r_c$, where the boson mass can be derived directly as the constant.

2. **Methodology**:

   In order to fit galaxies stellar profiles with the ψDM model:

   Step 1: Examine the stellar profiles of all local group dwarfs (well studied by independent teams), fitting our best ψDM stellar profile (section 3.3) to the observed stellar profile of the galaxy in order to quantify the core radius size (r_c) and the transition point (r_t) between the soliton and the NFW-like halo (as in section 4.2). These are about evenly divided into dSph and UFDs.

   In order to contrast with the scale free continuity expected for CDM galaxies and the inverse soliton density-radius expected for ψDM:

   Step 1: Extract the resulting core radius values of all the galaxies from the previous step's best fits. Listed in Tables 4.7 and 4.8.

   Step 2: Get the observable r_{half} and σ values form the bibliography to plot the next relations: Density vs. half light radius ($(\sigma/r_h)^2$), Density vs. core radius ($(\sigma/r_c)^2$) and Velocity dispersion vs. core radius (σ/r_c).

   Step 3: Calculate the medians of ($(\sigma/r_h)^2$) and ($(\sigma/r_c)^2$) relations in order to confirm the expected $\rho_c \propto r_c^{-4}$ trend.

Step 4: Compute the median of (σ/r_c) to compare it with the inverse relation required by the Uncertainty Principle.

In order to extract the boson masses:

Step 1: Extract the boson mass formula(Eq. 3.25), as explained in section 3.5.

Step 2: Compute the boson mass for each individual galaxy and calculate the median of all them at the end.

3. **Results**:

   Result 1: We show the capability of the ψDM stellar model (Eq. 3.16) to fit the stellar profiles for all these dwarfs independently to their host (Milky way or Andromeda) and to their class (UFD or classical). In good agreement with the possible solitonic cores and extended halos in the profiles of these dwarfs, as predicted in this context by our simulations of Wave Dark Matter. Figures 4.23 to 4.38.

   Result 2: Within each dwarf class we find the core radius R_c is inversely related to velocity dispersion σ, quite the opposite of standard expectations, but indicative of dark matter in a Bose-Einstein state, where the Uncertainty Principle requires $R_c \times \sigma$ is fixed by Planks constant, h. Figure 4.18.

   Result 3: We use the observed core radius derived above for each dwarf. Figure 4.17 shows this density looted against radius, revealing two parallel tracks defined by the dSph and UFDs respectively with a clear separation. It is interesting that these tracks form a steep relation that fits accurately the $\rho_c \propto r_c^{-4}$ (good fit to the slope, $d\log\rho_c/d\log R_c = -4$, for the time independent soliton solution of the Schrodinger-Poisson relation) relation predicated for ψDM which is a steep relation that follows from the inverse soliton core mass vs radio relation required by the Uncertainty Principle.

   Result 4: Finding that ultra-faint and dSph dwarfs lie on two parallel tracks of increasing radius with decreasing velocity dispersion, corresponding to two species of dark bosons separated by one order of magnitude gave us the possibility to estimate the boson masses for both the UFD and dSPh classes from the normalization between the core momentum $m_b\sigma_c$ and the width of the soliton standing wave so, $m_b = \hbar/2R_c\sigma_c$, fitted in Figure (4.17), obtaining $m_b = 2.27^{+1.79}_{-0.65} \times 10^{-21}$eV for the UFD's and $m_b = 1.85^{+0.66}_{-0.58} \times 10^{-22}$eV. This light boson solution for both the dSph and UFD dwarfs supports the generic "Axiverse" prediction of String Theory, where a discrete mass spectrum of light axions is predicted to span decades in mass, providing a unifying interpretation for the puzzling physical "diversity" of dark matter dominated dwarf galaxies.

4. **Conclusions**:

   Conclusion 1: Low mass galaxies in the Local Group are dominated by dark matter and comprise the well studied “dwarf Spheroidal" (dSph) class, with typical masses of $10^{9-10}M_\odot$ and also the equally numerous “ultra faint dwarfs" (UFD), discovered recently, that are distinctly smaller and denser with masses

of only $10^{7-8} M_{\odot}$. This bimodality amongst low mass galaxies contrasts with the scale free continuity expected for galaxies formed under gravity, as in the standard Cold Dark Matter (CDM) model for heavy particles. Within each dwarf class we find the core radius R_c is inversely related to velocity dispersion σ, quite the opposite of standard expectations, but indicative of dark matter in a Bose-Einstein state, where the Uncertainty Principle requires $R_c \times \sigma$ is fixed by Planks constant, h.

Conclusion 2: The most significant achievement of this work is the apparent need for two axion species following the ψDM relation set by the Uncertainty Principle. The "-4 slope" relation for the density-core of solitons and the "-1 slope" relation between σ_{los} and r_c for the solitons. Moreover, the observed results of these two relations are the opposite of what is expected for the CDM scenario where the opposite behavior is expected, where sizes should increase with increasing velocity dispersion generically.

Conclusion 3: The resulting boson masses, $m_b = h/R_c\sigma$, differ by one order of magnitude between the UDF and dSph classes, with $10^{-21.4}$eV and $10^{-20.3}$eV respectively. Two boson species is reinforced by parallel relations seen between the central density and radius of UDF and dSph dwarfs respectively, which both match the steep prediction, $\rho_c \propto R_c^{-4}$, for soliton cores in the ground state.

Conclusion 4: Multiple bosons may point to a String Theory interpretation for dark matter, where a discrete mass spectrum of axions is generically predicted to span many decades in mass, offering a unifying "Axiverse" interpretation for the physical "diversity" of dark matter dominated dwarf galaxies.

Conclusion 5: The detection of the core halo structure (first shown in subsection 4.2) in the stellar density profiles of almost all the galaxies of the Local Group, including the dwarfs from Andromeda, suggests the universality of this profile. A profile in which its well-established core and extended halo after a marked change of regime is a defining prediction of ψDM.

4.5 Galaxy formation with ψDM. The Core-halo structure. (Paper 5 to be submitted)

Here we present the preliminary results in collaboration with the CFA (Center for Astrophysics | Harvard & Smithsonian) with the objective of testing with new simulations the results of the star profile fitting presented in the thesis of section 3.3. As the presented data in this point is still not part of a formal paper and due to its methodology highly differing from the semi-analytical models explained in the rest of the Ph.D., we will present the full structure of the work with individual internal sections. All the next results have been possible using the CFA simulations data related to galaxy evolution for ψDM, WDM and CDM Mocz et al. (2019, 2020).

4.5.1 CFA simulations data

This hydrodynamical simulation describes the evolution of small, high resolution cosmological simulation volumes leading to predict the formation and evolution of galaxies, in terms of gas, stars and dark matter particles along different redshifts in the previously mentioned three DM scenarios, ψDM, WDM and CDM. We aim to test the empirical findings we have uncovered in section 3.3, as shown in figure 3.10. With that intention, we analyzed their data looking for the core-halo structure in the different DM cosmological evolution scenarios. We will start this section by describing the structure of the analyzed files:

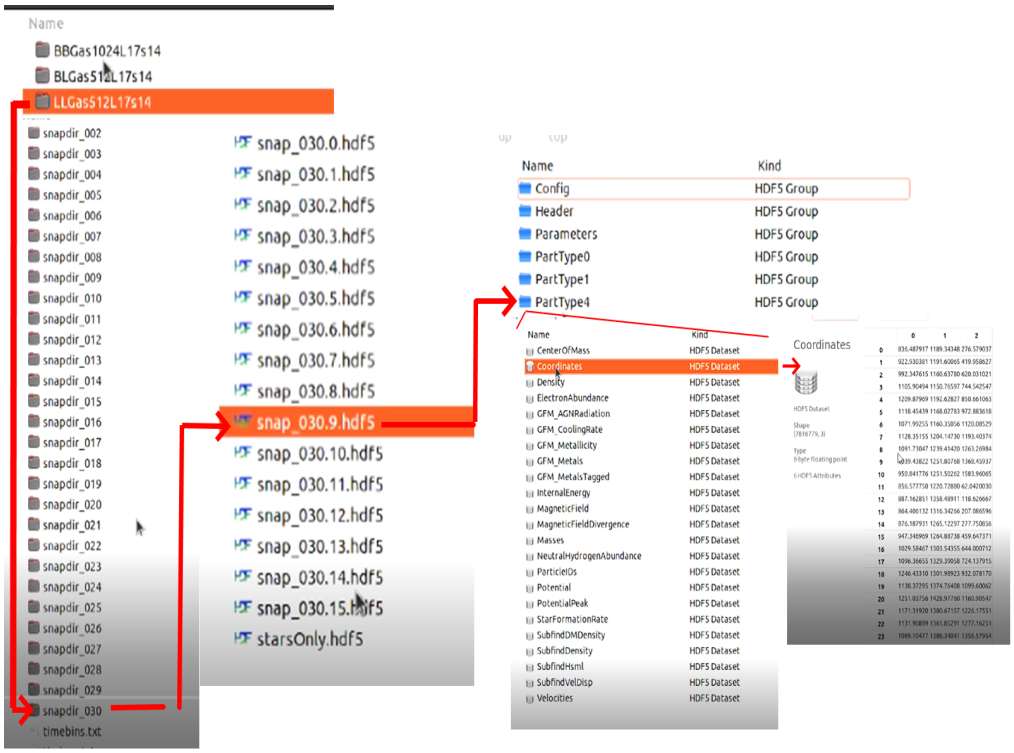

Figure 4.47: CFA simulations data. Structure of the analyzed files.

The simulation output files are in hdf5 format. The files are divided into different snapshots, where each snapshot represents the simulation data for each computed redshift. Every snapshot is divided into 16 files due to the practical limitations of saving all the information in one single file. These 16 files will have all the available data of gas (particle type 0), stars (particle type 4) and DM (particle type 1) particles computed in the simulations; velocities, 3D coordinates, gravitational potential, mass, ID, stellar birth rate...

4.5.2 Methodology

In order to confirm or discard the thesis of section 3.3, we needed to analyze/subtract the stellar profiles of the resulting dwarfs of the data. Here we will explain how we did it. The first thing to do to start with the stellar membership, was to localize and identify the three centers of the three galaxies. Two simple methods can be used for this; Detect the three smaller potential points or the three densest points, we selected the second method due to the lack of info about the gravitational potential for the ψDM simulation data. Is important to remark that due to the limit size of the simulations box (1700 kpc), in some snapshots, the particles were re-localized in incorrect coordinates (due to being calculated in coordinates out of the box), forcing us to rotate them (see figure 4.50). After localizing the three centers, we computed the stellar membership for each one in a simple way, just calculating the virial radius and considering all stars between each center and each individual radius part of the galaxy. To calculate the virial mass (M_{200}) and the virial radius (R_{200}), we just needed to know the center location of the halo, and find the radius R_{200} such that the enclosed mass (M_{200}) in the sphere of radius R_{200} was 200 $\times$ ρ_{crit} (where ρ_{crit} is the critical density of the universe). With the stellar membership done, we subtracted the stellar density profiles for each galaxy, calculating the density of stars (number of stars/ sphere volume) in bins of 0.01 kpc from the center to the virial radius. This process was repeated in all the snapshots susceptible of being interesting for the detection of the core-halo structure; The snapshots representing the data closer to redshift 0, 5.56 for ψDM and 2.3 for CDM and WDM.

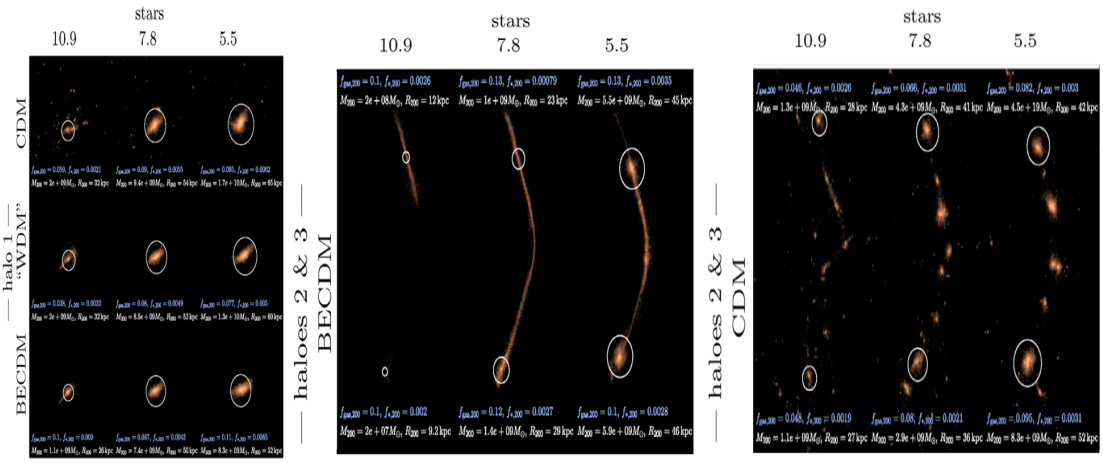

Figure 4.48: Mocz (2019) Mocz et al. (2019) simulation data. Evolution of the stellar structure of the three galaxies in ψDM and CDM scenarios from redshifts 10.9 to 5.56.

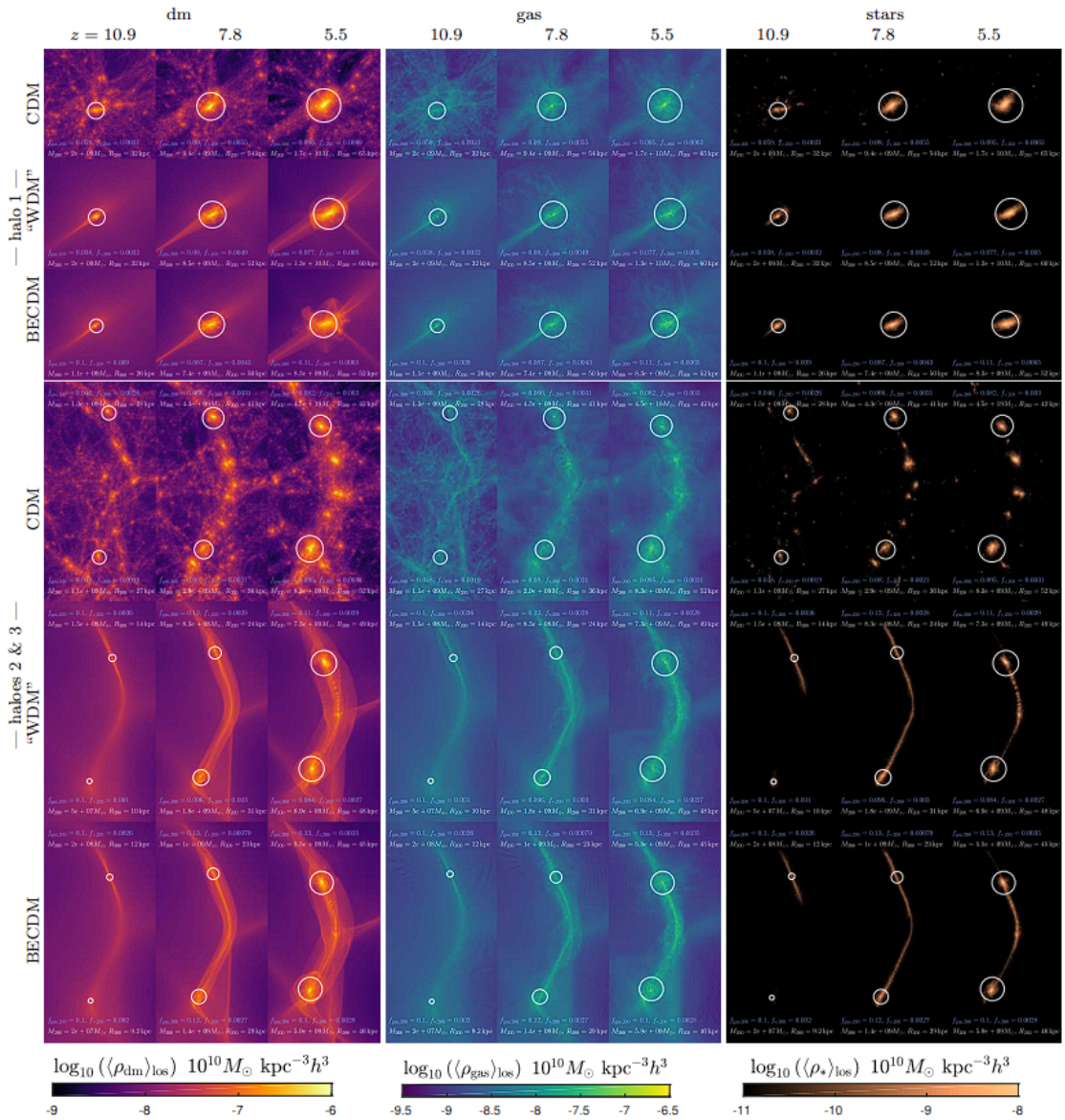

Figure 4.49: Mocz (2019) Mocz et al. (2019) simulation data. Diversity of structures in dark matter (orange/purple), gas (green/blue), and stars (black/yellow). Projected densities of the selected haloes simulated under the three different cosmologies (Mocz et al., 2020). Notice how WDM and ψDM evolve almost identically along all the different redshifts, indicating their big similarity in large-scale structures evolution, in contraposition to CDM.

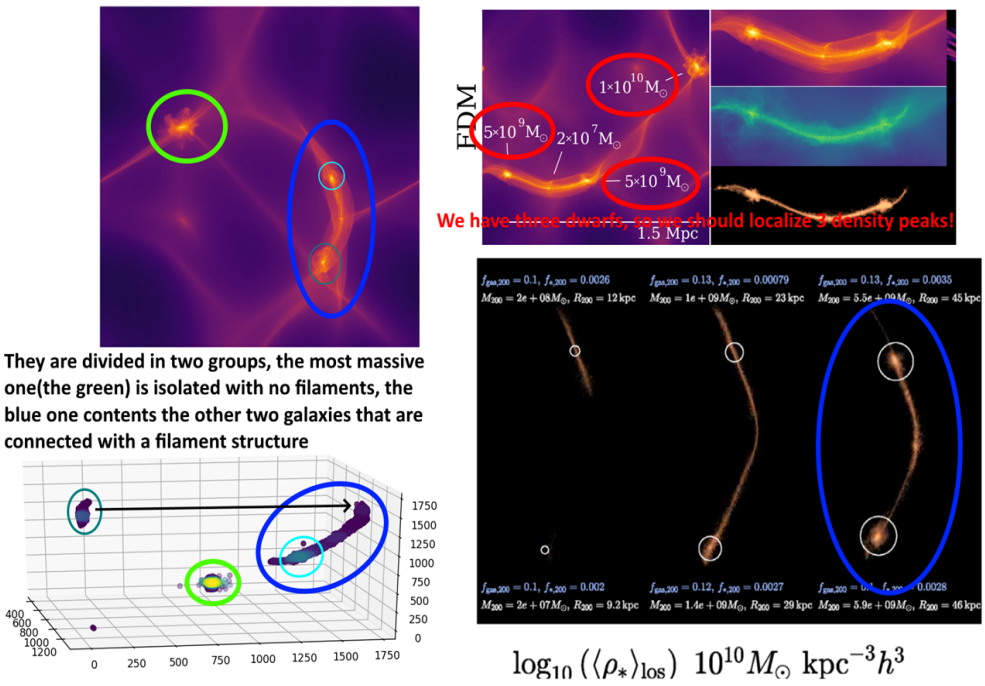

Figure 4.50: Mocz (2019) Mocz et al. (2019) simulation data. Visualization of the large-scale structure of the analyzed data in ψDM context.

4.5.3 Results

Results from the subtracted data at $z \simeq 5.56$

Due to limitations in resolving the smallest physical distance in ψDM in a fixed co-moving volume 1024^3 resolution-element simulation, the ψDM simulation stops at $z = 5.56$. We can clearly observe that CDM and ψDM have significant differences in large scales, with plenty of subhalos environment for CDM and filamentary structure for ψDM and WDM. Moreover, even if both have similar amounts of stars, in the ψDM context, the stars seem to be less concentrated, something that makes sense with the observed extended stellar halos (see figure 4.51). When we start zooming into the individual stellar profiles of the galaxies in the different DM scenarios, we can appreciate how in the case of ψDM, the profiles seem to be flatter in the inner parts, as expected for stars tracing the presence of the soliton in the core, while for WDM and CDM the lack of such soliton makes them have a cuspy inner profile. Nevertheless, the most important difference seems to arise in the isolated galaxy, where a primordial core-halo structure seems to appear for ψDM (figure 4.54). This core-halo structure was also observed even more clearly for WDM in the data referring to $z = 2.3$ for one of the filamentary galaxies. Such difference also seems to be lightly detected in the other two, but not clearly enough to identify it as a core-halo structure.

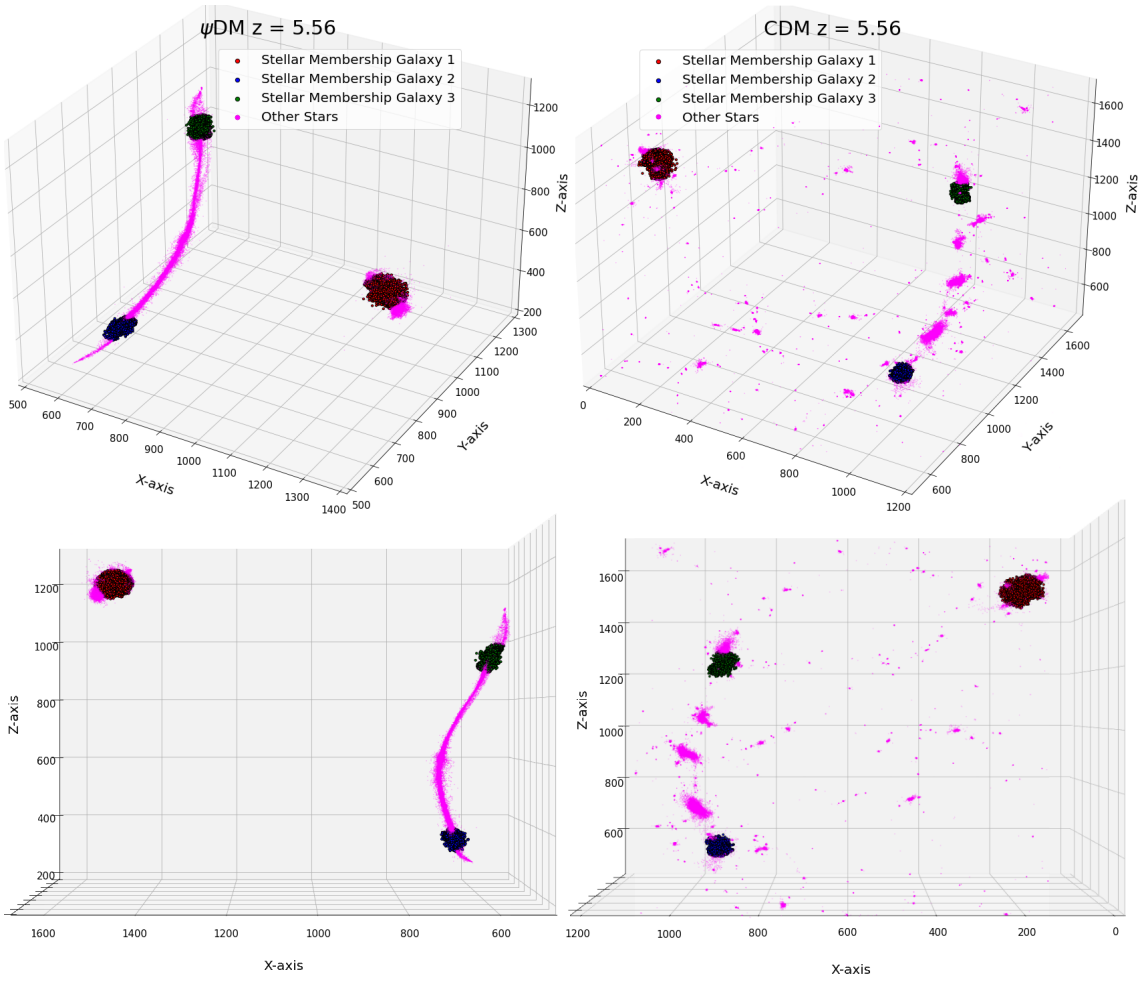

Figure 4.51: Mocz (2019) Mocz et al. (2019) simulation data. Stellar membership for ψDM and CDM in $z = 5.56$. The stars that belong to each galaxy have been painted with different colors; red for the isolated one and blue and green for the ones in the filamentary/subhalos structure. The figure shows the data in two different perspectives; 3D in the up row and 2D in the low one.

We can now readily appreciate in the small panels of figures 4.52 and 4.53, the main differences between these three galaxies in the two different DM scenarios are that the stars seem to be more concentrated for CDM with irregular structures. In contrast, for ψDM, a more elliptical shape can be appreciated, where the galaxies seem to have more extended stellar halos, making them see their stars farther from the center. It is curious to see how the stellar profiles are more extended for ψDM, even if the virial radius of these galaxies is smaller in this scenario. Nevertheless, these extended stellar profiles agree well with the softer DM profiles predicted for ψDM. On the other hand, we directly compare these three profiles for CDM and ψDM in figures 4.54 and 4.56, with a remarkable difference in the inner profile for galaxies two and three, in good agreement with the presence/lack of a soliton and the resulting core-cuspy disagreement. The main observed result is the presence of a possible primordial core-halo stellar structure in figure 4.54 (Zoom in fig. 4.55). The vertical line represents the comoving resolution, 0.19 kpc in this case. This value represents the limit where the subtracted data becomes unreliable beyond this

radius.

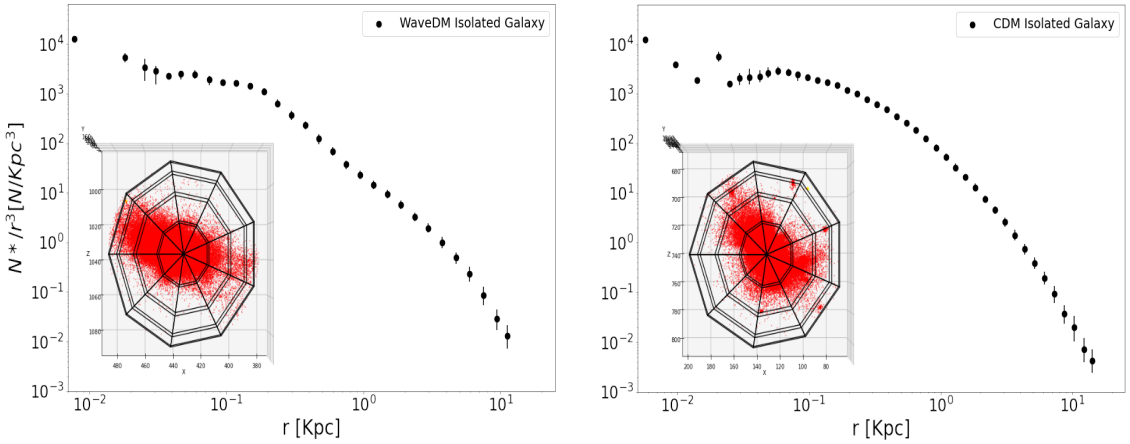

Figure 4.52: Mocz (2019) Mocz et al. (2019) simulation data. subtracted stellar profiles of the isolated galaxy in ψDM and CDM at $z = 5.56$. The small panels represent the morphology and distribution of the stars in the galaxy.

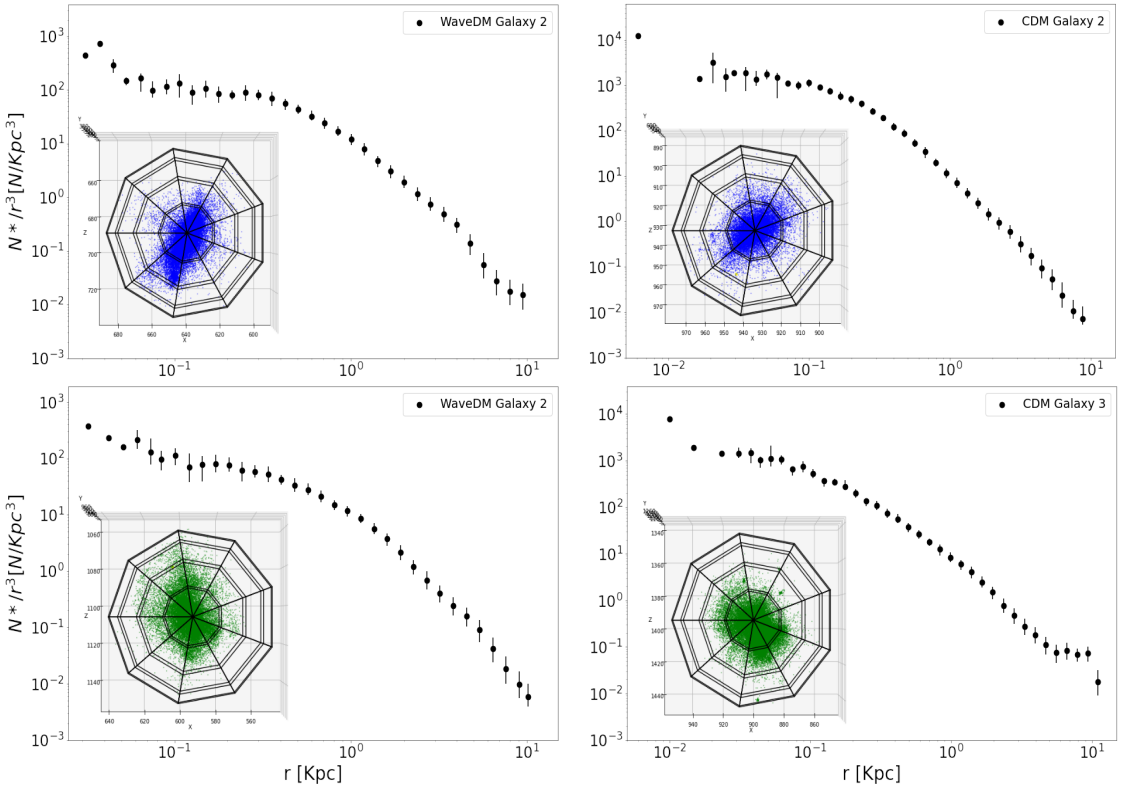

Figure 4.53: Mocz (2019) Mocz et al. (2019) simulation data. subtracted stellar profiles of the filamentary/subhalos galaxies in ψDM and CDM at z=5.56. The small panels represent the morphology and distribution of the stars in the galaxy.

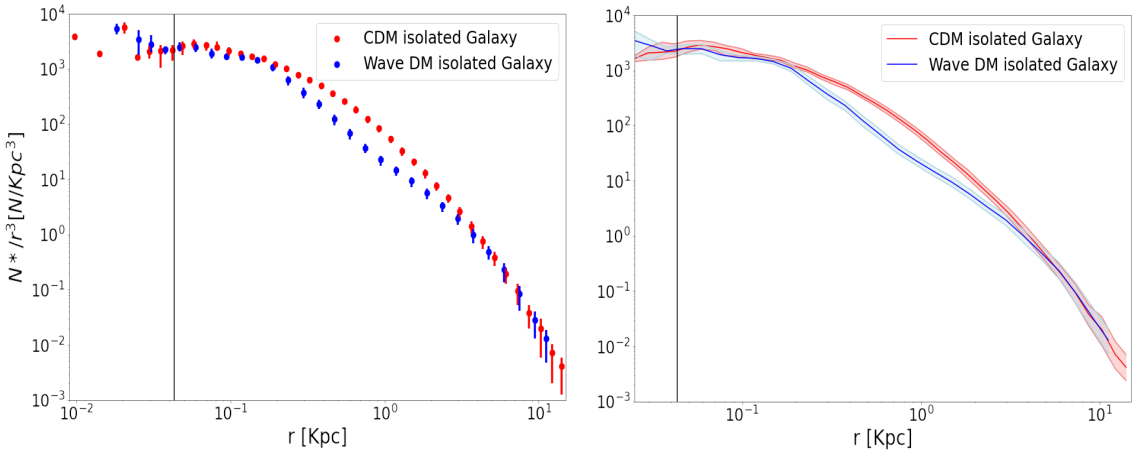

Figure 4.54: Mocz (2019) Mocz et al. (2019) simulation data. subtracted ψDM Vs CDM stellar profiles of the isolated galaxy. The left panel shows the subtracted stellar profile in 0.01 kpc bins style, while the right one shows exactly the same with continuous lines. Notice how there is a high discrepancy within the two models from 0.5 kpc to 5 kpc, suggesting a structure similar to the core-halo for the wave profile. The vertical black line represents the comoving resolution limit of the data, indicating that the data for values smaller than that limit are not reliable.

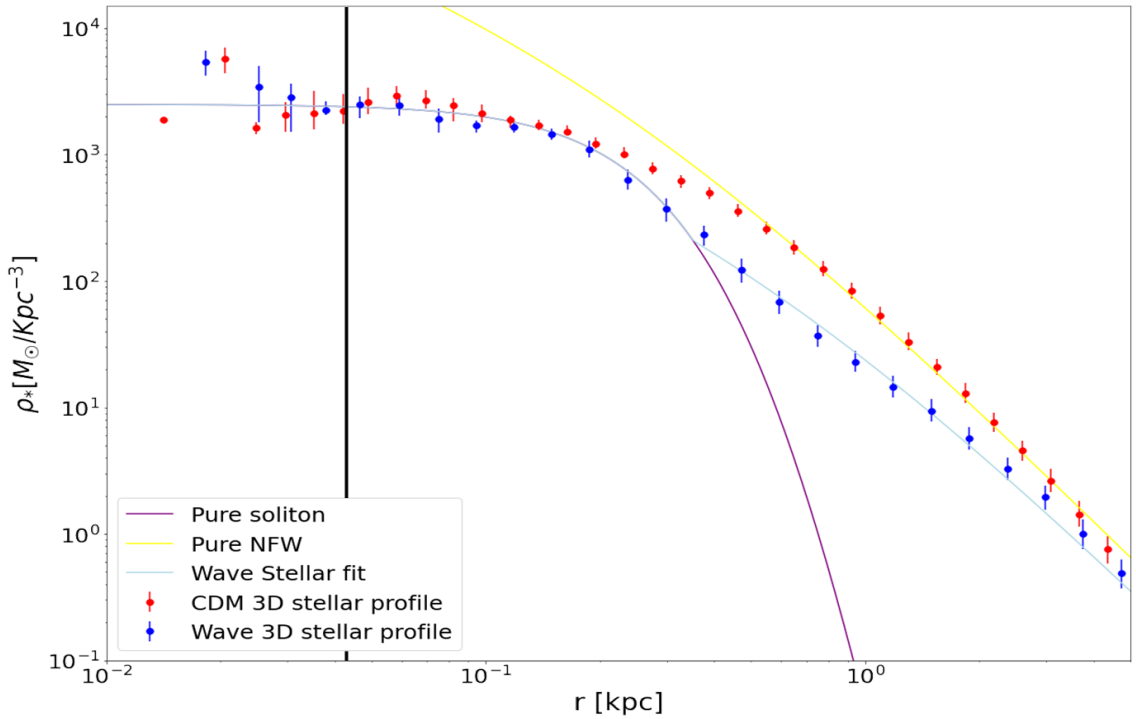

Figure 4.55: Mocz (2019) Mocz et al. (2019) simulation data. Zoom of the left panel of figure 4.54. Notice how the stellar wave profile is compatible with a core-halo structure (light blue fit). The transition point has been highlighted with the pure soliton profile, remarking the position where a change of regime is needed to continue explaining the observed stellar profile. The vertical black line represents the comoving resolution limit of the data, indicating that the data for values smaller than that limit are not reliable.

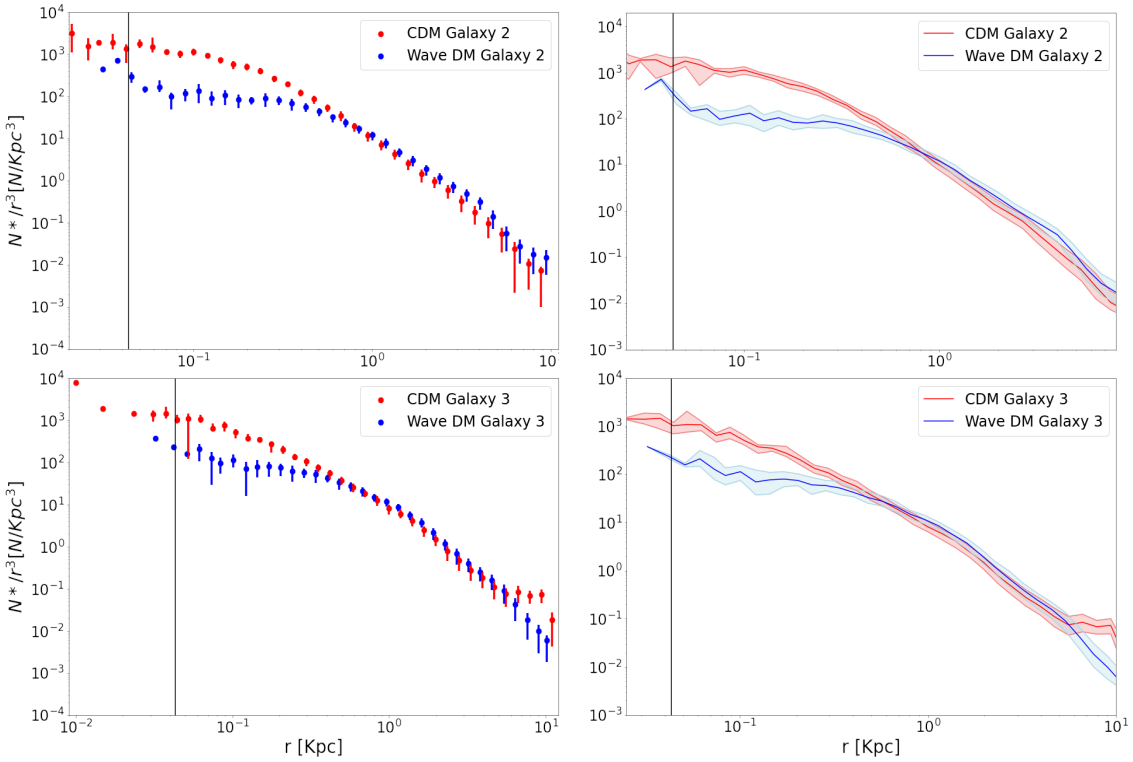

Figure 4.56: Mocz (2019) Mocz et al. (2019) simulation data. subtracted ψDM Vs CDM stellar profiles of the filamentary/subtracted galaxies. The left panel shows the subtracted stellar profile in 0.01 kpc bins style, while the right one shows exactly the same with continuous lines. Notice how there is a high discrepancy within the two models in the inner zone, suggesting a cored profile for wave galaxies and cuspy for CDM. The vertical black line represents the comoving resolution limit of the data, indicating that the data for values smaller than that limit are not reliable.

We now perform MCMC-based ψDM profile fits to the isolated dwarfs, shown in Figure 4.57. The core radius, r_c, fully characterizes the shape of the soliton core profile. For the halo, we fit an NFW profile with scale radius r_{s*} and normalization ρ_{0*}. The only other free parameter we require is the transition radius, r_t, defining the radius of the density transition between the soliton and NFW profile, which we vary within a prior range indicated by the ψDM simulations of 2–4 $\times r_c$. The only fixed parameter is the boson mass, with a value of 2.5×10^{-22}eV, which is precisely the same used for the simulations (Mocz et al., 2020). The best fit shows a resulting profile with a total mass of $5.8^{+0.24}_{-0.40} 10^9 M_\odot$, in good agreement with the computed one from Mocz et al. (2020) of $8.3 \times 10^9 M_\odot$ for this galaxy at this redshift. Moreover, the blue dashed profile shows the resulting profile where we repeat the analysis with the fixed total mass from Mocz et al. (2020) of $8.3 \times 10^9 M_\odot$. Notice how, if it is not as good as the free mass green profile, it is still in excellent agreement. Additionally, the resulting r_c and r_t ($0.15^{0.021}_{0.017}$ & $0.42^{0.063}_{0.055}$) are also inside the expected values for such kind of dwarf spheroidals (Pozo et al., 2020, 2023).

We continue comparing this profile with the two stellar profiles of the known dwarf galaxies orbiting the Milky Way and Andromeda with the most similar den-

sity gaps to it; Cetus and Andromeda XXI (Fig. 4.58). The left panel represents the profiles normalized in terms of stellar peak density, while the right panel is also normalized by their transition radii. The black profiles represent the mean stellar profile of all the Local Group dwarf spheroidal galaxies Pozo et al. (2023). The right panel is handy to see how the subtracted stellar profile (blue profile) is compatible with a real observed stellar profile, Andromeda XXI (red profile), indicating that this subtracted ψDM stellar profile is compatible with observable data, in contradiction to the CDM profiles. Moreover, this right panel makes more clear how the inner parts of the profiles are in good agreement, suggesting that all of them are consistent with a solitonic core.

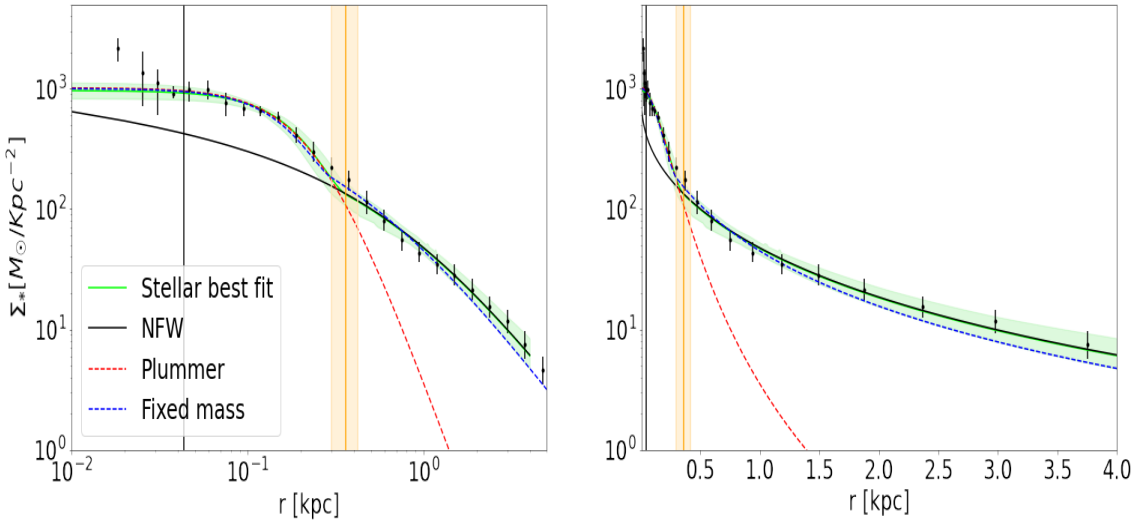

Figure 4.57: Mocz (2019) Mocz et al. (2019) simulation data. This figure shows the best fit of the projected star count profile of the ψDM isolated dwarf galaxy. An extended halo of stars is visible, stretching to $\simeq 4$ kpc and most evident on the linear scale of left-hand panel. A prominent core is also evident on a scale $<$ 0.5 kpc in each dwarf. These two characteristics seem to be in good agreement with the real dwarf spheroidals' stellar profiles observed in the Local Group Pozo et al. (2023). A standard Plummer profile (red dashed curve) is seen to fit approximately the core region but falls well short at large radius. Our predictions for the dSph class (2.5×10^{-22}eV) for ψDM are shown in green, where the distinctive soliton profile provides and excellent fit to the observed cores and the surrounding halo of excited states that average azimuthally to an approximately NFW-like profile beyond the soliton radius. The accuracy of the core fit to the soliton, is best seen on a log scale in the right panels, with linear scale of the left that shows the extent of the halo, including the characteristic density drop of about a factor of $\simeq 30$ in density, as predicted by ψDM between the prominent core and tenuous halo at a radius $\simeq 0.5$ kpc indicated by the vertical orange band. The blue dashed shows our prediction, but with a fixed mass of $8.3 \times 10^9 M_\odot$, exactly the expected one by Mocz et al. (2020) for this galaxy at this redshift.

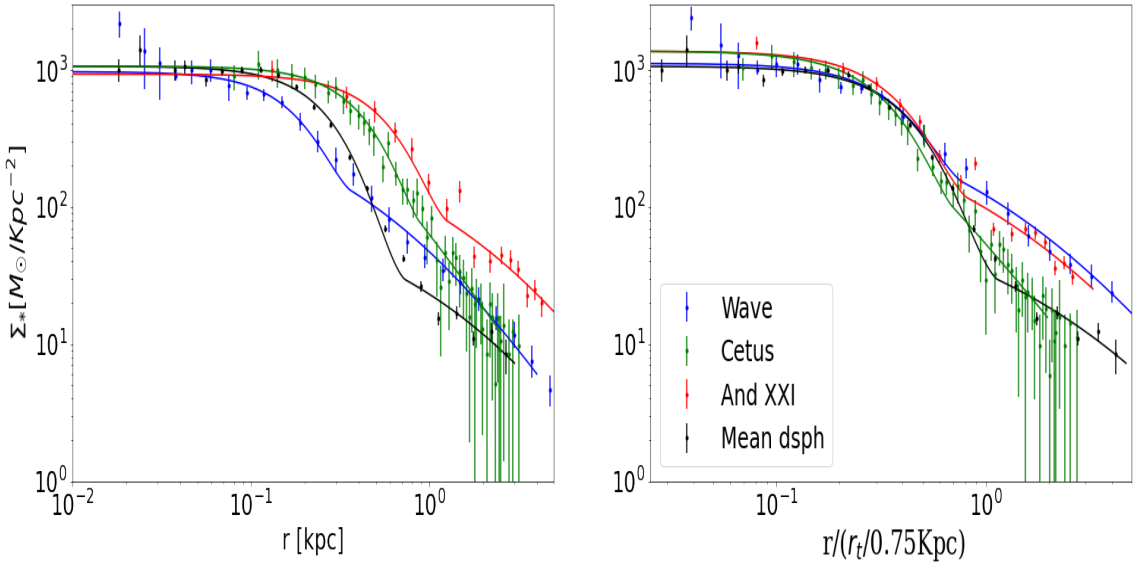

Figure 4.58: Mocz (2019) Mocz et al. (2019) simulation data. Comparison between the stellar profiles of the ψDM isolated galaxy, the mean profile of all the dwarf spheroidals of the Local Group (Pozo et al., 2023), and the two galaxies from Andromeda and the Milky Way with the most similar density gap between the core and the transition point. The left panel shows these four profiles normalized in their peak density value while in the right panel, they are also normalized in terms of the transition point. Notice how the subtracted profile from the data (blue line), is very similar in terms of shape to the subtracted profiles of the real observable galaxies. Moreover, this data's profile seems to coincide extremely well with Andromeda XXI's profile.

Results from the subtracted data at z $\simeq$ 2.23

Here now we repeat the analysis of the previous section but for the data at z $\simeq$2.23, for the simulations of WDM and CDM. Even though the main idea of the work is to compare ψDM evolved cosmological structures Vs CDM ones, the expected large-scale structures for WDM should be similar to ψDM. Notice in the central small panels of figure 4.60 how the resulting structures are almost identical for WDM and ψDM at z=5.56 (even in their internal halo structures differ in bigger proportion). This gives us the chance to use WDM data to make us an idea of how ψDM could look at this lower redshift. Moreover, analyzing CDM at this lower redshift compared to previous data will give us the opportunity to confirm if the non-detection of the core-halo structure at redshift 5.56 simply means that in CDM this structure seems to be formed later than in ψDM or not.

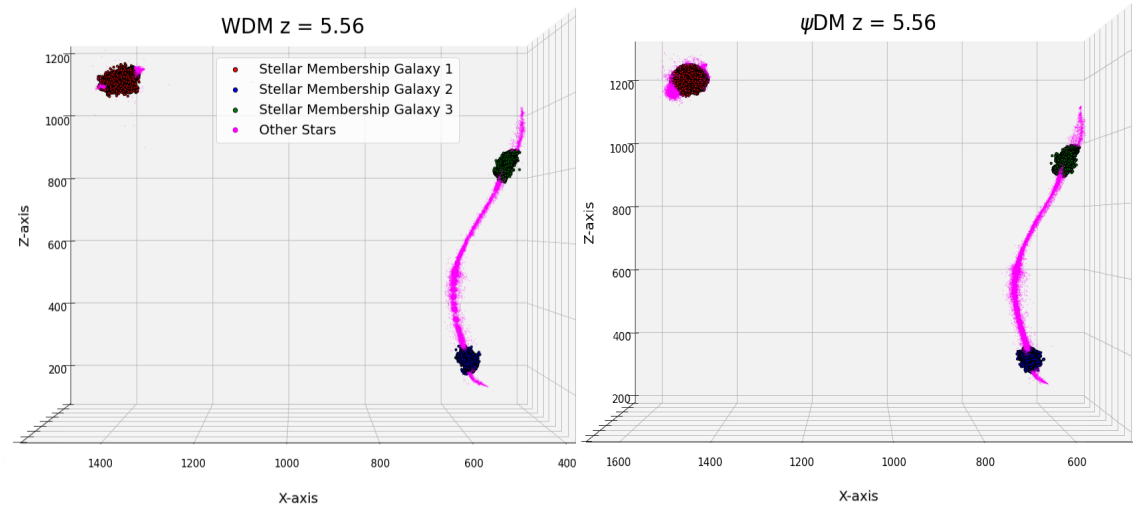

Figure 4.59: Mocz (2019) Mocz et al. (2019) simulation data. Stellar membership for WDM and ψDM in z=5.56. The main objective of this figure is to show how similar are WDM and ψDM structures at the last ψDM data redshift (z=5.56). This figure makes us conclude that the obtained results from WDM at z=2.23 are comparable to the ones that we would obtain at that redshift for a hypothetical ψDM data.

The resulting subtracted stellar profiles that can be seen in figure 4.61, seem to confirm the same results as in the previous redshift for CDM, where no presence or imprint of the core-halo structure has been founded in the halos of the three simulated galaxies. In contrast, the three WDM halos seem to have compatible core-halo stellar profiles, at least in a primordial way, still in construction for the isolated galaxy and galaxy number two. In addition, a well-defined core-halo structure is visible for the third, with a marked density drop from the core to the halo and the characteristic change of regime point (transition point, r_t), that marks the separation between the inner core and the outer halo (Low panels of figure 4.61).

We continue generating the previously presented stellar core-halo profile model for the WDM galaxy three (as we did for the ψDM isolated at z=5.56), where the core-halo shape is more visible. The resulting core radius (r_c) and transition point (r_t) values are listed along with the other variables in table 4.9. It is interesting how the resulting parameter values are inside of the expected ones compared to the extracted from the observed profiles of the observable Local Group dwarf classical spheroidals, even if the different redshift at which they were analyzed should make them differ a little bit, due to being still in construction the two ones analyzed in this paper. You can check the resulting parameter values of these two subtracted galaxies with the obtained values from the observable Local Groups dwarf spheroidals in table 4.9 (Pozo et al., 2023). Notice how the core values are in excellent agreement with the means obtained for such kinds of spheroidals in the Local Group. Moreover, the isolated galaxy from the ψDM simulation data ($\psi DM_{isolated}$) has a core radius similar to two satellite galaxies of the Milky Way; Leo II and Sculptor while on the other side the third galaxy from WDM simulation data (WDM_3), is in excellent agreement with the observed core of Sculptor and And IX. Both seem to differ

slightly in the transition point, something that could be reasonable if we take into account the redshift difference and in consequence the fact that these two simulated galaxies are in construction and therefore, we should expect more similar r_t values for z$\simeq$0. This seems to be supported by the observed r_t increment between $\psi DM_{isolated}$ and WDM_3, where the lower redshift goes in hand with a bigger r_t. However is interesting to point out that even with the redshift difference (almost 6 between the observed galaxies and the observable local group dwarfs), the r_c are similar, suggesting that the soliton is the first structure to be formed in this core-halo structure.

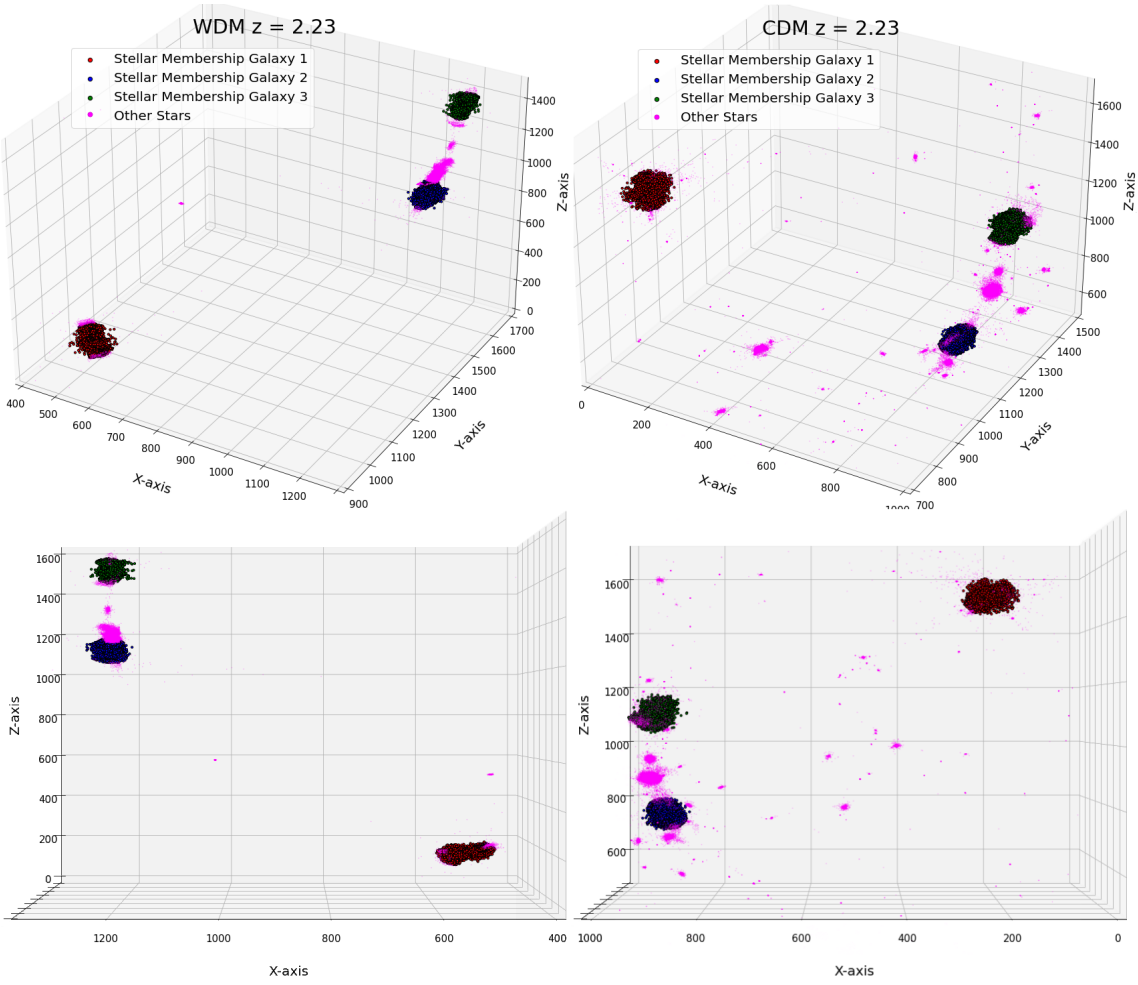

Figure 4.60: Mocz (2019) Mocz et al. (2019) simulation data. Stellar membership for WDM and CDM in z=2.23. The stars that belong to each galaxy have been painted with different colors; red for the isolated one and blue and green for the ones in the filamentary/subhalos environment. The figure shows the data in two different perspectives; 3D in the up row and 2D in the low one.

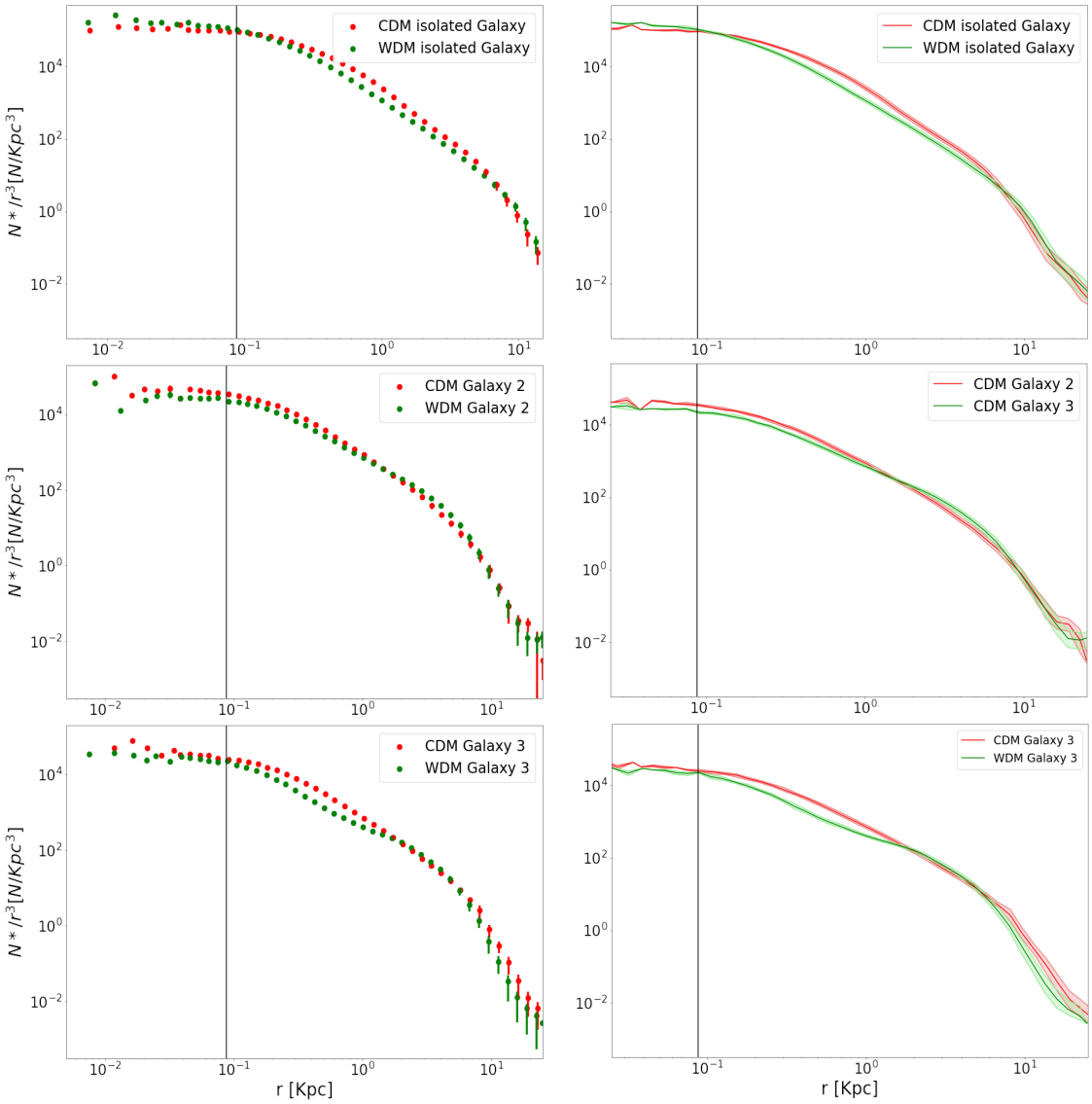

Figure 4.61: Mocz (2019) Mocz et al. (2019) simulation data. Subtracted WDM Vs CDM stellar profiles of the data's galaxies. The left panel shows the subtracted stellar profile in 0.01 kpc bins style, while the right one shows exactly the same with continuous lines. Notice how in this case there is not a high discrepancy between the two models in the inner zone, in good agreement with the expected cuspy profile for both. Nevertheless, we can observe a significative difference between the profile in positions close to the theoretical transition point for the three profiles, where the core-halo structure is easily observable for the last case (Galaxy 3). The vertical black line represents the comoving resolution limit of the data, indicating that the data for values smaller than that limit are not reliable.

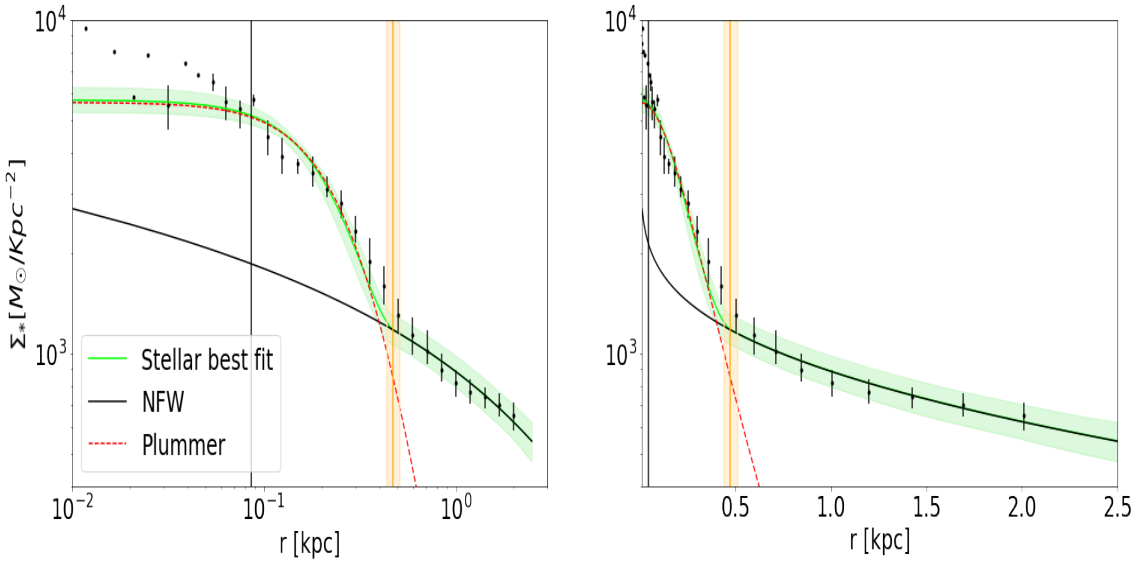

Figure 4.62: Mocz (2019) Mocz et al. (2019) simulation data. This figure shows the best fit of the projected star count profile of the WDM galaxy number three. An extended halo of stars is visible, stretching to $\simeq 3$ kpc and most evident on the linear scale of the left-hand panel. A prominent core is also evident on a scale < 0.5 kpc in each dwarf. These two characteristics seem to be in good agreement with the real dwarf spheroidals' stellar profiles observed in the Local Group (Pozo et al., 2023). A standard Plummer profile (red dashed curve) is seen to fit approximately the core region but falls well short at a large radius. Our predictions for the dSph class ($2.5 \times 10^{-22} eV$) for ψDM are shown in green, where the distinctive soliton profile provides an excellent fit to the observed cores and the surrounding halo of excited states that average azimuthally to an approximately NFW-like profile beyond the soliton radius. The accuracy of the core fit to the soliton is best seen on a log scale in the right panels, while the linear scale of the left shows the extent of the halo, including the characteristic density drop of about a factor of $\simeq 30$ predicted by ψDM between the prominent core and tenuous halo at a radius $\simeq 0.5$ kpc indicated by the vertical orange band. It is important to note that the green model tries to describe a solitonic core, making it unreasonable due to the lack of a soliton in WDM dwarfs. Nevertheless is important to point out that the transition point and the two different regimes are in contraposition to CDM.

Combinations	r_c (kpc)	r_t (kpc)	z	m_ψ 10^{-22}eV
$\psi DM_{isolated}$	$0.155^{+0.021}_{-0.017}$	$0.36^{+0.064}_{-0.056}$	5.56	2.5
WDM_3	$0.20^{+0.015}_{-0.015}$	$0.47^{+0.036}_{-0.035}$	2.23	2.5
$dSph_{Both}$	$0.21^{+0.003}_{-0.003}$	$0.71^{+0.021}_{-0.021}$	0	$1.85^{+0.66}_{-0.58}$
$dSph_{MilkyWay}$	$0.22^{+0.003}_{-0.003}$	$0.75^{+0.022}_{-0.023}$	0	$1.85^{+0.66}_{-0.58}$
$dSph_{Andromeda}$	$0.26^{+0.007}_{-0.006}$	$0.82^{+0.032}_{-0.028}$	0	$1.86^{+0.45}_{-0.53}$
Draco	$0.17^{+0.01}_{-0.01}$	$0.56^{+0.02}_{-0.02}$	0	-
Leo II	$0.17^{+0.01}_{-0.01}$	$0.66^{+0.02}_{-0.01}$	0	-
Sculptor	$0.21^{+0.01}_{-0.01}$	$0.72^{+0.07}_{-0.07}$	0	-
And IX	$0.22^{+0.02}_{-0.02}$	$0.70^{+0.08}_{-0.08}$	0	-
And XV	$0.19^{+0.02}_{-0.02}$	$0.65^{+0.08}_{-0.09}$	0	-

Table 4.9: Profile parameters for dwarfs associated with the Milky Way and Andromeda. Column 1: Dwarf Class or Dwarf individual name, Column 2: Core radius r_c, Column 3: Core-Halo transition radius r_t, Column 4: Redshift z, Column 5: Boson mass m_ψ.* We have to take into account that for WDM_3 the parameter values are not reliable cause the model is based in ψDM, expecting a soliton and a wave interference pattern, something that we will not have for a WDM galaxy. Nevertheless, the good agreement between the subtracted profile and the model is useful to understand and confirm that the core-halo structure also seems to arise in the WDM cosmological evolution, even if the physics are different from ψDM.

4.5.4 Tests feasible with JWST

The initial data from JWST seems capable of testing the rich non-linear coherent wave structure of the ψDM soliton structure for high redshift dwarf galaxies and the substructure around Einstein rings at the de Broglie scale. Evident in many of the lensed high redshift dwarf galaxies as shown in figure 4.63, for which we aim to provide a quantitative comparison with the model predictions in the next phase of my work in relation to the simulations and generic predictions analyzed in this thesis. Moreover, the data from JWST will also be crucial to distinguish between filamentary or subhalos structures in galactic environments, making a great point between the explained DM theories in this thesis.

Figure 4.63: Compilation of dwarf galaxies they are lensed by the SMACS0723 cluster. Notice how all of them seem to show a core, something expected by ψDM and difficult to explain by CDM. This high quality new data from JWST shows the feasibility of testing the competing profile predictions found in the simulations analysed in this thesis.

Summary & Conclusions

1. **Motivation**:

   Motivation 1: Look for the stellar core-halo structure (see section 4.2) in the three dark matter scenarios: WDM, CDM, and ψDM.

   Motivation 2: Analyze the simulations of the three DM models in order to find an observable different impact on stellar behavior and stellar structural development; Do stars trace dark matter?

   Motivation 3: Look for the soliton's imprint in the expected core profiles of ψDM, and the lack of it in WDM and CDM.

2. **Methodology**:

   Stellar membership of each galaxy

   Step 1: Localize the three galaxies dark matter centers detecting the three densest points.

   Step 2: Rotate the 3D coordinates of the particles if it was necessary.

   Step 3: Calculate the virial radius for each galaxy in order to establish all the stars between the virial radius of a halo and its center as stars that belong to that galaxy. To calculate the virial mass (M_{200}) and the virial radius (R_{200}), we just needed to know the center location of the halo, and find the radius R_{200} such that the enclosed mass (M_{200}) in the sphere of radius R_{200} was 200 $\times$ ρ_{crit} (where ρ_{crit} is the critical density of the universe).

Extract the stellar density profiles of each galaxy

Step 1: Subtract the stellar density profiles for each galaxy, calculating the density of stars (number of stars/ sphere volume) in bins of 0.01 kpc from the center to the virial radius.

Step 2: Repeat this process in all the snapshots susceptible of being interesting for the detection of the core-halo structure; The snapshots representing the data closer to redshift 0, 5.56 for ψDM and 2.3 for CDM and WDM. Also, snapshots with higher redshift in order to determine when the core-halo structure first appears.

Find and fit a possible stellar-core halo structure

Step 1: Compare the obtained stellar profiles of the three galaxies in the three dark matter scenarios to find a possible core-halo structure.

Step 2: Fit our best ψDM stellar profile (section 3.3) to the observed stellar profiles that might be compatible with a core-halo structure in order to quantify the core radius size (r_c) and the transition point (r_t) between the soliton and the NFW-like halo.

3. **Results**:

   z$\simeq$ 5.56

   Result 1: Clear core-halo structure is most visible for the isolated galaxy of the ψDM data, figure 4.55 that we have shown is in quantitative agreement with the soliton+halo structure predicted in this thesis. Comparison of the three well defined galaxies that are formed in common in the CDM, WDM and ψDM simulations with a possible soliton imprint in the observed flatter inner profiles of wave dark matter (see figures 4.55, 4.54 and 4.56).

   Result 2: We show how ψDM stellar core-halo model (Eq. 3.16) can reproduce well the subtracted stellar profile from the ψDM simulation for the isolated galaxy, with the boson mass as the only fixed parameter; 2.5×10^{-22}eV (Mocz et al., 2019)(green line and shaded area of figure 4.57). Moreover, we also found satisfactory results if we repeat the same analysis with a fixed halo mass from Mocz et al. (2019) of $0.8 \times 10^9 M_\odot$, the dashed blue line of figure 4.57.

   z$\simeq$ 2.23

   Result 1: The core-halo structure is noticeable almost in the three WDM profiles but never for CDM. Being the third WDM galaxy the one with the most distinct core-halo structure (figure 4.61). The stellar profiles still differ a lot for the three WDM and CDM galaxies.

   Result 2: We show how ψDM stellar core-halo model (Eq. 3.16) can reproduce well the stellar profile from the WDM data for the third galaxy, with the boson mass as the only fixed parameter; 2.5×10^{-22}eV (Mocz et al., 2019)(green line and shaded area of figure 4.62).

4. **Conclusions**:

Conclusion 1: In comparison to ψDM, we are able to highlight the considerable discrepancy between the simulation data with CDM predictions. In addition, there are other reasons to prefer ψDM from WDM, for example, the lensing effects that see the granularity of the halo (which WDM does not have). Another crucial point is that no WDM particle has been found in the laboratory despite stringent searches designed to find it. This is not a problem for Wave DM, as the needed laboratory would have the size of 1 kpc to see such light bosons. So certainly, there is no such heavy DM particle.

Conclusion 2: It is interesting to see how the core-halo structure also appears for WDM in hand with the almost identical large-scale structures of these two types of DM for which the core-halo structure may be the product of the characteristical power spectrum small-scale cut-off of WDM and ψDM. This last idea could be further tested after tracking the stars of each galaxy along different epochs and observing their berth position, to examine in more detail if the stars that appear in the outer extended halos were born in their halo or the outer filamentary structures. Moreover, stars seem to trace DM, as the stellar profiles are different in each DM scenario, following the predicted behaviors for each DM scenario, with a cuspy profile for WDM and CDM and with the core-halo structure hypothetically product of a change of regime in a specific position of the halo that should be the product of a central soliton and an interference pattern in the outer zone of the galaxies, something impossible to observe and in apparent disagreement with CDM predictions.

Conclusion 3: Actually, as we can see in fig. 4.49, there is little difference between the final large-scale structures in WDM and ψDM made by Mocz et al. (2020). Taking into account that the main point that they have in common is the small-scale cut-off of the initial power spectrum. This common cut-off results in a length scale that is imprinted on the DM profile and communicated to the star profile. This must be the key to the core halo structure, more than the soliton, even if it is true that the physics of their outer halo is quite different, one is caustic, and the other is the result of quantum interference patterns. However, on macro scales, they are almost identical. So even though the physical cause of this cut-off is very different (you can not know this from the simulation data (Mocz et al., 2020)), the result is the same; this scale is imprinted on the profile. The only thing that seems to matter is that they have the same cut-off in origin, which is why they evolve in a similar way producing core-halo stellar profiles.

Conclusion 4: One of the points that need to be discussed is the apparent detection of the core-halo structure for WDM data even if the presence of a soliton for WDM is impossible. As the shape of the cut-off in the initial dark matter power spectrum is not quite the same for WDM, it is probably slightly smoother, making us conclude that the soliton itself is not the key to the presence of this core-halo structure in the stellar profiles. Nevertheless, this soliton discrepancy is not a discard factor as the transition feature is due to the cut-off of the power spectrum; whether the inner profile is a soliton or a smooth WDM core is not relevant to the existence of the transition. Nevertheless, the presence of the soliton might have an effect on the earliest presence of the core

halo structure for ψDM (z$\simeq$5.56) than for WDM (z$\simeq$2.23).

Bibliography

Abbott B. P., et al., 2016, *Observation of Gravitational Waves from a Binary Black Hole Merger.*, Phys. Rev. Lett., 116

Abraham R. G., van Dokkum P. G., 2014, *Ultra-Low Surface Brightness Imaging with the Dragonfly Telephoto Array.*, Publications of the Astronomical Society of the Pacific, 126, 55

Abraham R. G., Valdes F., Yee H. K. C., van den Bergh S., 1994, *The Morphologies of Distant Galaxies. I. an Automated Classification System.*, Astrophys. J., 432, 75

Adelberger K. L., et al., 2005, *The Connection between Galaxies and Intergalactic Absorption Lines at Redshift 2< z< 3*, Astrophys. J., 629, 636

Alcock C., et al., 1998, *EROS and MACHO Combined Limits on Planetary-Mass Dark Matter in the Galactic Halo.*, Astrophys. J., 499

Alcock C., et al., 2000, *The MACHO Project: Microlensing Results from 5.7 Years of Large Magellanic Cloud Observations.*, Astrophys. J., 542, 281

Alcock C., et al., 2001, *MACHO Project Limits on Black Hole Dark Matter in the 1-30 Msolar Range.*, Astron. Astrophys., 550, L169

Alexander S. G., et al., 2017, *MOND Calculations of Bulk Dispersions and Radial Dispersion Profiles of Milky Way and Andromeda Dwarf Spheroidal Galaxies.*, Astrophys. J., 835, 13

Amanullah R., et al., 2010, *Spectra and Hubble Space Telescope Light Curves of Six Type Ia Supernovae at 0.511 < z < 1.12 and the Union2 Compilation.*, Astrophys. J., 716

Amorisco N. C., Evans N. W., 2012, *Dark matter cores and cusps: the case of multiple stellar populations in dwarf spheroidals.*, Mon. Not. R. Astron. Soc., 419, 184

Anastassopoulos V., et al., 2017, *New CAST limit on the axion-photon interaction.*, Nature Phys., 13, 584

Aparicio A., Carrera R., Martínez-Delgado D., 2001, *The Star Formation History and Morphological Evolution of the Draco Dwarf Spheroidal Galaxy.*, Astronomical. J., 122, 2524

Aprile E., et al., 2011, *Dark Matter Results from 100 Live Days of XENON100 Data.*, Phys. Rev. Lett., 107

Aprile E., et al., 2018, *Dark Matter Search Results from a One Ton-Year Exposure of XENON1T.*, Phys. Rev. Lett., 121

Archambault S., et al., 2017, *Dark matter constraints from a joint analysis of dwarf Spheroidal galaxy observations with VERITAS.*, Phys. Rev. D., 95

Arkani-Hamed N., Maldacena J., 2015, *Cosmological Collider Physics*, Arxiv

Armengaud E., et al., 2017, *Constraining the mass of light bosonic dark matter using SDSS Lyman-α forest.*, Mon. Not. R. Astron. Soc., 471, 4606

Arraki K. S., et al., 2014, *Effects of baryon removal on the structure of dwarf spheroidal galaxies.*, Mon. Not. R. Astron. Soc., 438, 1466

Arvanitaki A. Dubovsky S., 2011, *Exploring the string axiverse with precision black hole physics.*, Phys. Rev. D., 83

Arvanitaki A., et al., 2010, *String axiverse.*, Phys. Rev. D., 81

Avila-Vergara N., Carigi L., Hidalgo S. L., Durazo R., 2016, *Chemical history of isolated dwarf galaxies of the Local Group - I. dSphs: Cetus and Tucana.*, Mon. Not. R. Astron. Soc., 457, 4012

Avrorin A. D., et al., 2015, *Search for neutrino emission from relic dark matter in the sun with the Baikal NT200 detector.*, Astroparticle Phys., 62, 12

Ayala A., et al., 2014, *Revisiting the Bound on Axion-Photon Coupling from Globular Clusters.*, Phys. Rev. Lett., 113

Bajkova A. T., Bobylev V. V., 2020, *Orbits of 47 Dwarf Satellite Galaxies of the Milky Way in Three Models of the Gravitational Potential with Different*, ArXiv

Bandara K., Crampton D., Simard L., 2009, *A Relationship Between Supermassive Black Hole Mass and the Total Gravitational Mass of the Host Galaxy.*, Astrophys. J., 704, 1135

Bar-Or B., Fouvry J.-B., Tremaine S., 2019, *Relaxation in a Fuzzy Dark Matter Halo.*, Astrophys. J., 871, 17

Bar-Or B., Fouvry J.-B., Tremaine S., 2021, *Relaxation in a Fuzzy Dark Matter Halo. II. Self-consistent Kinetic Equations.*, Astrophys. J., 915, 17

Bar N., Blum K., Lacroix T., Panci P., 2019, *Looking for ultralight dark matter near supermassive black holes.*, J. of Cosmology and Astroparticle Phys.

Barranco J., et al., 2011, *Are black holes a serious threat to scalar field dark matter models?*, Phys. Rev. D., 84

Battaglia G. o., 2011, *Study of the Sextans dwarf spheroidal galaxy from the DART Ca II triplet survey.*, Mon. Not. R. Astron. Soc., 411, 1013

Battaglia G., et al., 2008, *The Kinematic Status and Mass Content of the Sculptor Dwarf Spheroidal Galaxy.*, Astrophys. J. Lett., 681, L13

Battaglia G., Rejkuba M., Tolstoy E., Irwin M. J., Beccari G. A., 2012a, *A wide-area view of the Phoenix dwarf galaxy from Very Large Telescope/FORS imaging.*, Mon. Not. R. Astron. Soc., 424, 1113

Battaglia G., Rejkuba M., Tolstoy E., Irwin M. J., Beccari G. A., 2012b, *The extensive age gradient of the Carina dwarf galaxy.*, Astrophys. J., 761, 6

Battaglia G., et al., 2022, *Gaia early DR3 systemic motions of Local Group dwarf galaxies and orbital properties with a massive Large Magellanic Cloud.*, Astron. Astrophys., 657, 49

Baugh C. M., 2006, *A primer on hierarchical galaxy formation: the semi-analytical approach.*, Rep. on Progress in Phys., 69, 3101

Beasley M. A., et al., 2016, *An Overmassive Dark Halo around an Ultra-diffuse Galaxy in the Virgo Cluster.*, Astrophys. J. Lett., 819, 7

Becker G. D., et al., 2015, *Evidence of patchy hydrogen reionization from an extreme Lyα trough below redshift six.*, Mon. Not. R. Astron. Soc., 447, 3402

Behroozi P. S., Wechsler R. H., Conroy C., 2013, *The Average Star Formation Histories of Galaxies in Dark Matter Halos from z = 0-8.*, Astrophys. J., 770, 36

Belczynski K., et al., 2016, *The first gravitational-wave source from the isolated evolution of two stars in the 40-100 solar mass range.*, Nature, 534, 512

Bennet P., et al., 2020, *The Satellite Luminosity Function of M101 into the Ultra-faint Dwarf Galaxy Regime.*, Astrophys. J. Lett., 893, 7

Benítez-Llambay A., et al., 2019, *Baryon-induced dark matter cores in the EAGLE simulations.*, Mon. Not. R. Astron. Soc., 488, 2387

Bergström L., et al., 2013, *New Limits on Dark Matter Annihilation from Alpha Magnetic Spectrometer Cosmic Ray Positron Data.*, Phys. Rev. Lett., 111, 1158

Bertone G., Tait T. M. P., 2018, *A new era in the search for dark matter.*, Nature, 562, 51

Bertone S., White S. D. M., 2006, *How do galactic winds affect the Lyα forest?*, Mon. Not. R. Astron. Soc., 367, 247

Bertone G., Hooper D., Silk J., 2005, *Particle dark matter: evidence, candidates and constraints.*, Phys. Reports, 405, 279

Bettinelli M., et al., 2019, *The star formation history of the Sculptor dwarf spheroidal galaxy.*, Mon. Not. R. Astron. Soc., 487, 5862

Bhattacharya S., et al., 2013, *Dark Matter Halo Profiles of Massive Clusters: Theory versus Observations.*, Astrophys. J., 766, 16

Binney J., Gerhard O., Silk J., 2001, *The dark matter problem in disc galaxies.*, Mon. Not. R. Astron. Soc., 321, 471

Bird S., et al., 2016, *Did LIGO Detect Dark Matter?*, Phys. Rev. Lett., 116

Blaña M., Fellhauer M., Smith R., 2021, *Leo IV and V - A possible dwarf galaxy pair?*, Astron. Astrophys., 542, 7

Blumenthal G. R., et al., 1984, *Formation of galaxies and large-scale structure with cold dark matter.*, Nature, 311, 517

Borriello A., Salucci P., 2007, *The dark matter distribution in disc galaxies.*, Mon. Not. R. Astron. Soc., 323, 285

Bose S., Ginsburg I., Loeb A., 2018, *Dating the Tidal Disruption of Globular Clusters with GAIA Data on Their Stellar Streams*, Astrophys. J. L., 859, 6

Bose S., et al., 2019, *No cores in dark matter-dominated dwarf galaxies with bursty star formation histories.*, Mon. Not. R. Astron. Soc., 486, 4790

Bosma A., 1981, *21-cm line studies of spiral galaxies. II. The distribution and kinematics of neutral hydrogen in spiral galaxies of various morphological types.*, Astron. J., 86, 1825

Bosman S. E. I., et al., 2020, *Three Lyα Emitting Galaxies within a Quasar Proximity Zone at $z \sim 5.8$.*, Astrophys. J., 896

Bouwens R. J., et al., 2015, *UV Luminosity Functions at Redshifts $z \sim 4$ to $z \sim 10$: 10,000 Galaxies from HST Legacy Fields.*, Astrophys. J., 803, 49

Boyarsky A., Ruchayskiy O., Shaposhnikov M., 2009, *The Role of Sterile Neutrinos in Cosmology and Astrophysics.*, Annual Review of Nuclear and Particle Science, 59, 191

Boylan-Kolchin M., Bullock J. S.and Kaplinghat M., 2011, *Too big to fail? The puzzling darkness of massive Milky Way subhaloes.*, Mon. Not. R. Astron. Soc., 415, L40

Boylan-Kolchin M., Bullock J. S.and Kaplinghat M., 2012, *The Milky Way's bright satellites as an apparent failure of ΛCDM.*, Mon. Not. R. Astron. Soc., 442, 1203

Boylan-Kolchin M., Bullock J. S., Kaplinghat M., 2011, *Too big to fail? The puzzling darkness of massive Milky Way subhaloes.*, Mon. Not. R. Astron. Soc., 415, L40

Bozek B., Marsh D. J. E.and Silk J., Wyse R. F. G., 2015, *Galaxy UV-luminosity function and reionization constraints on axion dark matter.*, Mon. Not. R. Astron. Soc., 450, 209

Broadhurst T., Scannapieco E., 2000, *Detecting the Gravitational Redshift of Cluster Gas*, Astrophys. J., 533, L93

Broadhurst T., de Martino I., Luu H. N., Smoot G. F., Tye S. H. H., 2020, *Ghostly galaxies as solitons of Bose-Einstein dark matter.*, Phys. Rev. D., 101

Brockway J. W., Carlson E. D., Raffelt G. G., 1996, *SN 1987A gamma-ray limits on the conversion of pseudoscalars.*, Phys. Lett. B., 383, 439

Brook C. B., et al., 2014, *The Stellar-to-halo Mass Relation for Local Group Galaxies.*, Astrophys. J. Lett., 784, 4

Brooks A. M. o., 2013, *A Baryonic Solution to the Missing Satellites Problem.*, Astrophys. J., 765

Brooks A. M., Zolotov A., 2014, *Why Baryons Matter: The Kinematics of Dwarf Spheroidal Satellites.*, Astrophys. J., 786

Brown W. R., et al., 2010, *Velocity Dispersion Profile of the Milky Way Halo.*, Astron. J., 139, 59

Brownsberger S., Randall L., 2019, *Stellar Profile Independent Determination of the Dark Matter Distribution of the Fornax Local Group Dwarf Spheroidal Galaxy.*, Arxiv

Bryant G., 2018,] https://slideplayer.com/slide/12519459/

Buck T., et al., 2019, *NIHAO XV: the environmental impact of the host galaxy on galactic satellite and field dwarf galaxies.*, Mon. Not. R. Astron. Soc., 483, 1314

Bugaev E., Klimai P., 2011, *Constraints on the induced gravitational wave background from primordial black holes.*, Phys. Rev. D., 83

Bullock J. S., 2001, *Profiles of dark haloes: evolution, scatter and environment.*, Mon. Not. R. Astron. Soc., 321, 559

Bullock J. S., 2010, *Notes on the Missing Satellites Problem.*, Arxiv

Bullock J. S., Boylan-Kolchin M., 2017, *Small-Scale Challenges to the ΛCDM Paradigm.*, Annual Rev. of Astro. and Astrophys., 55, 343

C. M., et al., 2020, *Modelling the Canes Venatici I dwarf spheroidal galaxy*, Astron. Astrophys., 633, 10

Caldwell N., et al., 2017, *Crater 2: An Extremely Cold Dark Matter Halo.*, Astrophys. J., 839, 11

Capolupo A., 2019, *Axion-photon mixing in quantum field theory and vacuum energy.*, Phys. Rev. B., 790, 427

Carignan C. and; Beaulieu S., 1989, *Optical and H i Studies of the "Gas-rich" Dwarf Irregular Galaxy DDO 154.*, Astrophys. J., 347, 760

Carignan C., Freeman K. C., 1988, *DDO 154: A "Dark" Galaxy?.*, Astrophys. J., 332, L33

Carr B. J., 1975, *The primordial black hole mass spectrum.*, Astrophys. J., 201, 1

Carr B. J., Hawking S. W., 1974, *Black holes in the early Universe.*, Mon. Not. R. Astron. Soc., 168, 399

Carr B., Kühnel F., 2020, *Primordial Black Holes as Dark Matter: Recent Developments.*, Annual Review of Nuclear and Particle Science, 70, 355

Carr B. J., et al., 2010, *New cosmological constraints on primordial black holes.*, Phys. Rev. D, 81

Carrera R., Aparicio A., Martínez-Delgado D., Alonso-García J., 2002, *The Star Formation History and Spatial Distribution of Stellar Populations in the Ursa Minor Dwarf Spheroidal Galaxy.*, Astronomical. J., 123, 3199

Carroll S. M., Field G. B., Jackiw R., 1990, *Limits on a Lorentz- and parity-violating modification of electrodynamics.*, Phys. Rev. D., 41

Cautun M., et al., 2020, *The milky way total mass profile as inferred from Gaia DR2.*, Mon. Not. R. Astron. Soc., 494, 4291

Chadha-Day F., Ellis J., Marsh D. J. E., 2022, *Axion dark matter: What is it and why now?*, Science, 8

Chan H. Y. J. s. o., 2022, *The diversity of core-halo structure in the fuzzy dark matter model.*, Mon. Not. R. Astron. Soc., 511, 943

Chan J. H. H., Schive H.-Y., Wong S.-K., Chiueh T., Broadhurst T., 2020, *Multiple Images and Flux Ratio Anomaly of Fuzzy Gravitational Lenses.*, ArXiv

Chapman S. C., et al., 2013, Mon. Not. R. Astron. Soc., 430, 37

Chavanis P.-H., 2011, *Mass-radius relation of Newtonian self-gravitating Bose-Einstein condensates with short-range interactions. I. Analytical results.*, Phys. Rev. D., 84

Chen X., 2010, *Primordial Non-Gaussianities from Inflation Models.*, Advances in Astronomy

Chen D.-M., McGaugh S., 2010, *Contradiction between strong lensing statistics and a feedback solution to the cusp/core problem.*, Research in Astron. Astrophys., 10, 1215

Chen X., Wang Y., 2010, *Quasi-single field inflation and non-Gaussianities.*, Journal of Cosmology and Astroparticle Physics

Chen S.-R., Schive H.-Y., Chiueh T., 2017, *Jeans analysis for dwarf spheroidal galaxies in wave dark matter.*, Mon. Not. R. Astron. Soc., 468, 1338

Chiti A., et al.,, *An extended halo around an ancient dwarf galaxy.*, Nat. Astro.

Chiti A., et al., 2022, *Detailed chemical abundances of stars in the outskirts of the Tucana II ultra-faint dwarf galaxy.*, Arxiv

Choi K., et al., 2015, *Search for Neutrinos from Annihilation of Captured Low-Mass Dark Matter Particles in the Sun by Super-Kamiokande.*, Phys. Rev. Lett., 114

Church B. V., Mocz P., Ostriker J. P., 2019, *Heating of Milky Way disc stars by dark matter fluctuations in cold dark matter and fuzzy dark matter paradigms.*, Mon. Not. R. Astron. Soc., 485, 2861

Cicuéndez L., Battaglia G., 2018, *Appearances can be deceiving: clear signs of accretion in the seemingly ordinary Sextans dSph*, Mon. Not. R. Astron. Soc., 480, 251

Clesse S., García-Bellido J., 2015, *Massive primordial black holes from hybrid inflation as dark matter and the seeds of galaxies.*, Phys. Rev. D., 92

Clowe D. and; Gonzalez A., Markevitch M., 2004, *Weak-Lensing Mass Reconstruction of the Interacting Cluster 1E 0657-558: Direct Evidence for the Existence of Dark Matter.*, Astrophys. J., 604, 596

Clowe D., et al., 2006, *A Direct Empirical Proof of the Existence of Dark Matter.*, Astrophys. J., 648

Cole D. R., Dehnen W., Wilkinson M. I., 2011, *Weakening dark matter cusps by clumpy baryonic infall.*, Mon. Not. R. Astron. Soc., 416, 1118

Coleman M. G., Da Costa G. S., Bland-Hawthorn J., 2005, *The Absence of Extratidal Structure in the Sculptor Dwarf Spheroidal Galaxy.*, Astronomical. J., 130, 1065

Collaboration C., 2020, *Search for high mass dijet resonances with a new background prediction method in proton-proton collisions at* $\sqrt{s}$ *= 13 TeV.*, Journal of High Energy Phy., 2020, 33

Collaboration P., et al., 2015, *Planck 2015 results. I. Overview of products and scientific results.*, Astron. Astrophys., 594, 38

Collaboration P., et al., 2016, *Planck 2015 results. XIII. Cosmological parameters.*, Astron. Astrophys., 594, 63

Collaboration P., et al., 2018a, *Planck 2018 results. IX. Constraints on primordial non-Gaussianity.*, Astron. Astrophys., 641, 47

Collaboration P., et al., 2018b, *Planck 2018 results. VI. Cosmological parameters.*, Astron. Astrophys., 641, 67

Collaboration P., et al., 2020a, *Planck 2018 results. I. Overview and the cosmological legacy of Planck.*, Astron. Astrophys., 641, 56

Collaboration P., et al., 2020c, *Planck 2018 results. VII. Isotropy and statistics of the CMB.*, Astron. Astrophys., 641, 61

Collaboration P., et al., 2020d, *Planck 2018 results. VII. Isotropy and statistics of the CMB.*, Astron. Astrophys., 641, 61

Collaboration P., et al., 2020b, *Planck 2018 results. X. Constraints on inflation.*, Astron. Astrophys., 641, 61

Collaboration P., et al., 2020e, *Planck 2018 results. V. CMB power spectra and likelihoods.*, Astron. Astrophys., 641, 92

Collins M. L. M., et al., 2013, *A Kinematic Study of the Andromeda Dwarf Spheroidal System.*, Astrophys. J., 768, 36

Collins M. L., et al., 2019, *A detailed study of Andromeda XIX, an extreme local analogue of ultra diffuse galaxies.*, Mon. Not. R. Astron. Soc., 491, 3496

Collins M. L., et al., 2021, *Andromeda XXI – a dwarf galaxy in a low density dark matter halo.*, Arxiv

Contenta F., et al., 2018, *Probing dark matter with star clusters: a dark matter core in the ultra-faint dwarf Eridanus II.*, Mon. Not. R. Astron. Soc., 476, 3124

Crain R. A., et al., 2015, *The EAGLE simulations of galaxy formation: calibration of subgrid physics and model variations.*, Mon. Not. R. Astron. Soc., 450, 1937

Cyburt R. H., Fields B. D., Olive K. A., Yeh T.-H., 2016, *Big bang nucleosynthesis: Present status.*, Rev. of Modern Phys., 88

D. D. S., K. W., 1998, *Experimental studies of Bose-Einstein condensation.*, Optics Express, 2, 299

D'Odorico V., et al., 2016, *Metals in the $z \sim 3$ intergalactic medium: results from an ultra-high signal-to-noise ratio UVES quasar spectrum.*, Mon. Not. R. Astron. Soc., 463, 2690

Danieli S., et al., 2017, *The Dragonfly Nearby Galaxies Survey. III. The Luminosity Function of the M101 Group.*, Astrophys. J., 837, 12

Danieli S., et al., 2019, *Still Missing Dark Matter: KCWI High-resolution Stellar Kinematics of NGC1052-DF2.*, Astrophys. J. Lett., 874, 8

Davies E. Y., Mocz P., 2020, *Fuzzy dark matter soliton cores around supermassive black holes.*, Mon. Not. R. Astron. Soc., 492, 5721

Davis M., Efstathiou G., Frenk C. S. s., White S. D. M., 1985, *The evolution of large-scale structure in a universe dominated by cold dark matte.*, Astrophys. J., 292, 371

Davis T. M., et al., 2007, *Scrutinizing Exotic Cosmological Models Using ESSENCE Supernova Data Combined with Other Cosmological Probes.*, Astrophys. J., 666

Del Popolo A., Le Delliou M., 2009, *Small Scale Problems of the ΛCDM Model: A Short Review.*, Galaxies, 5, 17

Dentler M., et al., 2022, *Fuzzy dark matter and the Dark Energy Survey Year 1 data.*, Mon. Not. R. Astron. Soc., 515, 5646

Di Cintio A., et al., 2017, *Ultra-diffuse galaxies in the Auriga simulations.*, Mon. Not. R. Astron. Soc., 466, L1

Di Valentino E., Melchiorri A., Silk J., 2020, *Planck evidence for a closed Universe and a possible crisis for cosmology.*, Nature Astro., 4, 196

Diego J. M., et al., 2018, *Dark Matter under the Microscope: Constraining Compact Dark Matter with Caustic Crossing Events.*, Astrophys. J., 857, 27

Diego J. M., Broadhurst T., Smoot G. F., 2021, *Evidence for lensing of gravitational waves from LIGO-Virgo data.*, Phys. Rev. D., 104

Diemer B.and Kravtsov A. V., 2015, *A Universal Model for Halo Concentrations.*, Astrophys. J., 799, 16

Dine M., Fischler W., Srednicki M., 1981, *A simple solution to the strong CP problem with a harmless axion.*, Phys. Rev. D., 104, 199

Dome T., et al., 2023, *Cosmic Web Dissection in Fuzzy Dark Matter Cosmologies.*, Arxiv

Dooley G. A., et al., 2017, *An observer's guide to the (Local Group) dwarf galaxies: predictions for their own dwarf satellite populations.*, Mon. Not. R. Astron. Soc., 471, 4894

Doré O., 2014, *Cosmology with the SPHEREX All-Sky Spectral Survey.*, Arxiv

Du X., Schwabe B., Niemeyer J. C., Bürger D., 2018, *Tidal disruption of fuzzy dark matter subhalo cores.*, Phys. Rev. D, 97

Dubinski J., Berentzen I., Shlosman I., 2009, *Anatomy of the Bar Instability in Cuspy Dark Matter Halos.*, Astrophys. J., 697, 293

Durfee D., Ketterle W., 1998, *Experimental studies of Bose-Einstein condensation .*, Optics Express, 2

Dutton A. A., 2016, *NIHAO V: too big does not fail - reconciling the conflict between ΛCDM predictions and the circular velocities of nearby field galaxies.*, Mon. Not. R. Astron. Soc., 457, L74

Dutton A. A., et al., 2020, *A model for core formation in dark matter haloes and ultra-diffuse galaxies by outflow episodes.*, Mon. Not. R. Astron. Soc., 499, 2648

Eckert D., et al., 2013, *The X-ray/SZ view of the virial region. II. Gas mass fraction.*, Astron. Astrophys., 551, 5

Edward L. W., 2004,] https://astro.ucla.edu/ wright/Lyman-alpha-forest.html

Efstathiou G., Sutherland W. J., Maddox S. J., 1990, *The cosmological constant and cold dark matter.*, Nature, 348, 705

Efstathiou G., et al., 1992, *Suppressing the formation of dwarf galaxies via photoionization.*, Mon. Not. R. Astron. Soc., 256, 43P

El-Zant A., Shlosman I.and Hoffman Y., 2001, *Dark Halos: The Flattening of the Density Cusp by Dynamical Friction.*, Astrophys. J., 560, 636

Ellis J., Hagelin J. S., Nanopoulos D. V., Srednicki M., 1984, *Search for violations of quantum mechanics.*, Nuclear Phys. B, 241, 381

Emami R., et al., 2016, *Cosmological tests of an axiverse-inspired quintessence field.*, Phys. Rev. D., 93

Emami R., Broadhurst T., Smoot G., Chiueh T., Luu H. N., 2020, *Soliton solution for the central dark mass in 47-Tuc globular cluster and implications for the axiverse.*, Phys. Rev. D., 101

(Event Horizon Telescope Collaboration) Akiyama K., et al., 2019, *First M87 Event Horizon Telescope Results. I. The Shadow of the Supermassive Black Hole.*, Astrophys. J., 875, 17

Fabrizio M. o., 2016, *The Carina Project. X. On the Kinematics of Old and Intermediate-age Stellar Populations 1,2.*, Astrophys. J., 830, 17

Fattahi A., et al., 2016, *The cold dark matter content of Galactic dwarf spheroidals: no cores, no failures, no problem.*, Arxiv

Fattahi A., et al., 2018, *Tidal stripping and the structure of dwarf galaxies in the Local Group.*, Mon. Not. R. Astron. Soc., 476, 3816

Feng J. L., 2010, *Dark Matter Candidates from Particle Physics and Methods of Detection.*, Annual Rev. of Astro. and Astrophys., 48, 495

Ferrarese L., 2002, *Beyond the Bulge: A Fundamental Relation between Supermassive Black Holes and Dark Matter Halos.*, Astrophys. J., 578, 90

Ferrarese L., Merritt D., 2000, *A Fundamental Relation between Supermassive Black Holes and Their Host Galaxies.*, Astrophys. J., 539, L9

Ferrero I., Abadi M. G., Navarro J. F., Sales L. V., Gurovich S., 2012, *The dark matter haloes of dwarf galaxies: a challenge for the Λ cold dark matter paradigm?*, Mon. Not. R. Astron. Soc., 425, 2817

Foreman-Mackey D., 2016, *corner.py: Scatterplot matrices in Python*, The Journal of Open Source Software

Foreman-Mackey D., et al., 2013, *emcee: The MCMC Hammer.*, EAS Publications Series, 125, 306

Fraternali F., Tolstoy E., Irwin M. J., Cole A. A., 2009, *Life at the periphery of the Local Group: the kinematics of the Tucana dwarf galaxy.*, Astron. Astrophys., 499, 121

Freundlich J., et al., 2020, *A model for core formation in dark matter haloes and ultra-diffuse galaxies by outflow episodes.*, Mon. Not. R. Astron. Soc., 491, 4523

Frinchaboy P. M., et al., 2012, *A 2MASS All-sky View of the Sagittarius Dwarf Galaxy. VII. Kinematics of the Main Body of the Sagittarius*, Astrophys. J., 756, 19

Fritz T. K., et al., 2018, *Gaia DR2 proper motions of dwarf galaxies within 420 kpc. Orbits, Milky Way mass, tidal influences, planar alignments, and group infall.*, Astron. Astrophys., 619, 18

Frusciante N., Perenon L., 2020, *Effective field theory of dark energy: A review.*, Phys. Reports, 857, 1

Frye B., Benitez N., Broadhurst T., 2002, *Spectral Evidence for Widespread Galaxy Outflows at z>4.*, American Astronomical Society, 34, 705

Fu S. W., Simon J. D., J. A., G. A., 2019, *Dynamical Histories of the Crater II and Hercules Dwarf Galaxies.*, Astrophys. J., 883, 15

Gallart C., et al., 2018, *The ACS LCID Project: On the Origin of Dwarf Galaxy Types—A Manifestation of the Halo Assembly Bias?*, Astrophys. J., 811, 6

Gangolli N., et al., 2021, *Constraining reionization in progress at $z = 5.7$ with Lyman-α emitters: voids, peaks, and cosmic variance.*, Mon. Not. R. Astron. Soc., 501, 5294

Gao L., Theuns T., 2007, *Lighting the Universe with Filaments.*, Science, 317

Gardner S., Fuller G. M., 2013, *Dark matter studies entrain nuclear physics.*, Progress in Particle and Nuclear Physics, 71, 167

Garrison-Kimmel S., et al., 2014a, *ELVIS: Exploring the Local Volume in Simulations.*, Mon. Not. R. Astron. Soc., 438, 2578

Garrison-Kimmel S., et al., 2014b, *Too big to fail in the Local Group.*, Mon. Not. R. Astron. Soc., 444, 222

Garrison-Kimmel S., et al., 2017, *Organized chaos: scatter in the relation between stellar mass and halo mass in small galaxies.*, Mon. Not. R. Astron. Soc., 464, 3108

Garrison-Kimmel S., et al., 2019, *The Local Group on FIRE: dwarf galaxy populations across a suite of hydrodynamic simulations.*, Mon. Not. R. Astron. Soc., 487, 1380

Garzilli A., Boyarsky A., Ruchayskiy O., 2017, *Cutoff in the Lyman-α forest power spectrum: Warm IGM or warm dark matter?*, Phys. Rev. B., 773, 258

Garzilli A., et al., 2021, *How to constrain warm dark matter with the Lyman-α forest.*, Mon. Not. R. Astron. Soc., 502, 2356

Gatto A., et al., 2013, *Unveiling the corona of the Milky Way via ram-pressure stripping of dwarf satellites.*, Mon. Not. R. Astron. Soc., 433, 2749

Gebhardt K., et al., 2000, *A Relationship between Nuclear Black Hole Mass and Galaxy Velocity Dispersion.*, Astrophys. J., 539, L13

Geha M., et al., 2012, *A Stellar Mass Threshold for Quenching of Field Galaxies.*, Astrophys. J., 757, 8

Gelato S., Sommer-Larsen J., 1999, *On DDO 154 and cold dark matter halo profiles.*, Mon. Not. R. Astron. Soc., 303, 321

Gentile G., et al., 2004, *The cored distribution of dark matter in spiral galaxies.*, Mon. Not. R. Astron. Soc., 351, 903

Gentile G., et al., 2007, *NGC 3741: the dark halo profile from the most extended rotation curve.*, Mon. Not. R. Astron. Soc., 375, 199

Genzel R., et al., 2003, *Spatially Resolved Millimeter Interferometry of SMM J02399-0136: AVery Massive Galaxy at z = 2.8.*, Astrophys. J., 584, 633

Gibbons G. W., Werner M. C., 2008, *Applications of the Gauss Bonnet theorem to gravitational lensing.*, Mon. Not. R. Astron. Soc., 25

Glazebrook K., et al., 2004, *A high abundance of massive galaxies 3-6 billion years after the Big Bang.*, Nature, 430, 181

Gnedin O. Y., Zhao H., 2002, *Maximum feedback and dark matter profiles of dwarf galaxies.*, Mon. Not. R. Astron. Soc., 333, 299

Gnedin O. Y., et al., 2010, *The Mass Profile of the Galaxy to 80 kpc.*, Astrophys. J. Lett., 720, L108

Goerdt T., et al., 2010, *Core Creation in Galaxies and Halos Via Sinking Massive Objects.*, Astrophys. J., 725, 1707

Graham P. ., 2015, *Experimental Searches for the Axion and Axion-Like Particles.*, Annual Review of Nuclear and Particle Science, 65, 485

Green A. M., Hofmann S., Schwarz D. J., 2004, *The power spectrum of SUSY-CDM on subgalactic scales.*, Mon. Not. R. Astron. Soc., 353, L23

Gregory A. L., et al., 2019, *Kinematics of the Tucana dwarf galaxy: an unusually dense dwarf in the Local Group.*, Mon. Not. R. Astron. Soc., 485, 2010

Grin D., et al., 2007, *Telescope search for decaying relic axions.*, Phys. Rev. D., 75

Gronke M., et al., 2021, *Lyman-α transmission properties of the intergalactic medium in the CoDaII simulation.*, Mon. Not. R. Astron. Soc., 509, 3697

Gross E. P., 1961, *Structure of a quantized vortex in boson systems.*, Nuovo Cimento, 20, 454

Gu M., et al., 2018, *Low Metallicities and Old Ages for Three Ultra-diffuse Galaxies in the Coma Cluster.*, Astrophys. J., 859, 13

Hargis J. R., Willman B., Peter A. H. G., 2014, *Too Many, Too Few, or Just Right? The Predicted Number and Distribution of Milky Way Dwarf Galaxies.*, Astrophys. J. Lett., 795, 5

Haslbauer M., et al., 2019, *The ultra-diffuse dwarf galaxies NGC 1052-DF2 and 1052-DF4 are in conflict with standard cosmology.*, Mon. Not. R. Astron. Soc., 489, 2634

Hayashi E., et al., 2004, *The inner structure of ΛCDM haloes - II. Halo mass profiles and low surface brightness galaxy rotation curves.*, Mon. Not. R. Astron. Soc., 355, 794

Hayashi K., et al., 2018, *Dark halo structure in the Carina dwarf spheroidal galaxy: joint analysis of multiple stellar components*, Mon. Not. R. Astron. Soc., 481, 250

Hayashi K., Chiba M., Ishiyama T., 2020, *Diversity of dark matter density profiles in the Galactic dwarf spheroidal satellites.*, Astrophys. J., 904, 19

Held E., Saviane I., Momany Y., 1999, *Stellar populations in the PHOENIX dwarf galaxy.*, Astron. Astrophys., 345, 747

Hermosa Muñoz L., et al., 2017, *Kinematic and metallicity properties of the Aquarius dwarf galaxy from FORS2 MXU spectroscopy.*, Astron. Astrophys., 634, 13

Hildebrandt H., et al., 2017, *KiDS-450: cosmological parameter constraints from tomographic weak gravitational lensing.*, Mon. Not. R. Astron. Soc., 465, 1454

Hinshaw G., et al., 2013, *Nine-year Wilkinson Microwave Anisotropy Probe (WMAP) Observations: Cosmological Parameter Results.*, Astrophys. J. Supp., 208, 25

Hlozek R., Grin D., Marsh D. J. E., Ferreira P. G., 2015, *A search for ultralight axions using precision cosmological data.*, Phys. Rev. D., 91

Hložek R., Marsh D. E., Grin D., 2018, *Using the full power of the cosmic microwave background to probe axion dark matter.*, Mon. Not. R. Astron. Soc., 476, 3063

Hogan C. J., Rees M. J., 1988, *Axion miniclusters.*, Phys. Rev. D., 205, 228

Hsu Y.-H., Chiueh T., 2021, *Evolution of perturbation and power spectrum in a two-component ultralight axionic universe.*, Phys. Rev. D., 103

Hu W., Barkana R., Gruzinov A., 2000, *Fuzzy Cold Dark Matter: The Wave Properties of Ultralight Particles.*, Phys. Rev. Lett., 85, 1158

Hu W., et al., 2001, *Cosmic Microwave Background Observables and Their Cosmological Implications.*, Astrophys. J., 549, 669

Hu E. M., et al., 2016, *An Ultraluminous Lyα Emitter with a Blue Wing at z = 6.6.*, Astrophys. J. Lett., 825

Hui L., 2020, *Ultralight scalars as cosmological dark matter*, Phys. Rev. Lett., 95

Hui L., Joyce A., Landry M. J.and Li X., 2020, *Vortices and waves in light dark matter*, Arxiv

Ibata R., Lewis G. F., Irwin M., Totten E., Quinn T., 2001, *Great Circle Tidal Streams: Evidence for a Nearly Spherical Massive Dark Halo around the Milky Way.*, Astrophys. J., 551, 294

Irwin M., Hatzidimitriou D., 1995, *Structural parameters for the Galactic dwarf spheroidals.*, Mon. Not. R. Astron. Soc., 277, 1354

Irwin M. J., et al., 2008, *Andromeda XVII: A New Low-Luminosity Satellite of M31.*, Astrophys. J. Letters, 676

Iršič V., et al., 2017a, *New constraints on the free-streaming of warm dark matter from intermediate and small scale Lyman-α forest data.*, Phys. Rev. D., 96

Iršič V., et al., 2017b, *First Constraints on Fuzzy Dark Matter from Lyman-α Forest Data and Hydrodynamical Simulations.*, Phys. Rev. Lett., 119

J. B., S. T., 2008, *Galactic Dynamics: Second Edition*, Princeton Univ.

Jardel J. R., Sellwood J. A., 2009, *Halo Density Reduction by Baryonic Settling?*, Astrophys. J., 691, 1300

Jason S. K., et al., 2010, *The SPLASH Survey: Internal Kinematics, Chemical Abundances, and Masses of the Andromeda I, II, III, VII, X, and XIV dSphs.*, Astrophys. J., p. 24

Javanmardi B., et al., 2016, *DGSAT: Dwarf Galaxy Survey with Amateur Telescopes. I. Discovery of low surface brightness systems around nearby spiral galaxies.*, Astron. Astrophys., 588, 12

Jenkins S. A. o., 2021, *Very Large Telescope Spectroscopy of Ultra-faint Dwarf Galaxies. I. Boötes I, Leo IV, and Leo V.*, Astrophys. J., 920, 25

Ji A. P., et al., 2021, *Kinematics of Antlia 2 and Crater 2 from The Southern Stellar Stream Spectroscopic Survey (S5).*, Arxiv

Jimenez R., et al., 2003, *Constraints on the Equation of State of Dark Energy and the Hubble Constant from Stellar Ages and the Cosmic Microwave Background.*, Astrophys. J., 593

Jing Y. P. ad Suto Y., 2000a, *The Density Profiles of the Dark Matter Halo Are Not Universal.*, Astrophys. J., 529, L69

Jing Y. P., 2000b, *The Density Profile of Equilibrium and Nonequilibrium Dark Matter Halos.*, Astrophys. J., 535, 30

Jungman G., Kamionkowski M., Griest K., 1996, *Supersymmetric dark matter.*, Phys. Reports, 267, 195

Kamionkowski M., Koushiappas S. M., 2008, *Galactic substructure and direct detection of dark matter.*, Phys. Rev. D., 77

Kamionkowski M., Pradler J. W., E. D. G., 2014, *An M theory solution to the strong CP-problem, and constraints on the axiverse.*, J. of High E. Phys., 2010

Kang H. D., Ricotti M., 2019, *Ghostly haloes in dwarf galaxies: constraints on the star formation efficiency before reionization.*, Mon. Not. R. Astron. Soc., 488, 2673

Kang J.-G., et al., 2020, *Cosmological constraints on ultra-light axion fields.*, Astron. Astrophys., 20, 8

Kapteyn J. C., 1922, *First Attempt at a Theory of the Arrangement and Motion of the Sidereal System.*, Astrophys. J., 55, 302

Katz H., et al., 2017, *Testing feedback-modified dark matter haloes with galaxy rotation curves: estimation of halo parameters and consistency with ΛCDM scaling relations.*, Mon. Not. R. Astron. Soc., 466, 1648

Kauffmann G., White S. D. M., Guiderdoni B., 1993, *The formation and evolution of galaxies within merging dark matter haloes.*, Mon. Not. R. Astron. Soc., 264, 201

Kaufmann T., 2006, *Cooling flows within galactic haloes: the kinematics and properties of infalling multiphase gas.*, Mon. Not. R. Astron. Soc., 370, 1612

Kawasaki M., Nakayama K., 2013, *Axions: Theory and Cosmological Role.*, Annual Review of Nuclear and Particle Science, 63, 69

Kazantzidis S., Łokas E. L., Mayer L., Knebe A., Klimentowski J., 2011, *Formation of dwarf spheroidal galaxies via mergers of disky dwarfs.*, Astrophys. J., 740, 6

Kelly P. L., et al., 2018, *Extreme magnification of an individual star at redshift 1.5 by a galaxy-cluster lens.*, Nature Astro., 2, 334

Khlopov M. I., Malomed B. A., Zeldovich I. B., 1985, *Gravitational instability of scalar fields and formation of primordial black holes.*, Mon. Not. R. Astron. Soc., 215, 575

Kim D., et al., 2016, *Portrait of a Dark Horse: a Photometric and Spectroscopic Study of the Ultra-faint Milky Way Satellite Pegasus III.*, Astrophys. J., 833, 9

Kim S. Y., Peter A. H. G., Hargis J. R., 2018, *Missing Satellites Problem: Completeness Corrections to the Number of Satellite Galaxies in the Milky Way are Consistent with Cold Dark Matter Predictions.*, Phys. Rev. Lett., 121

Kim S., Peter A., Hargis J., 2019, *There is No Missing Satellites Problem.*, American Astronomical Society, 92

King I., 1962, *The structure of star clusters. I. an empirical density law.*, Astron. J., 67, 471

Kirby E. N., et al., 2001, *Elemental Abundances in M31: The Kinematics and Chemical Evolution of Dwarf Spheroidal Satellite Galaxies.*, Astronomical. J., 159, 20

Kirby E. N., et al., 2014, *The dynamics of isolated Local Group galaxies.*, Mon. Not. R. Astron. Soc., 439, 1015

Kirby E. N., et al., 2017, *A Chemistry and Kinematics of the Late-forming Dwarf Irregular Galaxies Leo A, Aquarius, and Sagittarius DIG*, Astrophys. J., 834, 19

Klimentowski J., et al., 2007, *Mass modelling of dwarf spheroidal galaxies: the effect of unbound stars from tidal tails and the Milky Way.*, Mon. Not. R. Astron. Soc., 378, 353

Klypin A., Kravtsov A. V., Valenzuela O. Prada F., 1999, *Where Are the Missing Galactic Satellites?*, Astrophys. J., 522, 82

Koch A., et al., 2007a, *Stellar Kinematics in the Remote Leo II Dwarf Spheroidal Galaxy-Another Brick in the Wall.*, Astronomical. J., 134, 566

Koch A., Wilkinson M. I., Kleyna J. T., Gilmore G. F., Grebel E. K., Mackey A. D., Evans N. W., Wyse R. F. G., 2007b, *Stellar Kinematics and Metallicities in the Leo I Dwarf Spheroidal Galaxy-Wide-Field Implications for Galactic Evolution*, Astrophys. J., 657, 241

Kolb E. W., Tkachev I. I., 1993, *Axion miniclusters and Bose stars.*, Phys. Rev. Lett., 71, 3051

Kolb E. W., Tkachev I. I., 1994a, *Nonlinear axion dynamics and the formation of cosmological pseudosolitons.*, Phys. Rev. D., 49, 5040

Kolb E. W., Tkachev I. I., 1994b, *Large-amplitude isothermal fluctuations and high-density dark-matter clumps.*, Phys. Rev. D., 50, 769

Komatsu E., et al., 2009, *Five-Year Wilkinson Microwave Anisotropy Probe Observations: Cosmological Interpretation.*, Astrophys. J. Supplement, 180, 330

Konoplya R. A., 2019, *Shadow of a black hole surrounded by dark matter.*, Phys. Lett. B., 795, 1

Koposov S. E., Belokurov V., Torrealba G., Evans N. W., 2015, *Beasts of the Southern Wild: Discovery of Nine Ultra Faint Satellites in the Vicinity of the Magellanic Clouds.*, Astrophys. J., 805, 18

Koposov S. E., et al., 2018, *Snake in the Clouds: a new nearby dwarf galaxy in the Magellanic bridge.*, Mon. Not. R. Astron. Soc., 479, 5343

Kowalski M., et al., 2008, *Improved Cosmological Constraints from New, Old, and Combined Supernova Data Sets.*, Astrophys. J., 686

Kuhlen M., Vogelsberger M., Angulo R., 2012, *Numerical simulations of the dark universe: State of the art and the next decade.*, Phys. Dark Universe, 1, 50

Kumar Poddar T., 2021, *Constraints on axionic fuzzy dark matter from light bending and Shapiro time delay.*, J. of Cosmo. and Astroparticle Phys., 2021, 19

Lacey C. G., Ostriker J. P., 1985, *Massive black holes in galactic halos ?*, Astrophys. J., 299, 633

Lasserre T., et al., 2000, *Not enough stellar mass Machos in the Galactic halo.*, Astron. Astrophys., 355, L39

Lazar A., et al., 2020, *A dark matter profile to model diverse feedback-induced core sizes of ΛCDM haloes.*, Mon. Not. R. Astron. Soc., 497, 2393

Leaman R., et al., 2013, *The Comparative Chemical Evolution of an Isolated Dwarf Galaxy: A VLT and Keck Spectroscopic Survey of WLM.*, Astrophys. J., 767, 16

Lee J.-W., 2016, *Characteristic size and mass of galaxies in the Bose-Einstein condensate dark matter model*, Phys. Lett. B., 756, 166

Lee J.-W., Koh I.-G., 1996, *Galactic halos as boson stars.*, Phys. Rev. D., 53, 2236

Leo M., otehrs 2017, *The effect of thermal velocities on structure formation in N-body simulations of warm dark matter.*, Journal of Cosmology and Astroparticle Physics

Leong K.-H., et al., 2019, *Cosmological simulations of intergalactic medium enrichment from galactic outflows.*, Mon. Not. R. Astron. Soc., 484, 4273

Leung E., et al., 2018, *Magnification Bias of Distant Galaxies in the Hubble Frontier Fields: Testing Wave Versus Particle Dark Matter Predictions.*, Astrophys. J., 862, 34

Leung G. Y. C., Leaman R., van de Ven G., Battaglia G., 2020, *A dwarf-dwarf merger and dark matter core as a solution to the globular cluster problems in the Fornax dSph.*, Mon. Not. R. Astron. Soc., 493, 320

Li T. S., et al., 2018, *The First Tidally Disrupted Ultra-faint Dwarf Galaxy?: A Spectroscopic Analysis of the Tucana III Stream.*, Astrophys. J., 866, 23

Liao S., et al., 2019, *Ultra-diffuse galaxies in the Auriga simulations.*, Mon. Not. R. Astron. Soc., 490, 5182

Lin W., Ishak M., 2016, *Ultra faint dwarf galaxies: an arena for testing dark matter versus modified gravity.*, Journal of Cosmo. and Astroparticle Phy.

Liu T., Smoot G., Zhao Y., 2020, *Detecting axionlike dark matter with linearly polarized pulsar light.*, Phys. Rev. D., 101

Liu I.-K., Proukakis N. P., Rigopoulos G., 2022, *Coherent and incoherent structures in fuzzy dark matter halos.*, Arxiv

Lora V., Magaña J., Bernal A. and; Sánchez-Salcedo F. J., Grebel E. K., 2012, *On the mass of ultra-light bosonic dark matter from galactic dynamics.*, Journal of Cosmology and Astroparticle Physics

Lovell M. R., et al., 2014, *The properties of warm dark matter haloes.*, Mon. Not. R. Astron. Soc., 439, 300

Luu . N., Tye S. H. H., Broadhurst T., 2005, *Multiple ultralight axionic wave dark matter and astronomical structures.*, Phys. Dark Universe., 30

Luu H. N., Tye S. H. H., Broadhurst T., 2020, *Multiple ultralight axionic wave dark matter and astronomical structures.*, Phys. Dark Universe, 30

Macciò A. V., otehrs 2012, *Cores in warm dark matter haloes: a Catch 22 problem.*, Mon. Not. R. Astron. Soc., 424, 1105

Macciò A. V., et al., 2012, *Halo Expansion in Cosmological Hydro Simulations: Toward a Baryonic Solution of the Cusp/Core Problem in Massive Spirals.*, Astrophys. J., 744, 5

Madau P., Haardt F., 2015, *Cosmic Reionization after Planck: Could Quasars Do It All?*, Astrophys. J., 813, 6

Maldacena J., 2001, *Non-gaussian features of primordial fluctuations in single field inflationary models.*, Astrophys. J., 549, 669

Mandelbaum R., et al., 2006, *Galaxy halo masses and satellite fractions from galaxy-galaxy lensing in the Sloan Digital Sky Survey: stellar mass, luminosity, morphology and environment dependencies*, Mon. Not. R. Astron. Soc., 368, 715

Markevitch M., et al., 2004, *Direct Constraints on the Dark Matter Self-Interaction Cross Section from the Merging Galaxy Cluster 1E 0657-56.*, Astrophys. J., 606, 819

Marsh D. E., 2016, *Axion cosmology.*, Phys. Reports, 643, 1

Marsh D. J. E., Pop A.-R., 2015, *Axion dark matter, solitons and the cusp-core problem.*, Mon. Not. R. Astron. Soc., 451, 2479

Marsh D. J. E., Silk J., 2014, *A model for halo formation with axion mixed dark matter.*, Mon. Not. R. Astron. Soc., 437, 2652

Marsh D. J. E., et al., 2013, *Axiverse cosmology and the energy scale of inflation.*, Phys. Rev. D., 87

Martin N. F., et al., 2016, *The PAndAS View of the Andromeda Satellite System. II. Detailed Properties of 23 M31 Dwarf Spheroidal Galaxies.*, Astrophys. J., 833, 27

Martínez-Delgado D., Alonso-García J., Aparicio A., Gómez-Flechoso M. A., 2001, *A Tidal Extension in the Ursa Minor Dwarf Spheroidal Galaxy.*, Astrophys. J., 549, L63

Mashchenko S., 2015, *Mass Models of Dwarf Spheroidal Galaxies with Variable Stellar Anisotropy. I. Jeans Analysis.*, Arxiv

Mashchenko S., Couchman H. M. P., Wadsley J., 2006, *The removal of cusps from galaxy centres by stellar feedback in the early Universe.*, Nature, 442, 539

Mashchenko S., Wadsley J., Couchman H. M. P., 2008, *Stellar Feedback in Dwarf Galaxy Formation.*, Science, 319

Massari D., et al., 2020, *Stellar 3D kinematics in the Draco dwarf spheroidal galaxy*, Astron. Astrophys., 633, 11

Massó E., Toldrà R., 1997, *New constraints on a light spinless particle coupled to photons.*, Phys. Rev. D., 55, 7967

Mateo M. L., 1998, *Dwarf Galaxies of the Local Group.*, Annual Rev. Astron. Astrophys., 36, 435

Mateo M., et al., 1993, *The Carina Dwarf Spheroidal Galaxy: How Dark is it?.*, Astron. J., 105, 510

Matos T., Vázquez-González A., Magaña J., 2009, ϕ^2 *as dark matter*, Mon. Not. R. Astron. Soc., 393, 1359

May S., Springel V., 2021, *Structure formation in large-volume cosmological simulations of fuzzy dark matter: Impact of the non-linear dynamics.*, Mon. Not. R. Astron. Soc., 506, 2603

May S., Springel V., 2022, *The halo mass function and filaments in full cosmological simulations with fuzzy dark matter.*, Arxiv

McCarthy I. G., Bower R. G., Balogh M. L., 2007, *Revisiting the baryon fractions of galaxy clusters: a comparison with WMAP 3-yr results.*, Mon. Not. R. Astron. Soc., 377, 1457

McConnachie A. W., 2012, *The Observed Properties of Dwarf Galaxies in and around the Local Group.*, Astron. J., 144, 36

McConnachie A. W., Irwin M. J., 2006, *Structural properties of the M31 dwarf spheroidal galaxies.*, Mon. Not. R. Astron. Soc., 365, 1263

McConnachie A. W., Venn K. A., 2020, *Revised and New Proper Motions for Confirmed and Candidate Milky Way Dwarf Galaxies.*, Astronomical. J., 160

McConnachie A. W., Arimoto N., Irwin M., Tolstoy E., 2006, *The stellar content of the isolated transition dwarf galaxy DDO210.*, Mon. Not. R. Astron. Soc., 373, 715

McGaugh S., Milgrom M., 2013a, *Andromeda Dwarfs in Light of MOND.*, Astrophys. J., 766

McGaugh S., Milgrom M., 2013b, *Andromeda Dwarfs in Light of MOND. II. Testing Prior Predictions.*, Astrophys. J., 775

Mediavilla E., et al., 2009, *Microlensing-based Estimate of the Mass Fraction in Compact Objects in Lens Galaxies.*, Astrophys. J., 706, 1451

Mediavilla E., et al., 2017, *Limits on the Mass and Abundance of Primordial Black Holes from Quasar Gravitational Microlensing.*, Astrophys. J. Lett., 836, 5

Meszaros P., 1974, *The behaviour of point masses in an expanding cosmological substratum.*., Astron. Astrophys., 37, 225

Mitchell P. D., et al., 2013, *How well can we really estimate the stellar masses of galaxies from broad-band photometry?*, Mon. Not. R. Astron. Soc., 435, 87

Mo H. J., Mao S., 2004, *Galaxy formation in pre-processed dark haloes.*, Mon. Not. R. Astron. Soc., 353, 829

Mocz P., et al., 2017, *Galaxy formation with BECDM - I. Turbulence and relaxation of idealized haloes.*, Mon. Not. R. Astron. Soc., 471, 4559

Mocz P., et al., 2018, *Schrödinger-Poisson-Vlasov-Poisson correspondence.*, Phys. Rev. D, 97

Mocz P., et al., 2019, *First Star-Forming Structures in Fuzzy Cosmic Filaments.*, Phys. Rev. Lett., 123

Mocz P., et al., 2020, *Galaxy formation with BECDM - II. Cosmic filaments and first galaxies.*, Mon. Not. R. Astron. Soc., 494, 2027

Mohammadtaher S., Spergel D. N., 2020, *Ultra-light Dark Matter Is Incompatible with the Milky Way's Dwarf Satellites*, Astrophys. J., 893, 6

Molnar S. M., Broadhurst T., 2018, *Multi-phenomena Modeling of the New Bullet-like Cluster ZwCl 008.8+52 Using N-body/Hydrodynamical Simulations.*, Astrophys. J., 862, 11

Monroy-Rodríguez M. A., Allen C., 2014, *The End of the MACHO Era, Revisited: New Limits on MACHO Masses from Halo Wide Binaries.*, Astrophys. J., 790, 10

Moore B., 1994, *Evidence against dissipation-less dark matter from observations of galaxy haloes.*, Nature, 370, 629

Moore B., Quinn T., Governato F., Stadel J., Lake G., 1999a, *Cold collapse and the core catastrophe.*, Mon. Not. R. Astron. Soc., 310, 1147

Moore B., et al., 1999b, *Dark Matter Substructure within Galactic Halos.*, Astrophys. J., 524, L19

Moskowitz A. G., Walker M. G., 2020, *Stellar Density Profiles of Dwarf Spheroidal Galaxies .*, Astrophys. J., 892, 20

Moster B. P., et al., 2010, *Constraints on the Relationship between Stellar Mass and Halo Mass at Low and High Redshift.*, Astrophys. J., 710, 903

Moster B. P., Naab T., White S. D. M., 2013, *Galactic star formation and accretion histories from matching galaxies to dark matter haloes.*, Mon. Not. R. Astron. Soc., 428, 3121

Mutlu-Pakdil B., et al., 2018, *A Deeper Look at the New Milky Way Satellites: Sagittarius II, Reticulum II, Phoenix II, and Tucana III.*, Astrophys. J., 863, 11

Muñoz J. B., et al., 2016, *Lensing of Fast Radio Bursts as a Probe of Compact Dark Matter.*, Phys. Rev. Lett., 117

Muñoz R. R., et al., 2018, *A MegaCam Survey of Outer Halo Satellites. III. Photometric and Structural Parameters.*, Astrophys. J., 860, 54

Nadler E. O., et al., 2020, *Milky Way Satellite Census. III. Constraints on Dark Matter Properties from Observations of Milky Way Satellite Galaxies.*, Arxiv

Navarro J., Frenk C. S., 1996, *The Structure of Cold Dark Matter Halos.*, Astrophys. J., 462, 563

Navarro J. F., Frenk C. S., White S. D. M., 1997, *A Universal Density Profile from Hierarchical Clustering.*, Astrophys. J., 490, 493

Newby M., et al., 2013, *A Spatial Characterization of the Sagittarius Dwarf Galaxy Tidal Tails.*, Astronomical. J., 145, 19

Niemeyer J. C., 2020, *Small-scale structure of fuzzy and axion-like dark matter.*, P. in Particle & Nuclear Phys., 113

Nipoti C., Binney J., 2015, *Early flattening of dark matter cusps in dwarf spheroidal galaxies.*, Mon. Not. R. Astron. Soc., 446, 1820

Nori M., et al., 2019, *Lyman α forest and non-linear structure characterization in Fuzzy Dark Matter cosmologies.*, Mon. Not. R. Astron. Soc., 482, 3227

Ogiya G., Mori M., 2014, *The Core-Cusp Problem in Cold Dark Matter Halos and Supernova Feedback: Effects of Oscillation.*, Astrophys. J., 793, 12

Oguri M., et al., 2018, *Understanding caustic crossings in giant arcs: Characteristic scales, event rates, and constraints on compact dark matter.*, Phys. Rev. D., 97

Okamoto S., Arimoto N., Yamada Y., Onodera M., 2012, *Stellar Populations and Structural Properties of Ultra Faint Dwarf Galaxies, Canes Venatici I, Boötes I, Canes Venatici II, and Leo IV.*, Astrophys. J., 744, 13

Okamoto S., et al., 2017, *Population gradient in the Sextans dSph: comprehensive mapping of a dwarf galaxy by Suprime-Cam.*, Mon. Not. R. Astron. Soc., 467, 208

Oort J. H., 1932, *The force exerted by the stellar system in the direction perpendicular to the galactic plane and some related problems.*, Bulletin of the Astronomical Institutes of the Netherlands, 6, 249

Oppenheimer B. D., Davé R., 2006, *Cosmological simulations of intergalactic medium enrichment from galactic outflows.*, Mon. Not. R. Astron. Soc., 373, 1265

Ostriker J. P., Steinhardt P. J., 1995, *The observational case for a low-density Universe with a non-zero cosmological constant.*, Nature, 377, 600

Ostriker J. P., et al., 2019, *Mind the Gap: Is the Too Big to Fail Problem Resolved?*, Astrophys. J., 885, 9

Pace A. B., et al., 2020, *Multiple chemodynamic stellar populations of the Ursa Minor dwarf spheroidal galaxy.*, Mon. Not. R. Astron. Soc., 495, 3022

Paczynski B., 1986, *Gravitational Microlensing by the Galactic Halo.*, Astrophys. J., 304, 1

Padmanabhan H., Loeb A., 2021, *Distinguishing AGN from starbursts as the origin of double-peaked Lyman-alpha emitters in the reionization era.*, Astron. Astrophys., 646, 4

Pantig R. C., Övgün A., 2022a, *Black hole in quantum wave dark matter.*, Arxiv

Pantig R C., Övgün A., 2022b, *Dark matter effect on the weak deflection angle by black holes at the center of Milky Way and M87 galaxies.*, European Phys. J., 82, 5

Papastergis E., et al., 2013, *Is there a "too big to fail" problem in the field?*, Astron. Astrophys., 574, 16

Peccei R. D. snd Quinn H. R., 1977, *CP Conservation in the Presence of Pseudoparticles.*, Phys. Rev. Lett., 38, 1440

Peccei R. D., Quinn H. R., 1977a, *Constraints imposed by CP conservation in the presence of pseudoparticles.*, Phys. Rev. D., 16, 1791

Peccei R. D., Quinn H. R., 1977b, *CP conservation in the presence of pseudoparticles.*, Phys. Rev. Lett., 38, 1440

Peebles P. J. E., 1982, *Large-scale background temperature and mass fluctuations due to scale-invariant primeval perturbations.*, Astrophys. J., 263

Peebles P. J. E., 2000, *Fluid Dark Matter*, Astrophys. J., 534, L127

Percival W. J., et al., 2001, *The 2dF Galaxy Redshift Survey: the power spectrum and the matter content of the Universe.*, Mon. Not. R. Astron. Soc., 327, 1297

Pettini M., 1999, *Element Abundances at High Redshifts*, Chemical Evolution from Zero to High Redshift

Picozzi A., Garnier J., 2011, *Incoherent Soliton Turbulence in Nonlocal Nonlinear Media.*, Phys. Rev. Lett., 107

Plummer H. C., 1911, *On the problem of distribution in globular star clusters.*, Mon. Not. R. Astron. Soc., 71, 460

Pontzen A., Governato F., 2012, *How supernova feedback turns dark matter cusps into cores.*, Mon. Not. R. Astron. Soc., 421, 3464

Pooley D., et al., 2009, *The Dark-matter Fraction in the Elliptical Galaxy Lensing the Quasar PG 1115+080.*, Astrophys. J., 697, 1892

Pope A. C., et al., 2004, *Cosmological Parameters from Eigenmode Analysis of Sloan Digital Sky Survey Galaxy Redshifts.*, Astrophys. J., 607, 655

Portail M., Wegg C., Gerhard O., Ness M., 2017, *Chemodynamical modelling of the galactic bulge and bar.*, Mon. Not. R. Astron. Soc., 470, 1233

Pozo A., others. 2021a, *Understanding the "Feeble Giant" Crater II with tidally stretched Wave Dark Matter.*, Arxiv

Pozo A., others. 2021b, *Wave dark matter and ultra-diffuse galaxies.*, Mon. Not. R. Astron. Soc., 504, 2868

Pozo A., et al., 2020, *Detection of a universal core-halo transition in dwarf galaxies as predicted by Bose-Einstein dark matter.*, Arxiv

Pozo A., et al., 2023, *Dwarf Galaxies United by Dark Bosons.*, Arxiv

Putman M. E., et al., 2021, *The Gas Content and Stripping of Local Group Dwarf Galaxies.*, Astrophys. J., 913, 20

Quinn D. P., et al., 2009, *Structural analysis of the Sextans dwarf spheroidal galaxy.*, Mon. Not. R. Astron. Soc., 396, L11

Read J. I.and Agertz O., Collins M. L. M., 2016, *Dark matter cores all the way down.*, Mon. Not. R. Astron. Soc., 459, 2573

Read J. I., Erkal D., 2019, *Abundance matching with the mean star formation rate: there is no missing satellites problem in the Milky Way above M200* $\sim 10^9 M_\odot$., Mon. Not. R. Astron. Soc., 487, 5799

Read J. I., Gilmore G., 2005, *Mass loss from dwarf spheroidal galaxies: the origins of shallow dark matter cores and exponential surface brightness profiles.*, Mon. Not. R. Astron. Soc., 356, 107

Read J. I., Steger P., 2017, *How to break the density-anisotropy degeneracy in spherical stellar systems.*, Mon. Not. R. Astron. Soc., 471, 4541

Read J. I., et al., 2006a, *The tidal stripping of satellites.*, Mon. Not. R. Astron. Soc., 366, 429

Read J. I., et al., 2006b, *The importance of tides for the Local Group dwarf spheroidals*, Mon. Not. R. Astron. Soc., 367, 387

Read J. I., et al., 2017, *The stellar mass-halo mass relation of isolated field dwarfs: a critical test of* ΛCDM *at the edge of galaxy formation*, Mon. Not. R. Astron. Soc., 467, 2019

Read J. I., Walker M. G., Steger P., 2018, *The case for a cold dark matter cusp in Draco.*, Mon. Not. R. Astron. Soc., 481, 860

Read J. I., Walker M. G., Steger P., 2019, *Dark matter heats up in dwarf galaxies.*, Mon. Not. R. Astron. Soc., 484, 1401

Rees M. J., Ostriker J. P., 1977, *Cooling, dynamics and fragmentation of massive gas clouds: clues to the masses and radii of galaxies and clusters..*, Mon. Not. R. Astron. Soc., 179, 541

Reynolds C. S., et al., 2020, *Astrophysical Limits on Very Light Axion-like Particles from Chandra Grating Spectroscopy of NGC 1275.*, Astrophys. J., 890, 9

Ricotti M., 2007, *Contrasting Galaxy Formation from Quantum Wave Dark Matter.*, Astrophys. J., 662, 53

Ricotti M., Ostriker J. P., Mack K. J., 2008, *Contrasting Galaxy Formation from Quantum Wave Dark Matter.*, Astrophys. J., 680, 829

Riess A. G., et al., 1998, *Observational Evidence from Supernovae for an Accelerating Universe and a Cosmological Constant.*, Astron. J., 116, 1009

Riess A. G., et al., 2004, *Type Ia Supernova Discoveries at $z > 1$ from the Hubble Space Telescope: Evidence for Past Deceleration and Constraints on Dark Energy Evolution.*, Astrophys. J., 607

Riess A., et al., 2016, *A 2.4%Determination of the Local Value of the Hubble Constant.*, Astrophys. J., 826, 31

Riess A., et al., 2019, *Large Magellanic Cloud Cepheid Standards Provide a 1% Foundation for the Determination of the Hubble Constant and Stronger Evidence for Physics beyond ΛCDM.*, Astrophys. J., 876, 13

Robles V. H., Matos T., 2013, *Exact Solution to Finite Temperature SFDM: Natural Cores without Feedback.*, Astrophys. J., 763, 8

Robles V. H., et al., 2019, *The Milky Way's halo and subhaloes in self-interacting dark matter.*, Mon. Not. R. Astron. Soc., 490, 2117

Roderick T. A., Jerjen H., Da Costa G. S., Mackey A. D., 2016, *Structural analysis of the Sextans dwarf spheroidal galaxy.*, Mon. Not. R. Astron. Soc., 460, 30

Rogers K. K., Peiris H., 2021, *Strong Bound on Canonical Ultralight Axion Dark Matter from the Lyman-Alpha Forest.*, Phys. Rev. Lett., 126

Romano-Díaz E., et al., 2008, *Erasing Dark Matter Cusps in Cosmological Galactic Halos with Baryons.*, Astrophys. J. Lett., 685, L105

Romano-Díaz E., et al., 2009, *Dissecting Galaxy Formation. I. Comparison Between Pure Dark Matter and Baryonic Models.*, Astrophys. J., 702, 1250

Roy V., 2020, *Convergence Diagnostics for Markov Chain Monte Carlo.*, Annual Rev. of Statis. and Its App., 7

Rubakov V. A., 2000, *Relaxation of the cosmological constant at inflation?*, Phys. Rev. D., 61

Rubin V. C., et al., 1982, *Rotational properties of 23Sb galaxies.*, Astrophys. J., 261, 439

Rusakov V., et al., 2020, *The bursty star formation history of the Fornax dwarf spheroidal galaxy revealed with the HST.*, Arxiv

Sacchi E., et al., 2021, *Star Formation Histories of Ultra-Faint Dwarf Galaxies: environmental differences between Magellanic and non-Magellanic satellites?*, Arxiv

Safarzadeh M., Loeb A., 2021, *A New Challenge for Dark Matter Models.*, Arxiv

Sahni V., Wang L., 2000, *New cosmological model of quintessence and dark matter.*, Phys. Rev. D., 62

Sakamoto T., Chiba M., Beers T. C., 2003, *The mass of the Milky Way: Limits from a newly assembled set of halo objects.*, Astron. Astrophys., 397, 899

Samir Acharya B., Bobkov K., Kumar P., 2010, *Dark Energy from the String Axiverse.*, Phys. Rev. Lett., 113

Sand D. J., otehrs 2010, *A Deeper Look at Leo IV: Star Formation History and Extended Structure.*, Astrophys. J., 718, 530

Sanders J. L., Evans N. W., Dehnen W., 2018, *Tidal disruption of dwarf spheroidal galaxies: the strange case of Crater II.*, Mon. Not. R. Astron. Soc., 478, 3879

Saremi E., et al., 2020, *The Isaac Newton Telescope Monitoring Survey of Local Group Dwarf Galaxies. I. Survey Overview and First Results for Andromeda I.*, Astrophys. J., 894, 17

Sasaki M., et al., 2016, *Primordial Black Hole Scenario for the Gravitational-Wave Event GW150914.*, Phys. Rev. Lett., 117

Sawala T., et al., 2016, *The APOSTLE simulations: solutions to the Local Group's cosmic puzzles.*, Mon. Not. R. Astron. Soc., 457, 1931

Schaye J., et al., 2015, *The EAGLE project: simulating the evolution and assembly of galaxies and their environments.*, Mon. Not. R. Astron. Soc., 446, 521

Schive H.-Y., Chiueh T., Broadhurst T., 2014a, *Cosmic structure as the quantum interference of a coherent dark wave.*, Nature Phys., 10, 496

Schive H.-Y., et al., 2014b, *Understanding the Core-Halo Relation of Quantum Wave Dark Matter from 3D Simulations.*, Phys. Rev. Lett., 113

Schive H.-Y., Chiueh T., Broadhurst T., Huang K.-W., 2016, *Contrasting Galaxy Formation from Quantum Wave Dark Matter.*, Astrophys. J., 818, 14

Schive H.-Y., Chiueh T., Broadhurst T., 2020, *Soliton Random Walk and the Cluster-Stripping Problem in Ultralight Dark Matter.*, Phys. Rev. Lett., 124

Schwabe B., Niemeyer J. C., Engels J. F., 2016, *Simulations of solitonic core mergers in ultralight axion dark matter cosmologies.*, Phys. Rev. D., 94

Segall M., Ibata R. A., Irwin M. J., Martin N. F., Chapman S., 2007, *Draco, a flawless dwarf galaxy**, Mon. Not. R. Astron. Soc., 375, 831

Seidel E., Suen W.-M., 1991, *Oscillating soliton stars.*, Phys. Rev. Lett., 66, 1659

Servant G., others Tait T. M. P., 2003, *Is the lightest Kaluza-Klein particle a viable dark matter candidate?*, Nuclear Phys. B, 650, 391

Sikivie P., Yang Q., 2009, *Bose-Einstein Condensation of Dark Matter Axions*, Phys. Rev. Lett., 103

Simon J. D., 2019, *The Faintest Dwarf Galaxies.*, Annual Rev. of Astron. Astrophys., 57, 375

Simon J. D., Geha M., 2007, *The Kinematics of the Ultra-faint Milky Way Satellites: Solving the Missing Satellite Problem.*, Astrophys. J., 670, 313

Simon J., Verde L., Jimenez R., 2005, *Constraints on the redshift dependence of the dark energy potential.*, Phys. Rev. Lett., 71

Simon J. D., et al., 2015, *Stellar Kinematics and Metallicities in the Ultra-faint Dwarf Galaxy Reticulum II.*, Astronomical. J., 808, 14

Simon J. D., et al., 2020, *Birds of a Feather? Magellan/IMACS Spectroscopy of the Ultra-faint Satellites Grus II, Tucana IV, and Tucana V.*, Astrophys. J., 892, 16

Smercina A., et al., 2018, *A Lonely Giant: The Sparse Satellite Population of M94 Challenges Galaxy Formation.*, Astrophys. J., 863, 7

Sohn S., et al., 2007, *Exploring Halo Substructure with Giant Stars. X. Extended Dark Matter or Tidal Disruption?: The Case for the Leo I Dwarf Spheroidal Galaxy.*, Astrophys. J., 663, 960

Sohn S. T., et al., 2018, *Absolute Hubble Space Telescope Proper Motion (HST-PROMO) of Distant Milky Way Globular Clusters: Galactocentric Space Velocities and the Milky Way Mass.*, Astrophys. J., 862, 17

Songaila A., Cowie L. L., 1996, *Metal enrichment and Ionization Balance in the Lyman Alpha Forest at $Z = 3$.*, Astrophys. J., 112, 335

Spekkens K., Giovanelli R., Haynes M. P., 2005, *The Cusp/Core Problem in Galactic Halos: Long-Slit Spectra for a Large Dwarf Galaxy Sample.*, Astron. J., 129, 2119

Spencer M. E., Mateo M., Walker M. G., Olszewski E. W., 2017, *A Multi-epoch Kinematic Study of the Remote Dwarf Spheroidal Galaxy Leo II*, Astrophys. J., 836, 10

Spergel D. N., Flauger R. Hložek R., 2015, *Planck data reconsidered.*, Phys. Rev. D., 91

Spergel D. N., Steinhardt P. J., 2000, *Fuzzy Cold Dark Matter: The Wave Properties of Ultralight Particles.*, Phys. Rev. Lett., 84, 3760

Springel V., et al., 2008, *The Aquarius Project: the subhaloes of galactic haloes.*, Mon. Not. R. Astron. Soc., 391, 1685

Steinhardt P. J., Turok N., 2006, *Why the Cosmological Constant Is Small and Positive.*, Science, 312

Stern D., et al., 2010, *Cosmic chronometers: constraining the equation of state of dark energy. I: H(z) measurements.*, Journal of Cosmology and Astroparticle Physics

Stott M. J., Marsh D. J. E., 2018, *Black hole spin constraints on the mass spectrum and number of axionlike fields.*, Phys. Rev. D., 98

Suzuki N., et al., 2012, *The Hubble Space Telescope Cluster Supernova Survey. V. Improving the Dark-energy Constraints above $z > 1$ and Building an Early-type-hosted Supernova Sample.*, Astrophys. J., 746

Suárez A., Chavanis P.-H., 2017, *Cosmological evolution of a complex scalar field with repulsive or attractive self-interaction.*, Phys. Rev. D., 95

Svrcek P., Witten E., 2006, *Axions in string theory.*, J. of High Energy Phys.

Synge J. L., 1966, *The escape of photons from gravitationally intense stars.*, Mon. Not. R. Astron. Soc., 131, 463

Taibi S., et al., 2018, *Stellar chemo-kinematics of the Cetus dwarf spheroidal galaxy.*, Astron. Astrophys., 618, 22

Taibi S., et al., 2020, *The Tucana dwarf spheroidal galaxy: not such a massive failure after all.*, Astron. Astrophys., 635, 24

Tanabashi M., et al., 2018, *Review of Particle Physics*.*, Phys. Rev. D., 98

Taruya A., Saga S., 2022, *An analytical approach to core-halo structure of fuzzy dark matter.*, Arxiv

Tegmark M., et al., 2004, *The Three-Dimensional Power Spectrum of Galaxies from the Sloan Digital Sky Survey.*, Astrophys. J., 606, 702

Tisserand P., et al., 2007a, *Limits on the Macho content of the Galactic Halo from the EROS-2 Survey of the Magellanic Clouds.*, Astron. Astrophys., 469, 387

Tisserand P., et al., 2007b, *Limits on the Macho Content of the Galactic Halo from the EROS-2 Survey of the Magellanic Clouds.*, Astron. Astrophys., 469, 387

Tollerud E. J., Boylan-Kolchin M., Bullock J. S., 2014, *M31 satellite masses compared to ΛCDM subhaloes.*, Mon. Not. R. Astron. Soc., 440, 3511

Tomozeiu M., Mayer L., Quinn T., 2016, *Tidal Stirring of Satellites with Shallow Density Profiles Prevents Them from Being Too Big to Fail.*, Astrophys. J. Lett., 827, 7

Tonini C., Lapi A., Salucci P., 2006, *Angular Momentum Transfer in Dark Matter Halos: Erasing the Cusp.*, Astrophys. J., 649, 591

Torrealba G., Koposov S. E., Belokurov V., Irwin M., 2016, *The feeble giant. Discovery of a large and diffuse Milky Way dwarf galaxy in the constellation of Crater.*, Mon. Not. R. Astron. Soc., 459, 2370

Torrealba G., et al., 2019, *The hidden giant: discovery of an enormous Galactic dwarf satellite in Gaia DR2.*, Mon. Not. R. Astron. Soc., 488, 2743

Tremmel M. o., 2020, *The Formation of Ultra-Diffuse Galaxies from Passive Evolution in the RomulusC Galaxy Cluster Simulation.*, Ame. Astro. Society meeting, 52

Turk M. J., et al., 2011, *yt: A Multi-code Analysis Toolkit for Astrophysical Simulation Data.*, Astrophys. J. Supp., 192, 16

Ural U., et al., 2015, *A low pre-infall mass for the Carina dwarf galaxy from disequilibrium modelling.*, Nature Com., 6

V. B., 2016, *Stellar Dynamics and Structure of Galaxies.*, No one

Valinia A., others. 1997, *Gravitational Instability in Collisionless Cosmological Pancakes.*, Astrophys. J., 479, 46

Veltmaat J., Niemeyer J. C., Schwabe B., 2018, *Formation and structure of ultralight bosonic dark matter halos.*, Phys. Rev. D., 98

Veltmaat J., Schwabe B., Niemeyer J. C., 2020, *Baryon-driven growth of solitonic cores in fuzzy dark matter halos.*, Phys. Rev. Lett., 101

Venumadhav T., Dai L., Miralda-Escudé J., 2017, *Microlensing of Extremely Magnified Stars near Caustics of Galaxy Clusters.*, Astrophys. J., 850, 24

Verde L., 2007, *A practical guide to Basic Statistical Techniques for Data Analysis in Cosmology.*, Arxiv

Vicens J., Salvado J., Miralda-Escudé J., 2018, *Bosonic dark matter halos: excited states and relaxation in the potential of the ground state*, Arxiv

Viel M., et al., 2005, *Constraining warm dark matter candidates including sterile neutrinos and light gravitinos with WMAP and the Lyman-α forest.*, Phys. Rev. D., 71

Viel M., et al., 2013, *Warm dark matter as a solution to the small scale crisis: New constraints from high redshift Lyman-α forest data.*, Phys. Rev. D., 88

Villaescusa-Navarro F., Dalal N., 2011, *Cores and cusps in warm dark matter halos.*, Journal of Cosmology and Astroparticle Physics

Visinelli L., Vagnozzi S., 2019, *Cosmological window onto the string axiverse and the supersymmetry breaking scale.*, Phys. Rev. D., 99

Vogelsberger M., et al., 2013, *A model for cosmological simulations of galaxy formation physics.*, Mon. Not. R. Astron. Soc., 436, 3031

Walcher J., et al., 2011, *Fitting the integrated spectral energy distributions of galaxies.*, Astrophys. J., 331, 1

Walker M. G., 2012, *Dark Matter in the Milky Way's Dwarf Spheroidal Satellites.*, ArXiv

Walker M. G., Peñarrubia J., 2011, *A Method for Measuring (Slopes of) the Mass Profiles of Dwarf Spheroidal Galaxies.*, Astrophys. J., 742, 19

Walker M. G., et al., 2009, *A Universal Mass Profile for Dwarf Spheroidal Galaxies?*, Astrophys. J., 704, 1274

Wang J. and; White S. D. M., 2007, *Discreteness effects in simulations of hot/warm dark matter.*, Mon. Not. R. Astron. Soc., 380, 93

Wang Y., 2014, *Inflation, Cosmic Perturbations and Non-Gaussianities.*, Commu. in Theo. Phys., 62, 109

Wasserman A., et al., 2019, *Spatially Resolved Stellar Kinematics of the Ultra-diffuse Galaxy Dragonfly 44. II. Constraints on Fuzzy Dark Matter.*, Astrophys. J., 885

Webb J. J., Vesperini E., 2018, *The Structural and Kinematic Evolution of Central Star Clusters in Dwarf Galaxies and Their Dependence on Dark Matter Halo Profiles.*, Mon. Not. R. Astron. Soc., 479, 3708

Weinberg S., 1987, *Anthropic bound on the cosmological constant.*, Phys. Rev. Lett., 59, 2607

Weinberg S., 1989, *The cosmological constant problem.*, Rev. on Modern Phys., 61, 1

Weinberg D. H., 2015, *Cold dark matter: Controversies on small scales.*, Proceedings of the National Academy of Sciences, 112, 12249

Weinberg M. D., Katz N., 2002, *Bar-driven Dark Halo Evolution: A Resolution of the Cusp-Core Controversy.*, Astrophys. J., 580, 627

Weldrake D. T. F., de Blok W. J. G., Walter F., 2003, *A high-resolution rotation curve of NGC 6822: a test-case for cold dark matter.*, Mon. Not. R. Astron. Soc., 340, 12

Wesley A., 2004, Pearson Education

Wetzel A R., 2016, *Reconciling Dwarf Galaxies with ΛCDM Cosmology: Simulating a Realistic Population of Satellites around a Milky Way-mass Galaxy.*, The Astrophysical Journal Letters, 827, 6

Widrow L. M., Kaiser N., 1993, *Using the Schroedinger Equation to Simulate Collisionless Matter.*, Astrophys. J., 416, L71

Wilkinson M. I., et al., 2004, *Kinematically Cold Populations at Large Radii in the Draco and Ursa Minor Dwarf Spheroidal Galaxies.*, Astrophys. J., 611, L21

Wilkinson M. I., et al., 2006, *Probing the Dark Matter Content of Local Group Dwarf Spheroidal Galaxies with FLAMES*, The Messenger, 124, 25

Willman B., et al., 2005, *A New Milky Way Dwarf Galaxy in Ursa Major.*, Astrophys. J., 626, L85

Woo T. P., Chiueh T., 2009, *High-resolution simulation on structure formation with extremely light bosonic dark matter.*, Astrophys. J., 697, 850

Wu E., 2009, *Parity Violation Constraints Using 2006-2007 Quad Cmb Polarization Spectra.*, American Astro. Society, 41, 514

Wyrzykowski L., et al., 2009, *The OGLE view of microlensing towards the Magellanic Clouds - I. A trickle of events in the OGLE-II LMC data.*, Mon. Not. R. Astron. Soc., 397, 1228

Wyrzykowski L., et al., 2011, *The OGLE view of microlensing towards the Magellanic Clouds - IV. OGLE-III SMC data and final conclusions on MACHOs.*, Mon. Not. R. Astron. Soc., 416, 2949

Xu Z., et al., 2018, *Black hole space-time in dark matter halo.*, Phys. Rev. D

Xue X. X., et al., 2008, *The Milky Way's Circular Velocity Curve to 60 kpc and an Estimate of the Dark Matter Halo Mass from the Kinematics of ∼2400 SDSS Blue Horizontal-Branch Stars.*, Astrophys. J., 684, 1143

Yoo J., Chanamé J., Gould A., 2004, *The End of the MACHO Era: Limits on Halo Dark Matter from Stellar Halo Wide Binaries.*, Astrophys. J., 601, 311

Yoshida N., Sokasian A., Hernquist L., Springel V., 2003, *Early Structure Formation and Reionization in a Cosmological Model with a Running Primordial Power Spectrum.*, Astrophys. J., 598, 73

Zaggia S., Held E. V., Sommariva V., Momany Y., Saviane I., Rizzi L., 2011, *Phoenix Dwarf Galaxy Stellar Kinematics*, EAS Publications Series, 48, 215

Zentner A. R., et al., 2005, *The Physics of Galaxy Clustering. I. A Model for Subhalo Populations.*, Astrophys. J., 624, 505

Zhu L., et al., 2016a, *A discrete chemo-dynamical model of the giant elliptical galaxy NGC 5846: dark matter fraction, internal rotation, and velocity anisotropy out to six effective radii.*, Mon. Not. R. Astron. Soc., 462, 4001

Zhu L., et al., 2016b, *A discrete chemo-dynamical model of the dwarf spheroidal galaxy Sculptor: mass profile, velocity anisotropy and internal rotation.*, Mon. Not. R. Astron. Soc., 463, 1117

Zucker D. B., et al., 2006a, *A New Milky Way Dwarf Satellite in Canes Venatici.*, Astrophys. J., 643, L103

Zucker D. B., et al., 2006b, *A Curious Milky Way Satellite in Ursa Major.*, Astrophys. J., 650, L41

Zurek K. M., Hogan C. J., Quinn T. R., 2007, *Astrophysical effects of scalar dark matter miniclusters.*, Phys. Rev. D., 75

Zwicky F., 1933, *Die Rotverschiebung von extragalaktischen Nebeln.*, Helvetica Physica Acta, 6, 110

de Blok W. J. G., 2010, *The Core-Cusp Problem.*, Adv. in Astro.

de Blok W. J. G., Bosma A., 2002, *High-resolution rotation curves of low surface brightness galaxies.*, Astron. Astrophys., 385, 816

de Blok W. J. G., McGaugh S. S., 1997, *The dark and visible matter content of low surface brightness disc galaxies.*, Mon. Not. R. Astron. Soc., 290, 533

de Blok W. J. G., Bosma A., McGaugh S., 2003, *Simulating observations of dark matter dominated galaxies: towards the optimal halo profile.*, Mon. Not. R. Astron. Soc., 340, 657

de Boer T. J. L., Tolstoy E., Saha A.nd Olszewski E. W., 2013, *A new study of stellar substructures in the Fornax dwarf spheroidal galaxy.*, Astron. Astrophys., 551, 7

de Boer T. J. L., et al., 2014, *The episodic star formation history of the Carina dwarf spheroidal galaxy.*, Astron. Astrophys., 572, 14

de Martino I., Broadhurst T., Tye S. H. H., Chiueh T., Schive H.-Y., Lazkoz R., 2017, *Recognising Axionic Dark Matter by Compton and de-Broglie Scale Modulation of Pulsar Timing.*, Phys. Rev. Lett., 119

de Martino I., et al., 2020a, *Dark Matters on the Scale of Galaxies.*, Universe, 6, 107

de Martino I., Broadhurst T., Henry Tye S. H., Chiueh T., Schive H.-Y., 2020b, *Dynamical Evidence of a Solitonic Core of* $10^9 M_\odot$., Phys. Dark Universe, 491

de Rujula A., Jetzer P., Masso E., 1992, *On the nature of the dark halo of our galaxy.*., Astron. Astrophys., 254, 99

del Pino A., Aparicio A., Hidalgo S. L., 2015, *Merger traces in the spatial distribution of stellar populations in the Fornax dSph galaxy.*, Mon. Not. R. Astron. Soc., 454, 3996

van Dokkum P. G., et al., 2015, *Forty-seven Milky Way-sized, Extremely Diffuse Galaxies in the Coma Cluster.*, Astrophys. J. Lett., 798, 8

van Dokkum P. G., et al., 2016, *A High Stellar Velocity Dispersion and ∼100 Globular Clusters for the Ultra-diffuse Galaxy Dragonfly 44.*, Astrophys. J. Lett., 828, 6

van Dokkum P., et al., 2018a, *A Revised Velocity for the Globular Cluster GC-98 in the Ultra Diffuse Galaxy NGC-1052-DF2.*, American Astronomical Society, 2, 54

van Dokkum P., et al., 2018b, *A galaxy lacking dark matter.*, Nature, 555, 629

van Dokkum P., et al., 2018c, *An Enigmatic Population of Luminous Globular Clusters in a Galaxy Lacking Dark Matter.*, Astrophys. J. Lett., 856, 7

van Dokkum P., et al., 2018d, *The Distance of the Dark Matter Deficient Galaxy NGC 1052-DF2.*, Astrophys. J. Lett., 864, 7

van Dokkum P., et al., 2019a, *A Second Galaxy Missing Dark Matter in the NGC 1052 Group.*, Astrophys. J. Lett., 874, 8

van Dokkum P., et al., 2019b, *Spatially Resolved Stellar Kinematics of the Ultra-diffuse Galaxy Dragonfly 44. I. Observations, Kinematics, and Cold Dark Matter Halo Fits.*, Astrophys. J., 880, 26

van den Bergh S., 1994, *The Evolutionary History of Low-Luminosity Local Group Dwarf Galaxies.*, Astrophys. J., 428, 617

van den Bosch F. C., Swaters R. A., 2001, *Dwarf galaxy rotation curves and the core problem of dark matter haloes.*, Mon. Not. R. Astron. Soc., 325, 1017

Łokas E. L., 2009, *The mass and velocity anisotropy of the Carina, Fornax, Sculptor and Sextans dwarf spheroidal galaxies.*, Mon. Not. R. Astron. Soc., 394, L102

Łokas E. L., Mamon G. A., 2003, *A discrete chemo-dynamical model of the dwarf spheroidal galaxy Sculptor: mass profile, velocity anisotropy and internal rotation.*, Mon. Not. R. Astron. Soc., 343, 401

Łokas E. L., Mamon G. A., Prada F., 2005b, *Dark matter distribution in the Draco dwarf from velocity moments.*, Mon. Not. R. Astron. Soc., 363, 918

Łokas E. L., Mamon G. A., Prada F., 2005a, *The mass and velocity anisotropy of the Carina, Fornax, Sculptor and Sextans dwarf spheroidal galaxies.*, Mon. Not. R. Astron. Soc., 363, 918

Appendix

Extra section to comment the following Monte Carlo Markov Chain characteristics and the resulting corner plots of the previously correspondent results. The explanation refers to the exact methodology followed for the MCMC of sections 4.2, 4.3, 4.4 and 4.5. Due to being all the MCMC done exactly except the one refereed to section 4.1, which their explanation is on their caption (Figure 4.64):

We have explored the full range of relevant parameter space with the Monte Carlo Markov Chain (MCMC) technique based on the Metropolis-Hastings sampling algorithm to obtain the core radius that characterises fully the soliton profile, r_c, and the scale radius and the normalization of the stellar density profile,r_{s*} and ρ_{0*}, and the also the transition radius r_t between the core and halo profiles. We allow for an adaptive step size in order to reach an acceptance rate between 20% and 50%, computing 4 chains of 10000 iterations for each variable(r_c, r_t, ρ_{0*} and r_{s*}) in each galaxy. Each chain's serial correlation was checked by correlograms (ACF plots), ensuring that the autocorrelation of the terms dropped to zero before 250 lags (Roy, 2020). We ensure the convergence relying on the Gelman-Rubin criteria adopting a Max Gelman–Rubin Rc below to 1.2 (Roy, 2020). Once the convergence criteria are satisfied, the chains are combined to compute the total likelihood, together with the 1D marginalized likelihood distribution with the corresponding expectation value and variance. The results for the above free parameters and their uncertainties of section 4.2, 4.3, 4.4 and 4.5 are shown in Table 4.4, Table 4.5 and Tables 4.6 and 4.9 respectively. We also show the covariances between the free parameters for each required figure-result with the following corner plots. We set flat priors for all the galaxies MCMC calculations, with the following uniform distribution for the two main parameters: $r_c(kpc) \sim \mathcal{U}(0.1,\, 0.75)$ and $r_t(kpc) \sim \mathcal{U}(0.75,\, 1.5)$ to span a wide range of ψDM simulation expectations (Schive et al., 2014a, 2016). **All the calculations have been done with a fixed boson mass of $\simeq 1.5 \times 10^{-22}$ eV.** We decided to focus this paper cataloging the core size and the transition point of each galaxy as a natural characteristic of ψDM by fixing the boson mass to plausible theoretical values stipulated in previous works (Schive et al., 2014a, 2016) to avoid any type of degeneracy with the halo mass, M_h, due to equation(3.4) .

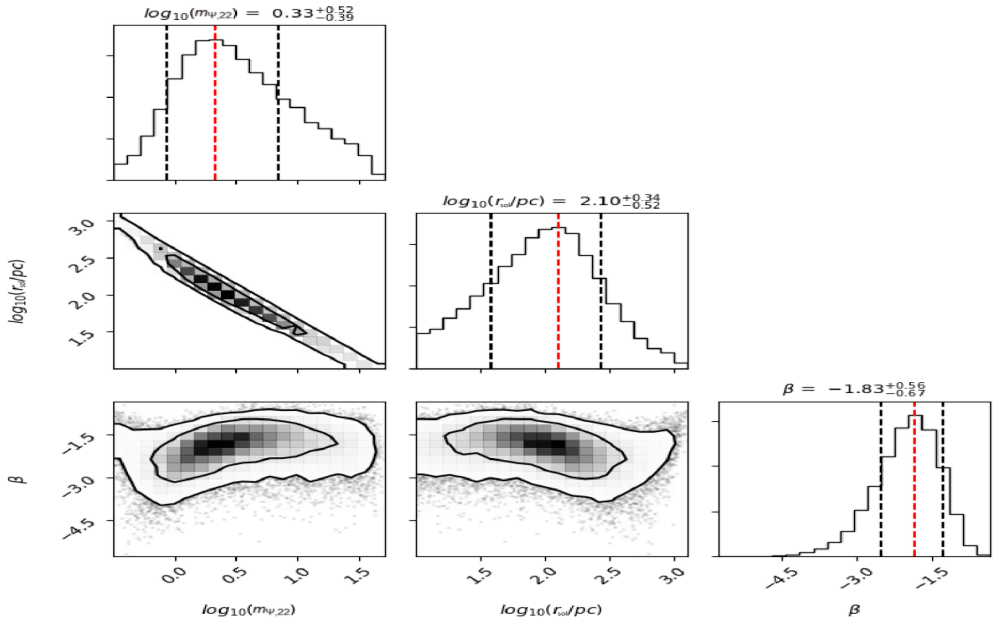

Figure 4.64: Respective corner plot of Figure 4.5. Correlated distributions of free parameters: boson mass, core radius and anisotropy from MCMC simulation. Transition factor distribution is not shown here due to its uniformity. Note, the 1D and 2D posterior distributions of four UFDs taken from MCMC chains using emcee (Foreman-Mackey et al., 2013), plotted using corner package (Foreman-Mackey, 2016)

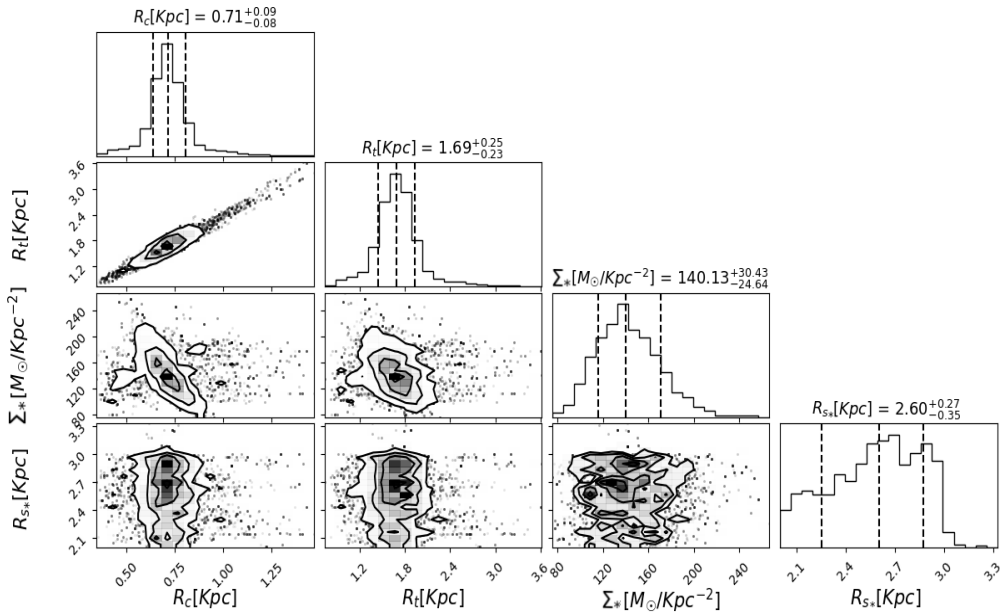

Figure 4.65: Respective corner plot of Figure 4.12. Crater II: correlated distributions of the free parameters. As can be seen the core radius and transition radius are well defined despite the flat input priors, indicating a reliable result. The contours represent the 68%, 95%, and 99% confidence levels. The best-fit parameter values are the medians(with errors), represented by the dashed black ones, and tabulated in Table4.5.

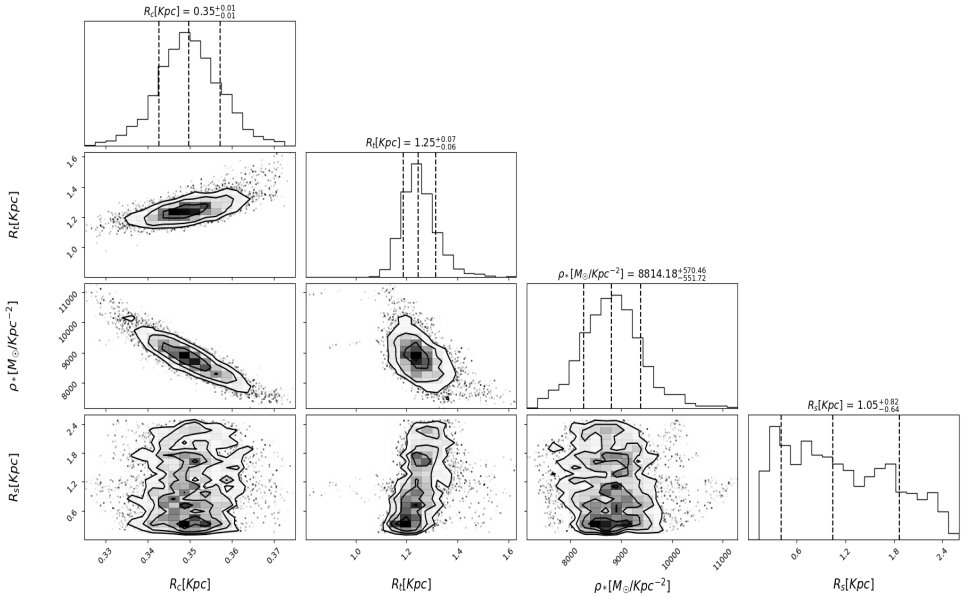

Figure 4.66: Respective corner plot of Figure 4.7. Aquarius' correlated distributions of free parameters from MCMC simulation. The core radius and transition radius is well defined here, despite the flat input priors, indicating a reliable result. The contours represent the 68%, 95%, and 99% of confidence level. The best-fit parameter values are the medians, represented with the vertical red lines while the black ones show their errors.

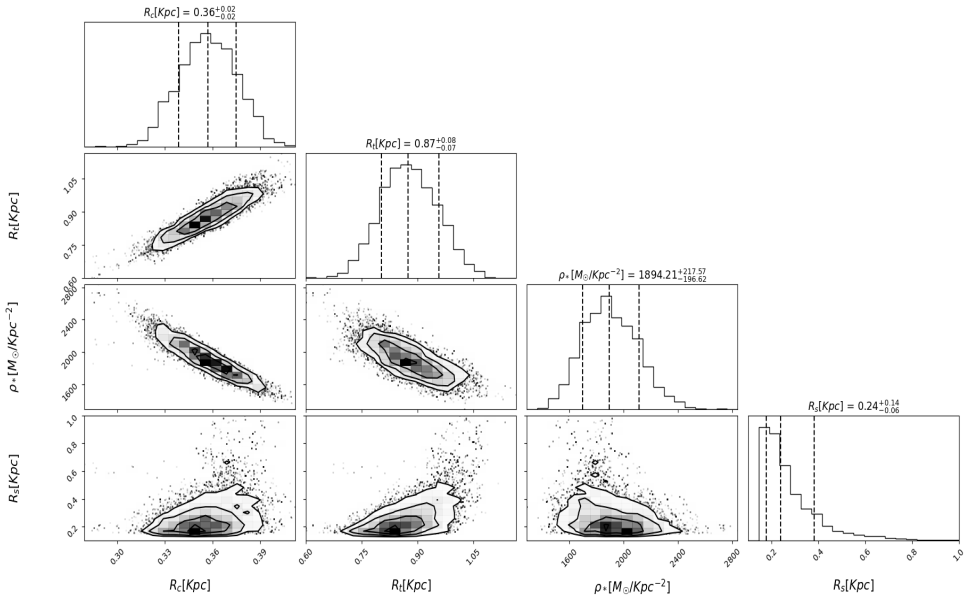

Figure 4.67: Respective corner plot of Figure 4.7. Cetus' correlated distributions of the free parameters. As can be seen the core radius and transition radius are well defined despite the flat input priors, indicating a reliable result.The contours represent the 68%, 95%, and 99% of confidence level. The best-fit parameter values are the medians, represented with the vertical red lines while the black ones show their errors.

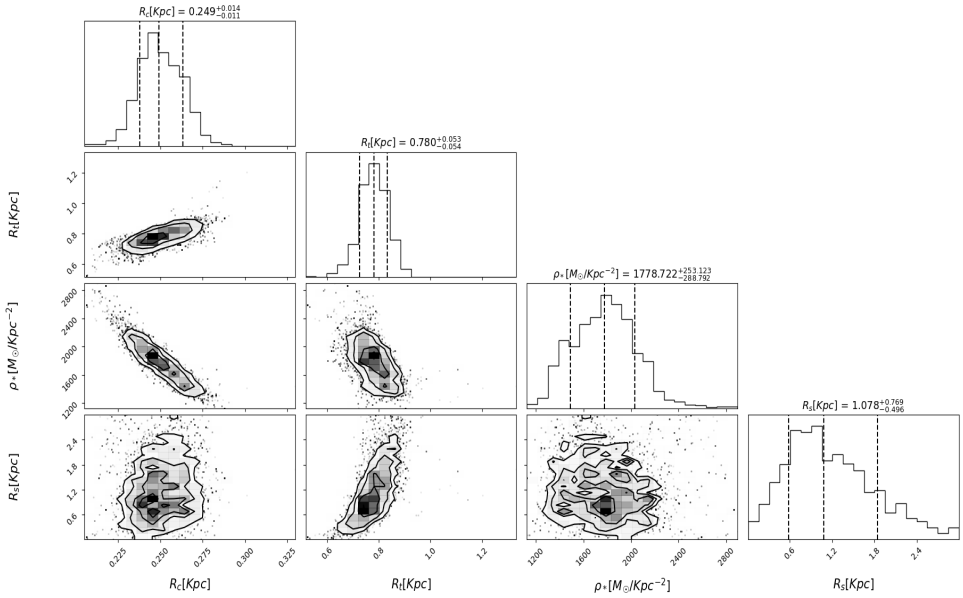

Figure 4.68: Respective corner plot of Figure 4.7. Tucana's correlated distributions of free parameters. As can be seen the core radius and transition radius are well defined despite the flat input priors, indicating a reliable result with a well constrained core and transition radius.The contours represent the 68%, 95%, and 99% of confidence level. The best-fit parameter values are the medians, represented with the vertical red lines while the black ones show their errors.

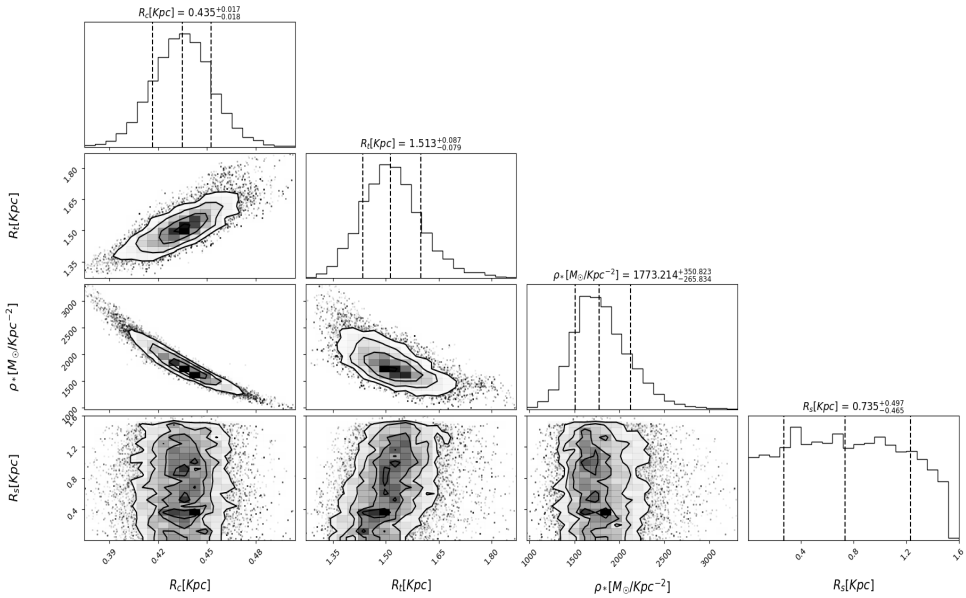

Figure 4.69: Respective corner plot of Figure 4.7. Leo A's correlated distributions of free parameters. As can be seen the core radius and transition radius are well defined despite the flat input priors, indicating a reliable result.The contours represent the 68%, 95%, and 99% of confidence level. The best-fit parameter values are the medians, represented with the vertical red lines while the black ones show their errors.

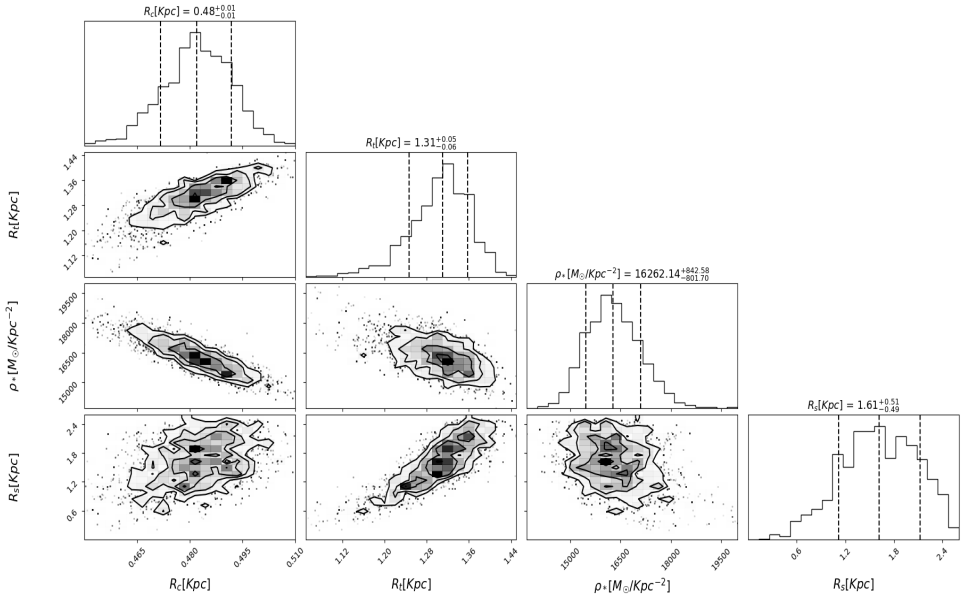

Figure 4.70: Respective corner plot of Figure 4.11. Sextans' correlated distributions of free parameters. As can be seen the core radius and transition radius are well defined despite the flat input priors, indicating a reliable result.The contours represent the 68%, 95%, and 99% of confidence level. The best-fit parameter values are the medians, represented with the vertical red lines while the black ones show their errors.

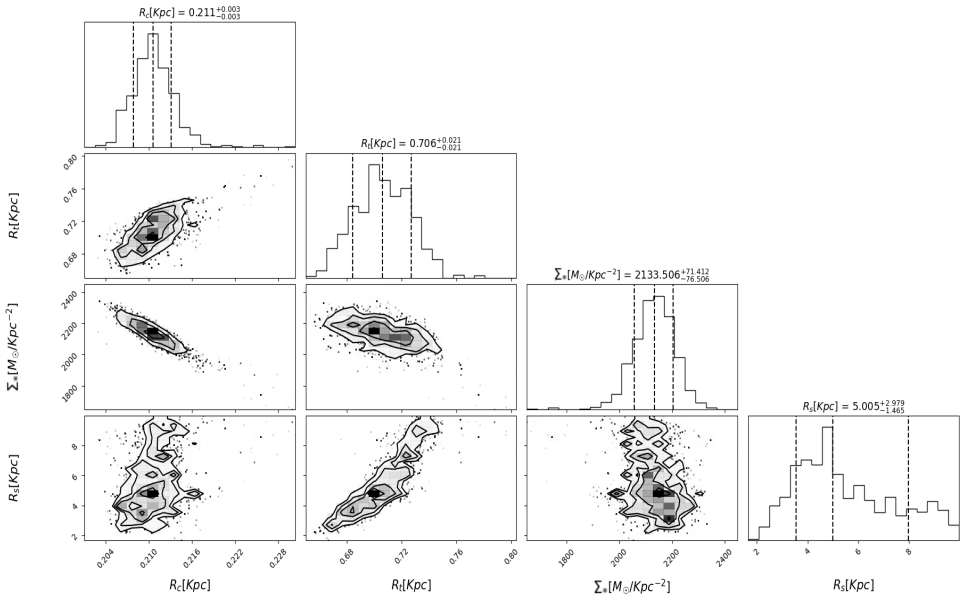

Figure 4.71: All dSph/ Respective corner plot of Figure 4.19 top panel: Classical dwarfs mean profile: correlated distributions of the free parameters. As can be seen the core radius and transition radius are well defined despite wide Gaussian priors, indicating a reliable result. The contours represent the 68%, 95%, and 99% confidence levels. The best-fit parameter values are the medians (with errors), represented by the dashed black ones, and tabulated in Table 4.6.

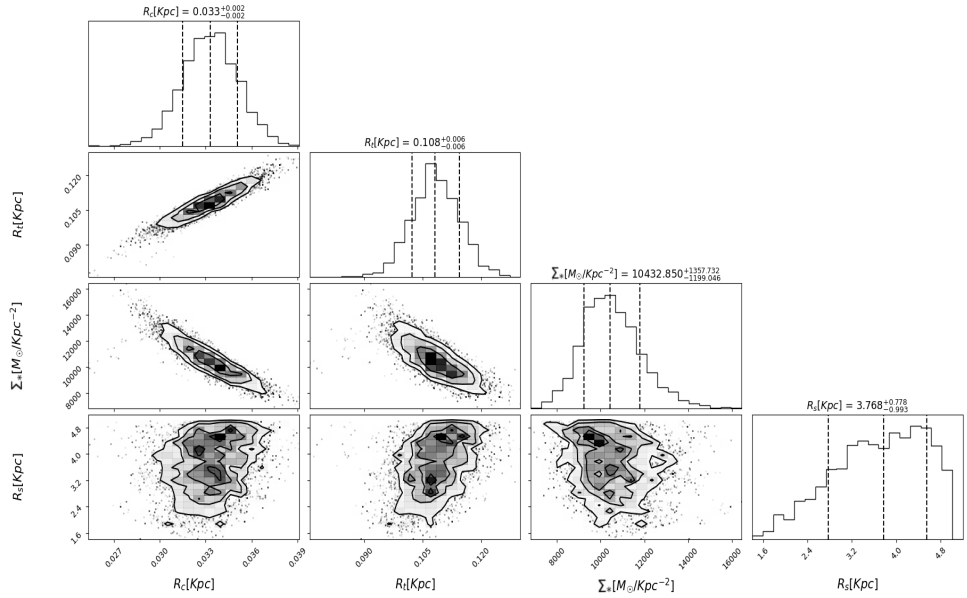

Figure 4.72: All UFD / Respective corner plot of Figure 4.19 low panel:Ultra faint dwarfs mean profiles: correlated distributions of the free parameters. As can be seen the core radius and transition radius are well defined despite wide Gaussian priors, indicating a reliable result. The contours represent the 68%, 95%, and 99% confidence levels. The best-fit parameter values are the medians(with errors), represented by the dashed black curve, and tabulated in Table 4.6.

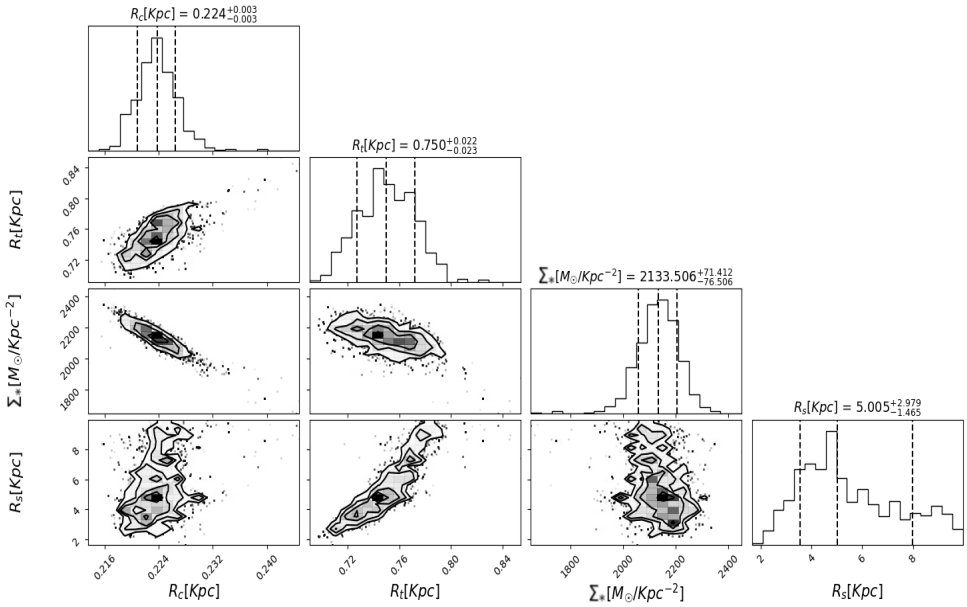

Figure 4.73: Respective corner plot of Figure 4.39 top panel: Milky's dSph mean: correlated distributions of the free parameters. As can be seen the core radius and transition radius are well defined despite the Gaussian input priors, indicating a reliable result. The contours represent the 68%, 95%, and 99% confidence levels. The best-fit parameter values are the medians(with errors), represented by the dashed black ones, and tabulated in Table 4.6.

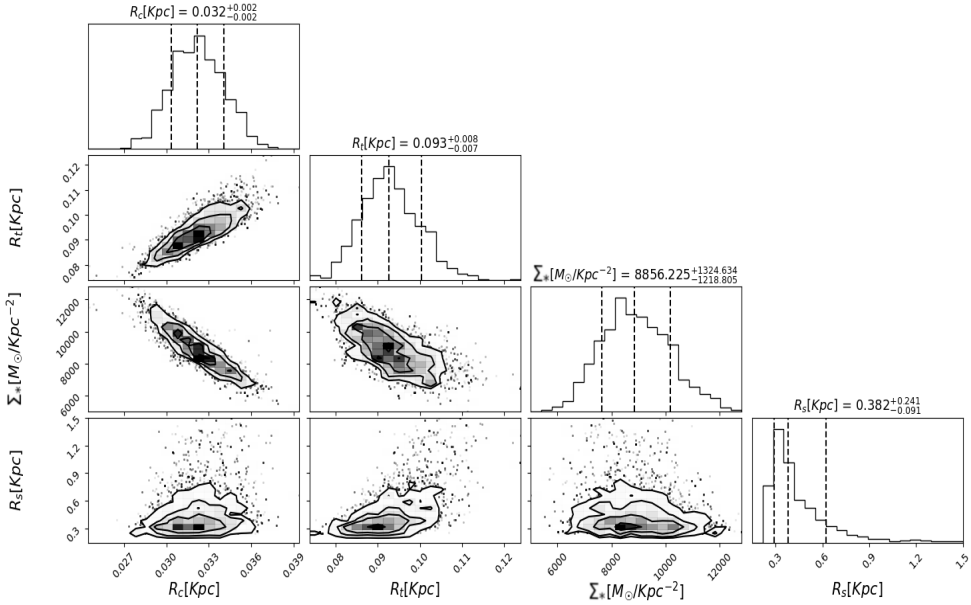

Figure 4.74: Respective corner plot of Figure 4.39 low panel Milky's UFD 2 mean: correlated distributions of the free parameters. As can be seen the core radius and transition radius are well defined despite the wide Gaussian priors, indicating a reliable result. The contours represent the 68%, 95%, and 99% confidence levels. The best-fit parameter values are the medians(with errors), represented by the dashed black ones, and tabulated in Table 4.6.

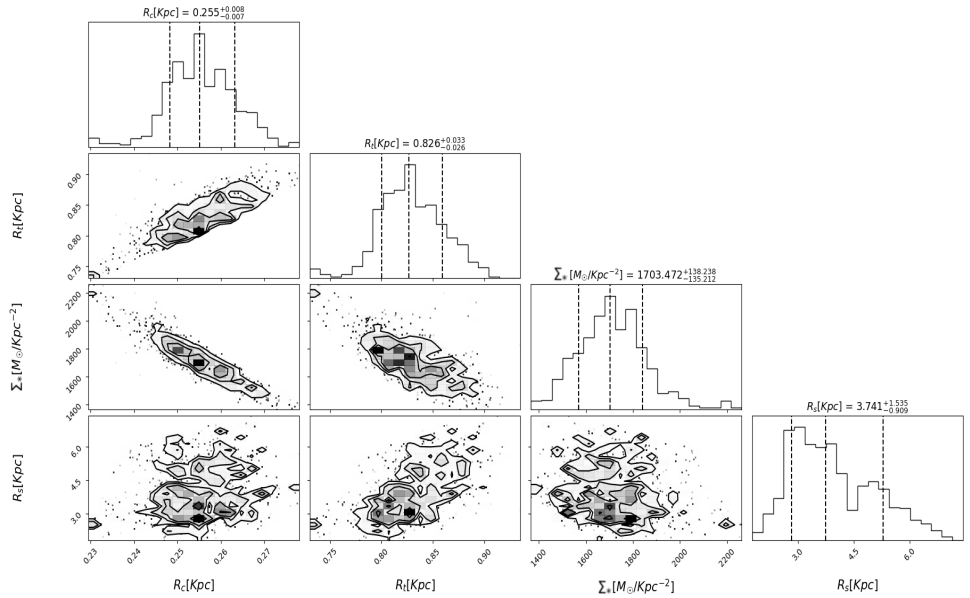

Figure 4.75: Respective corner plot of Figure 4.43 top panel Andromeda's dSph 1 mean: correlated distributions of the free parameters. As can be seen the core radius and transition radius are well defined despite wide Gaussian priors, indicating a reliable result. The contours represent the 68%, 95%, and 99% confidence levels. The best-fit parameter values are the medians(with errors), represented by the dashed black ones, and tabulated in Table 4.6.

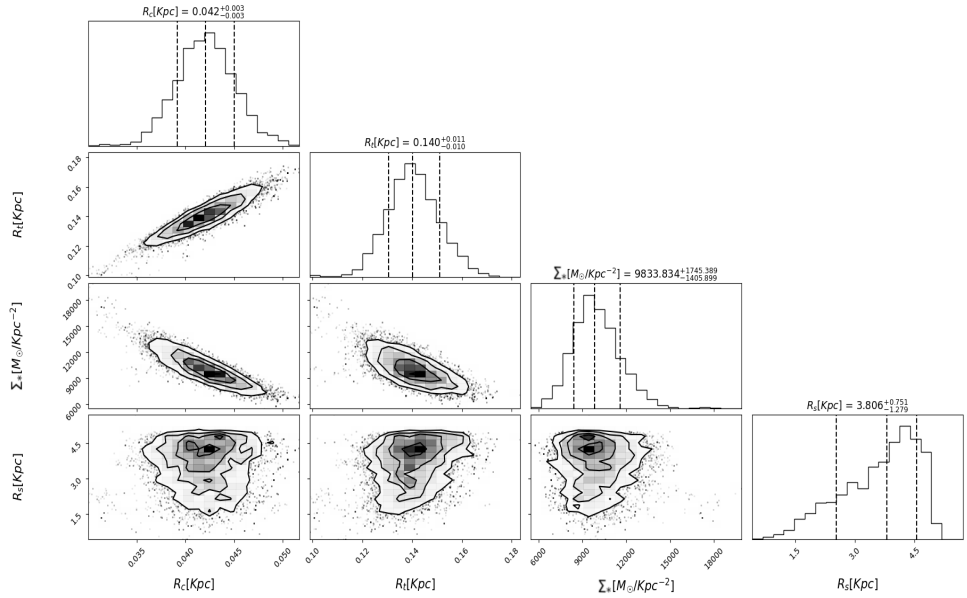

Figure 4.76: Respective corner plot of Figure 4.43 low panel top panel Andromeda's UFD 2 mean: correlated distributions of the free parameters. As can be seen the core radius and transition radius are well defined despite the Gaussian input priors, indicating a reliable result. The contours represent the 68%, 95%, and 99% confidence levels. The best-fit parameter values are the medians(with errors), represented by the dashed black ones, and tabulated in Table 4.6.

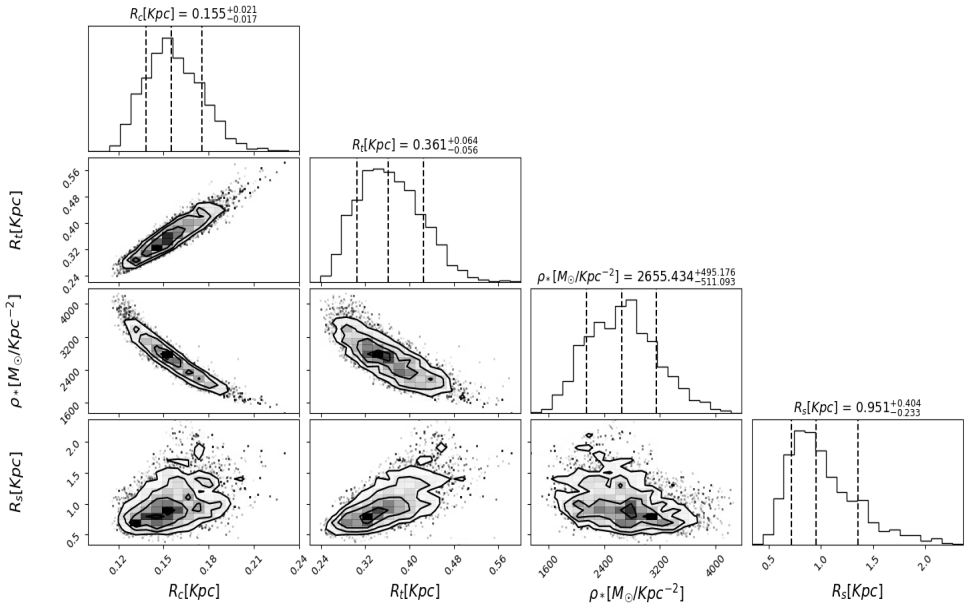

Figure 4.77: Respective corner plot of Figure 4.57 . Correlated distributions of the free parameters. As can be seen the core radius and transition radius are well defined despite the Gaussian input priors, indicating a reliable result. The contours represent the 68%, 95%, and 99% confidence levels. The best-fit parameter values are the medians(with errors), represented by the dashed black ones, and tabulated in Table 4.9.

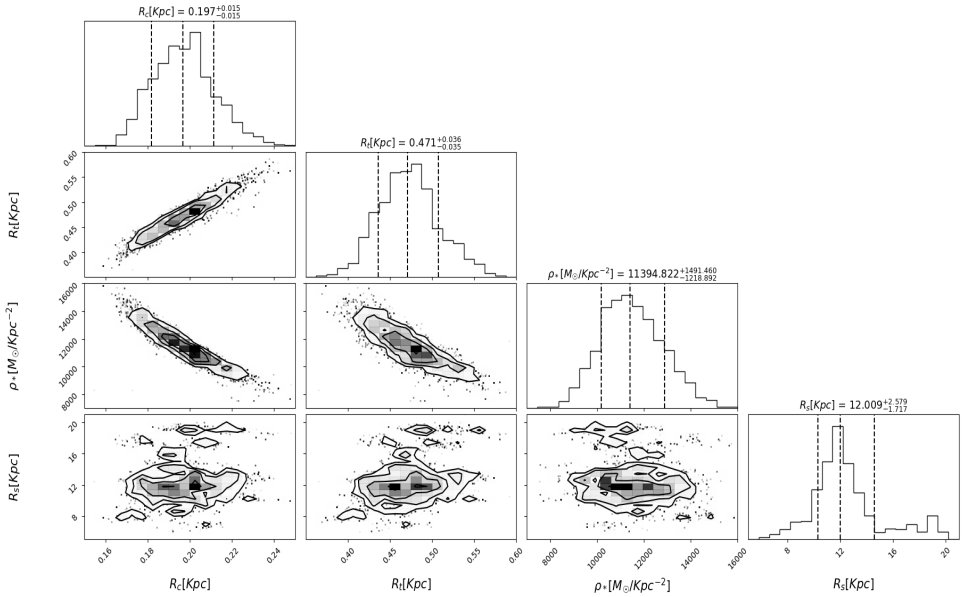

Figure 4.78: Respective corner plot of Figure 4.62 . Correlated distributions of the free parameters. As can be seen the core radius and transition radius are well defined despite the Gaussian input priors, indicating a reliable result. The contours represent the 68%, 95%, and 99% confidence levels. The best-fit parameter values are the medians(with errors), represented by the dashed black ones, and tabulated in Table 4.9.